The Henryk Niewodniczański Institute of Nuclear Physics
Polish Academy of Sciences
Department of Complex Systems Theory

Multiscale financial correlations in Ising-inspired agent-based models

mgr inż. Rafał Kowalski

This thesis was done under the supervision of
dr hab. inż. Paweł Oświęcimka.
Auxiliary Supervisor: dr Rafał Rak

Kraków 2021

Acknowledgements

First and foremost, I would like to express my gratitude to my supervisor dr hab. Paweł Oświęcimka, for his guidance, attention, and invaluable help during the course of this thesis. I would also like to thank my auxiliary supervisor, dr Rafał Rak for his remarks and assistance. Last but not least, I am indebted to prof. dr hab. Stanisław Drożdż, Head of the Department of Complex Systems Theory, and dr hab. Jarosław Kwapień for their support and creation of friendly atmosphere throughout my studies.

This research was supported in part by PL-Grid Infrastructure

Contents

Chapter 1

Introduction

The intricacy of the financial markets attracts the interest not only of economists and mathematicians but also of physicists. An extremely complicated structure, a multitude of dependencies between market elements, and herding behaviour among investors causes financial markets to resemble the complex systems found in nature, which can be quantitively described within formalisms commonly used in physics [1, 2, 3, 4, 5].

One phenomenon characteristic of complex systems in general also observed in the financial markets is the emergence. The market itself can be perceived as a set of individual entities having various objectives and strategies, possessing different resources, and, importantly, having the ability to interact with one another. The fact that traders exchange information and opinions about financial instruments can influence their investment decisions. For example, when a known trader shares his thoughts about a particular stock in public, other investors can follow this opinion, and, as a result, may tend to align their trading actions. Dependencies between market participants, which are not very interesting when a single entity is viewed, can lead to intriguing phenomena observed on a global scale. Speculative bubbles and market crashes exemplify this tendency [6]. In this context, financial markets have much in common with the emergence existing e.g., in biological [7, 8, 9, 10], sociological [11, 12, 13, 14, 15], and physical systems [16, 17, 18, 19].

The complexity of financial markets also reveals itself in the rate of return signals. Interestingly, regardless of the asset or market being considered, financial time series have common properties, known customarily as *stylized facts*. One of the most significant features of this signal type is its distribution. Originally, as proposed by Louis Bachelier in his doctoral thesis [20], price fluctuations were modeled using the Wiener process and relied on the assumption that returns follow a normal distribution. This work provided the foundation of modern quantitative finance and was inspirational for many researchers (e.g., Merton, Black and Scholes, who included Wiener process in their famous Black-Scholes option pricing formula [21]). However, as has been well established, rates of return do not enter into a Gaussian distribution. In fact, the distribution of asset price changes consists of an elongated central part with fat-tails that usually scale themselves according to the power law [22, 23, 24, 25, 26]. In physics, this characteristic of system fluctuations is commonly observed in near-critical states [27, 28], and so is another similarity between physical

systems and financial markets.

The power law dependency of returns distribution is related to another interesting feature of the financial time series: multifractality. In 1963, Mandelbrot noticed that an asset's price movement, considered on different time scales, have similar trajectories [29]. This finding set up the foundation of a new branch of mathematics. The fractal analysis in question, focuses on the multiscale regularities observed in various objects. In the following years, it has been completed with the more advanced theory of the multifractals, which are the convolution of fractal structures. The new formalism has been successfully applied in different areas of science including physics [30, 31], biology [32, 33], chemistry [34, 35], geophysics [36, 37], linguistics [38, 39], and primarily, quantitative finance [40, 41, 42, 43, 44, 45, 46, 47, 48, 49]. The multifractal nature of the rate of return signals indicates the presence of nonlinear, long-range dependencies, which are also manifested by the slow decay of the absolute returns autocorrelation function [23]. Interestingly, at the same time, these signals do not reveal significant linear autocorrelations [50]. The dependencies existing in financial time series become even more intriguing when multiple assets are considered; typically, the correlations between different financial instruments also exhibit a multiscale character. It has substantial practical implications as the correlation, and cross-correlation analysis constitutes the foundation of modern portfolio theory [51] that enable financial market practitioners to minimize the investment risk.

The complexity of the financial markets and the nontrivial character of returns are difficult to model using mathematical formulas. Therefore, in recent years, another approach, agent-based modeling (ABM), has gained popularity in the financial area. In this technique, instead of building complicated mathematical expressions that try to capture entire dynamic of the market, the considered system is divided into multiple, relatively small, and interacting elements (agents), which, by exchanging information, can generate signals characterised by nonlinear correlations. This approach has its roots in the von Neumann machine and cellular automata, and nowadays it is applied in multiple areas of science, including physics [52, 53, 54], biology [55, 56, 57], geology [58, 59, 60], sociology [61, 62, 63, 64, 65], and economics [66, 67, 68, 69]. Since financial markets consist of numerous and vastly different parts, the modeling of such a system where every element has a mathematical representation might be complicated and heavy in terms of required computational resources. In fact, crucial features of the financial markets, including stylized facts, can be relatively easily reproduced by agent-based models in the form of cellular automata. These models are often inspired by natural phenomena, such as phase transition in ferromagnetic materials and naturally make use of frameworks commonly applied in physics, such as the Ising Model. A notable example of a financial market model inspired by physical phenomena is the framework proposed by Iori [70] which is a variation of Random Field Ising Model adapted to stock market conditions. Another example is the model introduced by Bornholdt, in which the classical two-dimensional Ising Model is enriched with a minority game factor [71]. These two frameworks are well-recognized in the literature and have been studied in different contexts [69, 72, 73, 74, 75]; therefore, they constitute the foundation of the multiscale correlation analysis in Ising-inspired agent-based models presented in

this dissertation.

This work has two primary objectives. The first is the multifractal analysis of daily data from major stock exchanges (DJIA, DAX, NIKKEI, NASDAQ, and FTSE from 1950-2020[1]) and components quoted within DJIA (from 1962 to 2020), emphasizing the time evolution of the multifractal properties of different assets and a network-based analysis of their cross-dependencies. The second, more important objective is related to modeling of the financial time series properties mentioned above using agent-based models. Besides examining the frameworks mentioned above, the authorial, Ising-inspired **Multi-Asset Three-State Agent-Based Model** of the financial market is proposed and then comprehensively analysed in the context of the multiscale properties of signals it generates.

The dissertation contains nine chapters. Chapter Two introduces the fundamental quantities used in the financial time series analysis and includes an examination of the basic statistical properties of returns, such as fluctuations distribution and autocorrelation functions.

In Chapter Three, the analysis is extended to an examination of nonlinear dependencies, preceded by a comprehensive introduction to the fractal and multifractal formalism. The emphasis in this part of the thesis is on a multifractal rolling window analysis of the returns[2] as well as network analysis of the multiscale cross-correlations between assets.

Chapter Four introduces agent-based modeling. Using two fundamental models, namely, Schelling segregation model [77], and Boids model [78], it has been shown how emergent behaviour and phenomena having the appearance of a phase transition can be reproduced within this type of framework. In the next sections, the criticality of the agent-based models, in the form of cellular automata is discussed more formally, and simulation of such models using Monte Carlo methods is demonstrated. Subsequently, two Ising-inspired financial market frameworks, namely Iori's model and Bornholdt's model, are described and examined in the context of reproducing stylized facts observed in the financial time series.

Chapter Five contains a theoretical description and examination of the fundamental statistical and multifractal properties of the time series generated by the single-instrument variant of the authorial multi-asset three-state model of the financial market with default parameters.

Chapter Six is entirely devoted to analyzing the model's microscopic dynamics and the impact of its parameters on the multiscale characteristics of the generated signals. Moreover, it is shown which elements of the model stand behind the hierarchical organization of the signals it produces and how the richness of the generated structures can be controlled. Additionally, in this chapter, multifractal rolling window analysis is used to demonstrate, how the framework can recreate the dynamical changes of returns multiscale properties.

In Chapter Seven, the analysis of the model is extended to two asset scenarios. This part is focused on understanding how simulating multiple linked financial instruments influences the nonlinear properties of the time series generated by the

[1]DAX and NASDAQ datasets are limited to the range 1962-2020 and 1971-2020, respectively

[2]This part is an extended version of an analysis originally presented in the article [76], to which the author of this thesis contributed.

model. To improve clarity, the analysis has been divided into three parts; the first quantifies the impact of the global coupling between subsystems, the second focuses on the linkage between assets on the agent-agent level, whereas in third it was demonstrated how the combination of both types of interactions leads to nonlinear cross-correlations similar to those observed in the financial markets.

Chapter Eight discusses practical applications of the model. Here, the fully-fledged variant of the framework is presented and used for building two artificial indices. The first one, which consists of ten assets, demonstrates how the proposed solution can resemble stock market dynamics, including temporal correlation and decorrelation phases. The second, inspired by DJIA, consists of thirty linked assets. This section demonstrates how the model can reproduce a non-trivial multiscale cross-correlations structure, captured here using a complex network analysis. The last chapter contains a comprehensive summary and concludes this dissertation.

Chapter 2

Fundamental statistical properties of financial time series

The financial market is an example of a complex system, which analysis, in order to provide adequate and valuable insight, has to incorporate multiple factors and capture changes in market dynamics over time. One of the primary methods used in analyzing financial markets is examining the basic statistical properties of the rate of return time series. Such analysis facilitates observation of the market dynamics, and if extended to a multi-asset scenario, can help in understanding the relationship between financial instruments.

This chapter introduces the basic statistical methods commonly applied in the analysis of financial time series. Based on the major stock indices and DJIA components data, the characteristic features including fluctuations clustering, fat-tailed distributions of returns, and volatility correlations are presented. Examination of these properties provides a foundation for further discussion of the nonlinear dependencies existing in financial time series.

2.1 Probability distributions of returns

Financial assets, as any goods and services, are subject to the law of supply and demand [79]. The number of asset units available on the market and the demand for it brings changes in a financial instrument valuation, which is reflected in its price. This law applies to any kind of assets including stock shares, contracts, and currencies [23, 50]. Universal character and ubiquity make price a fundamental quantity used in financial analyses and modeling. However, direct examination of price, even using simplified models, could be complicated. The primary issue is that time series made up of prices in consecutive time steps are non-stationary. Moreover, from the investor perspective, more important than asset valuation is an asset's price change over time, which is usually expressed as a percentage value. Therefore, consideration of price differences, measured by logarithmic rates of return is more suitable:

$$R \equiv R(t, \Delta t) = \ln(P(t + \Delta t)) - \ln(P(t)), \tag{2.1}$$

where $t = 1, ..., N$ is the time instant, Δt indicates the analysed scale, and $P(t)$ corresponds to the asset's price at a given point of time. Rate of return, defined in such a way, is more convenient for statistical analysis than price, as the first moment of a returns signal for large scales is typically stable over time. Moreover, it facilitates capturing the percentage changes in the price asset over time, which, as mentioned above, is one of the main objectives of the financial market practitioners. Naturally, investors often compare different assets; thus, in practical applications, standardized returns (shortly called returns) are typically used:

$$r(t, \Delta t) = \frac{R(t, \Delta t) - u}{\nu}, \tag{2.2}$$

where ν is the standard deviation and u is an average of returns, both calculated for the entire analysed period. Despite having completely different prices and therefore unrelated absolute daily price changes, financial instruments typically have similar percentage returns, thus making comparison of different assets at the $r(t, \Delta t)$ level is an apparent choice. Furthermore, for large time intervals, returns are usually proportional to asset valuation. However, analysis of relative, standardized differences in the price nullifies this effect and allows comparison of a given asset in distinct periods of time. Due to the benefits mentioned above, further calculations in this study uses standardized logarithmic returns (shortly called returns). It is worth noting that this definition is not free of defects. In fact, for high-frequency data (e.g., tick-by-tick) and idiosyncratic financial instruments, returns are primarily independent of asset price. Such a situation commonly occurs on the foreign exchange and option markets [50].

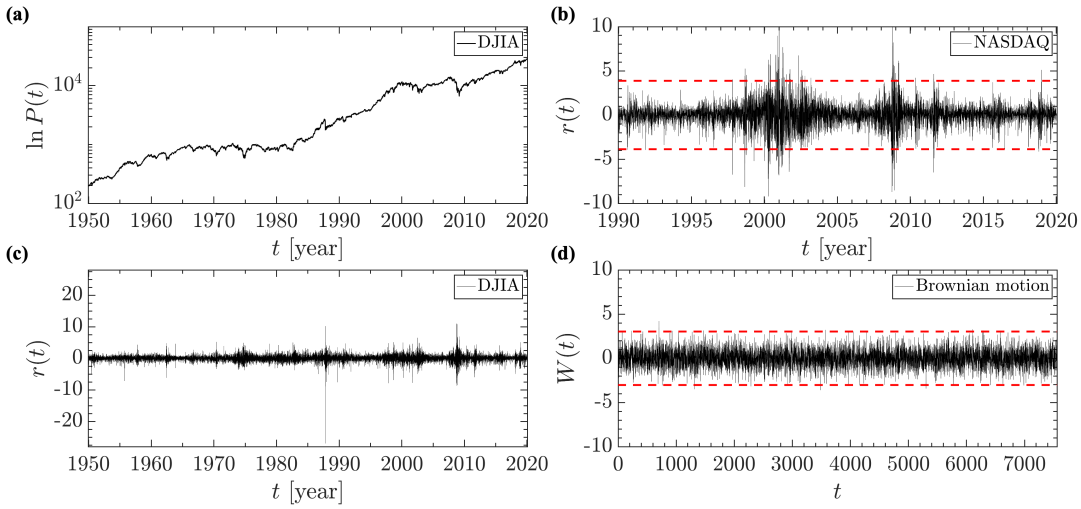

Figure 2.1: Logarithm of daily closing prices (panel **(a)**) and returns (panel **(c)**) of Dow Jones Industrial Average (DJIA) from 1950 to 2020. NASDAQ daily rates of return from 1990 to 2020 (panel **(b)**) and increments of Brownian motion (panel **(d)**). Red dotted lines in panels (b) and (d) denote $\pm 3\sigma$ range.

A vital part of the modern financial market analysis and modeling is related to risk management. The primary measure used for quantification of the risk associated with the investment in the particular asset is its *volatility*. By definition, it refers to the amount of uncertainty related to the size of changes in a security's value. A

higher volatility means that an asset's valuation can potentially be spread out over a more extensive range of values, and hence, its price can change dramatically over a short period, in either direction. On the other hand, lower volatility means that a financial instrument's value does not fluctuate significantly and tends to remain relatively steady over time. In general, volatility can be estimated using various parametric and nonparametric models. The former approach is based on an explicit functional formula, e.g., the stochastic volatility model [80]. Usually, parametric models are relatively easy to use; however, they have recently become increasingly restrictive, and so there has been a movement toward the use of more flexible and computationally simple nonparametric measures [81]. One of the most commonly used nonparametric methods of quantification of instrument price volatility is based on tracking the *absolute return* values. This approach is the basis of much of the modeling efforts presented in the literature, and in recent years has shown itself to be one of the most accurate measurements of the volatility [82], and thus, it is used in analyses presented in later sections of this dissertation.

Historically, returns, and consequently volatility time series, were modeled using Gaussian-distributed random variables. This idea became very popular in the 1950s, and it is one of the main ingredients of the famous Black-Scholes option pricing formula [21]. Indeed, if one considers each price change as a sum of many small and independent random contributions from various market factors, the Central Limit Theorem suggests the Gaussian as a natural candidate. In some financial problems, this model is still in use, mainly because of its simplicity, though it does not correspond to reality. Based on the empirical studies, it is well established that returns do not follow the Gaussian distribution [23, 50]. To see this phenomenon, it is sufficient to look at Figure 2.1 which shows returns of NASDAQ index from 1990 to 2019 (7560 data points) and increments of Brownian motion (panels (b) and (d), respectively). As is clearly visible, in the case of Gaussian-distributed variables, almost all observations are within a $\pm 3\sigma$ range (denoted by the red dotted lines), whereas for the returns signal, in periods of increased volatility (e.g., NASDAQ in years 1997-2003), this range is significantly and repeatedly exceeded. In general, distributions of returns are leptokurtic, and exhibit an elongated central part and *fat tails* (also called heavy tails), which scale according to the power law:

$$P(r > x) \sim x^{-\mu}, \tag{2.3}$$

where the μ exponent typically assumes values of 3 to 5; however, for immature markets and those having low liquidity, this can be around 2 and below (e.g., cryptocurrencies [83]). Scaling of this type can be observed not only in financial markets, but is also common in other areas of science, e.g., physics [84, 85], linguistics [86, 87], neuroscience [88], and many more [89]. Mathematically speaking, the power law relation may introduce extra calculation issues, as the variance is finite only for $\mu > 2$, which can, in turn, lead to major flaws in commonly accepted theories. For example, an infinite variance in the formalism of equilibrium statistical mechanics would lead to infinite temperature [90]. From a financial-analysis point of view, the power law dependency usually indicates the structural self-similarity of the considered signal and the existence of huge fluctuations, which are typically observed during financial crashes [6].

Figure 2.2 presents cumulative distribution functions of absolute returns calculated for major stock indices (panel (a)) and companies quoted within the DJIA index (panel (b)). For all analysed assets, fat tailed distributions are observed. The scaling exponent for indices, estimated using the least squares method, varies from $\mu = 3.33 \pm 0.20$ for the NASDAQ to $\mu = 3.84 \pm 0.24$ for the DAX, while for DJIA components, it fluctuates between $\mu = 2.64 \pm 0.10$ for GE and $\mu = 4.24 \pm 0.18$ for BA (see Appendix A for a full list of components).

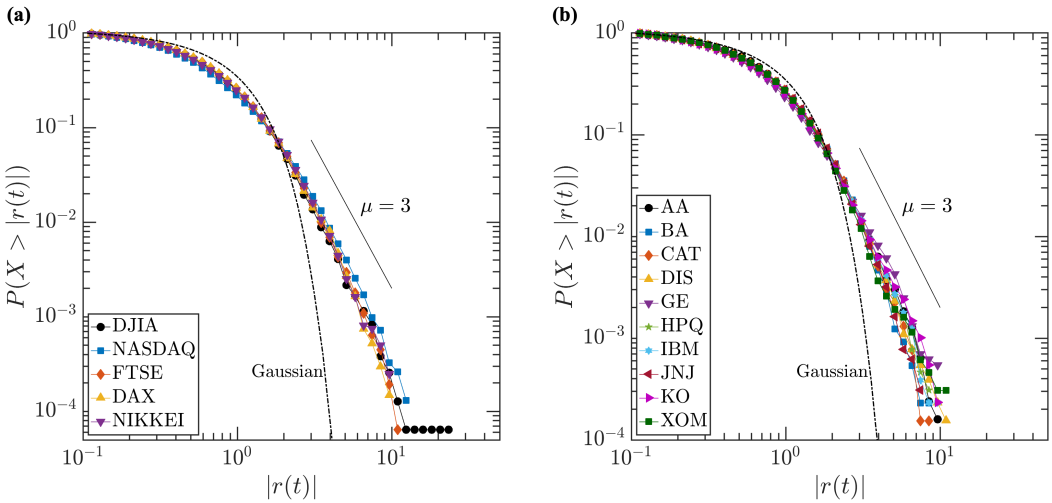

Figure 2.2: Cumulative distributions of daily absolute rates of return for major stock indices (panel **(a)**) and components of Dow Jones Industrial Average index (panel **(b)**).

Worth noting is that return distributions converge to the Gaussian as the time scale increases. However, this transition is slower than that observed for random signals, possibly indicating the presence of correlations in the examined series [91]. Indeed, as will be demonstrated in later sections of this study, financial time series are characterized by non-trivial self- and cross-dependencies, which underlie the fractal nature of the examined processes.

2.2 Autocorrelation and cross-correlation in financial data

Analysis of the stochastic processes governing asset price changes, in addition to distribution examination, requires quantification of correlations. In the case of financial time series, correlation analysis is critical as it constitutes a foundation of modern portfolio management strategies, and enables market participants to balance risk against performance [51].

The primary measure of the temporal self-dependencies found in time series is an autocorrelation function. It determines the influence of previous signal values (within a given time lag τ) on the current observation and can assume positive values (in range $(0, 1]$), if changes in the signal are in the same direction, or are negative (in range $[-1, 0)$), if changes in the signal are in opposite directions. For random data, it quickly converges to 0. Formally, the autocorrelation function of a

signal $X(t)$ with respect to the lag τ can be calculated as follows:

$$C_x(\tau) = \frac{\mathrm{E}[(X(t) - \overline{X})(X(t+\tau) - \overline{X})]}{\sigma^2}, \tag{2.4}$$

where σ^2 is the variance of the time series being analysed. As reported in numerous studies [23, 50] and shown in Figure 2.3, the rates of return time series are not characterised by linear correlations. In the case of daily returns of selected indices and stocks (panel (a)), the autocorrelation function drops to zero for τ greater than one and does not exceed the noise level indicated by the red dotted lines. The situation is slightly different in the case of one-minute data. As presented on the panel (b) of Figure 2.3, for returns of selected stocks, for a small lag ($\tau = 1$) a weak, negative, autocorrelation appears. Usually, this effect is related to the occurrence of zero values in the time series being examined; therefore, it is assumed to be a computational artifact. However, in the case of the analysed assets, similar results were obtained, even when zeros were removed from the signal, indicating that, on the short time scales, positive and negative returns are more likely to be interlaced than is typically observed on larger time scales. This phenomenon can be linked with a relatively low supply and demand inequilibrium combined with the continuous flow of orders placed by market makers. On the small time scales, when the buy and sell orders are almost balanced, the clear trend manifested by a consecutive chain of positive or negative returns cannot develop. In fact, price is more likely to fluctuate up and down rather than move firmly in either direction. Even though for high-frequency data and small lags τ weak negative correlations were observed, over a long range, returns are not linearly correlated regardless of the time scale being considered.

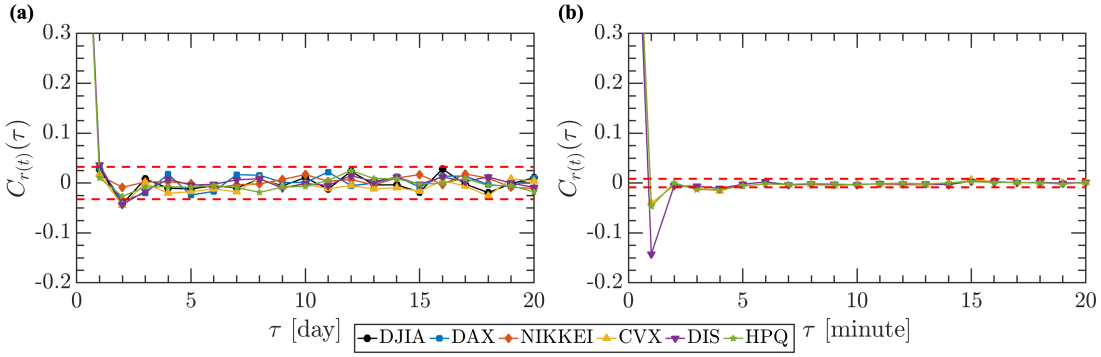

Figure 2.3: Autocorrelation functions of daily (panel (a)) and one-minute (panel (b)) returns of the selected indices and stocks. Red dotted lines indicate noise level.

Based on the returns' autocorrelation function, one might conclude that the process governing price fluctuations has no memory. However, the lack of linear correlation does not imply independent returns since higher order correlations may exist. It is sufficient to look at panels (b) and (d) of Figure 2.1, which present the daily NASDAQ returns from 1990 to 2019 (panel (b)) and increments of Brownian motion (panel (d)) to notice that financial fluctuations size changes over time. For example, returns in years 2000-2003 are significantly larger than in years 1993-1997, and, hence volatility in these periods differs. Such grouping of volatility is called

volatility clustering, and it is observed in many financial instruments. In comparison, increments of Brownian motion, an example of a homoscedastic process, have the same volatility across the entire dataset. In fact, the volatility signal has temporal correlations. Therefore, if at a given point of time t, rate of return assumes a large value, it is highly probable that it will have a large value in the next time step $t + 1$ as well (analogously for small fluctuations). Figure 2.4 presents the volatility autocorrelation function of the selected indices and stocks calculated for daily (section (a)) and one-minute (section (b)) absolute returns. In both time scales, the autocorrelation function declines slowly and maintains a statistically significant level for approximately 10^3 time steps for daily volatility and more than 10^5 time steps for one-minute data. Additionally, the autocorrelation function for high-frequency data in lag range $\tau \in [3 * 10^2, 3 * 10^3]$ fluctuates substantially. These oscillations are related to the daily trading cycles observed in the financial markets. The number of orders placed by investors is not constant over time and regular periods of increased activity in the market, and, thus increased volatility can be identified. Usually, the market is more volatile during session opening, when pre-market orders are executed, and in the last hour before market closure, as intraday traders close their positions.

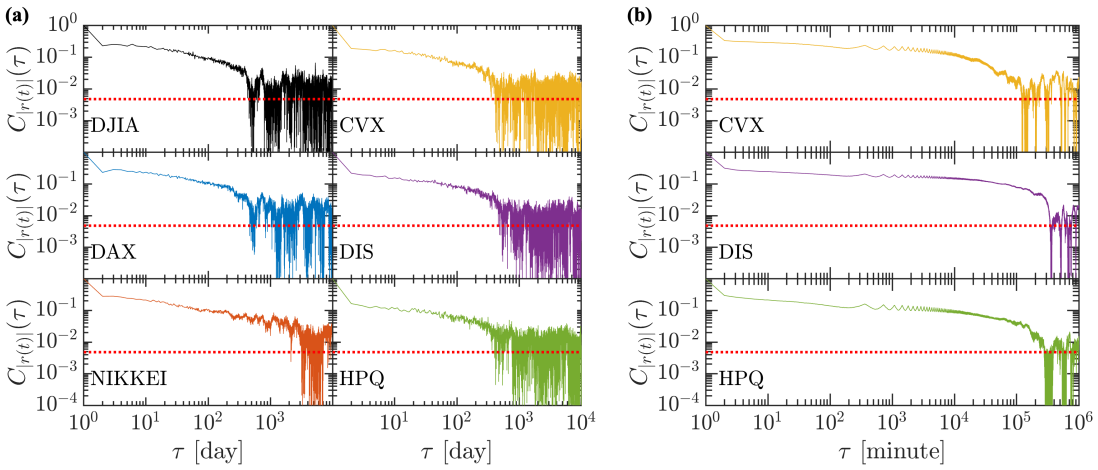

Figure 2.4: The autocorrelation function of the daily (section **(a)**) and one-minute (section **(b)**) absolute returns of the selected indices and stocks. Red dotted lines indicate the noise level.

Naturally, examination of financial data correlations can be extended to analysis of multiple assets. The basic technique used for a quantitative description of the interrelation between financial instruments is based on a cross-correlation function, which measures the degree to which the series follow one another when shifted by lag τ. Formally, when two time series $X(t)$ and $Y(t)$ are considered, the cross-correlation function can be calculated as follows:

$$C_{xy}(\tau) = \frac{\mathrm{E}[(X(t) - \overline{X})(Y(t+\tau) - \overline{Y})]}{\sigma_x \sigma_y}, \tag{2.5}$$

where σ_X and σ_Y are the standard deviations of the respective series and $\overline{X}$ and $\overline{Y}$ are the averages calculated for the entire signals. For $C_{xy}(\tau = 0)$, this formula comes down to the Pearson correlation coefficient, and its interpretation is analogous.

The coefficient assumes values from $-1 < C_{xy} < 1$ where $C_{xy} = 1$ means perfect correlation, $C_{xy} = -1$ indicates ideal anti-correlation, and $C_{xy} = 0$ corresponds to independent signals.

Figure 2.5 shows $C_{xy}(\tau)$ functions calculated for daily (panel (a)) and one-minute (panel (b)) volatility of selected pairs of assets. In the case of DJIA and NASDAQ daily data, the interdependencies have a long-range character and maintain the statistically significant level for more than 10^3 time steps, while the cross-correlations between DJIA and NIKKEI are substantially weaker and fluctuate around noise level (denoted by the red dotted line). This discrepancy is naturally related to the fact that DJIA and NASDAQ are indices quoted on the US market and multiple NASDAQ components are also present in the DJIA index, while DJIA and NIKKEI are technically separate assets.

Slight differences in volatility interdependencies are also visible on the level of the individual components. Here, three pairs of companies representing information technology (HPQ, IBM), consumer goods (DIS), and industrial (GE) sectors are considered on the daily (panel (a)) and one-minute (panel (b)) time scales. Naturally, regardless of the frequency of the data, the correlations between components from the same sector (HPQ-IBM, yellow line) are stronger than those observed for companies belonging to different baskets, e.g., HPQ-DIS (orange line) and HPQ-GE (purple line).

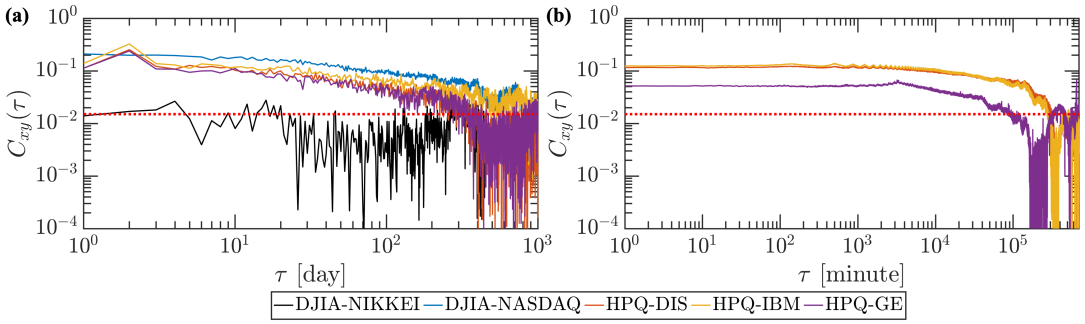

Figure 2.5: Volatility cross-correlations of selected market indices and stocks calculated for daily (panel **(a)**) and one-minute data (panel **(b)**). The red dotted lines denote the noise level.

Analysis of autocorrelation and cross-correlation functions of returns and volatility provides valuable insight into financial market dynamics and can help market practitioners build optimal portfolios. However, these methods do not differentiate fluctuations with respect to their size. In order to investigate the dependencies of the financial time series in a multiscale manner, considering the magnitude of the fluctuations, a multifractal analysis is usually employed. Related formalism and techniques are discussed in the next chapter.

Chapter 3

Multifractal concept and its application to financial time series

Temporal self- and cross-dependencies of the financial time series have a multiscale character, which cannot be precisely described using basic statistical methods such as a linear autocorrelation function, a power spectrum, or a Pearson cross-correlation coefficient. To analyse the signals characterized by long-range, non-linear dependencies, the multifractal methods are typically used.

In this chapter, the necessary fractal formalism as well as two analysis methods, MFDFA (Multifractal Detrended Fluctuation Analysis) and MFCCA (Multifractal Cross-Correlation Analysis), are introduced and then applied to investigate the hierarchical organization of the selected indices and DJIA components. Extra emphasis is placed on the time evolution of the returns' multifractal properties, captured using rolling window analysis. Moreover, the structure of the multiscale cross-correlations is investigated on the basis of the complex network formalism. This comprehensive multiscale analysis aims at quantifying financial time series non-linear dependencies at different levels, and the results obtained are used to examine the agent-based models, discussed in the later chapters of this dissertation.

3.1 Fractal and Multifractal formalism

The world around us is irregular and filled with roughness; therefore, an attempt to characterize the shape of real objects within a Euclidean geometry formalism can be laborious and sometimes even impossible. The mathematical approach to such structures changed in 1970s, when Mandelbrot developed the foundation of so-called *fractal geometry* [92]. The word fractal itself is derived from the Latin *fractus* and means fractional or broken. The term is applied to the irregular objects that exhibit self-similarity. In this context, self-similarity means that the part of the structure is similar to the entire object, regardless of the scale being considered. Fractal geometry allows the investigation of the complex, apparently chaotic structures from which an ordered and hierarchical picture can emerge. Such objects can be created relatively easily using recurrent, or iterative procedure. Examples are the Sierpinski triangle [93], which is created by an iterative division of an equilateral triangle into four pieces and removal of the center part, or Koch curve [94] which also results

from an altering an equilateral triangle (Figure 3.1, panels on the left-hand side).

Interestingly, fractal features are present not only in abstract mathematical constructs. The shapes of a leaf, snowflake, shoreline, or cardiovascular system are examples of natural objects which exhibits self-similarity, however only in a statistical sense (Figure 3.1, panels on the right-hand side). Such structures, usually called *stochastic fractals* [95], may differ in details depending on the scale being considered, but, in terms of general statistical properties, are nonetheless the same.

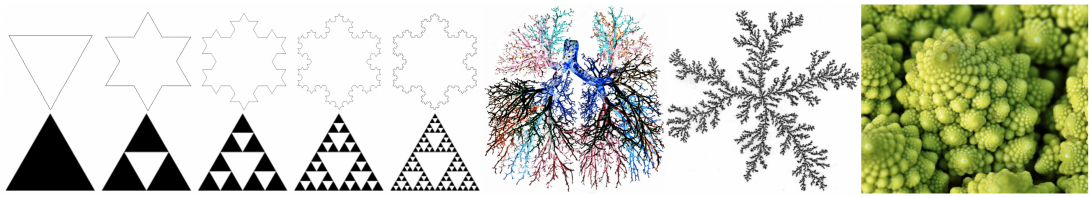

Figure 3.1: Examples of fractal structures. On the left-hand side: a mathematical fractals development procedure diagram (Koch curve on the top and Sierpinski triangle at the bottom). On the right-hand side, three examples of natural fractals: pulmonary vessels, a Diffusion Limited Aggregation process, and detailed photography of a broccoli.

Importantly, the financial time series also have a fractal nature. Basic, visual analysis of the price trajectory presented in Figure 3.2, shows that respective parts of such time series are similar to the entire structure. Moreover, if multiple financial time series on different scales are considered, distinguishing which series has a particular time scale is difficult, meaning that financial time series exhibit not only spatial self-similarity but also self-similarity within the time dimension.

Despite the frequent occurrence of the fractal structures in nature and mathematics, a single definition that facilitates the classification of a particular object as a fractals does not exist. However, based on the work done by Mandelbrot [92], which Falconer extended [96], the set of features characteristic of fractal objects was established:

- Fractals are self-similar (at least in statistical sense)
- Fractals have a structure that can be investigated in detail on arbitrarily small scale
- Fractals are so irregular that they cannot be described with a Euclidean geometry formalism
- Fractals can have non-integer dimension, usually ones greater that their topological dimension

The properties presented above are not specific; however, in practice, they allow unambiguous determination of whether the analysed object is a fractal or not.

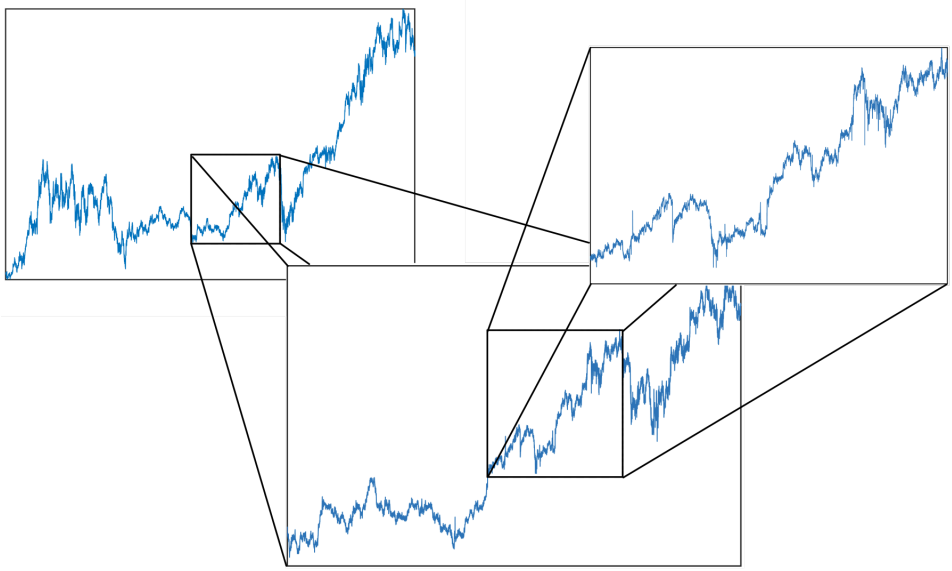

Figure 3.2: Self-similarity of the IBM price trajectory.

3.1.1 Self-similarity, self-affinity, and fractal dimensions

Fractals are inextricably linked with the concept of self-similarity, which, as mentioned previously, can be interpreted in a strict sense (mathematical fractals) or be limited to the statistical sense (stochastic fractals). Self-similarity is characterised by isotropy. It means that the translation, rotation, reflection, and scaling operations, that constitute the similarity transformation are identical in all directions. However, many natural fractals cannot be reproduced by isotropic transformation; therefore, the generalized concept of self-affinity and a corresponding affine transformation are typically employed. In contrast to a similarity transformation, an affine operation can depend on the direction and so is anisotropic in nature. Formally, an affine transformation can be defined as follows:

$$S(x) = T(x) + b, \tag{3.1}$$

where T is a linear transformation, usually represented by an $n \times n$ matrix, and b is vector in $\mathbb{R}^n$. Moreover, transformation S: $\mathbb{R}^n \to \mathbb{R}^n$ for $x, y \in \mathbb{R}^n$ defined as follows: $|S(x)-S(y)| \leq c|x-y|$ is contraction mapping if $c \in (0, 1)$. If foregoing weak inequality is reduced to an equation, then S describes the similarity. Worth noting is that self-similarity (self-affinity) does not imply the fractal nature of the analysed object. For instance, although a square or a line can be divided into fragments by using a similarity (affinity) transformation, they are not fractals.

Apart from their irregular shape, roughness, and self-similarity, fractals have another interesting feature. For example, let consider the mass of the Sierpinski triangle. It can be calculated according to the formula $M = \left(\frac{3}{4}\right)^n$, where n is a number of performed divisions of the triangle. As can be easily seen, the object's mass decreases with every alternation of the original structure and, hence it can be infinitely small after large number of iterations. Moreover, when the object's side length is doubled, then the mass increases three times. Formally, mass can be

expressed as a function of triangle side length:

$$M(L) \sim L^{d_f}, \tag{3.2}$$

where exponent $d_f = \frac{\log 3}{\log 2} \approx 1.585$[1]. The relation above is a form of the power law, typical for the fractal objects. The same kind of dependency can be observed not only in mathematically created structures but also in stochastic fractals existing in nature, including financial time series. Assuming that $f(x)$ represents the self-affine signal, it satisfies the following relationship [97]:

$$f(x) \cong \lambda^{-H} f(\lambda x) \tag{3.3}$$

where $\lambda > 0$ and H is the Hurst exponent which describes the level of long-range dependencies present in the signal. It indicates, whether the signal being considered is random ($H = 0.5$), persistent ($0.5 < H \leq 1$) or anti-persistent $0 \leq H < 0.5$ in a linear sense.

The scale-free character of fractal structures manifested by the power law relationship constitutes the foundation of the quantitative description of this type of objects. Scaling and self-affinity is usually quantified by so-called *fractal dimension*. For ordinary Euclidean spaces, the topological dimension (Lebesgue covering dimension) can be defined as the number of the coordinates required to unambiguously specify the location of the point within a given object (i.e 0 for point, 1 for line, 2 for surface etc.). In the case of fractal structures, the dimension can be calculated employing a few different procedures, and importantly, can assume fractional values.

The fundamental fractal dimension is the self-similarity dimension d_s, which describes the number of parts N into which an object can be divided using the given scale s:

$$d_s = \frac{\log N}{\log 1/s}. \tag{3.4}$$

For basic geometric objects such as a line, a square, or a cube, the self-similarity dimension has an integer value that equals the topological dimension. Nonetheless, for a fractal structure, such as Sierpinski triangle, the self-similarity dimension is fractional and, naturally differs from topological dimension. Practically, obtained result means that the Sierpinski triangle is a structure between a line and a surface. The self-similarity dimension is useful in the investigation of the fractal structures; however, it can be applied only to objects that exhibit strict self-similarity.

Felix Hausdorff [98, 99] proposed a more general approach that can be employed in studying the natural fractals. In order to discuss it, firstly the Hausdorff measure must be introduced. Let U be a non-empty set in $\mathbb{R}^n$, with diameter $U = \sup |x - y| < \epsilon : x, y \in U$. Moreover, let U_i be a countable set, which covers the set F and has diameter less than ϵ. If $F \subset \bigcup_{i=1}^{\infty} U_i$, scale $s > 0$ and $F \in \mathbb{R}^n$, then $\mathcal{H}^s_\epsilon = \inf \{ \bigcup_{i=1}^{\infty} |U_i|^s : \{U_i\} \}$ is ϵ-cover of the set F. Practically, this means that set F is covered with subsets U_i having a diameter ϵ, and the one with the smallest sum

[1] An increase in Sierpinski triangle side length causes mass to increase three times and thus, $2^{d_f} = 3 \rightarrow d_f = \frac{\log 3}{\log 2} \approx 1.585$

of s-degree exponents is selected. As diameter $\epsilon \to 0$ the more detailed view on the set is obtained. In most cases, the Hausdorff measure is equal to 0 or ∞. However the critical value s for which the $\mathcal{H}^s$ assumes value in between exists, and it is called *Hausdorff dimension* d_H:

$$\mathcal{H}^s_\epsilon(F) = \begin{cases} \infty & \text{for } s < d_H \\ 0 & \text{for } s > d_H \end{cases}. \tag{3.5}$$

Due to the complex calculations involved, the Hausdorff dimension is difficult to apply in practice, and so, alternatively, the *box-counting dimension* is commonly used. Assuming that F is a set in $\mathbb{R}^n$ and $N_\epsilon(F)$ is a smallest number of sets with diameter ϵ covering the set F, the box-counting dimension is defined as follows:

$$d_b = \lim_{\epsilon \to 0} \frac{\log N_\epsilon(F)}{-\log \epsilon}. \tag{3.6}$$

The huge advantage of this procedure is its simplicity; however, in practical application, the box-counting dimension is burdened with greater error than the one proposed by Hausdorff [100]. Nevertheless, it can be successfully employed in some problems, especially when a large dataset is available. Worth noting is that fractal dimensions calculated using different procedures can vary, although, in most cases, the Hausdorff dimension equals box-counting dimension. In general, the relationship between dimensions being considered assumes the form:

$$d_T \leq d_H \leq d_b. \tag{3.7}$$

3.1.2 Singularity spectrum

Examination of the fractal dimension does not always provide complete information about the object being investigated and the nature of the processes governing its development. In many instances, analysed structures are a convolution of multiple fractals, each having a different fractal dimension. Mathematically speaking, the fractal measure is not uniform, and multiple distributions of this measure for a given topological support are possible. Hence, determining the fractal dimension of the entire object provides averaged information. In order to describe such a structure precisely, studying its local properties is necessary. Consequently, specific changes in the formalism are required.

Assuming that, in the vicinity of point x_0, in scale ϵ, local scaling fulfills the relation which can be expressed by measure μ:

$$\mu(B_{x_0}(\epsilon)) \sim \epsilon^{\alpha(x_0)}, \tag{3.8}$$

where $B_{x_0}(\epsilon)$ is a sphere with radius ϵ centered at x_0. The $\mu(B_{x_0}(\epsilon))$ can be interpreted as a distribution of the measure in the vicinity of point x_0. Then, the so-called *singularity exponent* α can be calculated using the following formula [98, 97]:

$$\alpha(x_0) = \lim_{\epsilon \to 0} \frac{\log \mu\left(B_{x_0}(\epsilon)\right)}{\log \epsilon}. \tag{3.9}$$

The greater the value of singularity exponent, the more uniform the measure is in the vicinity of x_0 and the weaker is singularity. Usually, to quantitively describe the distribution of α for given structure, the *singularity spectrum* $f(\alpha)$ is calculated:

$$f(\alpha) = d_H\{x_0 \in \text{supp } \mu : \alpha(x_0) = \alpha\}. \tag{3.10}$$

The function obtained is interpreted as a Hausdorff dimension of the support for which the singularity assumes particular value $\alpha(x) = \alpha$. The singularity spectrum facilitates distinguishing between homogenous (monofractal) measures, where the singularity spectrum assumes a pointwise form, and heterogenous (multifractal) measures, where the $f(\alpha)$ function assumes a shape similar to an inverted parabola spread between α_{min} and α_{max}, which reflects strongest and weakest singularities, respectively (see Figure 3.3). Practically, to describe local properties of the object, the structure is decomposed by the value of the measure, using the partition function [101], as is done here:

$$Z(q, \epsilon) = \sum_{i=1}^{N} \mu_i^q(\epsilon), \tag{3.11}$$

where N is the number of bins in the histogram of singularity spectrum of α for $\epsilon \to 0$ and $q \in \mathbb{R}$. The relation between singularity exponent α and measure μ shown in equation (3.8) implies that the distribution of α for a given ϵ has the form $\varrho(\alpha)\epsilon^{-f(\alpha)}$, which, combined with equation (3.11), yields the following:

$$Z(q, \epsilon) \simeq \int \varrho(\alpha)\epsilon^{q\alpha - f(\alpha)} \mathrm{d}\alpha, \tag{3.12}$$

where partition function $Z(q, \epsilon)$, assuming $\epsilon \to 0$, fulfils the power law dependence:

$$Z(q, \epsilon) \sim \epsilon^{\tau(q)}, \tag{3.13}$$

and $\tau(q)$ is a scaling function typically called *generalized scaling exponent*. The primary input to the integral above is the α for which the expression $q\alpha - f(\alpha)$ assumes its lowest value. Thus:

$$\tau(q) = \min_{\alpha}(q\alpha - f(\alpha)). \tag{3.14}$$

From the equation above, the inverted Legendre transformation can be employed to obtain singularity spectrum $f(\alpha)$:

$$f(\alpha) = \min_{q}(q\alpha - \tau(q)). \tag{3.15}$$

In general, the relation between generalized scaling exponents $\tau(q)$ and singularity spectrum $f(\alpha)$ can be expressed by the following system of equations:

$$\begin{cases} q = \mathrm{d}q/\mathrm{d}\alpha \\ \tau(q) = q\alpha - f(\alpha) \end{cases} \qquad \begin{cases} \alpha = \mathrm{d}\tau/\mathrm{d}q \\ f(\alpha) = q\alpha - \tau(q). \end{cases} \tag{3.16}$$

It has to be emphasized that the foregoing transformation does not affect the information included in $\tau(q)$. Moreover, from partition function $Z(q, \epsilon)$ one can obtain *generalized fractal dimension*:

$$d_q = \frac{-1}{q-1} \lim_{\epsilon \to 0} \frac{\log Z(q, \epsilon)}{\log \epsilon}, \tag{3.17}$$

that can be also expressed as follows:

$$d_q = \frac{\tau(q)}{q-1} \quad \text{or} \quad d_q = \frac{1}{q-1}(q\alpha - f(\alpha)). \tag{3.18}$$

The dimension specified in this way has few characteristic values. Namely, for $q = 0$ the singularity spectrum $f(\alpha)$ has a maximum value, and $d_{q=0}$ is a topological support of measure μ. Moreover, for $q = 1$ and normalized measure $Z(1, \epsilon) = \sum \mu(\epsilon) = 1$ (thus $\tau(0) = \min_\alpha(\alpha - f(\alpha)) \to f(\alpha(q = 1)) = \alpha(q = 1)$) the corresponding value d_1 is an information dimension, which indicates change in amount of information needed for describing the point in a set, as scale ϵ changes [98]. Finally, values for $q \geq 2$ refer to the correlation dimension having degree q, which measures the probability that two randomly chosen points from the object are away from each other by a certain distance [102]. The exemplary singularity spectrum with characteristic values is presented in the figure below.

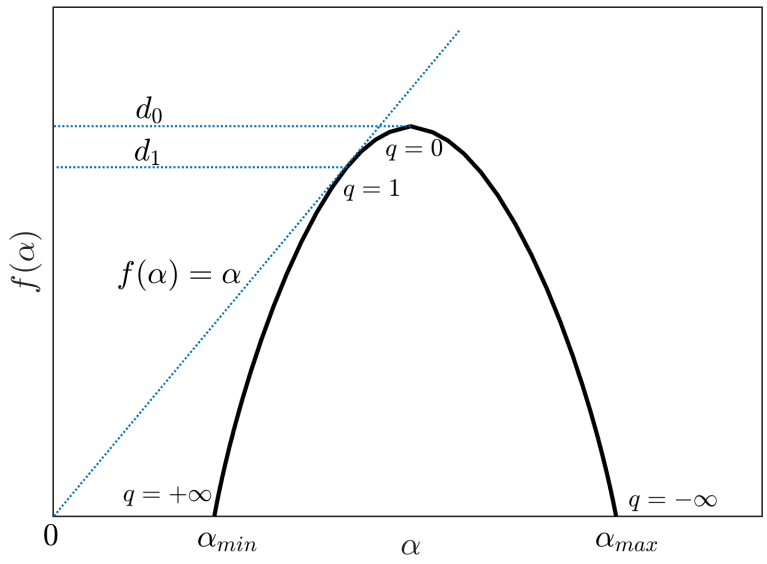

Figure 3.3: Schema of singularity spectrum $f(\alpha)$.

Furthermore, the multifractal formalism presented in this chapter can be directly linked with the concepts employed in thermodynamics [95]. As shown in study [95], the partition function $Z(q, \epsilon)$ is formally analogous to the partition function $Z(\beta)$ in thermodynamics, and thus $f(\alpha)$ can be interpreted as the entropy of the system.

3.1.3 Multiscale analysis methods

Quantification of the non-linear correlations and memory present in time series typically reduces to an examination of its multifractal properties. Currently, there are two commonly accepted and complementary methods that facilitate description of the time series multifractality, even in case of non-stationary signals. The first, the Wavelet Transform Modulus Maxima (WTMM) [97], makes use of the wavelet expansion of the series under consideration. The basis of the second method, Multifractal Detrended Fluctuation Analysis (MFDFA) is investigation of the scaling properties of different moments of the detrended signal [103, 104]. Both algorithms are relatively simple to implement, and therefore, are regularly used in different branches of the science, including physics [105, 106], biology [107, 108], chemistry [34], natural language analysis [38, 39], and economics [40, 41, 47, 109, 110]. However, the latter method often appears to be more accurate, numerically stable [111], and can be extended to the cross-dependence analysis of the time series [112]; therefore it will be used in the later sections of this dissertation.

Multifractal Detrended Fluctuation Analysis method (MFDFA)

Multifractal Detrended Fluctuation Analysis method is a generalization of the commonly used DFA method [113], which allows identification of correlations in the non-stationary signals. The algorithm consists of a few steps, and yields a singularity spectrum or generalized Hurst exponents. Assuming that x_i is a one-dimensional time series of length N where $i = 1, ..., N$, the MFDFA procedure consists of the following steps:

1. The profile function $Y(j)$ is calculated according to the formula:

$$Y(j) = \sum_{i=1}^{j} [x_i - \overline{x}], \tag{3.19}$$

   where $\overline{x}$ is a mean value of the entire signal.

2. The time series is divided into $M_s = \lfloor \frac{N}{s} \rfloor$ segments, each having length s. In order to avoid exclusion of the elements at either end of the signal, the procedure is repeated twice - once from the beginning in the natural order and again from the end in reversed order. In result, one obtain the $2M_s$ segments ν.

3. For each interval ν, the trend, represented by polynomial function $P_\nu^{(m)}$ of degree m, is subtracted from the profile signal $Y(j)$. The variance of each of segment is then determined as follows:

$$F_x^2(\nu, s) = \frac{1}{s} \sum_{i=1}^{s} [Y((\nu - 1)s + i) - P_\nu^{(m)}]^2. \tag{3.20}$$

   The detrending character is determined by the degree of the polynomial function. In financial applications, typically, the quadratic function is used ($m = 2$) [114].

4. Next, the average of the variance of each segment ν, called the *fluctuations function*, is calculated:

$$F_x(q,s) = \left\{ \frac{1}{2M_s} \sum_{\nu=1}^{2M_s} [F_x^2(\nu,s)]^{q/2} \right\}^{1/q}, \quad q \in \mathbb{R}\backslash\{0\} \tag{3.21}$$

where exponent q allows examination of the signal with respect to the size of its fluctuations. For positive q, the main input to $F_x(q,s)$ comes from the large values of the original signal, whereas for negative ones it comes from the small fluctuations.

If the calculated fluctuations function $F_x(q,s)$ follows power law relationship:

$$F_x(q,s) \sim s^{h(q)}, \tag{3.22}$$

then the signal being analysed has the fractal properties described by the generalized Hurst exponent $h(q)$. For monofractal structures $h(q)$ is constant and equal to the Hurst exponent $h(q) \equiv H$, whereas, for multifractal time series, $h(q)$ depends on scaling parameter q. Since returns and volatility distributions are leptokurtic the moments for exponents $q > 4$ are divergent [41]; thus the range of considered values is usually limited to $q \in [-4, 4]$.

Based on the calculated exponents $h(q)$, using transformation $\tau(q) = qh(q) - 1$ and equation (3.15) the multifractal spectrum can be determined. Figure 3.4 shows singularity spectra (panel (a)) and corresponding fluctuation functions calculated for Brownian motion (panel (c)), which is an example of the random process, and a log-normal cascade (panel (b)) which is a multifractal structure[2]. For non-autocorrelated time series, the singularity spectrum is narrow and reaches its maximum at $\alpha \approx 0.5$. Theoretically, it should scale down to a single point; however, due to the limited size of the data, a blur is observed. On the other hand, for non-linearly correlated signals, the multifractal spectrum has the shape of a wide, inverted parabola. The width of the $f(\alpha)$ function is measured as follows:

$$\Delta\alpha = \alpha(q_{min}) - \alpha(q_{max}). \tag{3.23}$$

This function quantifies the diversity of individual fractal structures that constitute analysed time series. The greater is $\Delta\alpha$, the reacher is the dynamics of the process governing the considered series and the stronger are non-linear correlations between the individual elements making up the signal. Naturally, spectrum width is used to distinguish between monofractal and multifractal signals. In this dissertation, the series is considered as a multifractal, if $\Delta\alpha \geq 0.1$.

The difference between multifractal and monofractal time series is also visible on the level of the fluctuations functions. As shown on the panel (c) of Figure 3.4, for random processes, the $F_x(q,s)$ function for different q are parallel to each other, which corresponds to the constant value of $h(q)$. In contrast, for the non-linearly correlated signal (panel (b) of Figure 3.4), the slope of the fluctuation function depends on the value of exponent q and $h(q)$ is a decreasing function of q.

[2]Detailed description of log-normal cascade can be found in study [115]

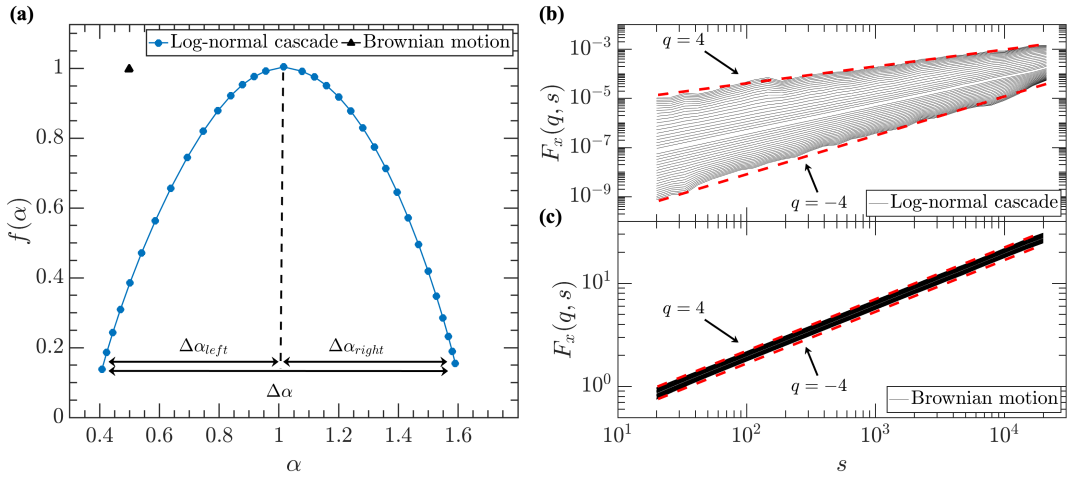

Figure 3.4: Singularity spectra $f(\alpha)$ (panel **(a)**) and corresponding fluctuations functions $F_x(q,s)$ determined for examples of multifractal (Log-normal cascade - panel **(b)**) and monofractal (Brownian motion - panel **(c)**) signals.

The example of a multifractal signal being considered has a symmetrical singularity spectrum, where the width of the left part is almost identical to that of the right. However, many series observed in nature, including financial data, are characterised by asymmetric singularity spectrum [105]. In order to quantify this feature, the asymmetry coefficient A_α is typically used:

$$A_\alpha = \frac{\Delta\alpha_{left} - \Delta\alpha_{right}}{\Delta\alpha_{left} + \Delta\alpha_{right}}, \tag{3.24}$$

where $\Delta\alpha_{left} = \alpha_0 - \alpha_{min}$ and $\Delta\alpha_{right} = \alpha_{max} - \alpha_0$. As reported in a study [105], multifractal spectra of financial time series usually exhibits left-sided asymmetry of the spectrum, suggesting that the correlations in large fluctuations are significantly stronger than those observed in small changes in a signal's value.

Multifractal Cross-Correlations Analysis method (MFCCA)

Analysis of non-linear correlations of time series is not only limited to investigation of internal dependencies but is often extended to an examination of the relationship between separate signals. The Multifractal Cross Correlations Analysis method is a consistent extension of the Detrended Cross-Correlation Analysis (DCCA) [116], which is able to detect multifractal cross-correlations between signals [112]. Assuming that x_i and y_i are time series of length N where $i = 1, ..., N$, then MFCCA is a procedure consisting of the following steps:

1. The profile functions are calculated for signals being analysed according to the following formulas:

$$X(j) = \sum_{i=1}^{j} [x_i - \overline{x}], \quad Y(j) = \sum_{i=1}^{j} [y_i - \overline{y}], \tag{3.25}$$

where $\overline{x}$ and $\overline{y}$ are the average values of the respective time series.

2. Each time series is divided into $M_s = \lfloor \frac{N}{s} \rfloor$ segments ν of length s. In order to avoid exclusion of values at either end of the series, the procedure is repeated twice - once from the beginning in the natural order then again from the end in reversed order. For each series, $2M_s$ segments ν are thus obtained.

3. For each interval ν of the respective profiles $X(j)$ and $Y(j)$ the polynomial trend of degree m is calculated: $P^{(m)}_{X,\nu}$, $P^{(m)}_{Y,\nu}$. Similarly to the MFDFA method discussed in a previous section, the degree of polynomial typically used in financial application has $m = 2$.

4. In the next step, the trend in each segment is subtracted from the examined series and the detrended cross-covariance is then calculated according to the following formula:

$$F^2_{xy}(\nu, s) = \frac{1}{s} \sum_{k=1}^{s} \left\{ (X((\nu-1)s+k) - P^{(m)}_{X,\nu}(k))(Y((\nu-1)s+k) - P^{(m)}_{Y,\nu}(k)) \right\}. \tag{3.26}$$

5. Then, a fluctuations function of degree q is calculated and averaged over all intervals ν as follows:

$$F^q_{xy}(s) = \frac{1}{2M_s} \sum_{\nu=1}^{2M_s} \text{sign}(F^2_{xy}(\nu, s)) |F^2_{xy}(\nu, s)|^{q/2}, \tag{3.27}$$

where $\text{sign}(F^2_{xy}(\nu, s))$ determines the sign of the function $F^2_{xy}(\nu, s)$ and $q \in \mathbb{R}\backslash\{0\}$ is an exponent that decomposes the time series with respect to the fluctuation size. Since distributions of the financial time series are typically leptokurtic, moments for exponents $q > 4$ are divergent, and thus the range of q is limited to $-4 \leq q \leq 4$. For a positive q, the primary input to the $F^q_{xy}(s)$ comes from large fluctuations, whereas, for negative values of q the small changes in the time series are amplified and thus, are the predominant component of the fluctuations function. For $q = 0$, the following formula is used:

$$F^0_{xy} = \frac{1}{2M_s} \sum_{\nu=1}^{2M_s} \text{sign}(F^2_{xy}(\nu, s)) \ln |F^2_{xy}(\nu, s)|. \tag{3.28}$$

The procedure presented above, using the sign function preserves the original direction of signal changes, and prevents numerical errors related to exponentiate negative values. It also prevents the occurrence of the complex values in the fluctuations function, which may appear when other methods, such as MFDXA [45] or MFHXA [117], are used. As in the MFDFA method, MFCCA calculates fluctuations function for different scales s, and, thus if the cross-correlations between signals have a fractal nature, the fluctuation function scale itself according to the power law:

$$F^q_{xy}(s)^{1/q} = F_{xy}(q, s) \sim s^{\lambda_q} \tag{3.29}$$

or $\exp\big(F^0_{x,y}\big) = F_{x,y}(0, s) \sim s^{\lambda_0}$ for $q = 0$, where λ_q is the corresponding scaling exponent, whose range of dependence on q quantifies the degree of complexity in the signal. The multifractal character of the relationship between analysed signals is

manifested by the existence of multiple λ_q values which change along with considered q parameter, while for monofractal relationship λ_q is constant and independent of q. Based on the examination of the cross-covariance function $F^q_{xy}(s)$ obtained through use of MFCCA method, the cross-correlation coefficient ρ^q can be calculated as follows:

$$\rho^q(s) = \frac{F^q_{xy}(s)}{F^{q/2}_x F^{q/2}_y}, \tag{3.30}$$

where F^q_x and F^q_y are the detrended fluctuation functions determined by the MFDFA method. The cross-covariance function and the fluctuation function are computed for $q \in \mathbb{R}$ parameter, which in financial applications is typically limited to the range $-4 \leq q \leq 4$. This cross-correlation measure allows quantification of the dependence degree between two time series x_i and y_i at different scales s and, by manipulation of q, makes possible estimation of the correlations, dependent on the magnitude of the fluctuations. The filtering ability of $\rho^q(s)$ constitutes a crucial advantage of this method, as financial time series cross-correlations typically vary depending on the size of the considered fluctuations. However, convenient use of this cross-dependency measure necessitates additional adjustment. Even though, for $q \geq 0$ the $\rho^q(s)$ always assume value from range $[-1, 1]$, for negative q exponents the obtained results might be slightly different. Namely, for weakly correlated processes, for $q < 0$, the numerator in the formula (3.30) is much greater than the denominator, and therefore, the cross-correlation coefficient may go far beyond interval $[-1, 1]$. In order to overcome this issue, the coefficient is adjusted as follows:

$$\rho^q_{xy}(s) = \begin{cases} \rho^q(s) & \text{for } |\rho^q(s)| \leq 1 \\ (\rho^q(s))^{-1} & \text{for } |\rho^q(s)| > 1 \end{cases}. \tag{3.31}$$

Cross-correlation coefficient $\rho^q_{xy}(s)$ defined in such a way always assumes values in range $\rho^q_{xy}(s) \in [-1, 1]$, thereby simplifying interpretation and being compatible with the Pearson cross-correlation coefficient. Moreover, for $q = 2$, it reduces to the classic DCCA method.

3.2 Multiscale analysis of returns: autocorrelation and cross-correlation case

The formalism introduced above facilitates quantification of the non-linear correlations in financial time series on the single-asset level as well as between different instruments. In this section, presented techniques are applied to the returns of the major stock indices and components of the DJIA. Next, the analysis is extended to a multi-asset scenario, and the cross-correlation are measured using coefficient ρ^q_{xy}.

Figure 3.5 shows fluctuation functions (section (a)) and the corresponding multifractal spectra (section (a)) calculated for daily returns of the major stock indices and selected DJIA components. Obtained $F_x(q, s)$, for all analysed assets, obey the power law over wide range of scales, which suggest the fractal nature and existence of non-linear, temporal dependencies in these signals. Since rates of return usually follow the leptokurtic distribution, and higher moments of the analysed series are

divergent, the fluctuation functions are limited to the range $q \in [-4, 4]$ with a step equal to 0.1, excluding $q = 0$. Naturally, due to the limited size of the analysed data, some distortions were observed for large values of s. However, power law dependence of $F_x(q, s)$ spans, at least, over two orders of magnitude of scales. For each of the analysed assets, the scaling range used for determining the multifractal spectra was adjusted individually, as denoted by the black dotted lines.

The fractal nature of the time series being considered is noticeable in obtained singularity spectra as well. Spectrum width, which measures the degree of the signal hierarchical organization, significantly exceeds the assumed multifractality threshold ($\Delta\alpha > 0.1$). As shown in Table 3.1 in case of indices it varies from $\Delta\alpha = 0.20$ for DAX to $\Delta\alpha = 0.30$ for DJIA returns, while for stocks from $\Delta\alpha = 0.21$ for BA to $\Delta\alpha = 0.40$ for DIS. Interestingly, some discrepancies are visible in the asymmetry coefficient A_α, which in case of indices vary from $A_\alpha = -0.68$ for FTSE to $A_\alpha = 0.83$ for NIKKEI, while for stocks vary from $A_\alpha = 0.05$ for CVX to $A_\alpha = 0.55$ for KO. Typically, financial time series reveals left-sided asymmetry $A_\alpha > 0$, suggesting the strong hierarchical organization of large fluctuations, whereas the dynamics of the small fluctuations remain relatively poor [105]. However, for analysed daily returns of selected DJIA components, almost symmetrical singularity spectra are observed, meaning that non-linear self dependencies are present in large as well as small fluctuations.

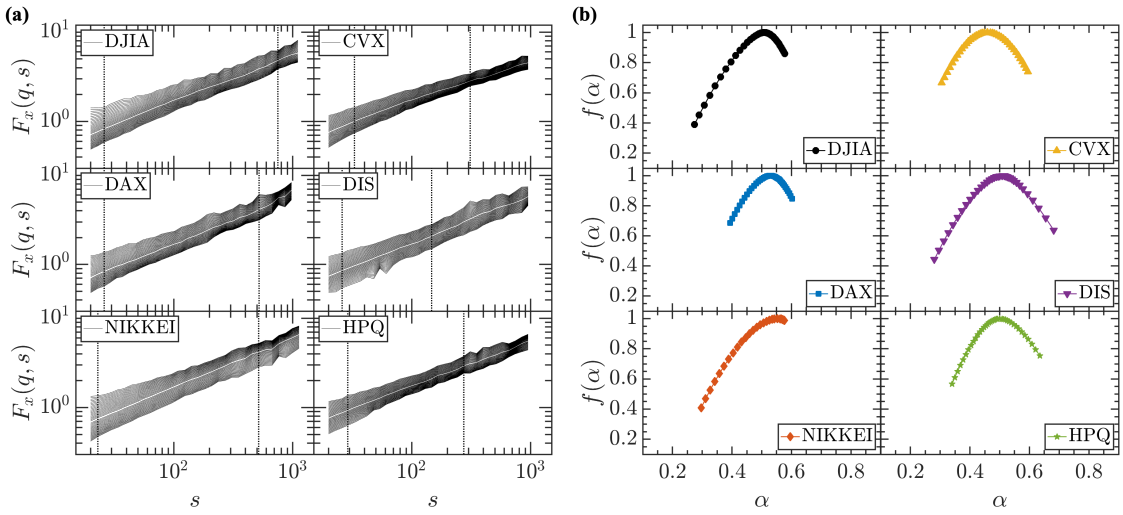

Figure 3.5: Fluctuation functions (panels in section **(a)**) and corresponding multifractal spectra (panels in section **(b)**) obtained for daily returns of major stock indices and selected companies from DJIA.

Besides quantifying non-linear dependencies, a multifractal analysis provides information about the linear correlations in the signal. Since, generalized Hurst exponent for $q = 2$ equals the ordinary Hurst exponent ($h(q = 2) \equiv H$) the linear, long-range correlations can be measured. For analysed indices, the Hurst exponent varied from $H = 0.44$ for DJIA to $H = 0.5$ for FTSE, whereas for DJIA components it fluctuated between $H = 0.39$ for CVX to $H = 0.48$ for IBM and BA. This result indicates that signals being analysed reveal slight anti-persistence or are linearly independent, which is typical for the financial time series. Worth noting is that the

level of long-range anti-correlation observed for CVX stands out significantly from the results obtained for other assets. Practically speaking, it means that periods of high and low returns of CVX are more likely to interlace.

Table 3.1: Spectra width ($\Delta\alpha$), asymmetry (A_α), and Hurst exponent (H) obtained for daily returns of selected indices and stocks.

	DJIA	**NASDAQ**	**FTSE**	**DAX**	**NIKKEI**
$\boldsymbol{\Delta\alpha}$	0.30	0.29	0.26	0.20	0.27
$\boldsymbol{A_\alpha}$	0.55	0.57	-0.68	0.31	0.83
$\boldsymbol{H}$	0.44	0.47	0.50	0.47	0.44

	AA	**BA**	**CVX**	**DIS**	**GE**	**HPQ**	**IBM**	**JNJ**	**KO**	**XOM**
$\boldsymbol{\Delta\alpha}$	0.27	0.21	0.28	0.40	0.22	0.29	0.27	0.32	0.28	0.35
$\boldsymbol{A_\alpha}$	0.26	0.18	0.05	0.13	0.42	0.08	0.28	0.12	0.55	0.33
$\boldsymbol{H}$	0.44	0.48	0.39	0.44	0.45	0.45	0.48	0.46	0.42	0.46

As mentioned previously, multifractality is a non-linear phenomenon; therefore, non-linear dependencies can only be its source. However, the scaling observed on the level of the fluctuations function can be, to some degree, caused by the heavy-tailed distribution of the analysed data [118, 119, 120]. For example, as shown in studies [121, 122], for uncorrelated time series characterized by a q-Gaussian distribution with a sufficiently large value of q, the scaling of the fluctuations function may appear and can lead to incorrect conclusions about correlations in analysed signal.

To quantify the impact of broad data distribution and confirm that wide singularity spectra observed for the returns being analysed is not a spurious effect, two different techniques were applied. The first one is based on random shuffling of the signal, which preserves the distribution of the time series, while linear and non-linear correlations are destroyed. As shown on the left panel of Figure 3.6, the singularity spectra calculated for shuffled time series are significantly narrower than was observed for the original signals. The width of the $f(\alpha)$ function for shuffled data varies from $\Delta\alpha = 0.05$ for DIS to $\Delta\alpha = 0.10$ for DJIA, both of which are below the assumed multifractality threshold.

The second technique applied in this study is based on the Fourier surrogate method [123]. This transformation combines two operations, namely, a Fourier Transformation and random mixing of the phases obtained. Next, using the inverted Fourier Transformation, the so-called Fourier surrogate signal is calculated. This modified time series has the same linear dependencies as the original one, but the non-linear correlations are destroyed, and data distribution is changed to the Gaussian. The right panel of Figure 3.6 shows the singularity spectra calculated for the returns modified using the technique described above. Similarly to the shuffled data, a significant reduction of the $f(\alpha)$ width is observed. Obtained singularity spectrum widths vary from $\Delta\alpha = 0.02$ for HPQ to $\Delta\alpha = 0.07$ for CVX, proving that the analysed rates of return multifractal character is rooted in the non-linear correlations.

The complex character of the financial markets is also visible in the cross-

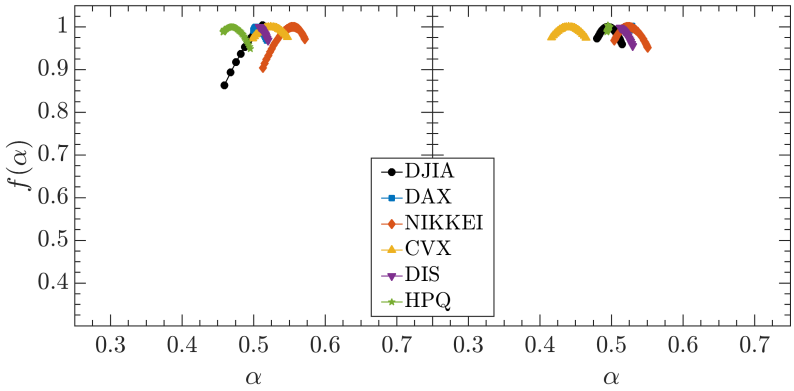

Figure 3.6: Multifractal spectra of the major stock indices and selected components of DJIA shuffled returns (panel on left-hand side) and signals transformed according to the Fourier surrogate method (panel on right-hand side).

dependencies between different assets. As shown in the previous chapter (see Figure 2.5), financial instruments quite commonly exhibit non-trivial cross-relationships. Interestingly, the dependencies between assets, like the temporal correlations analysed above, can have a multi-scale nature, especially when instruments from the same basket (sector) are considered. The panels in section (a) of Figure 3.7 present the cross-fluctuation functions $F_{xy}(q, s)$ of selected pairs of assets. In this analysis, considered values of scaling parameters were limited to the range $q \in [2, 4]$, as the cross-fluctuation functions of financial time series usually obey the power law only for positive values of q parameter [112].

The $F_{xy}(q, s)$ functions calculated for the stocks, and DJIA-NASDAQ pairs obey the power law in a relatively wide range of scales (varying from $s \in [30, 280]$ for HPQ-DIS pair to $s \in [25, 880]$ for DJIA-NASDAQ pair), whereas for DJIA-NIKKEI pair the cross-correlation does not have a multifractal character. Again, it has to be noted that the time series being considered span from 1950 up to 2020, and the results obtained are the averaged information. In past decades, due to geographical distance and differing monetary policies of US and Japan [124], these assets were, to some degree, decoupled. However, due to globalization, Japanese and US companies are in a strong economic relationship nowadays; thus, major indices from these countries reveal strong cross-correlations.

Discrepancies in synchronisation between assets with respect to the analysed size of fluctuations are also visible in the differences between scaling exponent $\lambda(q)$ and the mean value of the generalized Hurst exponents $\overline{h(q)} = (h_x(q) - h_y(q))/2$, which is usually measured by $d(q) = \lambda(q) - \overline{h(q)}$. The lower the value of $d(q)$, the more synchronised signals are, and in the case of perfect alignment between analysed series, $d(q) = 0$. As shown in the panels in section (c) of Figure 3.7, for analysed pairs of indices (DJIA-NASDAQ, plot on the left-hand side) and companies from the same sector (HPQ-IBM, third plot from the left), the difference between $\lambda(q)$ and $\overline{h(q)}$ yields $d(q) \approx 0.07$ and $d(q) \approx 0.025$, respectively, and does not significantly change with the increase of considered size of fluctuations. On the other hand, when the assets being analysed belong to different sectors $d(q)$ substantially decreases for larger returns: from $d(2) \approx 0.09$ to $d(4) \approx 0.04$ for HPQ-DIS and from $d(2) \approx 0.07$ to

$d(4) \approx 0.03$ for HPQ-GE pair. As these findings show, synchronization of the indices having common components and companies from the same sector maintain similar level regardless of the considered size of fluctuations (medium or large), whereas, when components represent different areas of the economy, alignment between large fluctuations is significantly stronger than that observed for medium-sized returns. From the practical application perspective, it means that highly correlated assets are synchronized regardless of the financial market cycle, as companies from different baskets become more aligned during crises or other economic events characterized by large fluctuations.

In order to quantify the multifractal cross-correlations between the instruments being analysed, $\rho^q_{xy}(s)$ coefficients were determined[3]. As shown in section (b) of Figure 3.7, the pair DJIA-NASDAQ has strongest inter-dependencies, which, regardless of the fluctuation size being considered (examined q) reach maximum value $\rho^q_{xy}(s) \approx 0.9$ for middle and large scales ($s > 3 * 10^3$, which corresponds to approximately 12 years). Interestingly, for small scales, the cross-correlations are significantly weaker, meaning that for short time spans (days), the fluctuations of DJIA and NASDAQ are more loosely coupled ($\rho^q_{xy}(s) \approx 0.65$), whereas over longer time periods (months, years) they are almost fully aligned. The high level of cross-correlations between considered indices is rooted in the components which comprise each of them. As has been noted, most of the tech companies (e.g., APPL, CSCO, INTC, MSFT) quoted within DJIA are also components of the NASDAQ index.

On the level of individual stock shares, multifractal cross dependencies are also significant; however, some discrepancies of value $\rho^q_{xy}(s)$ can be observed. The yellow, orange, and purple lines on plots in section (b) represent three different pairs of assets: HPQ-IBM, HPQ-DIS, HPQ-GE, respectively. The analysed instruments were chosen so that cross-correlation between assets from the same sector (IT sector, pair HPQ-IBM) and different buckets could be captured (IT and Consumer Goods sectors, pair HPQ-DIS and IT and conglomerate, HPQ-GE pair). Naturally, in the range of small scales $s < 10^2$, the multi-scale cross-correlation between assets from the same sector is significantly higher than is observed for instruments representing different areas of the economy. This effect is even more pronounced when medium-sized fluctuations are examined ($\rho^q_{xy}(s) \approx 0.7$ versus $\rho^q_{xy}(s) \approx 0.6$ for the HPQ-IBM and HPQ-DIS(GE) pairs, respectively). On the other hand, when longer time spans $s > 10^2$, or larger fluctuations ($q \in [3, 4]$) are considered, the difference in the strength of multifractal cross-dependencies becomes less meaningful. From a practical application perspective, analysis of $\rho^q_{xy}(s)$ for different pairs of assets shows that, over relatively short time spans, the actual similarity between instruments (belonging to the same sector or having common components) plays an important role, whereas for larger scales the global economic trends enter into the equation, causing higher alignment, even between instruments associated with different business areas.

[3]Due to lack of scaling observed for DJIA-NIKKEI pair, it was omitted in further analysis of multifractal cross-correlations

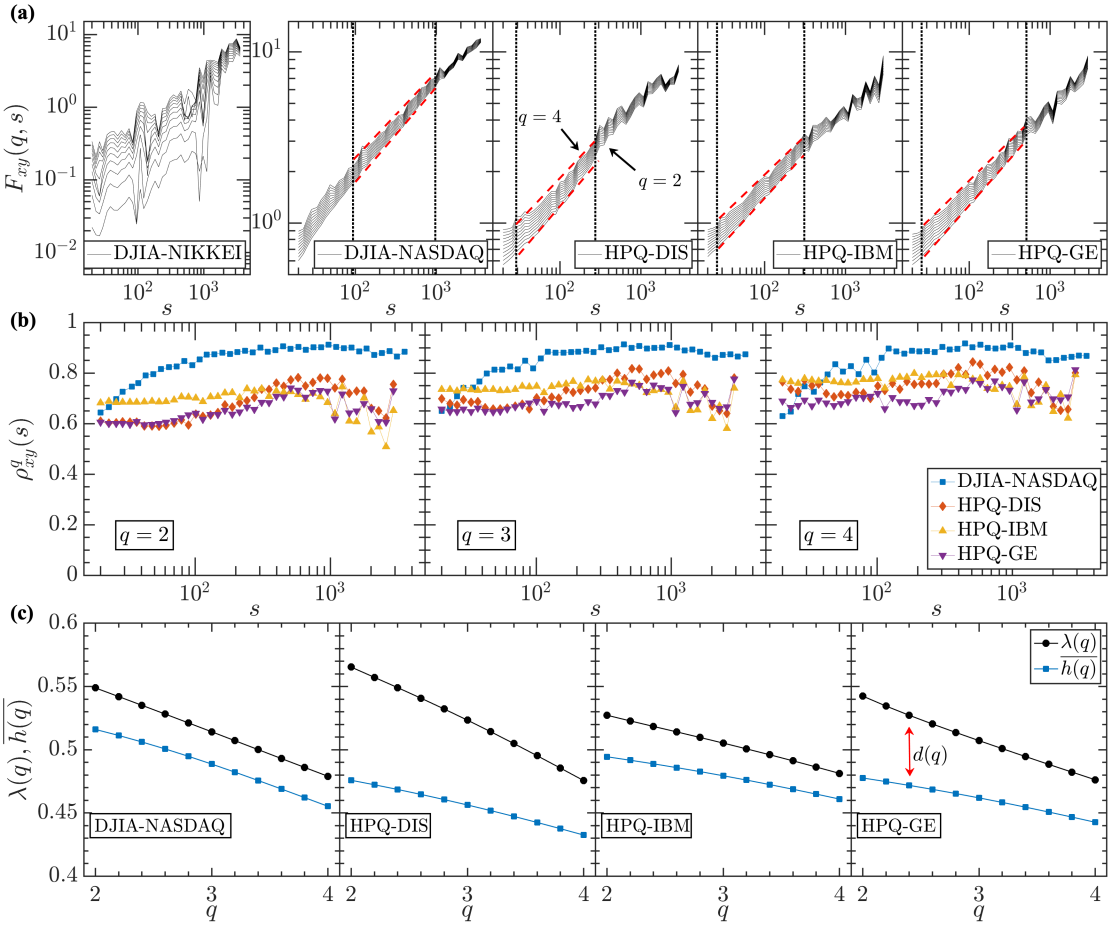

Figure 3.7: Multiscale cross-dependencies analysis of selected indices and stocks. Section **(a)**: cross-fluctuations functions $F_{xy}(q,s)$ calculated for exponents $q \in [2,4]$, black dotted lines indicate range of scaling. Section **(b)**: cross-correlation coefficients $\rho^q_{xy}(s)$ for scaling parameters $q \in [2,4]$. Section **(c)**: Scaling exponents $\lambda(q)$ (black line), and mean generalized Hurst exponents $\overline{h(q)}$ (blue line). Due to lack of scaling, the pair DJIA-NIKKEI is not included in the $\rho^q_{xy}(s)$ and $\lambda(q)$, $\overline{h(q)}$ analyses (sections (b) and (c)).

3.3 Network representation of financial time series non-linear cross-dependencies

Financial time series are characterized by non-linear cross-dependencies, which can be quantified using generalized cross-correlation coefficients $\rho^q_{xy}(s)$. Examination of the multiscale dependencies between assets can provide valuable information about the hierarchical organization of the financial market. However, analysis and interpretation of coefficient $\rho^q_{xy}(s)$ for multiple instruments on different scales could be difficult. In this section, the non-linear correlations are examined using techniques commonly applied in complex network analysis. Based on the calculated $\rho^q_{xy}(s)$ coefficients, the minimal spanning trees (MSTs) are built and then analysed in respect of their properties including the node degree distribution, the average short path length, and betweenness coefficient.

The minimal spanning tree can be defined as follows: having the graph G with V nodes, a set of edges $E \in \{\{u,v\} : u,v \in V\}$, and edge weights c_{xy}, the graph T

with V nodes and $D \in E$ edges constitutes a minimal spanning tree if the sum of the edge weights ω_e is the smallest possible. In order to build such a network, the distance between considered time series must be determined. In this dissertation it is defined as follows: $d_{xy}(q,s) = \sqrt{2(1-c_{xy}^{s,q})}$, where $c_{xy}^{s,q}$ is the matrix of $\rho_{xy}^{q}(s)$ coefficients determined for given scale s and q parameter. For fully correlated signals, $d_{xy}(q,s) = 0$; for anti-correlated signals $\sqrt{2} < d_{xy}(q,s) \leq 2$, while for uncorrelated signals $d_{xy}(q,s) = \sqrt{2}$. The distance measure $d_{xy}(q,s)$ must meet the triangle inequality, namely $d_{ab}(q,s) + d_{bc}(q,s) \geq d_{ac}(q,s)$, where a, b and c denote time series. The condition above, as shown in the study [125], is fulfilled only for positive q parameters, thus in further analysis only $q \in [2,4]$ will be considered. With a metric defined, in the Kruskal's algorithm of building MSTs [126], that was employed here, the time series are sorted by the distances between them, ranked in increasing order and then connected with respect to $d_{xy}(q,s)$ in such a way that each node can be attached only once. The result is the network having the smallest possible sum of the edge weights ω_e.

In addition to a visual representation of the relationships between financial time series, the quantitative description of the network features allows numerical examination of the market structure. The fundamental characteristic of the network is the distribution of node degree $P(k)$, which communicates the probability that a randomly selected node has k connections with other nodes. Mathematically, it is expressed as follows:

$$P(k) = \frac{N_k}{N}, \tag{3.32}$$

where N_k is the number of nodes with defined degree k and N is the total number of nodes in the graph.

The important feature, commonly observed in the real-world networks (e.g. social networks [127, 128, 129], semantic networks [130], or airline networks [131]) is the power law character of node degree distribution $P(k) \sim k^{-\eta}$. Networks of this type, customarily called scale-free, are also observed in the financial market e.g., currency comovements for which the distribution scaling exponent vary from $\eta = 2.4$ to $\eta = 2.7$ [132, 133].

One of the characteristic feature of the scale-free networks is their relatively small average shortest path length, which, for network having N nodes and shortest path $l(j,k)$ between nodes j and k, can be calculated using the following formula:

$$L = \frac{1}{N(N-1)} \sum_{j \neq k} l(j,k). \tag{3.33}$$

The average path length provides information about level of concentration of the network; the greater the average path L, the more scattered the network is.

Moreover, analysis of the financial data correlations usually requires identification and quantification of the most important assets quoted within the considered index. Using network representation, one can relatively easily obtain this information by calculating betweenness, which describes the significance of a particular node i in the network. More formally, it measures the number of shortest paths between

nodes that are passing through node i:

$$b_i = \sum_{j \neq k} \frac{n_i(j,k)}{n(j,k)}, \tag{3.34}$$

where $n_i(j,k)$ is the number of shortest path between nodes j and k passing through the node i, while $n(j,k)$ is the total number of shortest paths in the network. Besides the quantification of the node importance, the betweenness can also be interpreted as a measure of the influence of a particular node on the information propagation throughout the network.

Figure 3.8 presents the minimal spanning trees based on thirty companies quoted (currently or historically) within DJIA from 02.01.1981 to 31.12.2019 (see Appendix A for a full list of components). The analysis covers scaling parameters $q \in [2, 3, 4]$ and three scales $s \in [20, 63, 249]$, which correspond approximately to one trading month, one quarter, and one year, respectively. Moreover, components were divided into six sectors, each denoted by a different-colored nodes: Industrials (black), Finance (blue), Information technology (orange), Energy (purple), Consumer goods (yellow), and Healthcare (green). The size of the node indicates the value of the betweenness coefficient, according to the legend presented in the bottom right corner of the figure.

For medium-sized fluctuations ($q = 2$) and a monthly scale (panel (a)), the largest group of assets (10 components) is formed from companies belonging to the Financial and Consumer goods industries, and its hub (AXP) has the highest node degree in the graph ($k = 9$). Such a cluster, which represents a combination of assets from the Financial and Consumer goods sectors, is not surprising, as individual customers, who are the main source of income for the companies from the Consumer goods sector, strongly rely on the financing provided by banking institutions and payment operators such as American Express (AXP). In general, clusters built of components belonging to different sectors are quite common, as the areas in which companies operate often overlap. Interestingly, the node with the highest degree (AXP) is not the crucial one from a structural point of view. The most important node, which concatenates all clusters in the graph, is General Electric ($b_{GE} = 0.77$, $k = 5$). The central position of the GE, which was also observed in study [125], is understandable, as this company is a huge conglomerate that operates and usually plays a dominant role in multiple industries (e.g., aviation, technology, renewable energy, finance). Furthermore, as marked with dotted lines, in addition to Financial/Consumer goods sector, other three clusters can be extracted, namely Information technology with IBM ($b_{IBM} = 0.19$, $k = 4$) as a cluster hub, Industrials with RTX ($b_{RTX} = 0.42$, $k = 5$) as a hub and Consumer goods/Healthcare with KO ($b_{KO} = 0.31$, $k = 4$) in the center.

The structure of component cross-correlations changes slightly when larger fluctuations are considered. For $q = 3$ still, pronounced clusters are visible; however, GE loses its importance ($b_{GE} = 0.62$, $k = 4$), whereas the Consumer goods/Healthcare cluster becomes tightly coupled with the Finance sector and the AXP becomes the node with the highest betweenness and degree ($b_{AXP} = 0.71$, $k = 7$). For the largest returns, the structure becomes more dispersed, and three nodes from different sectors play a major role in terms of information propagation in the network

(XOM - $b_{XOM} = 0.59$, DIS - $b_{DIS} = 0.66$, AXP - $b_{AXP} = 0.54$). Additionally, for the largest fluctuations, General Electric becomes a marginal node, tightly coupled with Citibank.

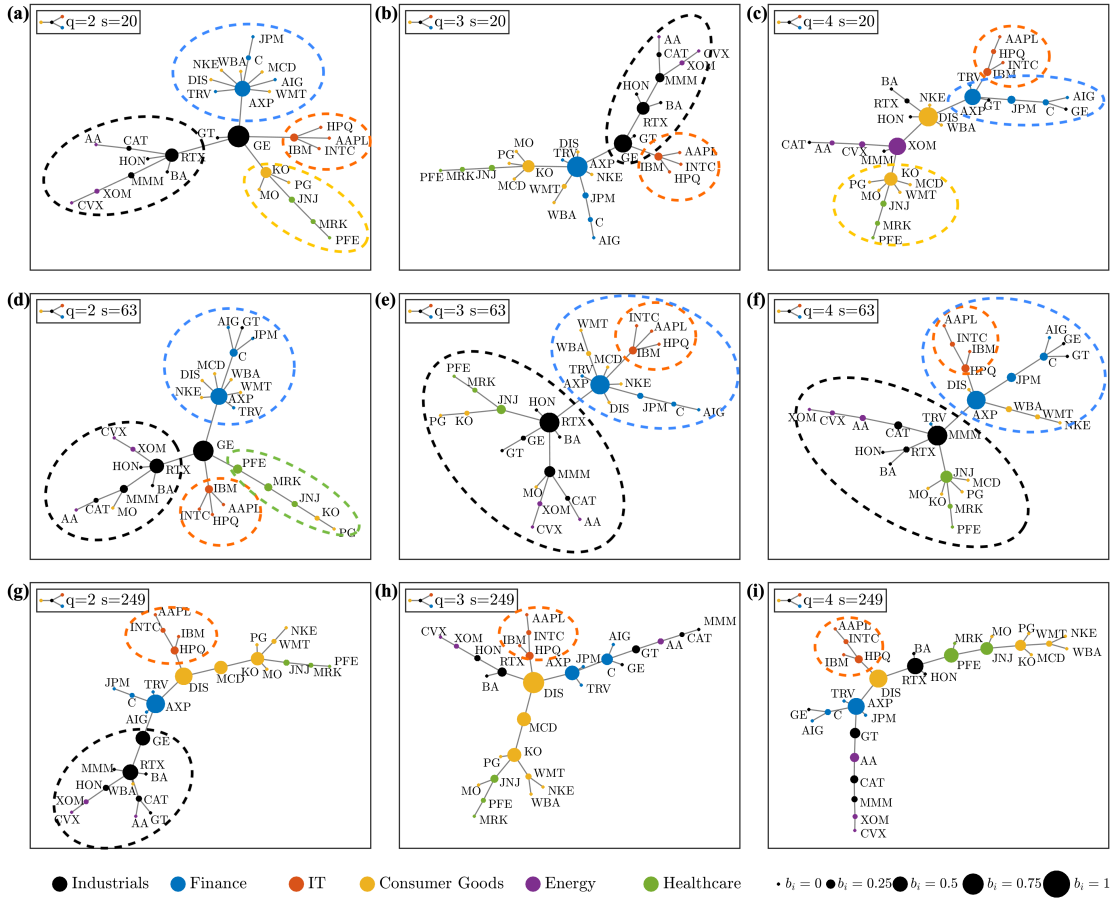

Figure 3.8: Minimal spanning trees build upon the multiscale cross-correlation coefficient $\rho^q_{xy}(s)$ calculated for three scales: monthly, quarterly and yearly ($s \in [20, 63, 249]$) and three different q parameters: $q \in [2, 3, 4]$. Each row of the panels corresponds to single scale s, whereas each column contains graphs calculated for same q. The color of the nodes in the graph indicates the sector to which particular asset belongs (black: Industrials, blue: Finance, orange: Information technology, yellow: Consumer goods, green: Healthcare and purple: Energy). Moreover, dotted lines denotes the clusters of highly coupled stocks. The size of the node indicates the value of the betweenness coefficient, as shown in the figure legend.

For medium-sized fluctuations, the market structure viewed on a quarterly scale, is similar to one observed for a monthly scale. Again, four clusters are pronounced, with GE in the center. However, here, a certain shift is visible for larger fluctuations. For $q = 3$ (panel (e)) GE loses its importance in favour of RTX ($b_i = 0.71$, $k = 6$), and the entire market can be divided into two parts: the first is dominated by companies from Industrial area and the second consists of assets representing Finance, Consumer goods and Information technology sectors with AXP acting as a hub ($b_i = 0.67$, $k = 8$). A similar structure is also visible for $q = 4$ (panel (f)).

Considering the yearly scale and medium-sized fluctuations ($q = 2$), one can notice that clusters of the companies representing the same or highly coupled sectors

exist; however, there is no central node that concatenates different sectors, and the graph assumes a more chain-like structure. A similar shape is also noticeable for larger q exponents (panels (h) and (i)).

Interestingly, regardless of the analysed scale or size of the fluctuations, clusters of IT companies (marked with orange dashed lines) are always distinguishable, indicating that stocks belonging to this sector are highly coupled and are driven by the same factors during periods of stability on the market as well as in volatile phases. Another observation having practical applications is that for medium-volatile and volatile market phases considered in quarterly scale ($q = 3$, $q = 4$, and $s = 60$, panels (e) and (f) of Figure 3.8) the structure can be divided into two parts (denoted by blue and black dotted lines). Therefore, in the market phases mentioned above, from a non-linear cross-correlation perspective, the risk exposure can be minimized by simultaneously investing in companies from both of these uber-clusters.

As mentioned above, one of the fundamental characteristics of the network is the distribution of node degrees. In the analysis performed in this dissertation, due to a relatively small number of analysed assets (30 companies), the fully legitimate, power law distribution cannot develop. However, as shown in the Figure 3.9 even for such a small number of nodes the incipient of this type of characteristic is noticeable. The slopes of the obtained distributions are approximately $\eta \approx 2$ regardless of analysed scale and size of the fluctuations, which is in consonance with the value reported for the entire New York Stock Exchange in the study [134] ($\eta \approx 2.1$).

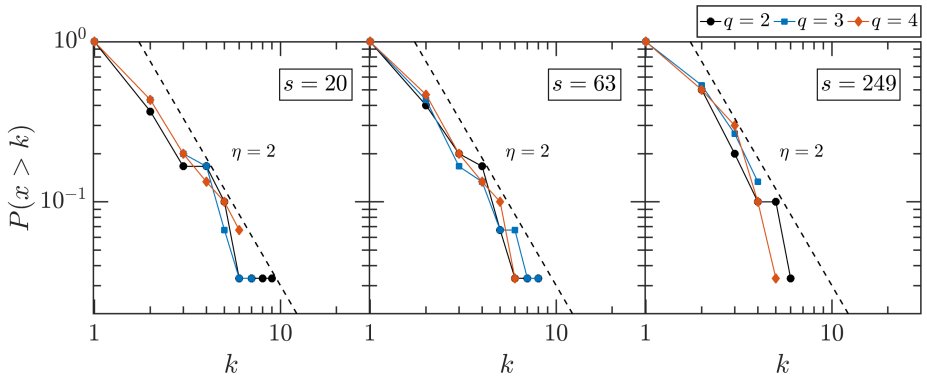

Figure 3.9: Cumulative distributions of the node degree determined for MSTs built for three different scales: monthly (panel on the left-hand side), quarterly (middle panel), yearly (panel on the right-hand side) and three different scaling parameters $q = 2$ (black circles), $q = 3$ (blue squares), $q = 4$ (orange diamonds).

Moreover, for each graph the average shortest path length L was determined (see Table 3.2). In general, as the considered scale or q exponent increases, the network becomes increasingly dispersed (the exception here is the value of L for $q = 3$ on the quarterly scale).

As the presented analysis shows, DJIA structure measured by non-linear cross-correlations, evolves along with the magnitude of considered returns and scales. The most significant changes are observed for small scales, for which the market structure transits from a centric layout with GE as a dominant node (for $q = 2$) to an increasingly dispersed arrangement. The common feature of obtained minimal spanning trees is the sectorial division of the nodes that is manifested by clusters

Table 3.2: Average path length L of the Minimal Spanning Trees based on non-linear cross-correlation coefficients $\rho^q_{xy}(s)$ between components of DJIA determined for three exponents $q \in [2, 3, 4]$ and three scales: monthly, quarterly and yearly.

L	$\mathbf{q = 2}$	$\mathbf{q = 3}$	$\mathbf{q = 4}$
Monthly	3.59	3.96	4.07
Quarterly	3.93	3.59	4.02
Yearly	4.72	4.74	5.11

formed by companies operating in the same or similar business areas. These sectors are usually connected with one another by single component e.g General Electric (GE, e.g panels (a) and (d) of Figure 3.8) or by two dominant nodes e.g United Technologies Corporation/American Express (RTX/AXP, e.g panels (e),(f) Figure 3.8). However, the sector-based structure of the market becomes less and less evident as the size of considered fluctuations (q exponent) increases, indicating that the sectorial binding between companies is typical for moderate returns. For large fluctuations, due to investors' herding behaviour all stocks become volatile and the fact that a particular company belongs to a given sector plays less significant role. This effect is also manifested by the increased value of the average shortest path length (see Table 3.2) observed for $q = 4$. It is worth noting that such representation of the cross dependencies between assets can have practical applications. The minimal spanning trees build on linear correlation coefficients are already used in the investment portfolio diversification [135]. Extending this approach to non-linear dependencies measured by the $\rho^q_{xy}(s)$ coefficient, allows more accurately identify the coupling between different financial instruments and thus better control risk exposure.

3.4 Time evolution of assets' singularity spectra

The hierarchical organization of the financial time series, as shown in previous sections, can be distorted. The effect is manifested by either the left- or right-side asymmetry of multifractal spectra. Detecting such distortions, combined with the examining widths of singularity spectra, provides valuable information about the mechanism governing the dynamics of particular time series. However, as shown in the study [76], asymmetry and width of the singularity spectrum may vary in time. Thus to better understand the underlying process dynamics, analysis of a multifractal spectrum's evolution over time is necessary. In this section, the changes in the multifractal properties of the major indices and selected stocks are investigated using the rolling window analysis method. The time evolution of the assets' self-dependencies are qualitatively analysed and also quantified by spectrum width $\Delta\alpha$, asymmetry coefficient A_α and Hurst exponent H. Performed analysis includes reference to the major economic events and their influence on financial market dynamics.

As mentioned above, in order to investigate changes in the multifractal properties of assets over different time periods, a rolling window analysis was applied. The

window length was 5000 data points, which corresponds to approximately 20 trading years, and a step size was 20 data points, reflecting about one trading month. The series of such a length, in presence of temporal, non-linear dependencies, are sufficiently long to detect it since the absence of such correlations demands significantly longer time series [121]. However, a single, outstanding fluctuation might affect the results obtained. As an example, such a return occurred on the 18th of October, 1987, in what is known as the Black Monday crash, during which the DJIA fell by 22.9%. In order to capture the general changes in dynamics of the processes governing the evolution of the multifractal properties of considered assets, the mentioned rate of return is omitted in the rolling window analysis.

Figure 3.10 shows the result of the rolling window analysis of singularity spectra for the DJIA index and HPQ company, calculated from January 1950 to December 2019 and January 1962 to December 2019, respectively. Panels (a) and (b) show a three-dimensional plot of the singularity spectra obtained consecutively for each window. In order to better visualize evolution of $\Delta\alpha$, A_α, and H the panels below contain two dimensional projections onto the time-α plane (plots (c) and (d)), with $f(\alpha)$ maxima denoted by red crosses and values of $\Delta\alpha$, A_α, H and rate of returns time series shown in the sections (e)-(f). Moreover, three historically significant events that influenced the financial markets are denoted by vertical dashed lines: the Black Monday crash - yellow line; Dot-com bubble - purple line; and bankruptcy of Lehman Brothers - green line.

Initially, the DJIA returns' singularity spectra expand gradually, with a local maximum $\Delta\alpha \approx 0.4$ occurring in 1984. The multifractal spectra, starting from 1985, become narrower ($\Delta\alpha \approx 0.25$), but this narrowing is primarily the result of shrinkage of the right arm of $f(\alpha)$, which is also manifested by an increase of A_α coefficient. From the time windows ending in 1993 up to 2007, the right side of $f(\alpha)$ almost disappears ($A_\alpha \approx 0.9$), suggesting weak or even lack of non-linear correlations in small fluctuations. However, after the Lehman Brothers bankruptcy, the singularity spectra begins to recover, with some fluctuation occurring in the years 2018-2020. On the level of the multifractal spectra width, this effect is visible in a gradual increase of $\Delta\alpha$ in recent years. Interestingly, before the Black Monday Crash and the Lehman Brothers bankruptcy, a significant decrease of singularity spectrum width is noticeable. Such a decrease means that, in the periods preceding these major market events, the dynamics of the process governing price changes became poorer. In terms of the long-range linear dependencies measured by the Hurst exponent, a clear, progressing downtrend is visible. Up to 1985, H fluctuates around 0.5, then it decreases significantly to $H \approx 0.42$, and, this level is maintained to date, with a slight increase for the windows that ends in period 2007-2009, indicating increased randomness in those years.

Slightly different characteristics are observed in the HPQ singularity spectra time evolution. Here, up to 1998, the multifractal spectrum is broad ($\Delta\alpha \approx 0.5$) and reveal left-side asymmetry ($A_\alpha \approx 0.5$). A significant change of the singularity spectrum's shape is noticeable for windows that end in period 1998-2000 (before Dot-com bubble crash), when, initially, the right-side of $f(\alpha)$, followed by the left-side, shrunk substantially. As a result the spectrum width decreased to $\Delta\alpha \approx 0.2$. The less hierarchical organization in the HPQ returns is observed up to 2010, when

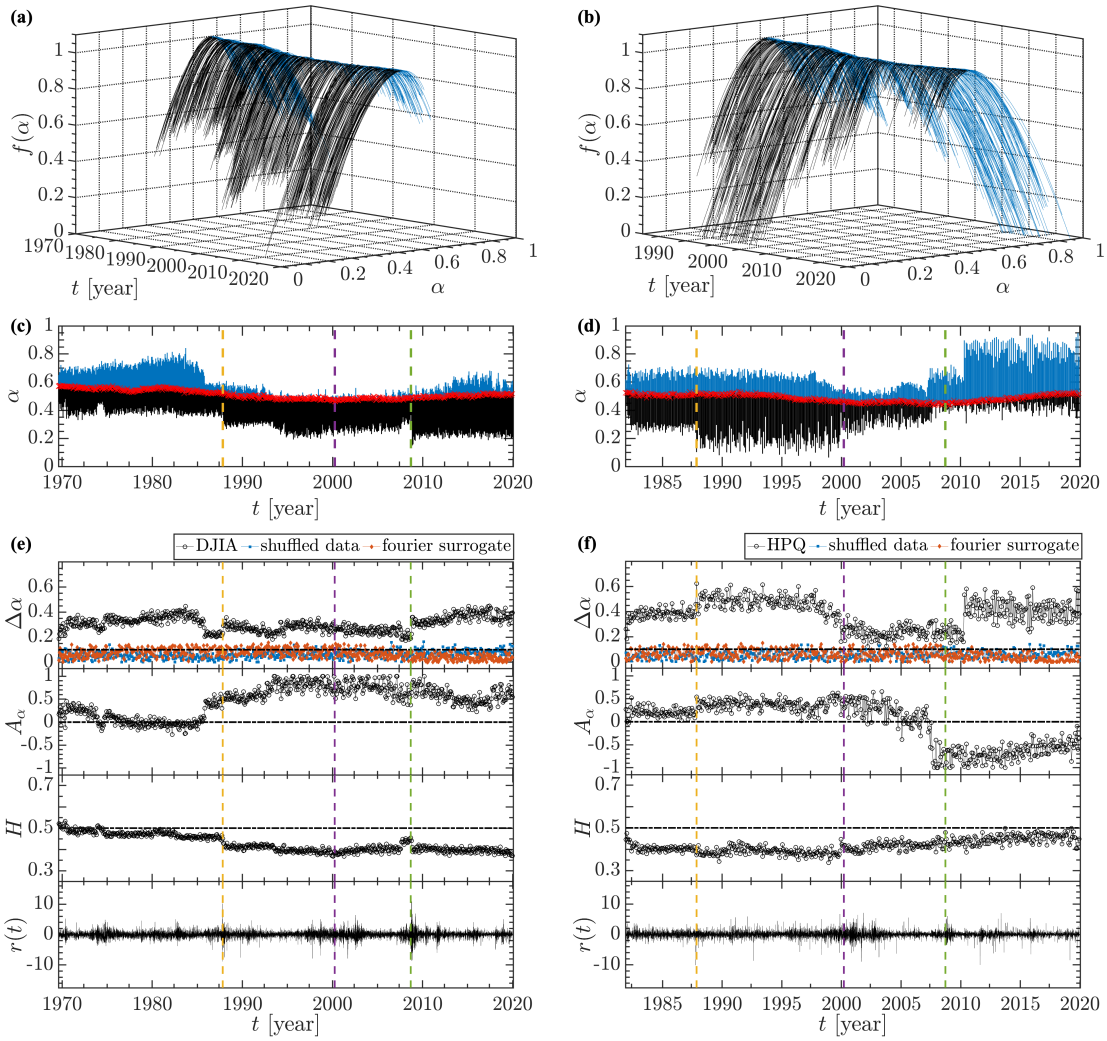

Figure 3.10: Multifractal rolling window analysis of DJIA (plots on the left-hand side) and HPQ (plots on the right-hand side). The panels **(a)** and **(b)** display a three-dimensional view of the singularity spectra of each window, where black and blue colors corresponds to left and right sides of $f(\alpha)$, respectively. Panels **(c)** and **(d)** show the projections of the multifractal spectra onto the time-α plane, where the red crosses illustrate displacement of maxima of $f(\alpha)$. Panels in section **(e)** and **(f)** show quantities describing the multifractal spectra (from top: width $\Delta\alpha$, asymmetry A_α and Hurst exponent H) as well as analysed return signals (bottom panels). The calendar date assigned to each data point corresponds to the end date of a window. The yellow, purple and green vertical lines in sections **(c)**-**(f)** indicate important economical events (Black Monday 19.10.1987, Dot com bubble crash - 13.03.2000, Bankruptcy of Lehman Brothers - 15.09.2008, respectively).

the right side of $f(\alpha)$ rapidly developed and the total width came back to previously observed levels. This effect is even more intriguing, as the left side of the singularity spectrum almost disappeared beginning in 2007 ($A_\alpha \approx -0.7$), and has shown gradual recovery in recent years. Thus, in the last two decades, large returns of HPQ were weakly correlated, which is unusual for financial time series. Moreover, in recent years, the weakening of the linear dependencies manifested by $H \approx 0.5$ is visible.

In order to verify that the multifractality of the time series in analysed windows is not a spurious effect caused by the broad distribution of the data, $f(\alpha)$ functions

were determined for randomly shuffled series and the signal modified according to the Fourier surrogate method (the procedures were applied in each window individually). The width of the obtained singularity spectra are presented in the upper panels of the sections (e) and (f) (blue squares and orange diamonds for shuffled data and the Fourier surrogate, respectively). For both assets, the width of $f(\alpha)$ for modified signals is substantially lower than observed for original data; however, for some windows, the assumed multifractality threshold ($\Delta\alpha = 0.1$) is violated, usually during turbulent market periods. This effect is primarily caused by the limited length of the data in each window (5000 data points), and qualitatively does not undermine the obtained results.

To some extent, similar changes in the multifractal properties are also visible for NIKKEI returns. As shown on the panels in section (a) of Figure 3.11, the index, which is commonly recognized as a barometer of the Asian economy, does not reveal changes in dynamics related to the Black Monday, which may be a result of the loose monetary policy of Japanese regulators, that reduced the impact of the 1987 crash [124]. However, such a policy led to the asset price bubble, which burst in late 1991 [136], and this is clearly visible in singularity spectra width - $\Delta\alpha$ decreased by approximately 0.12. Moreover, starting from the windows that end in 1992, a slow symmetrization of the multifractal spectrum is noticeable. The downward trend of A_α is interlaced with temporal increments of the asymmetry coefficient during the Dot-com and Lehman Brothers bankruptcy crises (purple and green dotted lines, respectively). These changes in multifractal characteristics are also accompanied by a gradual decrease of the linear correlations in period 1990-2009, reflected by the Hurst exponent value $H \approx 0.5$, and then were followed by an increase of the returns' anti-persistence starting from 2009 and continuing to date. In general, the multifractal rolling window analysis suggests that NIKKEI, and by extension the entire Japanese economy, was strongly influenced by the early 1990s' crash up to 2009, when the Bank of Japan announced another round of quantitative easing, which translated into richer dynamics of NIKKEI returns. The long-range effects of the Japanese bubble crash were described in studies [137, 138].

In contrast, the changes in singularity spectra width and asymmetry observed for DAX are not that sudden. In the 1990s, its returns exhibit a monofractal nature, and, starting from the beginning of the 20th century, the steady increase of the $\Delta\alpha$, accompanied by increasing symmetrization of $f(\alpha)$ and a slight downtrend in the Hurst exponent, is visible. Lack of sharp changes in its multifractal properties suggests that DAX was not significantly affected by crashes that occurred in past decades and, in terms of non-linear correlations, seems to be relatively poorer than other analysed assets.

Similar to the DAX index, the returns of CVX (section (b) of Figure 3.11) up to the window that ends in 2000, exhibit poor hierarchical organization, manifested by narrow singularity spectra ($\Delta\alpha \approx 0.18$) and accompanied by large fluctuations of the asymmetry coefficient. Starting from the beginning of the 20th century, correlations in the large CVX rates of return are gradually strengthen, as shown in the increased total width of the singularity spectra and the growth of A_α. Interestingly, conterminously to the DJIA, sudden reduction of the $\Delta\alpha$ and asymmetry coefficient are observed before the Lehman Brothers crash in 2007.

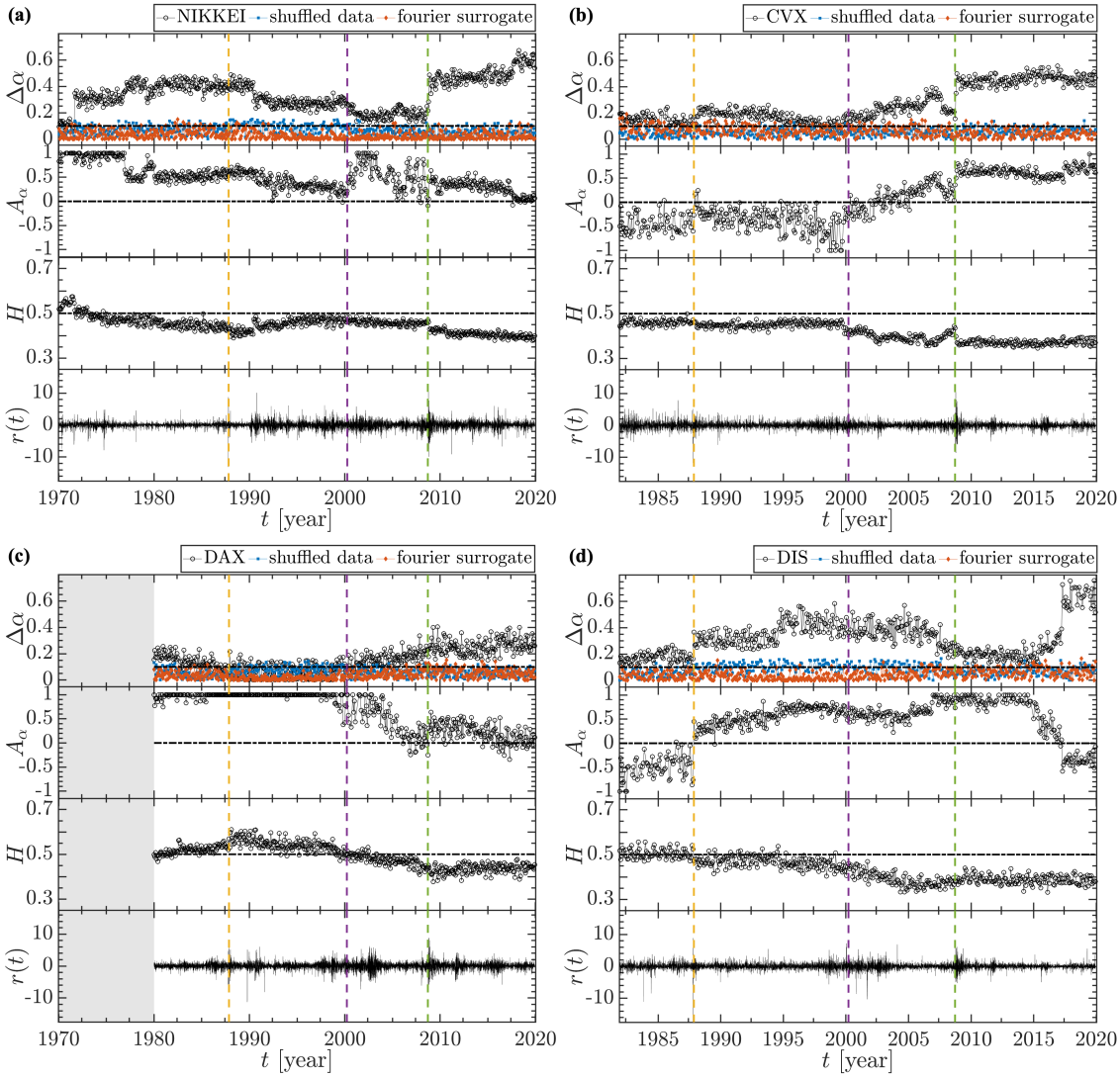

Figure 3.11: Time evolution of the multifractal properties of indices (section **(a)** - NIKKEI, section **(c)** DAX) and selected components of DJIA (section **(b)** - CVX, section **(d)** DIS)) rates of return. Each section contains four panels, from top: spectrum width $\Delta\alpha$ (calculated for original data (black dots), shuffled data (blue squares) and data modified accordingly to Fourier surrogate method (orange diamonds)), asymmetry A_α, Hurst exponent H and rates of return signal $r(t)$, respectively. The calendar date assigned to each data point corresponds to the end point within a window. The yellow, purple and green vertical lines indicates important economical events (Black Monday 19.10.1987, Dot-com bubble crash - 13.03.2000, and bankruptcy of Lehman Brothers - 15.09.2008, respectively). Due to limited DAX data availability, the analysis was not possible for time windows end dates in 1970-1980, indicated by grey area.

Decrease of hierarchical organization level before the recent crisis is also visible in the the DIS returns. Starting from the window that ends in 2005 a gradual decrease of $\Delta\alpha$ can be observed. The weakening of the non-linear correlations of returns $\Delta\alpha \approx 0.2$ is observed up to 2015, when the width surges to approximately $\Delta\alpha \approx 0.6$ and the singularity spectrum reveals right-hand side asymmetry $A_\alpha \approx -0.5$. In this context, the multifractal properties of DIS returns are to some degree similar

to those observed for HPQ indicating that these components might become non-linearly correlated. The source of such a similarity is probably related to the fact that Disney has became more involved in the technology sector in recent years.

Again, in order to confirm that the results described above were not significantly influenced by the limited size of the data and its broad distribution, as with the DJIA and HPQ analyses, the singularity spectrum width of the shuffled signal (blue squares) and that modified by Fourier surrogate method (orange diamonds) were calculated for each window. Regardless of the analysed asset, the width of the altered time series is significantly lower than was observed for original data; however, due to limited data size, the multifractality threshold (here set to $\Delta\alpha = 0.1$) is occasionally violated, usually during turbulent market periods.

Analysis of the changes in multifractal properties of the major stock indices and components from DJIA demonstrates that they evolve through a variety of shapes whose changes typically appear correlated with the historically most significant events experienced by the world economy. Notably, the variation in a hierarchical organization typically manifests prior to an asset's valuation collapse, thereby demonstrating the prediction potential of the applied method.

3.5 Variability of multiscale cross-correlations between financial instruments

Naturally, significant changes in multifractal features of the indices and stocks presented in the previous section reflect different market phases that vary in degree of coupling among the components [139]. In this section, these phases are investigated using a multifractal rolling window analysis of 10 selected components of DJIA as well as *Proxy Index* constructed from these companies. Examination of the multifractal properties' time evolution is supported with correlation matrix analysis.

The indices are built of components; thus, the hierarchical organization of the index is the superposition of the features observed on the stocks level. It is expected that multifractal properties of sum of many uncorrelated multifractal signals disappears along with an increasing number of the components [105]. However, stocks can be linearly and non-linearly correlated; thus, coupling among the companies quoted within the same index may produce interesting multifractal features observable on the global level. To study these effects, by summing up prices of 10 companies from DJIA, the proxy of the index was created (AA, BA, CVX, DIS, GE, HPQ, IBM, JNJ, KO, XOM from 02.01.1962 to 31.12.2019). Since DJIA is a price-weighted index ands the components of the proxy are dispersed across different sectors, the created instrument well approximates the real index, as shown in Figure 3.12.

For such created Proxy Index as well as its components, a rolling window analysis was performed. Again, to capture general changes in system dynamics, not dominated by outstanding fluctuations, the return that occurred on 18th October 1987 (the Black Monday crash) was omitted. Figure 3.13 displays the result of this analysis. To improve illustrative clarity, the multifractal spectra of the individual components, are represented by the average value, calculated separately for each window. The upper panels ((a) and (b)) show the $f(\alpha)$ function projected onto

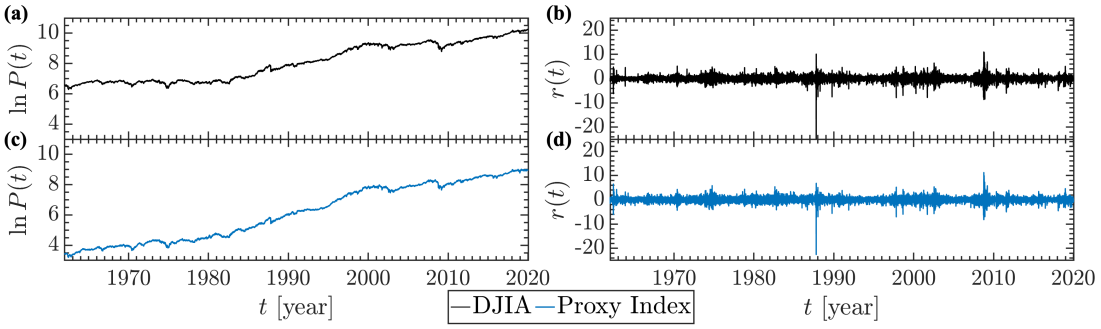

Figure 3.12: Daily prices (panels **(a)** and **(c)**) and returns (panels **(b)** and **(d)**) of the DJIA index and its proxy formed from 10 companies (AA, BA, CVX, DIS, GE, HPQ, IBM, JNJ, KO, XOM).

the time-α plane, the middle panels present the multifractal spectra properties of the corresponding assets (panel (c) - spectrum width $\Delta\alpha$, panel (d) - spectrum asymmetry A_α), and the panel (e) contains the obtained values of the Hurst exponent H. Clearly visible is the similarity of the changes in multifractal spectra shape and location for both analysed instruments, which is manifested by similar values of the asymmetry coefficient A_α and Hurst exponent H. However, the average $f(\alpha)$ spectrum is never narrower than the one obtained for the Proxy Index, which is understandable result, because equality is expected in the case of perfect correlation among price fluctuations of all participating companies. Interestingly, the discrepancy between Proxy Index spectra width and the average value $\Delta\alpha$ of its components is not constant over time. An especially noteworthy case occurs in the period between 1991 and 1994, indicated by the red area. In this period, the width of the mean singularity spectra of the considered companies stabilise around $\Delta\alpha \approx 0.22$ while the width of the Proxy Index enters into mono-fractal regime $\Delta\alpha < 0.1$. Such narrowing of the Proxy Index singularity spectra indicates that, in this period, the non-linear correlations among the components were weak. On the other hand, starting from 1995 up to 2003 (on Figure 3.13 marked with the green area), the hierarchical organization of the Proxy Index as well as its components are characterized by similar singularity spectra widths, suggesting a stronger coupling between companies. In recent years, the analysed companies seem to decorrelate again, a tendency manifested by a gradually increasing difference in $\Delta\alpha$ observed from 2005 to date, with the exception of the financial crisis period, during which the discrepancy in singularity spectra broadness shrunk.

In order to verify that the narrowing and broadening of the Proxy Index singularity spectra in different periods is related to suppression and amplification of the cross-correlations among components, a rolling window analysis of the correlation matrix was performed. Under the assumption that M denotes a $N \times T$ rectangular matrix formed from N time series $x_i(t)$ of length T, the correlation matrix can be defined as follows:

$$C = \left(\frac{1}{T}\right) MM^T. \tag{3.35}$$

The entries of matrix C constructed in such a way, correspond to the Pearson correlation coefficients, for which, by diagonalization ($Cv^k = \lambda_k v^k$), the eigenvalues

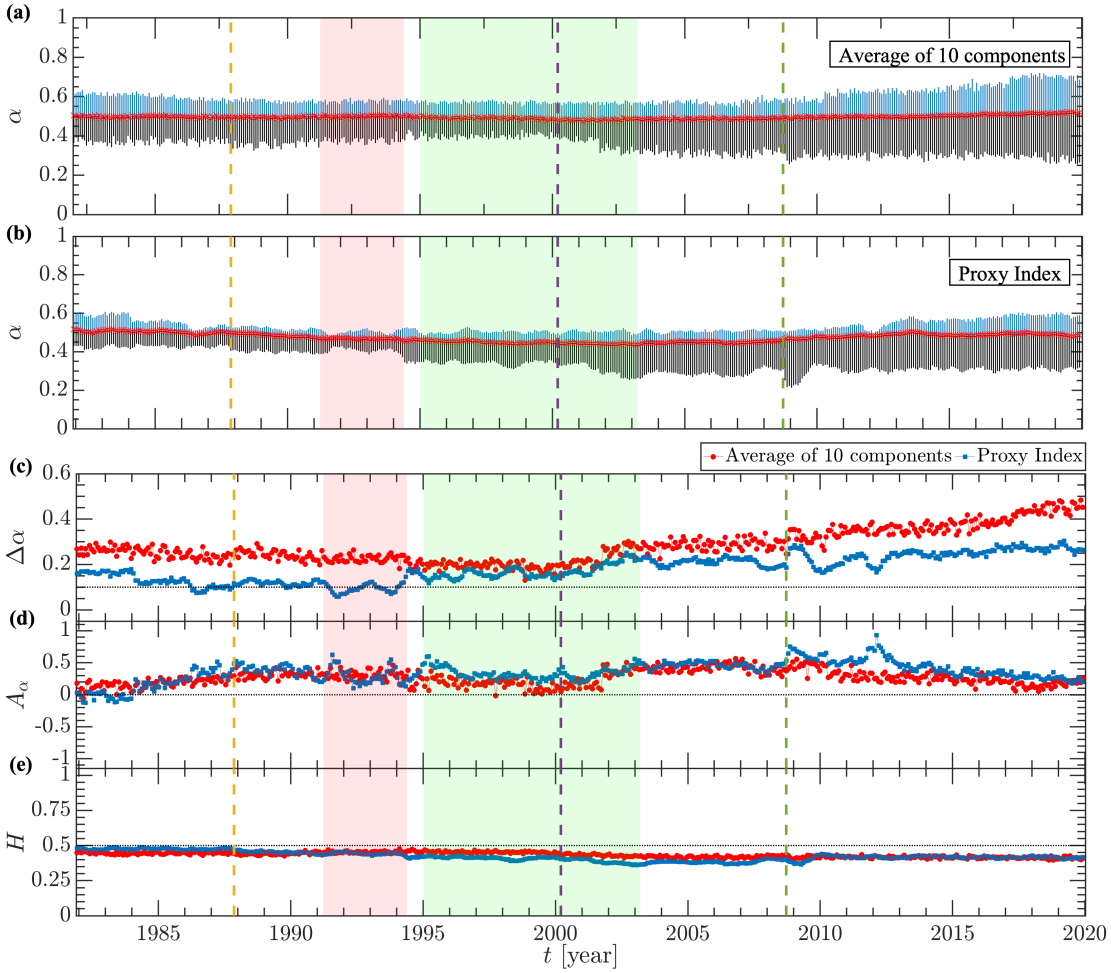

Figure 3.13: Multifractal rolling window analysis of the Proxy Index built of ten instruments quoted within DJIA (AA, BA, CVX, DIS, GE, HPQ. IBM, JNJ, KO, XOM) compared with average calculated for components individually. Panels **(a)** and **(b)** show sequence of singularity spectra calculated for average spectrum and Proxy Index, respectively. Panels **(c)** and **(d)** presents time evolution of the multifractal properties of analysed assets (red circles - average of the components, blue squares - Proxy Index), namely, spectra width $\Delta\alpha$ (panel **(c)**), spectra asymmetry A_α (panel **(d)**) and linear long-range correlations measured by Hurst exponent H (panel **(e)**). The black dotted line in plot (c) indicates assumed threshold of the multifractality $\Delta\alpha = 0.1$. The yellow, purple and green vertical lines indicate important economical events (Black Monday 19.10.1987, Dot-com bubble crash - 13.03.2000, bankruptcy of Lehman Brothers - 15.09.2008, respectively).

$\lambda_k (k = 1, ..., N)$ and corresponding eigenvectors v^k can be obtained. Accordingly to the Marchenko-Pastur law [140] for the entirely random signals, the density of eigenvalues $\rho_C(\lambda)$ is known analytically as follows:

$$\rho_C(\lambda) = \frac{Q}{2\pi\sigma^2} \frac{\sqrt{(\lambda_{max} - \lambda)(\lambda - \lambda_{min})}}{\lambda}, \tag{3.36}$$

where the λ_{min} and λ_{max} bounds are as follows:

$$\lambda_{min}^{max} = \sigma^2 \left(1 + \frac{1}{Q} \pm 2\sqrt{\frac{1}{Q}}\right). \tag{3.37}$$

In these equations, $Q = T/N$, and σ^2 is the variance of the analysed time series. The

degree of deviation of the largest eigenvalue λ_1 above λ_{max} measures the strength of the correlations among the time series used to construct the correlation matrix [1, 141]. Figure 3.14 presents the time evolution of the largest eigenvalue λ_1 (blue squares) for the window of length $T = 100$, moved by 20 data points each step. Moreover, in the same figure, the black circles represent the changes of the largest eigenvalue γ_1 of an analogous matrix composed of the multiscale cross-correlations coefficients $\rho^q_{xy}(s)$ for scale $s = 100$ and exponent $q = 2$. Clearly visible is the similarity in the time evolution of these two measures, both of which reach their minima in January 1994. In this period, the λ_1 touches the border of purely random series, while γ_1 drop to 2.5. Moreover, downtrend in the λ_1 and γ_1 is also noticeable in recent years, confirming that, in these periods, considered components are less correlated, thus explaining the narrow singularity spectra of the Proxy Index. On the other hand, in period 1995-2003 (green area), both measures maintain higher levels; however, the slight decorrelation followed by stronger coupling is observed during the dot-com bubble crash. Such an effect is typical for significant financial events when investors' panic behaviour and massive sell-offs observed on the market translate into the stronger coupling between companies.

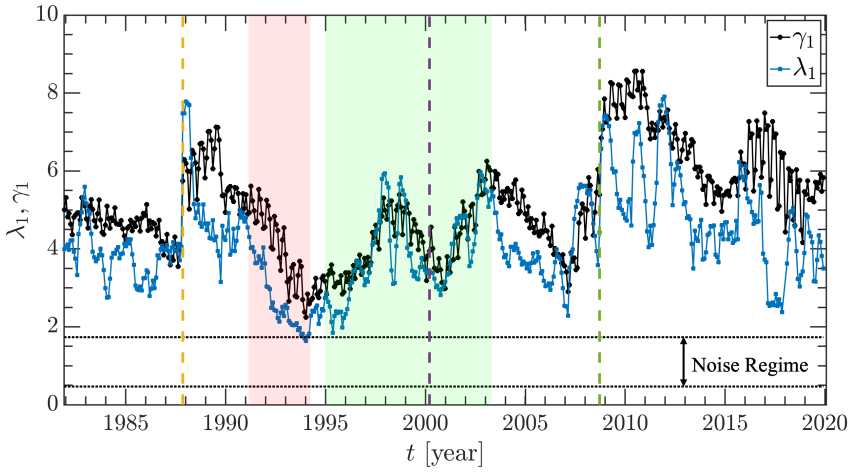

Figure 3.14: Rolling window analysis of the largest eigenvalue of correlation matrix (λ_1 - blue squares) and matrix composed of multiscale correlation coefficients $\rho^q_{xy}(s)$ (γ_1 - black circles). The horizontal black dotted lines indicate the noise regime of the correlation matrix calculated according to equation 3.37. The yellow, purple and green vertical lines indicate important economical events (Black Monday crash 19.10.1987, Dot-com bubble crash - 13.03.2000, Lehman Brothers bankruptcy - 15.09.2008, respectively).

The rolling window analysis of the Proxy Index and selected companies presented in this section shows that cross-correlations between companies are one of the main factors responsible for the dynamical variability of the hierarchical organization observed in financial market indices. Furthermore, the changes in coupling between companies are usually correlated with significant financial events and crashes. The approach introduced in this section constitutes a valuable tool that can be used as a confirmation method for other prediction techniques.

The multifractal analysis of the major stock indices and components of DJIA presented in this chapter shows that financial time series have non-trivial characteristics. Returns, beside incorporating non-linear autocorrelations can also be

non-linearly depend on one another. On top of that, the hierarchical organization of the financial time series is not constant in time. In different market phases the correlations among components can substantially increase or decrease, which results in intriguing phenomena observed on the index level. Producing signals characterised by the features mentioned above is not an easy task and require application of clever modeling techniques. Undoubtedly, one of such techniques is agent-based modeling. The fundamentals of this approach to generating time series, correspondence to models applied in physics and analysis of two, well-recognized agent-based models of financial markets are discussed in the next chapter.

Chapter 4

Agent-based modeling

Many processes appearing in the nature are marked by high degree of complexity. The interdependencies present in many physical, biological or environmental systems are too complicated to be modeled using conventional modeling tools and examining these using traditional deductive and inductive reasoning is therefore difficult [142]. Due to the economic development and increasing globalization, the same can be said about sociological and economical systems [143]. The intricacy of the world around us, and the need for simple techniques able to reproduce complex phenomena led to rapid development of a bottom-up approach to the modeling. In such a methodology, rather than creating general formula, which describes the entire considered process, the modeling effort is focused on dividing the system into multiple linked parts, which by defined interactions, are able to generate complex phenomena observed on the system level.

This chapter begins with an introduction to agent-based modeling. Using two fundamental models of this type, namely, Schelling segregation model [77] and Boids model [78] it is demonstrated how frameworks of this class can reproduce complex phenomena including herding and processes having the appearance of the phase transition. Moreover, using Ising Model as an example, it is shown how phase transition and criticality of the physical systems correspond to the phenomena observed in real financial markets and how such behaviour can be simulated with relative ease, using Monte Carlo methods. Finally, two financial agent-based frameworks inspired by Ising Model, namely Iori's model [70], and Bornholdt's model [71] are discussed and examined in the context of reproducing hierarchical organization of the returns.

4.1 Fundamentals

Agent-based modeling (ABM) is one of the primary methods belonging to the group of bottom-up, micro-scale modeling techniques. This approach represents a system as a collection of autonomous, interacting, decision-making agents, that operate in a defined environment [144]. An ABM's definition is abstract; nonetheless, two main components existing in every model of this class can be distinguished. Naturally, the first common element ABMs share is the presence of agents. Since these models are usually characterized in the context of their application, often using the jargon

of particular scientific field, no exact and standardized definition of 'agent' exists. However, definitions present in the literature tend to agree on more points than they disagree [142]. The list below contains several fundamental, but not obligatory properties of and agent [55, 59, 145, 146]:

- **Autonomy**: Agents are autonomous, self-directed units that are capable to operate independently in the environment.
- **Self-containedness**: Agents are discrete, identifiable individuals, that can be described through use of a set of properties. The agent's discreetness implies that they have well-defined boundaries, thereby one can simply and unambiguously determine whether part of the system is an agent or not.
- **Interactivity**: Agents are able to interact and exchange information with other entities existing in the system.
- **Heterogenity**: The state of an agent can vary across individuals and can change over time. For instance, an agent representing a human being, can posses attributes such as age, job or wealth, and these attributes can evolve as the simulation advances. On the other hand sex, nationality or race remains constant.
- **Reactiveness**: Agents are aware of their surroundings and can anticipate and react to signals coming from the simulation environment and other individuals. In more advanced models, agents can have memory and alter their state depending on previous states as well as learn and adapt.

Characteristics of an agent can be divided into two groups: attributes and methods. Attributes describe the state of a particular agent and, as mentioned above, can either be static (e.g., name, sex) or evolve over time (e.g., memory, wealth). On the other hand, methods specify the rules of the behaviour of an entity. In this context, ABMs are flexible and it fully lies in the modeler's hands, whether an agent takes action based on the simple if-else clauses or applies sophisticated decision trees or neural networks [147].

The second component which exists in every ABM is an environment. It defines the space in which agents operate and, in a basic scenario, provides information on the spatial location of an agent. In more advanced models, the environment may supply extra data that could affect agents behavior (e.g., global economic sentiment in financial market simulations [148, 149]). The topology of the environment is usually domain-specific and strongly depends on the problem that the model is designed to address. It can be an abstract non-spatial 'soup' (e.g., computational economy models [150]), an Euclidean space (e.g., flocking [78]), a two dimensional-lattice (e.g., game of life [151]) or spatial network (e.g., traffic jam model [152]). Importantly, model's topology usually defines an agent's *neighborhood*, which, in turn determines individuals that given agent can interact with. In the case of a two-dimensional lattice, von Neumann or Moore neighborhoods are typically applied (see Figure 4.1 left and central panels, respectively), whereas, for network-like environments, the individuals are linked according to node edges (see Figure 4.1, right panel).

The information exchanged by connected agents depends on the problem being considered and scientific field to which the model is being applied. In simple physical

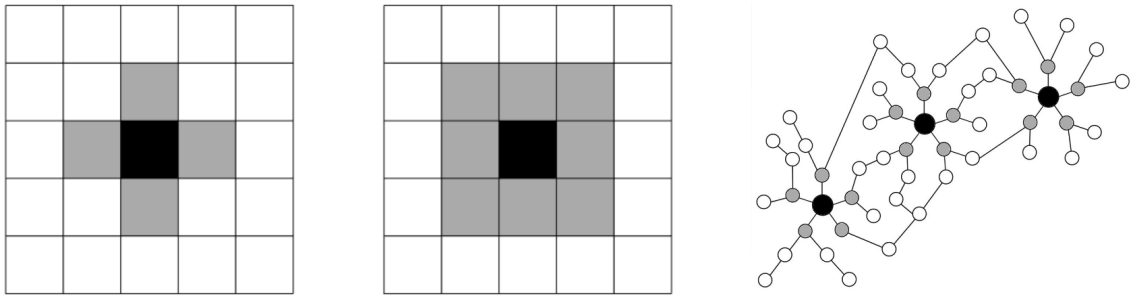

Figure 4.1: Examples of the topologies and neighbourhoods commonly employed in agent-based models. Left panel: von Neumann neighbourhood in the two-dimensional lattice, central panel: Moore neighbourhood in the two-dimensional lattice, right panel: neighbourhood in the network. The black color indicates selected agents and gray marks their neighbours.

models it could be a position (e.g., molecule position [52]), in biological systems the type of an agent (e.g bacteria, antibiotic, cell etc. [56, 153, 154]), while in sociological and economical models typically an opinion (e.g., voting preference [61, 72]) or sentiment is exchanged [67]. In general, individuals share details about their state with the entities in the vicinity and, based on the information received from neighbours agent modifies its state.

Lack of concrete definition of ABM and their ability to incorporate different agent's decision-making mechanisms (e.g., machine learning [155]) and environment topologies can lead some to view this modeling technique as complicated. This is partially true, for example in the case of so-called large-scale models, in whose the simulation can consist of thousands of widely varied agents behaving accordingly to the complex rules (e.g., models of global economy [68, 150]). However, many of ABMs, capable of generating complex phenomena can be implemented in a simple form such as cellular automata [156]. An example of such framework is the Schelling's segregation model [77], which reproduces the racial division in a society. This model is based on a two-dimensional lattice, and the agents are divided into two groups (A and B), representing people of different races. Each individual in the system can assume one of two states (happy and unhappy), and which entity assumes is determined by the percentage of units of the same type inhabiting its neighbourhood (a Moore neighbourhood in this case) and tolerance threshold $T \in [0, 1]$. If the percentage of agents of a different race in the neighbourhood exceeds the individual's tolerance threshold T, an agent is considered as unhappy, and thus, in the next time step, it randomly changes location to any other unoccupied cell in the system. In an extreme case, when $T = 0$ an individual is happy only when entities of the same type are in the vicinity, whereas for $T = 1$ agents are always happy, regardless of the type of units surrounding them. As shown in Figure 4.2, the dynamic of such a system significantly depends on the tolerance threshold.

For a high level of tolerance, the system remains unordered, and qualitatively, the agents' spatial distribution does not significantly change over time, whereas for tolerance values below the certain threshold ($T \leq 0.3$), strong spatial segregation emerges. In physics, such a dramatic change in system organization is characteristic of phase transitions and usually is associated with changes in the state of matter. The phenomenon itself, as well as techniques of modeling it, are described in more

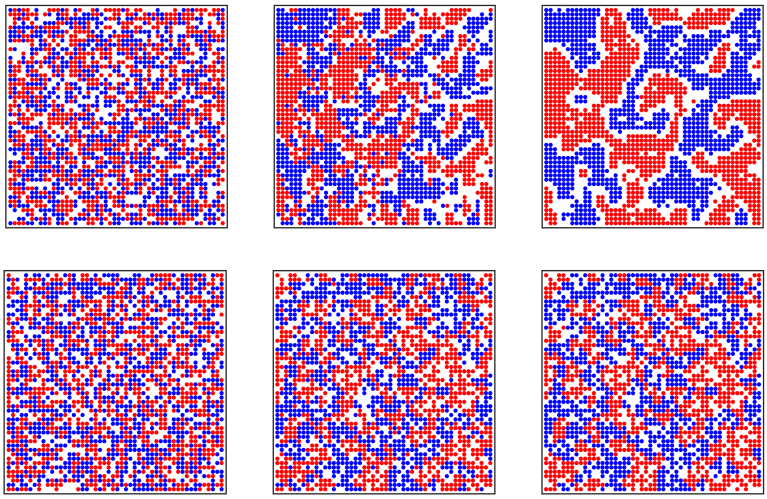

Figure 4.2: Time evolution of the Schelling's Segregation Model employing two different tolerance thresholds: $T = 0.3$ (upper panels) and $T = 0.7$ (bottom panels). The lattice has size 100x100 and 70% of the cells are occupied by agents of type A (blue dots) or B (red dots). The plots in the same column show the configuration of the system in the initial state, after 5 time steps and after 20 time steps, respectively. For a low tolerance threshold $T = 0.3$, the spatial segregation occurs, and clusters of agents of the same type, separated by empty cells, are formed. This phenomenon does not appear for a high tolerance threshold $T = 0.7$. In this case agents are distributed more uniformly.

detail in the next section.

The second, crucial observation with regard to Schelling's segregation model dynamic is that simple, local interactions between agents lead to creation of clusters of individuals belonging to the same group. Such collective, organized behaviour observed on the system level and rooted in local interactions is called *emergence*. This phenomenon is even more visible in the Boids model [78], which imitates the movement observed in the flock of animals such as fishes or birds. The model's environment is a two-dimensional Euclidean space with periodical boundaries, and agents move according to three basic rules:

1. **Cohesion:** Each agent steers toward the central of the mass of the entities in the neighbourhood.
2. **Separation:** Each agent avoids collisions.
3. **Alignment:** Each agent steers towards the average direction of the entities in the neighbourhood.

As shown in Figure 4.3, initially, agents have randomly assigned orientations and locations on the plane. As the simulation proceeds, the rules mentioned above make the movement appear purposeful and coordinated. Worth noting is that the model does not assume any kind of leadership by any agent (or agents), and the same rules govern all individuals in the system. Such herding behaviour is observed not only among animals but also appears in human actions (in sociological systems and financial markets, for instance). Moreover, many believe that herding behavior is the root cause of the formation of speculative bubbles and crashes [75, 157, 158].

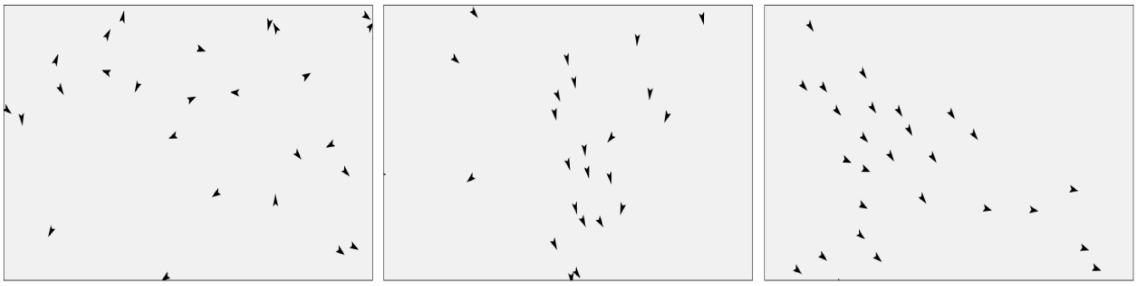

Figure 4.3: Time evolution of the Boids model consisting of 25 agents. The panels present the initial configuration of the system, configuration after 50 time steps and configuration after 150 time steps, respectively. As the simulation proceeds, the movement of the individuals appears increasingly coordinated, and in final state, the flock is formed as almost all entities steer towards the same direction.

The examples considered above reveal the fundamental features that underlie the popularity of the agent-based modeling. The ability to reproduce complex phenomena, including spontaneous change of the system dynamic and emergence manifested by collective actions taken by agents, have found applications in many areas of science spanning social, economic, physical, and biological systems. Not without significance is the flexibility of the agent-based models and rapidly advancing computational power, which allows performing large-scale simulations that would not have been feasible a few years ago.

In the context of the agent-based modeling applications, worth noting is that, based on the degree of the complexity and purpose of the model, two different approaches can be distinguished. The first one entails a detailed representation of the analysed system. These models, whose primary purpose is to predict system behaviour, usually have plenty of parameters and utilize huge data sets. This modeling approach is often used in the analysis of individual countries' economic policies and their influence on the global market. Here, the advantage of agent-based modeling over traditionally used econometric and dynamic stochastic general equilibrium models (DSGE) is indisputable [66], as these models are not able to simulate interdependencies between different economic components.

The second approach, preferred by physicists, is based on building simple, elegant models with a limited number of parameters and an appropriate generalization level. Simulation of the phenomenon in controllable conditions facilitates analysis of the system dynamics and provides valuable insight into the considered process. A small number of free parameters simplify interpretation of results and aid in identification of the crucial mechanisms underlying phenomenon being analysed. Moreover, such models usually focus only on one segment of the large system. A prominent example here are the models of financial markets which simulates trading preferences of the investors. Naturally, prediction capabilities of such models are limited; however, they are able to provide an explanations for stock market bubbles and crashes [159, 160, 161, 162], that do not appear in econometric or equilibrium models [66]. Interestingly, many agent-based models of financial markets were designed originally by physicists and consequently, are inspired by frameworks commonly used in physics [71, 163, 164, 165, 166]. A typical example of a model that comes from physics but has found applications in multiple areas of science is the Ising Model.

Its properties and applications are presented in the next section of this dissertation.

4.2 Ising Model and criticality of financial markets

Agent-based models, as shown in the previous section, are able to reproduce collective behavior and phenomena having the appearance of the phase transition. In the context of the financial markets modeling, the former feature is especially compelling. Phase transitions are usually associated with the thermodynamic processes in which the state of matter change, for instance, from liquid to solid. Such a dramatic alternation of system properties can also be observed in ferromagnetic materials, liquid helium, superconductors, and many more [167]. In this section, phase transitions and criticality of the physical systems are compared to phenomena observed in the financial markets during the crises and bubble bursts. Next, it is demonstrated how phase transitions in the ferromagnetic materials can be easily reproduced using the Ising Model and Monte Carlo methods.

Based on the behaviour of the system in the vicinity of a transition temperature, two types of phase transitions are possible, namely, first-order and second-order phase transitions. Considering a system in the thermodynamic equilibrium, a first-order phase transition is a process in which a sharp, noncontinuous change of a thermodynamic function, such as entropy or specific heat, is observed. During such a transition, the system can release (or absorb) a significant amount of energy without changing the temperature. This stage of the process is called a mixed-phase regime, in which only a fraction of the system completes the transition, with the rest remaining in its original phase. A typical example is boiling water, which, before completely turning into vapor occupies a mixed-phase regime manifested by a turbulent mixture with bubbles.

Alternatively, in the second-order phase transition the system's state function changes continuously. For instance, in a ferromagnetic material, the spontaneous magnetization of the system disappears above a certain temperature called Curie Temperature (also called critical temperature). Practically speaking, the assignment of a particular process to a type of phase transition is performed based on latent heat, which can be defined as the amount of energy required to change the phase of a single particle at a given temperature. First-order transitions are processes in which latent heat is observed; thus, during the transition, a finite amount of energy is released (or absorbed), whereas, for second-order transitions, the latent heat does not appear.

From the perspective of the system microstructure, a distinguishing feature of most phase transitions is the appearance of a non-zero value of the order parameter in the system's ordered phase but zero (or nearly zero) in its disordered phase [168]. The order parameter definition depends on the type of the considered system. For instance, in a liquid-to-crystal transition, it will be the orientational order of the particles, whereas, in liquid-to-gas, the order parameter is the difference in the density between the material in these two phases. Typically, the order parameter assumes a scalar form; however, it may also take on a multi-component or tensorial value.

Phase transitions are interesting, extensively studied phenomena that have coun-

terparts in different areas of science. In the context of this effect's multidisciplinary applications, especially compelling is the second-order phase transition. In the vicinity of a critical point, fluctuations of many quantities, such as energy or magnetization increase significantly. Interestingly, the distributions of these quantities often assume power law characteristic, suggesting the existence of a non-trivial hierarchical organization and non-linear correlations. Moreover, correlation does not appear only in the time dimension, but strong spatial dependencies are observable as well. As a result, when the system is in a near-critical state, any small, local change in the system has global effects that can lead to macro-consequences.

As mentioned in the previous section, dramatic changes in system dynamics having an appearance of a phase transition are observed in non-physical systems as well. It is sufficient to look at Schelling segregation model time evolution (see Figure 4.2) to notice that the significant increase of the order is observed for simulation performed with tolerance threshold above certain value. In this case, the simplest measure of the order of the system is the average number of neighbours of a different type in the agent's vicinity. Assuming that 70% of the cells in the system are occupied and tolerance threshold $T = 0.3$ (see Figure 4.2, upper panels), the average number of the individuals of different race drops to zero after approximately 30 time steps, while for $T = 0.7$ it stabilises around 1.6 (see Figure 4.2, bottom panels).

Phenomena exhibiting signs of a phase transition also occur in the financial markets [6, 169, 170]. According to the theory introduced by Sornette, formation of bubbles and crashes in financial asset valuation has multiple features in common with phase transition. Cooperative actions taken by investors eventually put the market into a metastable phase, where even a small disturbance can trigger instability that results in a crash. Increased sensitivity of markets is similar to the behaviour of a physical system, e.g., ferromagnetic material, in the vicinity of its critical temperature, where a little adjustment causes a dramatic change of the system properties. Interestingly, when the financial market drifts towards its critical point, the precursory fingerprints in the stock prices can be observed [6, 171] and even modeled using, for instance using, Log-Periodic Power Laws (LPPL) method [172, 173, 174].

The most popular and, at the same time the simplest physical model that is able to reproduce a second-order phase transition is the Ising Model [167]. In some metals, such as iron or nickel, spins spontaneously orientate in one direction, and in consequence, a macroscopic resultant magnetic field is observed. However, above Curie temperature, these materials lose their magnetic properties and become paramagnetic. Simulation of such phase transition was the initial intention of Lenz, who in 1920 proposed the model [175], which was developed and solved analytically in one dimension by Ising in 1925 [176].

The model consists of discrete variables that represent the nuclear magnetic moment and, in a basic scenario, are arranged in a chain, where each variable has two neighbors. For instance, let consider a chain of ions with spin $s = 1/2$ and internal magnetic moment μ_0, which are influenced by an external magnetic field. According to quantum mechanics, such spin can be oriented in one of the directions, namely, along with the external field (customarily called 'up'), and in opposition to the external field (customarily called 'down'). Hamiltonian of such system can be

calculated as follows:

$$H = -J \sum_{<i,j>} \sigma_i \sigma_j - h \sum_i \sigma_i \tag{4.1}$$

where $< i, j >$ is the sum over the nearest neighbours, σ_x denotes spin, J is a coefficient that determines the preference of the spins, and h is the energy of spin in an external magnetic field. For $J > 0$ the spins orient in the same direction as in ferromagnetic materials, whereas for $J < 0$, an alternate configuration of the spins, typical for antiferromagnetic materials, is favored. By convention, the entire component is multiplied by -1; however, it does not have any physical interpretation, and the change of the sign comes down to the flipping of all spins in the system. The second part of the equation is the sum of all spins existing in the system, scaled by an external magnetic field h. At this point, one can notice that the parts of the Hamiltonian represent different types of interactions, namely, local (with the nearest neighbors) and global (with an external magnetic field), which as will be demonstrated in later sections of this dissertation is crucial in modeling of financial markets multiscale properties. Mathematically, solution of the Ising Model, as with other systems considered within thermodynamics formalism, comes down to the calculation of the partition function:

$$Z = \sum_N \exp(-E/k_B T), \tag{4.2}$$

where E is the total energy of the system (value of the Hamiltonian H), k_B is a Boltzmann constant, and T is the temperature. The sum of equation 4.2 is over all N possible states of the system, and so depends on the size and number of degrees of freedom of each variable. The partition function is used to determine the probability of the particular state of the system, as follows:

$$P_u = \frac{\exp(-E_u/k_B T)}{Z}, \tag{4.3}$$

where E_u is the energy at state u (i.e., value of the Hamiltonian H in the state u). Moreover, from the partition function, by use of the procedures of statistical mechanics, the thermodynamic functions of the system, such as free energy, entropy, and internal energy can be derived. As shown by Ising [176], in the one-dimension case, no phase transition to the ordered state occurs at any temperature. In other words, the ordered state is unstable at any finite temperature because a single thermal fluctuation manifested by the spin oriented in the opposite direction destroys the ordering in all consecutive spins in the chain, until another thermal fluctuation appears. As a result, a break in "communication" between different parts of the system occurs.

Interestingly, such behavior is strictly connected to the number of neighbors of a given spin. For instance, two-dimensional Ising Model with von Neumann neighborhood, or a one-dimensional chain with long-range interactions, undergo the phase transition from the ferromagnetic to the paramagnetic state and vice versa. The former case, in a basic scenario without external field, was analytically solved by Onsager in 1944 [177] and the transition appears at critical temperature T_c:

$$T_c = \frac{2J}{k_B \log\left(1 + \sqrt{2}\right)}, \tag{4.4}$$

where J is an interaction coefficient and k_B is a Boltzmann constant. Despite its simplicity Ising Model can be strictly solved only for one-dimensional chains and two-dimensional lattices without an external magnetic field. Other cases can be puzzled out by usage of various approximation methods, such as mean-field approximation or renormalization techniques.

4.2.1 Monte Carlo methods for Ising Model

In practice, one of the most convenient ways to solve the Ising Model is through use of Monte Carlo numerical methods, which are relatively simple and typically provide accurate results. In this section, the fundamentals of employing Monte Carlo methods to solve an Ising Model, including different dynamics, are presented.

Considering a system in thermal equilibrium at given temperature T, from basic principles of thermodynamics, it is known that the probability of finding the system in a given state u is described by Boltzmann distribution (4.3). Now, let X_u be an observable of the system that characterises the state u; for example, this could be the energy or entropy of the system. Then, at the given temperature, the average value of the observable can be calculated as follows:

$$\langle X \rangle = \sum_u P_u X_u, \tag{4.5}$$

where P_u is the probability that system is in the state u, and X_u is a value of investigated thermodynamical quantity in this state. From the perspective of probability theory, X is an ordinary random variable that assumes one of the possible values X_u accordingly to distribution P_u. Now, to obtain the average value, the possible states u can be randomly drawn from the configuration space. This technique, though correct, is inefficient. Even a small system can have a tremendous number of possible configurations; for instance, the Ising Model, which consist of $N = 200$ spins, has 2^{200} possible configurations. Another issue that arises in this context is that the Ising Model's Hamiltonian (4.1) describes only the system in thermodynamical equilibrium and thus does not provide any information concerning system dynamics. Nonetheless, both of these issues can be overcome through use of Markov chains. The concept itself corresponds to the stochastic process, in which the current state depends only on its immediate predecessor. Stated more formally, a Markov chain is a stochastic, discrete process x_{t_n} (where $t_1 < t_2 < ... < t_n$) occurring in the system which has finite number of the possible states $S_1, S_2, ..., S_N$, if the conditional probability:

$$P(x_{t_n} = S_{u_n} | x_{t_{n-1}} = S_{u_{n-1}}, ..., x_{t_1} = S_{u_1}) \tag{4.6}$$

is not 0 only for the previous state of the system: $P(x_{t_n} = S_{u_n} | x_{t_{n-1}} = S_{u_{n-1}})$. Thus, this conditional probability can be interpreted as a transition probability of the system's moving from state u to v [167]:

$$W_{u \to v} = P(x_{t_n} = S_v | x_{t_{n-1}} = S_u). \tag{4.7}$$

Naturally, $W_{u \to v}$ is greater than or equal to 0, and the sum over all possible transitions is normalized. Now, having the definition of the transition probability, for

infinitely small time steps, one can write the master equation as follows:

$$\frac{\mathrm{d}P_u(t)}{\mathrm{d}t} = -\sum_{u \neq v}[P_u(t)W_{u\to v} - P_v(t)W_{v\to u}], \tag{4.8}$$

where $P_u(t)$ and $P_v(t)$ are probabilities that the system, at time t, has state u, v respectively. Worth noting is that the basic property of Markov processes that the next state of the system depends only on the current state, is not typical for all physical systems, and only some of them have dynamics compatible with the equation (4.8) [178]. As long as the examined process can be described as a Markov chain, the derivative in the formula above is equal to 0, and thus the terms on the right-hand side must be equal. This leads, in turn, to the expression known as *detailed balance*:

$$P_u(t)W_{u\to v} = P_v(t)W_{v\to u}. \tag{4.9}$$

Under the assumption that, at some point in time, the system reaches its equilibrium, and that the probability of given state is given by the 4.3, following condition occurs:

$$Z^{-1}\exp(-E_u/k_BT)W_{u\to v} = Z^{-1}\exp(-E_v/k_BT)W_{v\to u}, \tag{4.10}$$

which, by basic transformations, leads to the formula for determining the probability of the transition:

$$\frac{W_{u\to v}}{W_{v\to u}} = \frac{\exp(-E_u/k_BT)}{\exp(-E_v/k_BT)} = \exp(-(E_u - E_v)/k_BT). \tag{4.11}$$

The formula above does not explicitly define the transition probabilities between given states, and any form that satisfies the *detailed balance* is acceptable. In statistical physics, the dynamics proposed by Metropolis [179] is commonly used:

$$W_{u\to v} = \begin{cases} \tau_0^{-1}\exp(-\Delta E/k_BT) & \text{if } \Delta E > 0 \\ \tau_0^{-1} & \text{if } \Delta E \leq 0, \end{cases} \tag{4.12}$$

where $\Delta E = E_u - E_v$ and τ_0 is the time required to attempt a spin-filp, which is customizable and usually set to $\tau_0 = 1$. In practice, assuming that the system is in the initial state (usually generated randomly), the algorithm can be described as a few steps procedure:

1. Choose a site k
2. Calculate the resultant change in energy ΔE in case of flipping the spin at site k
3. If $\Delta E \leq 0$, flip the spin and repeat the procedure, starting from point 1; otherwise continue to the next step
4. Generate random variable r from the uniform distribution
5. If $r \leq \exp(-\Delta E/k_BT)$, then flip the spin; otherwise the site k remains unchanged. Continue from the step 1.

This procedure is repeated for each site, and one full cycle is considered to be a typical measure of Monte Carlo time (MCS/site). Optionally, the sites can be chosen randomly. In such a scenario, assuming that the system consists of N sites, 1 MSC/site corresponds to N random selections of the site. This technique is usually applied when not only static equilibrium properties but also the dynamic correlation functions of the stochastic model being studied [167]. Once a sufficient number of cycles are completed the average of the discretionary thermodynamic quantity can be calculated according to equation 4.5. Figure 4.4 shows the example of time evolution of the magnetization and energy for the two-dimensional Ising Model in a zero magnetic field. In the initial phase, the system drifts towards the equilibrium state, where both internal energy and magnetization stabilise. Moreover, as the simulations proceeds, a global spin inversion is observed. This effect is related to the finite size of the system; however, these states have equal energy and differ only in sign.

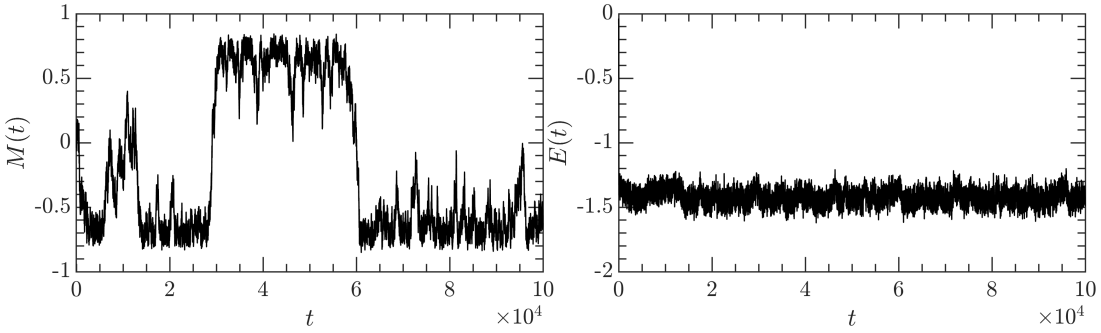

Figure 4.4: Time evolution of magnetization, here calculated as the sum of all spins in the system $M(t) = \sum_{k=1}^{K} \sigma_k$ (panel on the left-hand side) and the energy (panel on the right-hand side) for a two-dimensional Ising Model without an external magnetic field at temperature $T_c \approx 2.26$.

Worth noting is that the Metropolis algorithm works well for a limited range of temperatures. If the system has high temperature, $T \to \infty$ the probability of flipping the spin drifts toward 1, which, in practice, means that with every sweep spins are overturned. Such a process is the direct opposite of the *ergodicity* principle, which states that any state of the system should be reachable from any other state. In fact, however, many of the transition rates from and to a particular state can be zero, but given two arbitrary states u and v there should exist, at the very least, a single path of the transitions having non-zero rates and so able to connect them. An alternative dynamics, that lacks this defect, is Glauber dynamics [180]. It uses a single-flip transition rate defined as follows:

$$W_{u \to v} = (2\tau_0)^{-1}[1 + \sigma_k \tanh(E_k / k_B T)] \tag{4.13}$$

where $\sigma_k E_k$ is the energy of the kth spin in state u and τ_0 is a time required to attempt a spin-filp. Using Glauber dynamics, at a high temperature probability of flipping the spin approaches 1/2 (assuming $\tau_0 = 1$). Thus the process remains ergodic.

Another approach, commonly used in Ising-like models of sociological and economical systems, is called the *heatbath method*. Instead of calculating the change

in the energy between two spin configurations and then accepting or rejecting the new configuration, in the heatbath method, the spin direction is chosen randomly and compared with the Boltzmann probability of the trial configuration. For instance, assuming that each spin can have one of two different values $\sigma_k = +1$ with probability p_k and $\sigma_k = -1$ with probability $1 - p_k$, where:

$$p_k = \frac{\exp(2/k_B T) \sum_{j \in nn} \sigma_j}{1 + \exp(2/k_B T) \sum_{j \in nn} \sigma_j} \tag{4.14}$$

then by generating a random number r new state can be calculated: $\sigma'_k = \text{sign}(p_k - r)$. The probability of the spin's being up or down is the same as in Glauber dynamics, meaning that the process is ergodic; however, the implementation is slightly different:

$$\sigma'_k = \begin{cases} \text{sign}(r - (1 - p_k)) & \text{if } \sigma_k = +1 \\ \text{sign}(p_k - r) & \text{if } \sigma_k = -1 \end{cases}. \tag{4.15}$$

The heatbath algorithm is not very efficient, and other methods such as the Wolff algorithm [181] (which is a cluster flipping technique), typically yield better performances with acceptable levels of accuracy [167]. However, the heatbath method is useful in systems where determining the energy of the entire system is time-consuming, and the acceptance rate of the new configuration is relatively low. As mentioned previously, heatbath algorithm is commonly applied in Ising-like models of the sociological and economical systems, including models of financial markets; thus, it was used in the research being described herein and so appears in later sections of this dissertation.

4.3 Spin models of financial markets

Thanks to their simplicity and ability to reproduce complex phenomena, use of spin models of financial markets is now widely accepted in the economic mainstream. A significant portion of these models are rooted in the statistical mechanics and derive from the solutions commonly used in physics, including Ising and Percolation models. Combination of the local interactions, similar to Ising Hamiltonian, with finance specific components, appears to generate signals with properties resembling those observed in financial time series. The dynamics of such systems, coupled with their ability to perform simulation in, to some extent, controllable conditions, facilitates analysis of the processes governing the financial markets and the behaviour of its participants. Worth noting is that physics-inspired spin models are applied not only to simulate financial markets and related trading activity [182, 183], but also to reproduce different aspects of economy such as bankruptcies [184], systematic risk in the inter-bank lending system [185] or impact of the crisis on the global financial sector [186].

In this section, two fundamental agent-based frameworks inspired by Ising Model are examined in the context of reproducing stylized facts, including the hierarchical organization of the generated signals. Extra emphasis is placed on the strengths and weaknesses of these models as well as their practical applications.

4.3.1 Modified Random Field Ising Model

A common variation of the Ising Model successfully applied in financial market modeling is the modified Random Field Ising Model (RFIM) [187] proposed by Iori in 1999 [70]. The model is based on a two-dimensional lattice with periodic boundaries, where each site represents an agent that communicates with others according to the von Neumann neighbourhood. An individual's investment decision is represented by state S_x, and it is driven by the influence of the entities in the vicinity as well as two types of idiosyncratic noise:

$$Y_i(t) = \sum_{<i,j>} J_{ij} S_j(t) + A v_i + B\epsilon(t), \tag{4.16}$$

where $< i, j >$ is the sum over the nearest neighbours, J_{ij} is the influence coefficients matrix that describes the strength of the interactions between agents, and S_j is a spin of the j-th neighbour. The spin can assume one of three possible values $S_x \in \{-1, 0, 1\}$ that correspond to the three positions of an agent in the market: sell, on-hold and buy, respectively. The first component of the equation above, except for the extra possible state, is similar to the original Ising Model and represents the local interaction between the investors. The modification is in the consecutive components of the Hamiltonian. The v_i is a random signal, usually drawn from a uniform distribution and it is scaled by arbitrary constant A. This term corresponds to the individual investment preferences of a given agent and can empower the total signal $Y_i(t)$ or lessen it. In turn, this may lead an investor to assume a neutral or opposite state relative to the neighbours. Moreover, the behaviour of the individuals can be disrupted by the global signal $\epsilon(t)$, which in the basic version of the model, assume non-zero value drawn from a uniform distribution with probability $p_\epsilon \approx 0.01$ or else it is equal to 0. The global signal can be interpreted as financial news appearing on the market, which is accessible by all agents in the system. In general, the individual signal $Y_i(t)$ is composed of the local interaction component (i.e., the sum over the spins of the neighbours), which lead to the collective behaviour of agents and random signals (i.e., $v_i(t)$ and $\epsilon(t)$) which can amplify or weaken synchronization of the investment decisions among individuals.

As mentioned above, the model generalizes the traditional Ising Model introducing additional state $S_i = 0$, which represents inactive agents. In this context, the Iori model can be seen as the Potts Model with $q = 3$ [188]. Bringing the additional state in requires modification of the rules that determine the position of a particular agent in the market. In the considered framework, the following threshold mechanism was proposed:

$$S_i(t) = \begin{cases} -1 & \text{if } Y_i(t) \leq -\xi_i(t) \\ 0 & \text{if } -\xi_i(t) < Y_i(t) < \xi_i(t) \\ +1 & \text{if } Y_i(t) \geq \xi_i(t), \end{cases} \tag{4.17}$$

where threshold ξ_i can be interpreted as trade friction related to transaction costs or imperfect capacity to access information and is calculated based on its previous value and the price of the modeled asset: $\xi_i(t+1) = \frac{P(t+1)}{P(t)}\xi_i(t)$. Consequently, in periods of increased volatility, agents tend to stay inactive, which, in turn slows

down the dynamics of the entire system. On the other hand, in case of low volatility, the threshold drifts towards 0, and the system behaves more like the ferromagnetic material in the classic Ising Model.

Another innovation introduced by Iori relates to the interaction-strength matrix J_{ij}. In the field of statistical physics, it is commonly known that the dynamics of the system significantly depends on the J_{ij} values. In many models, the interactions are symmetrical; thus, the J_{ij} reduces to the scalar, or it is randomly chosen from a Gaussian distribution, as in the spin-glass model [189]. In the basic version of the Iori's model $J_{ij} = 1$ with probability p and $J_{ij} = 0$ with probability $1 - p$. Such a rule applied to the interaction strength matrix suggest associations to the Percolation model. Indeed, as shown in the following paragraphs and in study [70], system behaviour depends to a great extent on the assumed value of p, and the richest dynamic is observed for probability rates around percolation threshold $p \approx p_c$, which, for a two-dimensional lattice, is approximately $p_c \approx 0.6$.

Moreover, the model introduces another few modifications directly related to the organization of the financial markets. Each agent has a certain amount of money and stock shares to trade with the *market maker*, which is also limited in terms of resources. The ability to reproduce stylized facts, especially non-linear correlations, is not significantly affected by these rules. However, if there are insufficient resources in the system, an agent's activity declines substantially, and, in extreme cases, trading entirely disappears. More important in terms of the system dynamic is the information-propagation procedure. Each time step consists of multiple consultation rounds, in which the agents exchange information and assume one of the three possible states. These consultation rounds are executed according to the heat-bath algorithm and are repeated until the state of the system converges, meaning that in the two consecutive consultation rounds, no agent changes its state. When the individual investment preferences of agents stabilize, the orders are placed and then simultaneously cleared by the market maker. Finally, the price for the next time step is calculated as follows:

$$P(t+1) = P(t)\left(\frac{D(t)}{Z(t)}\right)^{\alpha_v}. \tag{4.18}$$

$D(t)$ and $Z(t)$ in the equation above are demand and supply measured as a normalized numbers of agents having states $S_i = +1$ and $S_i = -1$, respectively, whereas α_v describes the asymmetric reaction of the market maker to imbalanced orders placed in periods of high, versus low trading activity. This is calculated according to the formula: $\alpha_v = a\frac{D(t)+Z(t)}{N}$, where a is discretionary constant and N is the number of individuals in the system. After a full cycle has been performed as described above, agents update their thresholds ξ_i and next cycle begins. Assuming that the system is initialized with resources (money and stocks) and default individual thresholds $\xi_i(0)$, the simulation algorithm consists of the following steps:

1. Each agent receives individual and global signals ($v_i(t)$ and $\epsilon(t)$, respectively)
2. Entities update their states according to equation (4.17). This step is repeated until the system converges.
3. Orders are cleared by the market maker.

4. Based on the supply and demand, the price in the next time step is calculated.
5. Agents update their threshold values $\xi_i(t+1)$, and the entire procedure is repeated.

In the model under discussion, the ability to generate time series resembling those observed in the financial markets strongly depends on the probability of interaction between agents p and the individual investment preferences represented by factor Av_i. If the entities willingly communicate with agents in the vicinity (i.e., p value equal to or greater than percolation threshold $p_c \approx 0.6$), then collectivity increases, and thus, large fluctuations can form. On the other hand, when entities mostly rely on their individual investment preferences (i.e., the value of A is considerable), then the generated signal has a white-noise character. Based on these observations and the results presented in study [70], the further analysis of the model focuses on the variant that seems to be an optimal balance between agents' collectivity and independence ($p = 0.6$, $A = 0.2$ and $B = 0$).

As shown in Figure 4.6 (panel (a)) for selected parameters, the model reproduces the typical price trajectory observed on the financial markets and is able to form bubbles and crashes manifested by large fluctuations (e.g., in period $t \in [6 * 10^4, 8 * 10^4]$). Oscillations observed on the rates of return level obey the power law with slope $\mu \approx 3$ (Figure 4.6, panel (e)), a value commonly seen for real financial time series (see Figure 2.2). However, the system generates large fluctuations only for relatively low prices (less than 1). The reason for such behaviour is the threshold mechanism design and price impact function (equation 4.18). The thresholds $\xi_i(t)$ are based on the price ratio in subsequent time steps, which is not symmetrical. For example, assuming that $\xi_i(1) = 1$ and that price decreases by 20 percent in five consecutive time steps, $\xi_i(5) = 0.3277$, whereas in the opposite scenario, when price increases by 20 percent in five consecutive time steps $\xi_i(5) = 2.4883$. This asymmetry has a direct impact on the transaction volume. Low thresholds encourage agents to invest; thus, the total transaction volume in the system increases, and the α_v exponent in the price impact function reaches its maximum ($\alpha_v = a$), which in turn translates into large price fluctuations.

Such a construction of the threshold mechanism and price impact function led to an important problem, namely, model instability. Since the volatility clustering and other properties typical of the financial market appear in the time series generated by the model characterised by interaction probability close to the percolation threshold, quite commonly, at some point of the simulation, the system becomes dominated by one group of agents, usually those having sell positions on the market. If a large cluster of individuals having state $S_i = -1$ forms, then, accordingly to equation (4.18) the asset price drops. As a result, as shown in Figure 4.5, extremely low values of the price translates into large fluctuations observed on the rates of return level. Even though the system is usually able to recover from a non-stable regime (see price trajectory for $t \in [4.5 * 10^5, 5 * 10^5]$), such simulations must be rejected, significantly limiting the practical applications of the model.

Despite the limitations mentioned above, the returns generated by the stable realizations of the model, similarly to the ones observed in real financial markets, are not linearly correlated (see Figure 4.6, panel (b)), but show strong temporal dependence on the level of volatility signals (see Figure 4.6, panel (d)). The autocorrelation

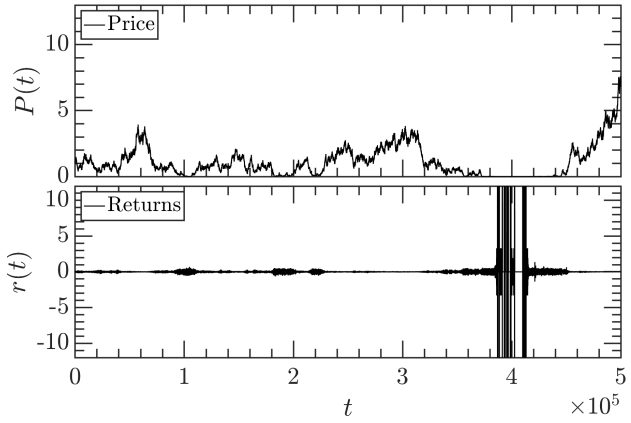

Figure 4.5: Example of unstable price signal (upper panel) and corresponding returns (bottom panel) generated by Iori's model. The system collapses in the period $t \in [3.7 * 10^5, 4.5 * 10^5]$.

function of the rates of return decreases immediately and does not exceed statistical significance thresholds (denoted by the red dotted lines), while absolute rates of return remain at relatively high levels for more than 10^4 time steps. Long-range nonlinear correlations of the returns are also visible on the fluctuations function level (see Figure 4.6, inset of panel (f)) which obeys the power law for scales $s \in [20, 10^4]$. Scaling of the fluctuations function translates into relatively wide singularity spectra (see Figure 4.6, panel (f), black dots) with width $\Delta\alpha \approx 0.21$ and strong left-hand side asymmetry $A_\alpha \approx 0.97$. In order to verify that the multifractality of the series generated by the model is not a spurious effect, singularity spectra of shuffled data (blue squares) and signal modified according to Fourier surrogate procedure (orange diamonds) were determined. In both cases, the $f(\alpha)$ is considerably narrower than for the original series, and hovers around $\Delta\alpha \approx 0.1$ for shuffled data and $\Delta\alpha \approx 0.03$ for Fourier surrogate.

In general, the Iori model is able to reproduce stylized facts, including long-range non-linear correlations. However, the hierarchical organization of the time series generated by the framework might not be sufficient to model dynamics of financial instruments characterized by a wide singularity spectrum, for which $\Delta\alpha > 0.3$. Moreover, model implementation, especially the sequential character of the consultation round, significantly impacts the computational effort and time required to generate sufficiently long time series that, combined with the instability issues described above, inhibit the use of the model in practice. Nevertheless, the relevance of this framework in the context of the analysis of multiscale correlations is indisputable, and the model itself constitutes a good foundation for further study of the subject.

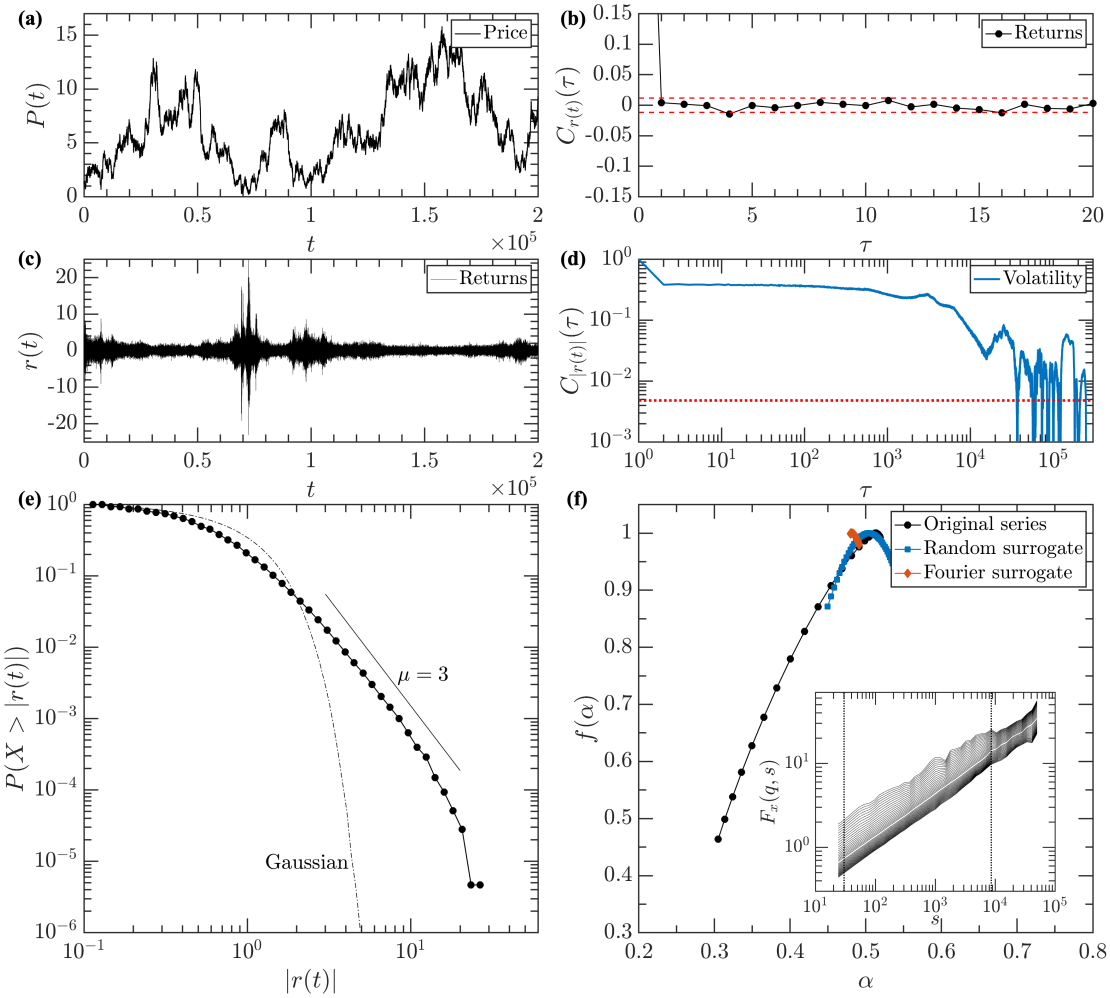

Figure 4.6: Statistical properties of the example of signal generated by the Iori's model based on the square lattice $L \times L = 100 \times 100$ and the following parameters: $p = 0.6, J = 0.2, A = 0.2, B = 0, a = 1.0$. Panel **(a)**: price trajectory, panel **(b)**: autocorrelation function of returns, panel **(c)**: rates of return, panel **(d)**: autocorrelation function of volatility, panel **(e)**: cumulative distribution function of absolute returns, panel **(f)**: singularity spectrum and corresponding fluctuations function (inset).

4.3.2 Fundamentalists and chartists in financial market modeling

Another group of spin models of financial markets that have had a profound influence on the further research in this area, are those that introduced division of the market participants into groups. In this section, two fundamental models, that incorporate such a division are examined. Next, one of these, namely Bornholdt's model [71] is investigated in the context of reproducing features observed in financial data.

The innovation of the first framework discussed here, the Lux-Marchesi model [190], relates to the division of the agents into two groups: fundamentalist, who follow the premise of the efficient market hypothesis, and chartists (also called noise traders), who can be associated with the technical traders that do not trust in the fundamental value of an asset. In practice, a fundamentalist trades the assets

in the belief that price follows imposed fundamental value, whereas chartists' investment decisions are driven by a so-called investment mood, which assumes two values: optimistic and pessimistic. Noise traders switch between possible moods with a probability defined as an exponential function. Moreover, agents are allowed to change their strategy, that is, they can change from being chartists to become fundamentalists and vice versa. Such a transition is driven by difference in profits between these groups as well as a transition probability factor. Naturally, agents prefer to belong to the group, having better performance. As a result, the number of individuals in these groups determines the difference between demand and supply, which in, turn causes price adjustments that affect an agent's choice of strategy. Such a feedback loop leads to permanent fluctuations in the number of agents in a particular group and works as a self-stabilizing mechanism, that does not allow all individuals to use the same strategy.

Interestingly, as shown in [191, 192], price fluctuations generated by the Lux-Marchesi model reveal non-trivial hierarchical organization and reproduce the non-linear correlations existing in financial time series. Moreover, the size of the fluctuations generated by the system is directly linked to the number of noise traders, and the periods of increased volatility interlace with times of lower agents activity. Theoretical analysis showed that the critical value that determines the dynamics of the system exists, and the system has the richest dynamics, when a number of noise traders drifts close to the critical value [190]. As in the Iori's model, large fluctuations generated by the Lux-Marchesi framework, result from continuous skirmishing of two different forces, where one support collective behaviour (chartist traders) and the other, that depending on the system's state, can amplify or weaken synchronization among agents (fundamentalists).

The Lux-Marchesi model well reflects the dynamics of financial markets and is able to reproduce a great deal of the stylized facts; however, from a practical point of view, it has one major drawback - complexity. Analysis of the model, which contains more than ten free, adjustable parameters, is inconvenient. This, among other factors, led Bornholdt to propose another, similar but simpler framework [71].

Bornholdt's model is based on the two-dimensional lattice, where each node is occupied by an agent that communicates with others according to von Neumann neighbourhood, and, similarly to the Lux-Marchesi model, individuals belong to one of two groups: fundamentalist or chartists (noise traders). The agent (spin) can assume one of two possible values, +1 and -1, which reflects buy and sell sentiments, respectively, and is determined by the following formula:

$$S_i(t+1) = \begin{cases} +1 & \text{with } p = 1/(1+\exp(-2\beta h_i(t))) \\ -1 & \text{with } 1-p, \end{cases} \tag{4.19}$$

where i is an index of the individual and its state calculation is based on a Boltzmann-like distribution, $h_i(t)$ is an individual signal received by the agent and β is an inverse temperature. In each iteration, performed with heatbath dynamics, the agents receive signal:

$$h_i(t) = \sum_{<i,j>} J_{ij} S_j - \alpha_c C_i(t) M(t), \tag{4.20}$$

where the first component is the local Ising Hamiltonian with nearest neighbours interactions. In the basic version, interaction strength matrix J_{ij} reduces to a scalar and typically $J_{ij} = J = 1$. The second term is related to *global coupling* and consists of the magnetization $M(t) = \frac{1}{N}\sum_{j=1}^{N} S_j(t)$ scaled by a discretionary constant $\alpha_c > 0$, where N donates the number of the spins in the system. Agent's strategies are represented by coefficient $C_i(t)$, which assumes one of two values +1 and -1. $C_i(t) = 1$ corresponds to anti-ferromagnetic global coupling and reflects fundamentalists who desire to join global minority in order to invest in possible future gains [71], whereas $C_i(t) = 1$ corresponds to ferromagnetic global coupling characteristic of the chartist traders, who tend to follow the trend on the market. If all agents in the system follow the same strategy, in other words, have the same value of $C_i(t)$ coefficient, the system dynamic is not very intriguing as $C_i(t) = 1$ lead to full oneness of the agents, even for temperatures lower than critical, while for $C_i(t) = -1$, in every single iteration of the heatbath algorithm, each spin is flipped to the opposite value. The time evolution of the system becomes much more complex once agents follow different strategies and are allowed to change them. The simplest possible scenario proposed by Bornholdt is that agents in the majority group may often tend to join the minority and vice versa. In the context of financial markets, this corresponds to the situation in which the majority opt to trade against the market for future prospective gains or to escape a future crash, while traders in the minority group are not satisfied with present returns and desire to follow the global trend. Formally, assuming that the change in the strategy can be performed instantaneously, without costs, the rules of the transition can be formulated as follows: $C_i(t) = S_i(t)$, and then the signal received by each agent has the form:

$$h_i(t) = \sum_{<i,j>} J_{ij} S_j - \alpha_c S_i(t)|M(t)|. \tag{4.21}$$

As in the models studied previously, the signal $h_i(t)$ that drives agents investment decisions is composed of two different components, representing possibly conflicting forces. The local interaction component leads to the collective behaviour of the agents, while the second term (global coupling) can encourage individuals to join the minority/majority and, as a result, amplify or weaken the signal $h_i(t)$.

Model dynamic is characterized by metastable phases, where periods of relative stability of the system interlace with intermittent phases of rapid rearrangements. Figure 4.7 shows snapshots of the system configuration extracted from an example simulation performed with the following parameters: $T = 1/\beta = 0.625$, $J = 1$, $\alpha_c = 30$, and lattice size $L = 120$.

The fluctuations of magnetization generated by the model have characteristics similar to those observed in financial time series, especially when the temperature is relatively low. Assuming that rate of return is equal to the difference of magnetization in consecutive time steps $r(t) = M(t) - M(t-1)$, periods of increased activity of the agents translates into increased volatility. As shown in Figure 4.8 (panel (e)), the distribution of the fluctuations, to some extent, obeys the power law, and has two different regimes. In the first regime, which includes returns $r(t) \in [1, 7]$, slope $\mu \approx 2$, while, the tails of the distribution are thinner - $\mu \approx 5$. Importantly, the generated signal is not linearly correlated. The autocorrelation function of the

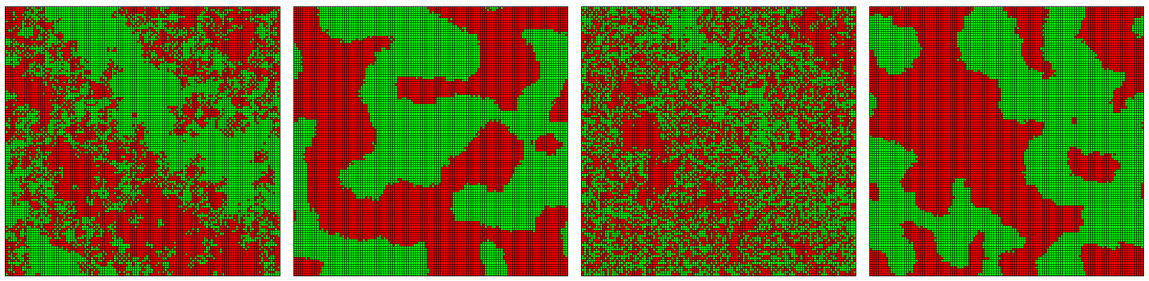

Figure 4.7: Snapshots of system configuration at temperature $T = 0.625$ ($\beta = 1.6$). Each square represents an agent, and the color indicates agent's state: green - $S_i(t) = 1$, red - $S_i(t) = -1$. First and third snapshots were taken during rearrangement periods, when the magnetization of the system fluctuates significantly. The second and fourth panel show configuration of the system in the metastable phase.

returns (see Figure 4.8, panel (b)) disappears after a few time steps and does not exceed statistically significant thresholds. Weak negative linear dependence is observed for small lags $\tau \in [1, 3]$, meaning that positive and negative returns are likely to interlace, a behaviour also observed in financial time series, especially when high-frequency data is considered (see Figure 2.3). Moreover, the fluctuation clustering present in the signal reveals itself in the long-range correlations of the absolute returns (Figure 4.8, panel (d)). In this case, self-dependencies last for more than 10^3 time steps, which is similar to that observed in the daily returns of common indices and stock shares (see Figure 2.4). Non-linear correlations of the produced returns are also manifested by the relatively wide singularity spectrum (panel (f)) which for the considered signal has width $\Delta\alpha \approx 0.24$, reveals left-hand side asymmetry $A_\alpha \approx 0.37$, while the Hurst exponent indicates weak negative autocorrelation $H \approx 0.45$. In order to confirm that the multifractality of the generated returns is not a spurious effect, the singularity spectra of shuffled data and Fourier surrogate were calculated. In both cases, the spectra obtained were significantly narrower and even converged to the point for Fourier surrogate ($\Delta\alpha \approx 0.04$ and $\Delta\alpha \approx 0.01$ for shuffled data and Fourier surrogate respectively).

The model proposed by Bornholdt is capable of producing signals that, to some degree resemble features observed in real financial time series. The major drawback of this framework is the inability to generate fluctuations characterized by extra rich hierarchical organization ($\Delta\alpha > 0.3$), which substantially limits the spectrum of possible practical applications. Also, worth noting is that, in this model agent state is reduced to only sell and buy (-1 and +1, respectively), and it does consider that investor might be out of the market. That in turn can influence the dynamic of the system, and potentially affects correlations in the generated signals.

Analysis of the popular Ising-inspired spin models of financial markets shows that frameworks of this type, despite their simplicity, are able, to some degree reproduce complex phenomena appearing in financial markets. Even though the models discussed above differ from each other, the common element can be extracted. The signal which drives the investment decision of the agent consists of two types of components where one supports collective behaviour (local) and the other can stand in opposition or amplify the herding (global). Such a composition of two, to some

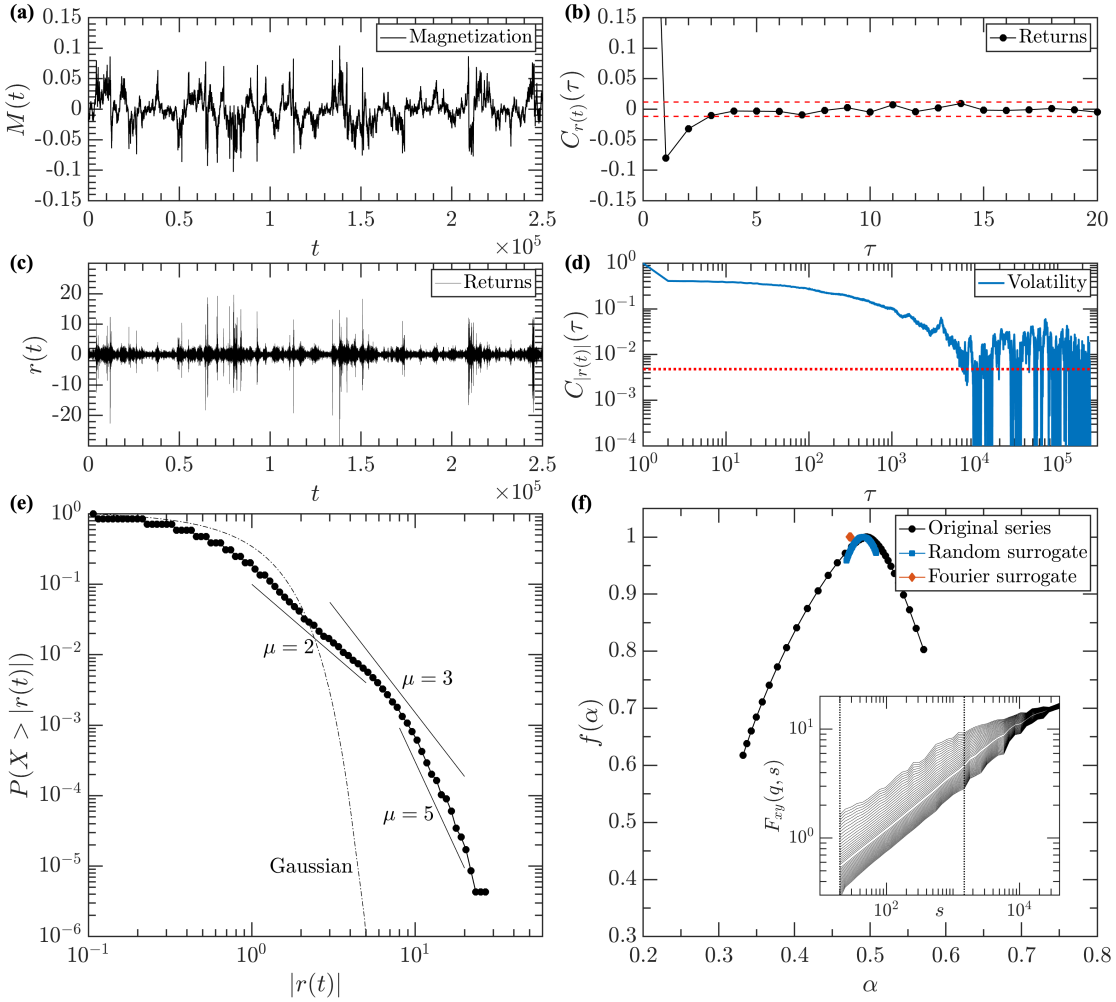

Figure 4.8: Statistical and multifractal properties of signal generated by the Bornholdt's model with the following parameters: $T = 1/\beta = 0.5$, $J_{ij} = J = 1$, $\alpha_c = 30$, and lattice size $L \times L = 120 \times 120$. Panel **(a)**: magnetization; panel **(b)**: autocorrelation function of returns (red dotted line denotes the noise regime); panel **(c)**: rates of return; panel **(d)**: volatility autocorrelation function (red dotted line denotes noise level); panel **(e)**: absolute returns cumulative distribution; panel **(f)** singularity spectrum of the returns (black dots) and shuffled signal (blue squares), and series modified according to Fourier surrogate method (orange diamonds). The inset plot contains fluctuations function of the generated signal, with black dotted lines denoting range of scaling.

degree, antagonistic forces leads to significant fluctuations of the entire system that, in their nature are similar to these observed during the phase transitions. More precisely, the system undergoes multiple phase transitions from ordered to disarranged state and vice versa. Based on these observations and known limitations of the presented models, in the next chapter, the generalized multi-asset, three-state model of the financial market is proposed.

Chapter 5

Multi-asset three-state model of financial market

The increasing popularity of ABMs inspired by physical phenomena, such as spontaneous magnetization in ferromagnetic materials, has led to development of multiple models, that are able to reproduce stylized facts observed in financial time series. As shown in previous sections and in study [193], not all of these solutions are able to reproduce the extremely rich hierarchical organization of returns signals. Moreover, some of the frameworks (e.g., Iori's model) have significant stability issues that limit their usefulness in practical applications.

Given these gaps, in this chapter, a new **multi-asset three-state model of financial market** is proposed. Design of this framework focuses on the ability to produce time series characterised by multiscale autocorrelations and cross-correlations. The following paragraphs describe the model and present statistical and multifractal properties of an example of the signal produced by the framework.

5.1 Motivation

In agent-based models, the ability to generate fluctuations characterized by a rich hierarchical structure could be linked with system criticality. As known from physics, power law characteristics and other free-scale features are intensified in a near-critical state of a system [194]. This has profound consequences on the practical applications of such models. Since the systems in the near-critical state are usually unstable, these models are not able to repeatedly generate signals characterized by similar statistical properties. This, in turn, affects the ability to study dynamics of these models. For example, the framework proposed by Iori, which, as shown in the previous chapter, is able to produce fluctuations characterized by non-linear, long-range correlations manifested by relatively wide singularity spectrum ($\Delta\alpha \approx 0.21$), however, these properties develop for interaction probabilities close to the percolation threshold, a not stable regime of the model. Simulations performed for the sub-critical value of the interaction probability quite often collapse, leading in turn to the dramatic decrease in modeled asset price and huge fluctuations (see Figure 4.5). Instability of the model combined with sequential character of the consultation round significantly reduce its usefulness in practical applications.

Nonetheless, multiple models are able to reproduce complex phenomena in a more repeatable manner, even for sub-critical values of the parameters. Many of them, similarly to the Lux-Marchesi model [190], are quite complicated due to the number of free parameters they contain. In turn, these models are more difficult to analyse and explicit identification of the source of the long-range, non-linear correlations in generated time series is tough. The framework proposed by Bornholdt constitutes a compromise between model complexity and the ability to produce multifractal signals. As was already shown in previous chapter (see Figure 4.8) and other studies [195, 196], Bornholdt model properly reproduces the most important stylized facts. However, like the Iori model, it is not able to generate time series characterized by extra rich hierarchical organization, manifested by wide singularity spectrum ($\Delta\alpha > 0.3$). Moreover, it does not consider some facts concerning financial market mechanisms, that are crucial from the perspective of the system dynamics and multifractality of the generated signals.

First, the model is based on the assumption that there are only two possible states of an agent, namely buy and sell. It ignores that investors might be out of the market, meaning that they do not actively participating in trading at a given point in time. Multiple reasons account for such behaviour of market participants, but the primary factor is the risk aversion. Well established is that many investors, especially those with a conservative, defensive approach to trading, avoid risk to the greatest extent possible. During a crisis, such investors move their funds to less risky instruments such as bonds or term deposits [197] or simply cash their assets out. On the other hand, a substantial number of market participants are professional, short-term speculators who prefer a volatile market since, higher risk typically goes hand in hand with the potential for higher profits.

Furthermore, similar to most of the spin models of financial markets, Bornholdt framework is limited to single-asset modeling and does not consider inter-asset dependencies. Investors usually trade multiple assets at the same time in an attempt to build an optimal, diversified portfolios, that fit their risk preferences. Hence, dependencies between assets have a significant impact on investors' investment decisions [51]. As an example, traders with high exposure to the commodity market avoid buying shares of companies from the mining industry. Such interdependencies occur not only between different asset classes (e.g., currency and shares, commodity and shares) but are also present within the same group of financial instruments. A typical example are correlations between assets belonging to the same sector, which, as shown in Chapter Three, can have linear and non-linear nature.

5.2 Model description

Given the gaps present in Bornholdt's model, the practical inconveniences inherent in use of the Iori's solution, and the complexity of other framework such as the Lux-Marchesi, new, generalized multi-asset three-state model of financial market is proposed. In the model agents are located on the square lattice with periodical boundaries and von Neumann neighbourhood. The agent can trade multiple assets at the same time, and on each of them (denoted by m) assume one of the three states, represented by the spin $S_x^{(m)} \in \{-1, 0, 1\}$, respectively. From the topological

perspective, the entire system can be perceived as a set of subsystems (lattices) linked together, where each subsystem reflects a single asset (see Figure 5.1). Spins in each subsystem are updated according to the following heatbath dynamics:

$$S_i^{(m)}(t+1) = \begin{cases} 0 & \text{if } -\kappa^{(m)}(t) < h_i^{(m)}(t) < \kappa^{(m)}(t) \\ & \text{else} \\ +1 & \text{with } p = 1/\left(1+\exp\left(-2\beta h_i^{(m)}(t)\right)\right) \\ -1 & \text{with } 1-p, \end{cases} \tag{5.1}$$

where $\beta = 1/T$ is the inverse temperature, $h_i^{(m)}(t)$ is the signal that agent i receives at given point of time t, and m is the record number of the traded asset (subsystem). As in Iori's model, the individual assumes on-hold state $S_i^{(m)}(t) = 0$ if the received signal does not exceed threshold $\kappa^{(m)}(t)$. The threshold itself is calculated as follows:

$$\kappa^{(m)}(t) = \kappa_c \frac{V^{(m)}(t-1)}{N}, \tag{5.2}$$

where κ_c is an arbitrary constant, $V^{(m)}(t-1) = N_+^{(m)}(t-1) + N_-^{(m)}(t-1)$ is the trading volume calculated by summing number of spins in subsystem m that have changed to $S_i^{(m)} = +1$ ($N_+^{(m)}(t-1)$) or to $S_i^{(m)} = -1$ ($N_+^{(m)}(t-1)$), and N is the total number of agents in the system. This definition of the trading threshold reflects mechanisms observed in real financial markets. In a period marked by high volatility, when many agents change positions, the threshold increases, and some individuals assume an on-hold state (also called out of the market state). On the other hand, when the market is quiet and price fluctuations are small, the value of $\kappa^{(m)}(t)$ decreases, and agents more willingly assume an active position. In the proposed definition of the threshold, the market dynamic is quantified by the transaction volume. In general, any other variable that captures the activity of traders can be used (e.g., rates of return). This procedure of determining the trading threshold is, similar to that proposed by Sieczka and Hołyst [198], where the threshold value is based on the absolute magnetization of the system in the previous time step $\kappa(t) \sim |M(t-1)|$. The primary difference between the approach proposed in [198] and the method introduced here is that former assumes investors to be less likely to trade extremely cheap/expensive stocks, whereas the procedure introduced here is based on the assumption that some investors are afraid of a market volatility, rather than the high or low pricing of an asset. Also worth noting is that, by distinguishing between positive and negative volume (i.e., agents that change state to positive or to negative, respectively), formula (5.2) can be modified to introduce asymmetric thresholds that vary with regard to the negative and positive value of the signal received by the agent and thus more granularly model agent's risk aversion.

The central element of the model that drives agents behaviour is signal $h_i^{(m)}$,

which individuals receive in each time step:

$$h_i^{(m)}(t) = \overbrace{\sum_{l=1}^{K} \underbrace{\sum_{<i,j>} J_{ij}^{lm} S_j^l(t)}_{\text{agent-agent local interaction}}}^{\text{agent-agent cross-asset local interaction}} - \underbrace{\alpha_c C_i^{(m)}(t)|M^{(m)}(t)|}_{\text{global coupling}} + \underbrace{\sum_{l=1, l\neq m}^{K} \gamma_{lm} M^l(t-1)}_{\text{inter-asset global coupling}}. \quad (5.3)$$

The primary innovation introduced here is an extension that allows simulation of multiple linked assets. As mentioned above, the model assumes that agents can trade K different assets at the same time. Investment decisions of agent i regarding asset m are determined by the signals $h_i^{(m)}$ calculated per financial instrument. The first term of the formula (5.3), is a modified version of the Ising Hamiltonian, which incorporates interaction with the neighbours on the level of a single subsystem (i.e., agent-agent local interaction, where $< i, j >$ denotes nearest neighbours) and also different subsystems (i.e., agent-agent cross-asset interaction at local scale, where l denotes considered subsystem). Interactions are weighted by four-dimensional influence strength matrix J_{ij}^{lm} that assumes non-zero values only for the agents in the vicinity of the individual under consideration.

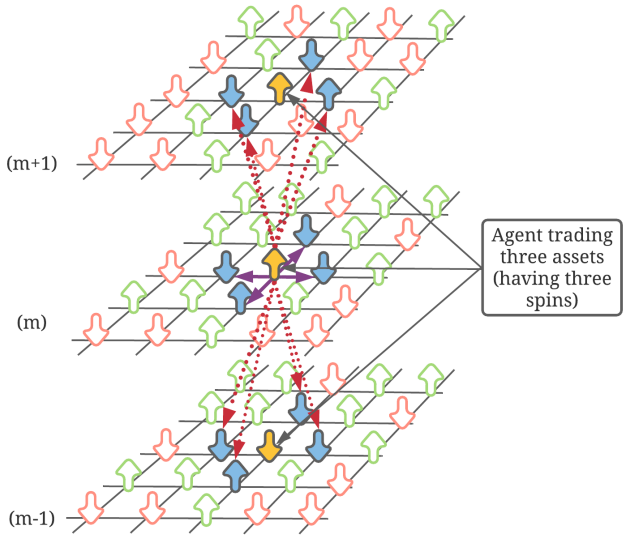

Figure 5.1: Schema of model that consists of three subsystems (i.e., models three assets). The yellow arrows indicate the agent under consideration and blue marks its neighbours' spins. Purple arrows indicate agent-agent local interaction between individual and its neighbours within considered subsystem. Red arrows show how agent interacts with the neighbours on the cross-asset level (i.e., agent-agent cross-asset local interaction).

The second component is similar to the one introduced in Bornholdt's model and represents global coupling to the magnetization of the given subsystem (i.e., global coupling term in equation 5.3). It reflects the different strategies adopted by agents: fundamentalists $C_i(t) = +1$ who, in addition to the ferromagnetic signal received from neighbours, prefer joining the subsystem minority, and chartists $C_i(t) = -1$

who follow the global trend and imitate the trading actions taken by the subsystem majority. Naturally, agents are allowed to change their strategies. Here, the simplest possible transition rule is adopted. Agents in the minority prefer joining the majority and vice versa, stated mathematically: $C_i^{(m)}(t) = S_i^{(m)}(t)$.

Moreover, the agents are influenced by the magnetization of other subsystems, which is reflected in the last component of formula (5.3). A similar term was originally proposed by Takaishi [199] as a form of global connection between assets. Coupling strength is controlled by matrix γ_{lm}, which assumes positive values for the correlated financial instruments, negative for anti-correlated stocks, and zero for independent assets. Such a linkage between different assets can exert considerable influence over system dynamics. For example, given two positively correlated instruments A and B, large magnetization of asset B, causes increase of the individual signal $h_i^A(t)$ that agents receive when trading asset A. As a result, individuals are more likely to buy the asset A rather than sell it, since $h_i^A(t)$ assumes higher values (analogously for negative magnetization of subsystem B). In general, depending on the γ_{AB} (γ_{BA}) values, magnetization trajectories of coupled assets tends to align (or disharmonize).

Based on individual signals $h_i^{(m)}(t)$ the magnetizations in subsystems are determined as follows: $M^{(m)}(t) = 1/N \sum_i^N S_i^{(m)}(t)$, where N is the number of agents in the system. Next, the returns are calculated $r^{(m)}(t) = M^{(m)}(t) - M^{(m)}(t-1)$, and standardized. It is worth noting that correlation properties of the signals generated by the model are influenced by the number of simulated agents, as larger number of entities translates into granularity of rates of return. On the other hand, excessive number of entities in the system significantly increase computational effort required to perform simulation. In the preliminary study of the model it was checked, that to generate stable, complex signals and fulfill technical requirements the reasonable size of the lattice is $L = 120$ (thus the system contains $N = 14400$ agents).

Simulation of the model where multiple assets are considered at the same time could also lead to extra concurrency issues. It is sufficient to look at formula (5.3) to notice that the signal $h_i^{(m)}(t)$ is determined based on the magnetization and spins at step t. However, when the individual signal for a particular agent is being calculated, other spins might not be updated. Combining it with a sequential procedure, where agents are visited one by one, always in the same order, may produce artificial regularities. In order to avoid such a behaviour of the system, spins are updated in random order.

Moreover, the same type of issue may arise on the cross-asset level since the last component of formula (5.3) depends on the magnetization of other subsystems. If assets are always updated in the same order, the subsystem that is revised in the first place is favored. As a result, instruments updated later follow the ones which were considered earlier (depending on the values of γ_{lm}). Again, to avoid such an artificial effect and fully control the global coupling between assets using γ_{lm} matrix, the magnetization in the cross-asset global interaction component of equation (5.3) is shifted in time $M(t-1)$. It is worth noting that without the time shift and by visiting the subsystems in random order, one can obtain similar results; however, in such a scenario, a detailed analysis of the model on the microscopic level as well as debugging is handicapped.

In general, model design is based on a combination of two types of interactions on two different levels. Namely, on the single subsystem level, agents interact with other individuals in their neighbourhoods (agent-agent local interaction term in the equation (5.3)) and their decisions are also influenced by the magnetization of a given subsystem, which can be interpreted as an average sentiment of agents regarding that asset (global coupling term in the equation (5.3)). The second level of the information propagation within the model is based on the inter-subsystem (inter-asset) interactions. Again, two types of forces come into play here, namely: agent-agent cross-asset local interaction, which is an extension of agent-agent local interaction, and inter-asset global coupling, which allows agents to obtain averaged information about positions of individuals on different assets.

Model that incorporates such a combination of interactions, can generate series characterized by non-linear autocorrelations and rich hierarchical organization on the cross-signal level. Moreover, the proposed model distinguishes itself as a highly reducible solution. For instance, considering a single subsystem (i.e., $K = 1$), automatically three state variation of Bornholdt's model is obtained, whereas, by additional assumption that $\kappa_c = 0$, the original version is recreated. Such extensible construction facilitates verification of the influence of particular parameters on system dynamics and the multi-scale correlations of the generated signals.

Figure 5.2 shows the characteristics of an example of signal generated by the model, in a basic, single-asset scenario with parameters $\beta = 2.0$, $J_{ij}^{11} = 1.0$, $\alpha_c = 30$ and $\kappa_c = 0.5$. The simulation was based on a two-dimensional square lattice with $N = 14400$ agents interacting according to a von Neumann neighbourhood. The total length of the signal was $3*10^5$ time steps; however first $0.5*10^5$ was considered as a system thermalization period and omitted. Thus, the effective length of the analysed signal is $2.5 * 10^5$.

The fluctuations generated by the model reveal strong clustering (panel (c)), while the distribution of the absolute returns, to some degree, obeys the power law with slope $\mu \approx 2.5$ in the middle section and $\mu \approx 6$ for the tail (panel (e)). Importantly, clustering of generated signals is also manifested by long-range correlation of the absolute returns, lasting $\tau \sim 10^4$ time steps (panel (d)), while the autocorrelation of the returns, for lag τ greater than two time steps does not exceed the statistical significance thresholds (panel (b)). Moreover, the proposed model generates signals characterized by rich hierarchical structure manifested by wide singularity spectrum $\Delta\alpha \approx 0.36$ with left-hand side asymmetry $A_\alpha \approx 0.37$ (panel (e)). In addition, the power law dependency of fluctuations function is observed for large range of scales $s \in [50, 4780]$ (inset of panel (e)). In order to verify that the multifractality of the generated signals is not a spurious effect, spectra of shuffled series (blue squares) and Fourier surrogates (orange diamonds) were determined. In both cases, $f(\alpha)$ function is significantly narrower than for original signal, exhibiting widths $\Delta\alpha \approx 0.07$ and $\Delta\alpha \approx 0.01$, respectively.

Introduction of a third possible state of the agent ($S_i^{(m)}(t) = 0$ - on-hold state) clearly impacts the multifractal characteristics of the generated signal, as manifested by a significant increase of the singularity spectrum width (i.e., from $\Delta\alpha \approx 0.24$ for Bornholdt's model to $\Delta\alpha \approx 0.36$ for proposed framework). Importantly, other statistical properties, including absolute returns distribution and returns linear de-

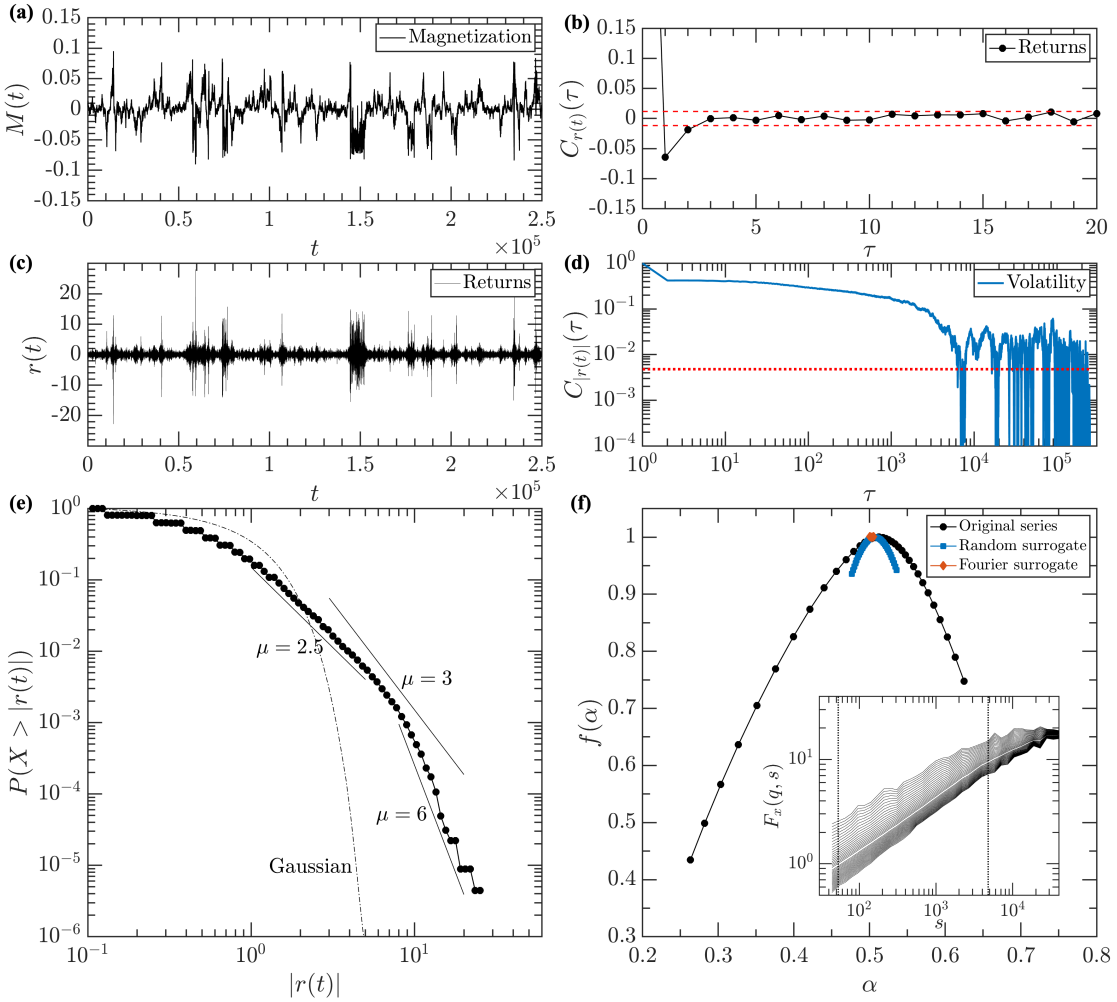

Figure 5.2: Statistical and multifractal properties of time series generated by the single-asset variant ($K = 1$) of the three-state multi-asset model with the following parameters: $\beta = 2.0$, $J_{ij}^{11} = 1$, $\alpha_c = 30$, and $\kappa_c = 0.5$. Panel **(a)**: magnetization; panel **(b)**: autocorrelation function of returns (red dotted line denotes the noise regime); panel **(c)**: rate of returns; panel **(d)**: volatility autocorrelation function (red dotted line indicates the noise regime); panel **(e)**: absolute rate of returns cumulative distribution; panel **(f)**: singularity spectrum of the returns (black dots) and shuffled signal (blue squares), and series modified according to Fourier surrogate method (orange diamonds). The inset plot contains fluctuations function of the original signal and black dotted lines denote the scaling range.

pendencies remained almost unchanged. Moreover, the choice of κ_c parameter value (here $\kappa_c = 0.5$, which is the model's default value) significantly affects the features of generated time series. The relation between the richness of produced signals and the threshold value is discussed in details in further sections of this dissertation.

Chapter 6

Multiscale analysis of the single-asset model variant

As shown in the previous section, proposed model can generate time series characterised by rich hierarchical organization ($\Delta\alpha > 0.3$). In the context of this result, two fundamental questions arise: Firstly, what is the model's dynamics, and how it translates into fluctuations clustering in the generated signals? Secondly, how particular parameters of the model affect the hierarchical organization of the produced time series? This chapter addresses these two major questions. Based on an investigation of the model dynamics, the elements of the framework that are responsible for the multifractality in generated signals were identified. Moreover, in the following subsections, each parameter of the single-asset variant of the framework is examined in the context of its impact on stylized facts, including non-linear autocorrelations[1].

6.1 Microscale dynamics of the model and fluctuations clustering effect

Multifractality of time series is inextricably linked with fluctuations clustering, meaning that signal can exhibit multiscale properties only if fluctuations of similar sizes are grouped together. In the model, fluctuations clustering is related to changes in the system configuration. This section comprehensively describes the microscale dynamic of the model and shows how it translates to clustering observed in the signals it produces.

In general, dynamics of the multi-asset three-state model can be described as interlaced periods of meta-stability and rearrangement phases (also called turbulent phases). The panels in section (a) of Figure 6.1, show the snapshots of system configuration in the meta-stable phases (outer panels) and during the turbulent periods (inner panels). The green, white, and red colors indicate agents having states +1, 0, and -1, respectively. The difference on the microscopic level is clearly visible. During the meta-stable phase, agents form large, relatively stable clusters of individuals with the same position in the market. Some fluctuations of the agent states exist

[1]Since the single-asset variant of the model is considered in this chapter $K = 1$, $m = l = 1$ and $\gamma_{lm} = 0$ in all equations and figures.

only on the boundaries of the clusters, as entities located in this area typically receive ambiguous signals from neighbours and, in turn, make investment decision in a more random manner. Mathematically speaking, for these agents, the local interaction term in the individual signal formula (see equation (5.3)) typically assumes value 0, and, in turn $h_i^{(m)}(t)$ has a relatively low value. In such a scenario, the probability function p, used for calculating a particular spin (see equation (5.1)) is closer 0.5, and thus, spin can assume value +1 or -1 with almost equal probability. Moreover, during a meta-stable period, agents view the market situation as nonhazardous, and, therefore, all individuals have active positions - either sell or buy. Naturally, such behaviour of entities results from the threshold mechanism construction and assumed κ_c value (here, it was set to default value of $\kappa_c = 0.5$). When the number of agents that change state in consecutive time steps is low, then transaction volume in the system is exiguous as well. In turn, the value of the threshold $\kappa^{(m)}(t)$ approaches 0. As the trading friction almost disappears, the number of agents being out of the market also vanishes.

System dynamics in a turbulent period is dramatically different. In this case, clusters of the agents having the same state are considerably smaller and are usually separated by an area of inactive individuals. During the rearrangement phase, entities that are not part of a cluster, willingly change their position in the market, causing total transaction volume to increase. In turn, according to equation 5.2, threshold $\kappa^{(m)}(t)$ rise as well, and the number of individuals who are out of the market increases. This behaviour corresponds to the situation in which investors avoid financial risk exposure due to high market volatility and the hazards associated with it.

The spin configurations observed during meta-stable and rearrangement periods, to some extent, resemble the behaviour of the physical systems in different phases. Large clusters of individuals having the same state, that are observed when the system is relatively stable, signifies the order existing among entities. On the other hand, during a rearrangement period, this order is, at least partially, broken. This effect is manifested by smaller clusters of the individuals characterised by the same state and through a substantial number of agents that assume on-hold position, scattered among the system.

On the microscopic level, analogous dynamics can be observed in ferromagnetic materials, for which, below the critical temperature, the order parameter has a non-zero value (i.e., the spontaneous magnetization occurs), whereas above this temperature, it drops to zero. The primary difference between ferromagnetic materials modeled using the Ising Model, and the proposed solution is the non-deterministic character of the phase transitions in the latter framework. In the multi-asset, three-state model, for a given temperature the system undergoes multiple phase transitions, moving from an ordered to an unordered state (and vice versa), and doing so in unpredictable manner.

The distinction between dynamics of the system in different phases is also visible in the fraction of agents having a particular value of the individual signal $h_i^{(m)}(t)$. The panels in section (b) of Figure 6.1 depict the normalized histogram of individuals depending on $h_i^{(m)}(t)$. The charts presented correspond to the system configuration snapshots discussed previously, and by colored, dashed lines are mapped to the

certain rates of return showed in the panel below (section (c)). For the three-state, single-asset variant of the model with two-dimensional lattice topology and von Neumann neighbourhood, the possible individual signal that agent can receive, depends on two factors. First one is the signal received from the entities in the vicinity (see first term of equation (5.3)), which for, $J_{ij}^{lm} = J = 1$, can assume values $[-4, -3, ..., 3, 4]$. The second, which shifts the resultant individual signal towards negative or positive values, is proportional to the magnetization (see the global coupling term of equation (5.3)). These two components reveal themselves in the location of $h_i^{(m)}(t)$ histogram's bars; they are located relative to reference points determined by the signal received from agents in the neighbourhood and are shifted proportionally to the magnetization.

Naturally, the polarized histogram of the individual signal, with peaks corresponding to two edge values of a possible signal coming from neighbours ($h_i^{(m)} \pm 4$), manifests the large clusters of agents having the same spin observed during the meta-stable phase. Moreover, as only entities located on the boundaries of the clusters can have $h_i^{(m)}$ values relatively close to 0, the inner bars of the histogram are significantly lower. Such a distribution of an agent's individual signal, combined with the probability function p used to determine the agent's state, results in the low fluctuations observed on the system magnetization level. On the other hand, during system rearrangements, the lack of large clusters of individuals having the same state translates into a Gaussian-like shape of the $h_i^{(m)}$ histogram. In such a situation, the probability of flipping a spin is high for a substantial number of agents. As these individuals frequently change the state, thereby possibly causing a significant imbalance between supply and demand and, consequently, leading to large fluctuations of the system magnetization.

As mentioned previously, high trading activity of agents impacts the values of $\kappa^{(m)}(t)$, which, on the histograms are denoted by black dotted lines. Clearly visible is that in the meta-stable phase, the thresholds drift towards 0, and none of the individuals assume an on-hold state. In the turbulent period, when trading is intensive, $\kappa^{(m)}(t)$ rises and numerous agents that receive ambiguous signals stay out of the market. In the context of the system dynamics, the threshold mechanism has a dual nature. On the one hand, it enriches system dynamics, as the number of possible configurations increases; on the other hand, during the rearrangement phase, a dozen agents assume on-hold position, resulting in the cooling down of the entire system (i.e., decrease in agent's trading activity).

The intermittent character of system dynamics is also visible in the time evolution of the individual signal distribution. Panel (d) of Figure 6.1 shows the two-dimensional, grayscale projection of $h_i^{(m)}(t)$ values over time, with color intensity indicating the number of agents having a particular value of individual signal. During a meta-stable phase (e.g., $t \in [10^4, 3 * 10^4]$), strong polarization with relatively small fluctuations of the individual signal value is observed, whereas, in a rearrangement period (e.g., $t \in [3.3 * 10^4, 4.6 * 10^4]$), the spectrum of assumed $h_i^{(m)}$ is significantly wider.

In terms of the fluctuations generated by the model, the crucial observation is relation between shape of the $h_i^{(m)}$ histogram and size of returns. Gaussian-like shape of $h_i^{(m)}$ histogram corresponds to large fluctuations, while polarized one,

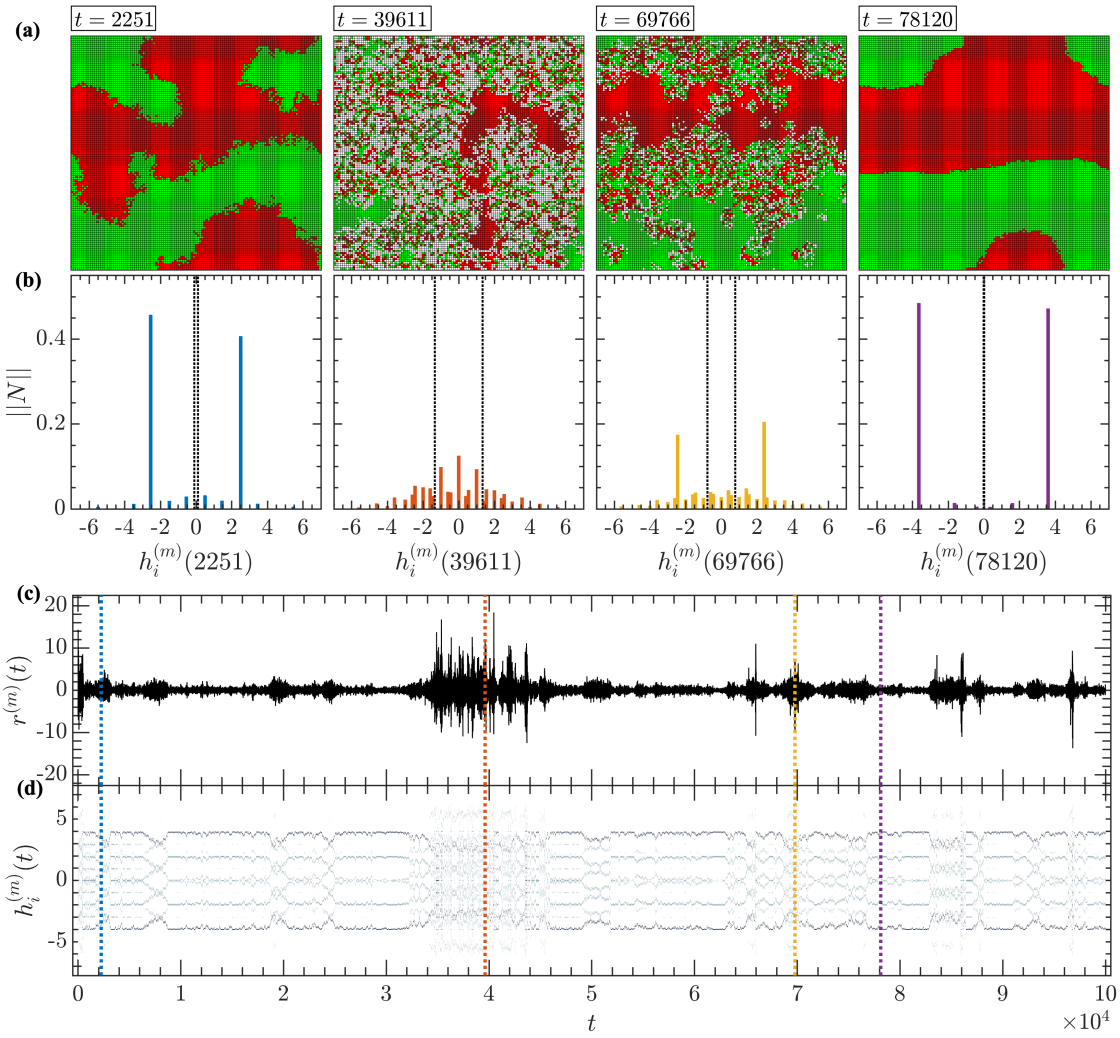

Figure 6.1: Dynamics of the single-asset variant of the model with parameters $\beta = 2.0$, $J_{ij}^{lm} = 1$ $\alpha_c = 30$, and $\kappa_c = 2.0$. Panels in section **(a)** present snapshots of system configuration in meta-stable phase (outer panels) and rearrangement periods (inner panels). Color of square indicates the state of an agent: red - $S_i^{(m)} = -1$, green - $S_i^{(m)} = +1$ and white - $S_i^{(m)} = 0$. Panels in section **(b)** display corresponding normalized histogram of agents having particular values of individual signal $h_i^{(m)}$ captured at certain time steps. Thresholds $\kappa^{(m)}(t)$ are denoted by black dotted lines. Panel in section **(c)** displays returns signal. Panel in section **(d)** presents two dimensional, grayscale projection of the time evolution of the individual signal. The intensity of the color indicates the number of agents having particular value of $h_i^{(m)}(t)$. Vertical colored lines in sections **(c)** and **(d)** corresponds to $h_i^{(m)}(t)$ histograms and configuration snapshots presented in sections **(a)** and **(b)** (assigned based on the colour).

dominated by two values, underlies small changes in system magnetization. As the simulation continues, these phases, manifested by a different type of individual signal distributions, interlace with each other in a nondeterministic manner, however, the meta-stable phase prevails most of the time.

Worth noting here is that the transition between different types of individual signal histograms is a smooth process without precipitous changes. Figure 6.2 presents the schematic transition that occurs when the system transforms from a meta-stable to a turbulent phase. For clarity, the process is shown in four stages, each presented

in a separate panel. Moreover, the two-state variant of the model $\kappa_c = 0$ is considered here; however, similar dynamic can be observed in the three-state variant of the model. The orange color denotes the fraction of the agents for whom the individual signal will change in the next time step, and the arrows indicate the values of $h_i^{(m)}$ that these entities will assume.

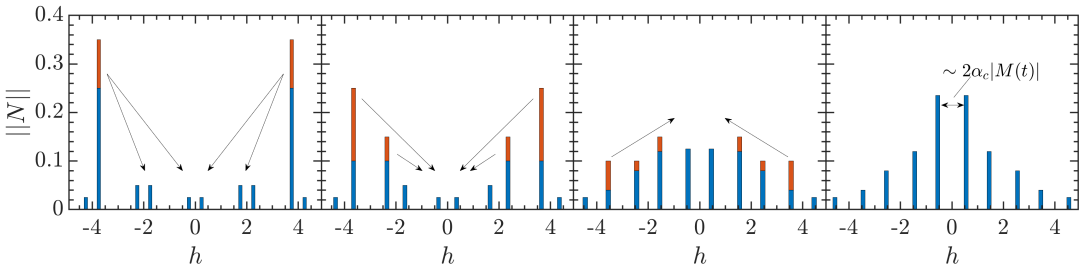

Figure 6.2: Schema of the individual signal histogram time evolution during transition from a meta-stable phase to a turbulent period. The orange color indicates the fraction of agents for whom individual signal will change in the next time step, whereas the arrows indicate the future values of $h_i^{(m)}$ assumed by these entities.

During the initial phase of the break down in agent clusterization, the number of individuals having $h_i^{(m)} \approx \pm 4$ significantly reduces in favour of units characterised by individual signal $h_i^{(m)} \approx \pm 2$. On the microscopic level, this corresponds to the blur of boundaries between clusters of agents having the same state (see configuration snapshot taken at $t = 69766$ in Figure 6.1). As the process continues, more and more individuals receive an ambiguous signal from their neighbours, a trend is manifested by an increased number of entities having $h_i^{(m)} \approx 0$. Finally, when clusters of agents having the same state almost disappear, the $h_i^{(m)}$ histogram resemble a bell-like curve centered at $h_i^{(m)} = 0$.

Moreover, the schema display another effect. As the magnetization of the system fluctuates, the values of $h_i^{(m)}$ assumed by the agents fluctuate as well. This phenomenon is related to global coupling (see the global coupling term in equation (5.3)). When magnetization increases, the pairs of possible $h_i^{(m)}$ values, that corresponds to the signal coming from neighbours (see the local agent-agent interaction term in the equation (5.3)) are more dispersed, as denoted on the last panel of Figure 6.2. These fluctuations does not significantly affect the clustering of generated signals, however it has impact on their hierarchical organization.

In order to show that, the following experiment was conducted. For each time step of the simulation performed with parameters[2]: $\beta = 1.6$, $\alpha_c = 30$, $J_{ij}^{lm} = 1$, and $\kappa_c = 0$ the signals $h_i^{(m)}$ were extracted and then reduced (or increased, depending on the spin sign) by factor $\alpha_c S_i |M(t)|$. In turn set of possible values of $h_i^{(m)}$ reduced to values equaling signal that agents can receive from their neighbours, namely $h_i^{(m)} \in [-4, -2, 0, 2, 4]$. Then, based on such artificially modified individual signals, according to equation (5.1) the states of the entities at each time step were determined, and finally, the magnetization was calculated. The procedure applied in this experiment substantially reduces the impact of the global coupling on individual

[2]For simplicity, in the experiment, the two-state version of the model was considered

signal $h_i^{(m)}$.

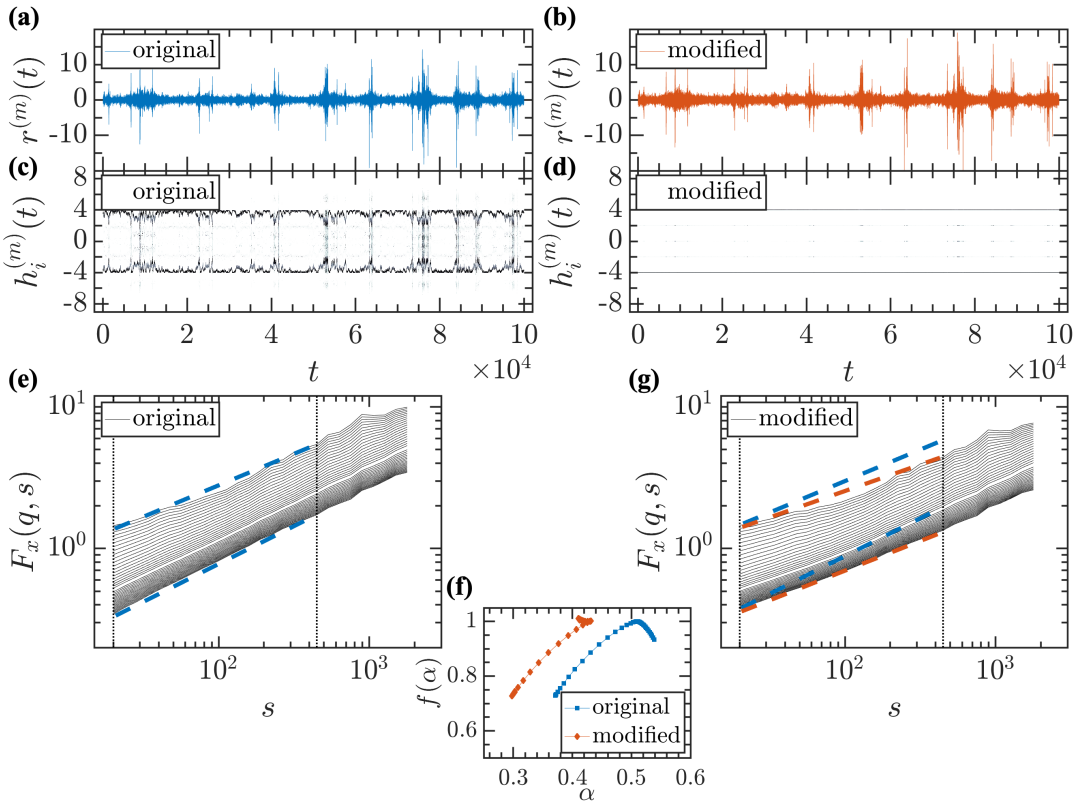

Figure 6.3: Comparison of returns (panels **(a)** and **(b)**), individual signal histograms time evolution (panels **(c)** and **(d)**), and fluctuation functions (panels **(e)** and **(g)**) generated by the original model (panels on the left-hand side) and by modified procedure explained above (panels on the right-hand side). The black dotted lines on panels (e) and (g) show the range of scaling. In order to highlight differences in fluctuation functions between the originally generated signal and produced in the experiment, the envelope of the $F_x(q,s)$ of the originally generated signal was projected to $F_x(q,s)$ plot of the returns produced by modified version of the model (blue dashed lines in panel (g)). Moreover, panel **(f)** presents corresponding singularity spectra.

Figure 6.3 presents a comparison of the original simulation results and those of simulation based on the modified individual signals. As shown in panels (a) and (b), the rates of return produced by these two variants of the model are almost identical and only a few discrepancies are noticeable (see the fluctuations for $t \approx 2.5 * 10^4$). Naturally, striking differences are visible in the $h_i^{(m)}(t)$ histograms time evolution, which, in case of the experimental simulation (panel (d)), is concentrated around $h_i^{(m)} = \pm 4$. Moreover, the fluctuations function calculated for the signal generated by the experimental simulation is similar to the fluctuations function of the original returns. However, closer inspection shows that the slope of $F_x(q,s)$ of originally produced time series is slightly higher (see the envelope of $F_x(q,s)$ of the original signal projected onto $F_x(q,s)$ obtained for the modified simulation - panel (g), shown with blue and orange dashed lines, respectively). Additionally, for the series generated by the experimental simulation, increased curvature of the fluctuations function is observed, meaning that scaling is poorer. These discrepancies are clearly visible on the singularity spectra level. As shown in panel (f), $f(\alpha)$ function of

the original signal has width $\Delta\alpha \approx 0.17$ accompanied by the left-hand side asymmetry $A_\alpha \approx 0.65$, whereas the singularity spectrum of the series generated in the experiment is narrower $\Delta\alpha \approx 0.12$. This narrowing is the result of the shrinkage observed in the right-hand side of $f(\alpha)$ function, while the left part remains almost the same. Moreover, the long-range linear correlations measured by Hurst exponent are also differ - $H \approx 0.39$ and $H \approx 0.47$ for the originally generated signal and series produced in the experiment, respectively. It means that global coupling is the element of the model, which does not significantly affect fluctuation clustering in the generated signals, however it influences the non-linear correlations of the generated time series, especially in the range of small fluctuations. Moreover, agents potential to have different strategies and ability to change them prevent the development of the linear dependencies.

6.2 Influence of system temperature on produced time series features

As shown in the previous section, the fluctuations clustering of the signals generated by the model, is rooted in the agents' collective behaviour, manifested by the presence of the meta-stable clusters of entities having the same position in the market, that are to some extent, broken up during the rearrangement phases, causing large fluctuations. The collective behaviour of the individuals in the model can be controlled in several ways. The natural choice is the β parameter, which changes the shape of probability distribution p used in the system dynamics equation (see equation (5.1)). This chapter contains a comprehensive exploration of the influence of this parameter on the stylized facts and multiscale characteristics of signals generated by the model.

Figure 6.4 shows a few examples of the probability functions p depending on individual signal $h_i^{(m)}$ for different values of parameter β. As is clearly visible, increase in β result in steeper probability distribution function in the vicinity of $h_i^{(m)} = 0$, which for large values of this parameter, assumes shapes similar to the signum function. The influence of probability function p on the collective behaviour of agents and, by extension, on system dynamics is essential. For instance, consider an agent that has state $S_i^{(m)} = -1$ and is surrounded by individuals having the same position on the market and, for sake of simplicity, assume that $M^{(m)}(t) = 0$. In such a scenario, the agent receives individual signal $h_i^{(m)} = -4$. Now, the probabilities that this entity will trade against its neighbours (will assume positive state $S_i^{(m)} = +1$) have values 0.018, $6.14 * 10^{-6}$, $2.06 * 10^{-9}$ for $\beta = 0.5$, $\beta = 1.5$, and $\beta = 2.5$, respectively. With $N = 14400$ agents in the system, roughly 259, 4.82, and $3 * 10^{-5}$ entities in each time step will trade against individuals in their vicinity, respectively [3]. Clearly visible is that statistically, number of agents trading against their neighbours dramatically decreases as the β parameter assumes higher values. Naturally, these numbers are higher when agents with the individual signal closer to 0 are considered, however this estimations well illustrates the influence of the β

[3] Trade against individuals means that agent that receive negative signal from neighbours assumes positive state, and vice versa.

parameter on the collectivity of the entities and thus on the stability of the agent's clusters.

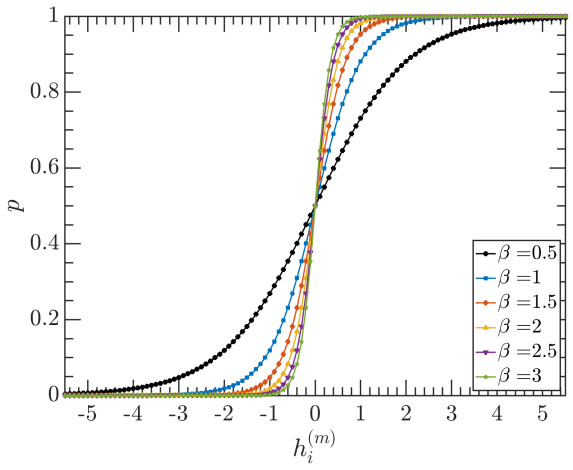

Figure 6.4: Probability function p in dependence of the value of agent's individual signal $h_i^{(m)}$ calculated for different values of $\beta \in [0.5, 1, 1.5, 2, 2.5, 3]$.

The dependence between agents collectivity and the β parameter has its reference in physical systems. In thermodynamics β is proportional to the inverse temperature $\beta \sim \frac{1}{T}$. A higher temperature (assuming that other parameters are kept constant) translates into a higher energy, which can introduce extra oscillations of the system observed on the microscopic level. In contrast, low temperatures (high values of β) correspond to system stabilization characterized by small fluctuations.

The impact of probability distribution function p on system dynamics is clearly visible in the temporal evolution of the individual signal's histograms as well. Figure 6.5 shows a two-dimensional, grayscale projection of $h_i^{(m)}(t)$, for different values of β. For relatively small values of β (e.g., $\beta = 0.8$ - panel (a)), which corresponds to the gradual rise (decline) of the probability function in the vicinity of $h_i(t) \approx 0$, the individual signal histogram flattens and has Gaussian-like shape during, virtually, the entire simulation. Such a system is almost constantly in the rearrangement phase and clusters of the individuals having the same state cannot develop. More collective behaviour of the agents is observed as β increases. For $\beta = 1.6$ (panel (b)) and $\beta = 2.0$ (panel (c)) the meta-stable phases manifested by the polarized distribution of the individual signal, with $h_i^{(m)} \approx \pm 4$ dominant, is noticeable. Moreover, as β increases, the rearrangement periods occurs with increasing rarity, and the system is in a meta-stable phase most of the time, e.g., $\beta = 2.3$ (panel (d)).

Analysis of the time evolution of individual signal histograms reveals the second element of system dynamics, that probability distribution function significantly affects, namely, the frequency of rearrangement periods. As mentioned above, for high values of β, turbulent phases occur sporadically, while, for low values, they dominate during almost the entire simulation. The reason for such system behaviour originates from the number of agents trading in opposition to the received individual signal. To be initialized, rearrangement phase requires a sufficient number of individuals that behave contrary to the entities in their vicinity. In the next time steps, these agents reduce the individual signal of their neighbours and trigger a peculiar

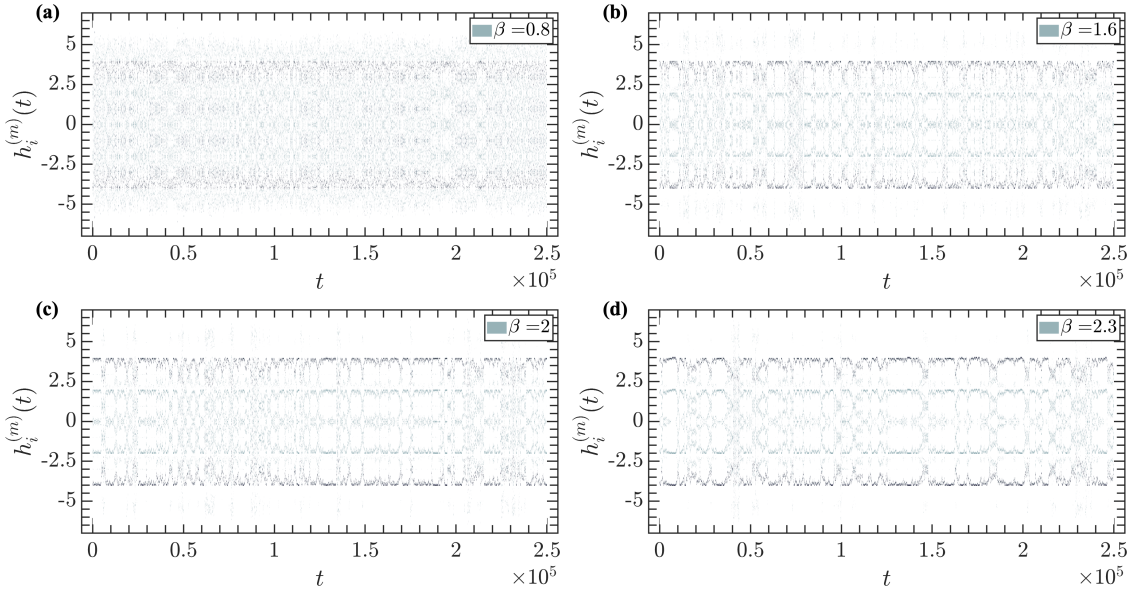

Figure 6.5: Two-dimensional, grayscale projection of time evolution of the agent's individual signal histogram $h_i^{(m)}(t)$ for an example model simulations with parameters: $J_{ij}^{lm} = 1$, $\alpha_c = 30$, $\kappa_c = 0.5$, and different values of $\beta \in [0.8, 1.6, 2.0, 2.3]$.

avalanche that leads to the breakdown of clusters. The number of agents required to initialize a transition between phases is hard to estimate as it depends not only on the total number of entities in the system but also on the shape of the clusters of agents having the same state, which is highly non-deterministic.

Naturally, differences observed on the individual signal distribution level reveal themselves in the character of the time series generated by the model. Figure 6.6 presents an example of system magnetization signals (panels on the left-hand side) and corresponding rates of return (panels on the right-hand side) obtained for β values given above. For small values of inverse temperature, the system's magnetization frequently fluctuates; however, these changes are relatively small. In result, rates of return, typically span over $r^{(m)}(t) \approx 6$ and $r^{(m)}(t) \approx -6$ and, to some degree, are similar to white noise. Along with increases in β, the collectivity of the agents behaviour increases, and thus meta-stable periods, characterized by low magnetization $M^{(m)}(t) \approx 0$ are extended. Additionally, the rearrangement phases are less likely to occur but are, however, more volatile. On the returns level, it brings about the interlaced periods of small and large oscillations with multiple spikes that resemble fluctuations observed in financial time series. Moreover, for $\beta = 2.3$, periods of the full stabilization of magnetization, manifested by $r^{(m)}(t) = 0$, are visible (e.g., $t = 136742$). In such a scenario, in two consecutive time steps, the magnetization does not change. This is possible only when exactly the same number of agents change their position in the market in opposite directions (from -1 to $+1$ and vice versa) or when the system configuration remains the same over consecutive time steps. In fact, for a large value of the β parameter, the former scenario is observed - the system temporarily freezes, and all agents preserve the positions they assumed in the previous time step.

Physically speaking, the system reaches its temporal equilibrium, a phenomenon

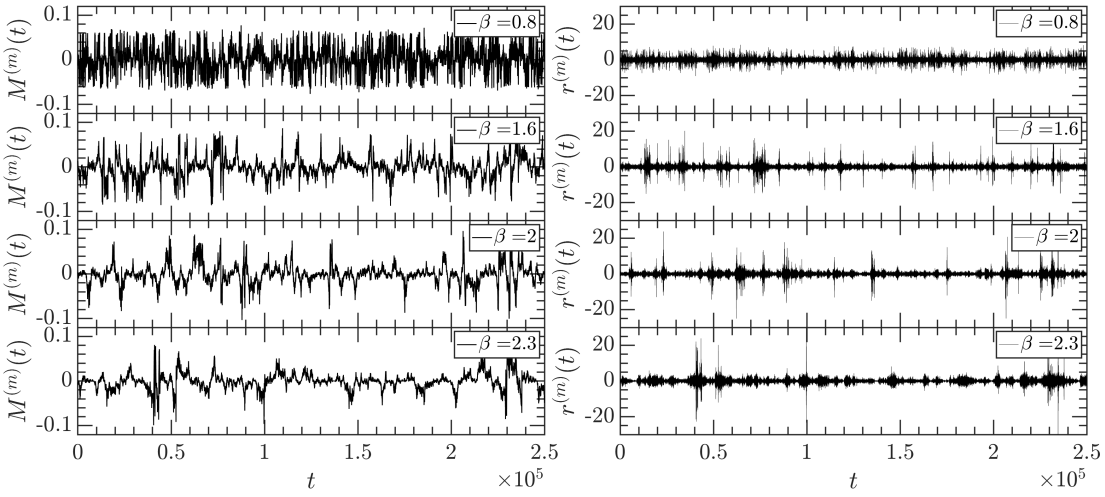

Figure 6.6: Magnetization (panels of the left-hand side) and corresponding rates of return (panels on the right-hand side) generated by the model with parameters: $J_{ij}^{lm} = J = 1$, $\alpha_c = 30$, $\kappa_c = 0.5$, and different values of $\beta \in [0.8, 1.6, 2.0, 2.3]$.

also observed in many natural systems. Since the model has its roots in the solution proposed by Ising [176], the dependence between system dynamics and temperature, to some degree, resembles the spontaneous magnetization observed in ferromagnetic materials. For high temperatures (low values of β), the system's energy is high, and thus spins are not aligned with each other. On the other hand, for low temperatures (immense values of β), the partial order, manifested by large clusters of the agents having the same state, emerges.

In the financial context, $1/\beta$ can be viewed as the market temperature. When it is high (e.g., $\beta = 0.8$), agents behave more independently and change position quite frequently. In financial markets, it corresponds to a situation when investor sentiment is uncertain. On the other hand, when the market temperature is low (e.g., $\beta = 2.0$), the agents behave more collectively and are less likely to change the position. and this reflects the stable situation in the economy, during which market participants make long-term investment decisions. Also worth noting is that for a system characterized by low temperature, the rearrangement periods are volatile, which resemble the crises and crashes observed in financial markets.

The influence of market temperature on the characteristics of generated time series is also visible on the absolute returns distribution level. As shown in Figure 6.7 (panel (a)), an increasing value of the β parameter results in heavier tails of the absolute returns distributions, which, for low temperatures, to some degree, obey the power law, with slope $\mu \approx 2.5$ in the middle section and $\mu \approx 5 - 6$ in the tail. For all analysed values of β, generated signals are characterized by weak, negative linear correlations for small lags τ and a lack of linear dependencies over larger time horizons. The existence of the negative correlations observed for small lags $\tau < 4$ is inextricably linked to the interlaced character of the model - the positive and negative returns tend to interlace as the firmly trend manifested by consecutive positive (negative) returns hardly develops. Moreover, since the β parameter's value enhanced the volatility clustering observed in the generated signals, differences in the absolute returns autocorrelation function are also noticeable (panel

(c)). The strongest volatility correlations are observed for $\beta = 2.0$, which naturally has its source in the strong collectivity of the agents; however, the range of these dependencies for the analysed set of βs does not change significantly and lasts for approximately $3 * 10^3$ time steps.

It is vitally important that the probability function and the associated β parameter affect the non-linear correlations of the generated time series. Panel (e) of Figure 6.7 shows the mean fluctuations functions calculated for ten consecutive simulations of the model for a given value of β (other parameters were set as follows: $J_{ij}^{lm} = 1$, $\alpha_c = 30$, $\kappa_c = 0.5$). The primary observation here is the distortion in the hierarchical organization of the signals, manifested by deformation of $F_x(q, s)$ that appears in the negative range of q (see equation 3.21) for low temperatures of the market. For $\beta = 2.0$ this effect is present only in the small range of scales $s \in [20, 30]$ and in general does not prevent calculation of the singularity spectra. However, for $\beta = 2.3$, the distortion spans a significant range of scales s. Thus these signals, in the range of the small fluctuations (negative q), cannot be considered to be multifractal. Mathematically speaking, the effect is caused by the temporal equilibrium phases that occur for low temperatures of the market and translate into periods without fluctuations (low variance). In turn, the value of the $F_x(q, s)$ decreases dramatically for negative q exponents. Moreover for $\beta = 2.0$ the range of scales where the fluctuation function obey the power law is slightly wider and approximately spans $s \in [20, 3 * 10^3]$ for $\beta = 2.0$ in contrast to $s \in [10, 2 * 10^3]$ for other values of β. In practice, this means that the non-linear correlation generated by the model with $\beta = 2.0$ lasts longer than for other values considered.

Naturally, features of the fluctuation functions reveal themself on the multifractal spectra level. Panel (d) of Figure 6.7 shows the mean singularity spectra calculated for $F_x(q, s)$ presented on the right-hand side of the figure. As expected, the higher collectivity among agents, which increases along with increasing values of β, resulted in a wider $f(\alpha)$ function. However for $\beta = 2.3$, it is impossible to determine the multifractal spectra in the range of negative q, thus only positive qs were considered resulting in a significantly lower $f(\alpha)$ width ($\Delta\alpha = 0.11 \pm 0.02$). For other considered values of β, the width $\Delta\alpha$ hovers from $\Delta\alpha = 0.16 \pm 0.01$ for $\beta = 0.8$ to $\Delta\alpha = 0.40 \pm 0.05$ for $\beta = 2.0$. Worth noting here is that, all obtained spectra are characterised by left-hand side asymmetry, that vary from $A_\alpha = 0.71 \pm 0.08$ for $\beta = 1.6$ to $A_\alpha = 0.29 \pm 0.11$ for $\beta = 2.0$. The properties of the multifractal spectra obtained are also presented in Table 6.1.

Table 6.1: Mean singularity spectra properties of the signals generated by the single-asset variant of the model with following parameters: $J_{ij}^{lm} = 1$, $\alpha_c = 30$, $\kappa_c = 0.5$, and different values of $\beta \in [0.8, 1.6, 2.0, 2.3]$.

	$\boldsymbol{\beta = 0.8}$	$\boldsymbol{\beta = 1.6}$	$\boldsymbol{\beta = 2.0}$	$\boldsymbol{\beta = 2.3}$
$\boldsymbol{\Delta\alpha}$	0.16 ± 0.01	0.21 ± 0.02	0.40 ± 0.05	0.11 ± 0.02
$\boldsymbol{A_\alpha}$	0.62 ± 0.11	0.71 ± 0.08	0.29 ± 0.11	$1.00 \pm --$
$\boldsymbol{H}$	0.35 ± 0.01	0.42 ± 0.02	0.45 ± 0.04	0.47 ± 0.03

In order to verify that the observed multifractality of the generated signals was

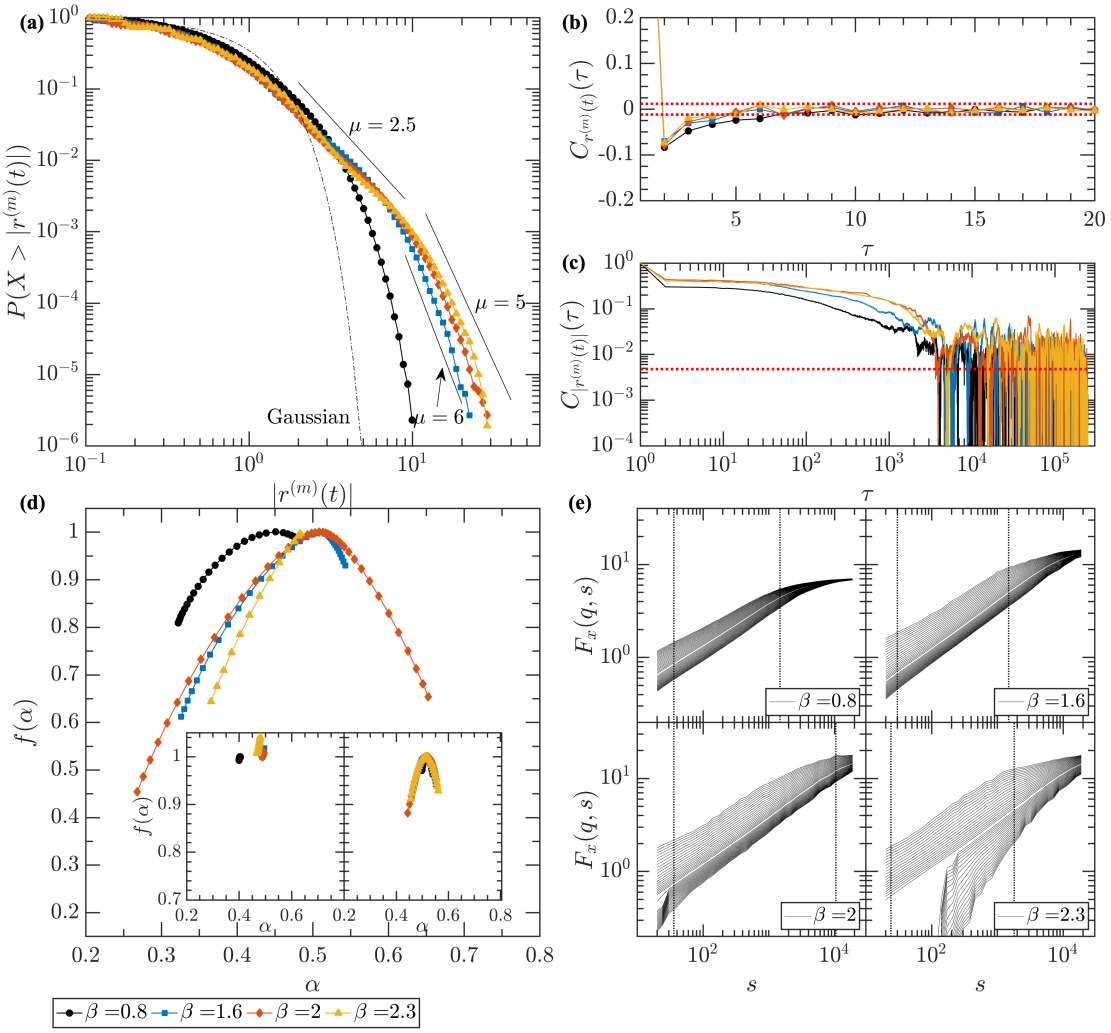

Figure 6.7: Mean statistical and multifractal properties of the series generated by the single-asset variant of the three-state multi-asset model based on a two-dimensional lattice $L \times L = 120 \times 120$ with von Neumann neighbourhood, the following parameters: $J_{ij}^{lm} = J = 1$, $\alpha_c = 30$, $\kappa_c = 0.5$, and different values of $\beta \in [0.8, 1.6, 2.0, 2.3]$. Panel **(a)**: distribution of the absolute returns; panel **(b)** autocorrelation function of the rates of return; panel **(c)**: autocorrelation function of the absolute returns (volatility); panel **(d)**: returns singularity spectra $f(\alpha)$ (main plot) and result obtained for signals modified by Fourier surrogates method (inset on the left-hand side) and shuffled data (inset on the right-hand side); panels in section **(e)**: mean fluctuation functions of the signals. The red dotted lines in plots **(b)** and **(c)** denote the noise level. The black dotted lines in section **(e)** denote range of scaling of the $F_x(q,s)$ functions. Presented results were calculated based on ten independent simulations of the model with the given parameters.

not a spurious effect, the singularity spectra for randomly shuffled signals (panel (d), right inset plot) and Fourier surrogates (panel (d), left inset plot) were determined. In both cases, the calculated $f(\alpha)$ functions widths were significantly lower than for the original signals and hovered from $\Delta\alpha = 0.05$ to $\Delta\alpha = 0.11$ for the shuffled signals, while for series modified by Fourier surrogate procedure, the spectra were pointwise.

The dependence between the richness of the hierarchical structure observed in the time series generated by the model and the shape of probability function p is

even more pronounced when a wide range of βs is considered. Figure 6.8, shows the width (panel (a)) and asymmetry coefficient (panel (b)) of the mean singularity spectrum as well as value of the Hurst exponent (panel (c)) in the function of inverse temperature $\beta \in [0.5, 2.5]$.

The multifractal spectra for large temperatures ($\beta \in [0.5, 0.6]$) are narrow and almost symmetrical, indicating a lack of the non-linear correlations in the analysed signals. This characteristic changes as the β parameter increases. In the range $\beta \in [0.6, 1]$, the widths of the singularity spectrum growth up to $\Delta\alpha \approx 0.2$ and exhibits left-hand side asymmetry as manifested by positive values of A_α. For these values of β, agents begin to act more collectively, and, as a result, the non-linear temporal dependencies emerge. Interestingly, the observed asymmetry of the singularity spectrum suggests that correlations of large fluctuations are significantly stronger than those existing in the low rates of return. Further reduction of the temperature ($\beta \in [1.1, 1.8]$) does not substantially affect the richness of the hierarchical organization of the generated time series ($\Delta\alpha$ stabilize around 0.2); however, an initial increase in the spectrum asymmetry, changes into a downtrend for $\beta > 1.4$. In fact, along with the increase in the β parameter, non-linear correlations emerge on the level of small fluctuations; thus, the spectrum becomes more symmetrical. This effect is dramatically amplified in the vicinity of $\beta = 2.0$, where spectrum width soars and reaches its maximum $\Delta\alpha = 0.40 \pm 0.05$, accompanied by a relatively low value of the asymmetry coefficient $A_\alpha = 0.29 \pm 0.11$. Successive increase of the inverted temperature value ($\beta > 2.05$) result in periods of temporal equilibrium of the system, which cause the distortion observed on the fluctuations functions level, that prevents calculation of the multifractal spectra in negative range of q parameter. In turn, the $f(\alpha)$ function demonstrate full, left-hand side asymmetry while its width declines significantly.

Singularity spectrum width describes the richness of the non-linear correlations present in the signal, thus measuring the non-linear order among agents. The dramatical narrowing of the $f(\alpha)$ function that occurs when a particular value of the β is exceeded, has the appearance of a phase transition. Moreover, the high value of $\Delta\alpha$ in the vicinity of a particular value of β resembles characteristics of physical systems that are in near-critical state, where free-scale properties are amplified.

The analogy between the change in the system dynamics observed for $\beta > 2.05$ and a phase transition raises the question of why this phenomenon occurs in the vicinity of the particular value of β. Of course, this is the resultant of all parameters present in the model; however, it depends primarily on the probability that the agent will act in opposition to the signal it has received. Two parameters, β and local interaction strength J_{ij}^{lm}, control this effect, as an increase in the value of either of these parameters amplifies collectivity among agents. Also significant is the number of individuals in the system. As mentioned above, the temporal equilibrium phases occur when no agents change position in the market over two or more consecutive time steps; thus, a higher number of individuals in the system increases likelihood that, even for low temperatures (or high interaction strength) at least one agent changes position and thereby prevents the freeze of the system configuration. In general, the strongest non-linear dependencies are observed in the series generated by the system, in which agent collectivity and independence are balanced.

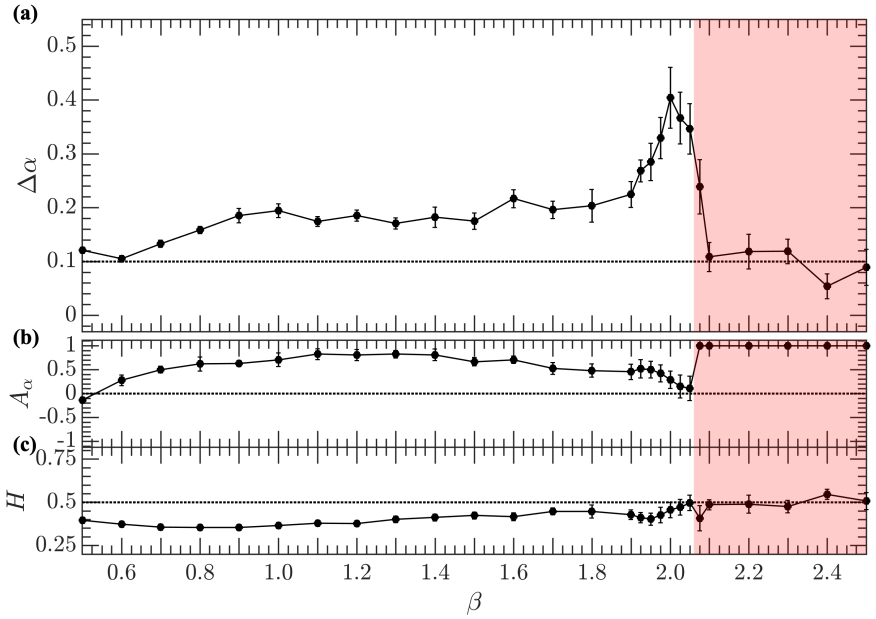

Figure 6.8: Mean multifractal properties of the time series generated by the single-asset variant of the model with following parameters $J_{ij}^{lm} = J = 1$, $\alpha_c = 30$, $\kappa_c = 0.5$, and different values of $\beta \in [0.5, 2.5]$. Panel **(a)**: spectrum width $\Delta\alpha$; panel **(b)**: spectrum asymmetry A_α; panel **(c)**: Hurst exponent H. The calculations are based on 10 independent realizations of the model for each considered value of β. The red area indicates the range of β values, where distortion of the fluctuations function $F_x(q, s)$ prevents calculation of the singularity spectra for negative q exponents.

6.3 Impact of agent-agent local interaction strength on model characteristics

Another element of the model that determines the level of collective behaviour among the individuals in the system, thus significantly impacts multiscale properties of generated signals, is agent-agent local interaction strength. This section focuses on studying influence of the J_{ij}^{lm} value on the dynamics of single-asset variant of the model and signals it generates.

In general, J_{ij}^{lm} can assume discretionary values, for example, drawn from Gaussian distribution[4]; however, in most of finance-related applications, interaction between agents is symmetrical and thus J_{ij}^{lm} can be reduced to a scalar usually equaling 1 (in a single-asset scenario $l = m = 1$ then, $J_{ij}^{lm} = J = 1$). From the $h_i^{(m)}$ histogram perspective, the interaction strength parameter determines the possible values of the signal that the agent receives from its neighbours (see the first term of equation (5.3)). For instance, in the single-asset model variant with symmetrical interaction between agents, when $J_{ij}^{lm} = 1$, the neighbour influence factor of the individual signal can assume integer values from interval $[-4, 4]$, while for $J_{ij}^{lm} = 0.5$ this range is reduced by 2 and includes fractional values $[-2, -1.5, -1, ..., 1, 1.5, 2]$.

Naturally, this effect is clearly visible in the time evolution of the individual signal histograms. As shown in Figure 6.9, in the case of low value of interaction strength

[4]In such a scenario, the spin-glass model is obtained [189].

($J_{ij}^{lm} = 0.5$, panel (a)), the $h_i^{(m)}$ histogram is more greatly centered around 0, than for higher values of J_{ij}^{lm}. Since an agent receives lower individual signal, the probability that an entity will act against its neighbours increases. As a result, individuals behave in a less collective manner, manifested by the Gaussian-like shape of $h_i^{(m)}$ histogram, meaning that the system is almost constantly in the rearrangement phase.

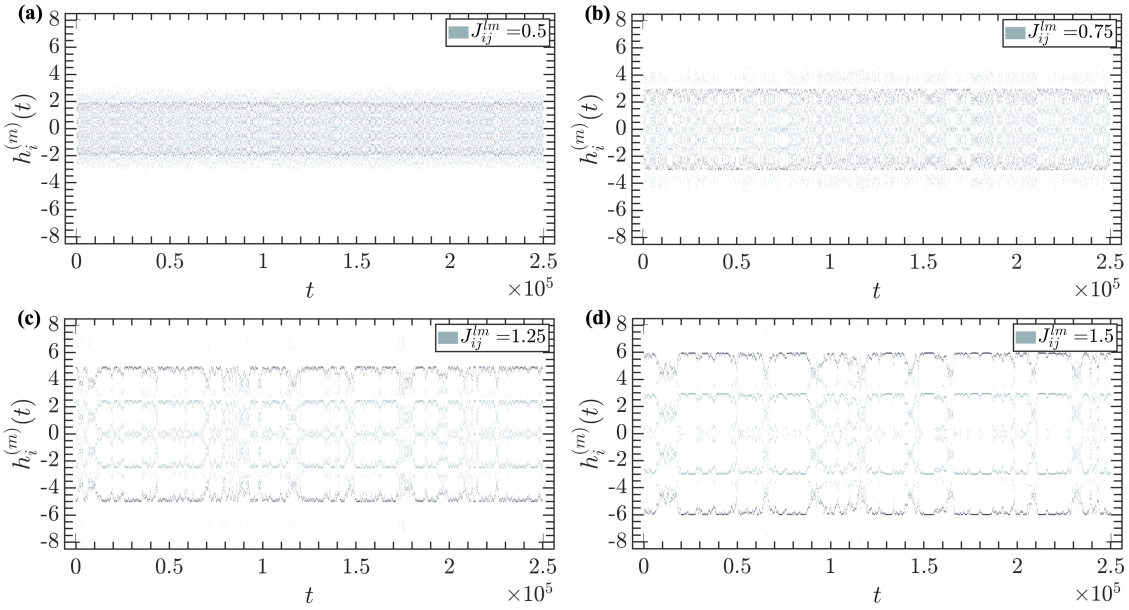

Figure 6.9: Two-dimensional, grayscale projection of the agent's individual signal histogram $h_i^{(m)}(t)$ time evolution in the single-asset variant of the model with the parameters $\beta = 1.6$, $\alpha_c = 30$, $\kappa_c = 0.5$ and different values of the agent-agent local interaction strength $J_{ij}^{lm} \in [0.5, 0.75, 1.25, 1.5]$.

Along with the increase in agent-agent local interaction strength, periods of metastability, manifested by the polarized distribution of $h_i^{(m)}$, begin to dominate, and the entire dynamics of the system, to some degree, resemble that observed for high values of β parameter. It should be emphasized that β and interaction strength J_{ij}^{lm} are a pair of parameters wherein either of the pair can, to some extent, cancel the influence of the other. When $\beta = 1.6$ and J_{ij}^{lm} parameter assumes low value, e.g., $J_{ij}^{lm} = 0.5$ as shown in the figure above the system constantly undergoes rearrangement. However, if β sufficiently increases, and as result the probability function p in the vicinity of $h_i^{(m)} = 0$ becomes steeper, system dynamics will resemble the one observed for pair $\beta = 1.6$ and $J_{ij}^{lm} = 1$. For instance, if $\alpha_c = 0$, the parameters pair $J_{ij}^{lm} = 0.5$ and $\beta = 3.2$ correspond to $J_{ij}^{lm} = 1$, $\beta = 1.6$ with respect to their effect on system dynamics.

Changes in collectivity of the agent behaviour affect the characteristics of the signals generated by the model. Figure 6.10 shows a time series of magnetization (panels on the left-hand side) and corresponding rates of return (panels on the right-hand side) for simulations performed with different values of $J_{ij}^{lm} \in [0.5, 0.75, 1, 1.25, 1.5]$. For small values of interaction strength ($J_{ij}^{lm} = 0.5$), system total magnetization fluctuates constantly; however, these oscillations are relatively small and exhibit an almost constant amplitude. As a result, the corresponding rates of return have a noise-like character. As the J_{ij}^{lm} increases, system magnetization tends to fluctuate

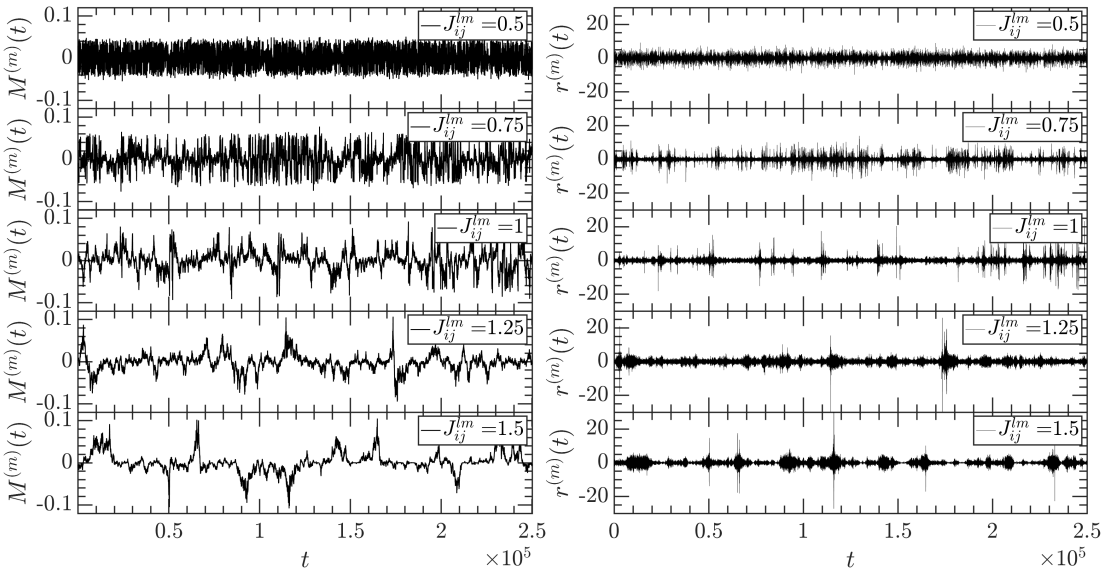

Figure 6.10: The magnetization (panels of the left-hand side) and corresponding rates of return (panels on the right-hand side) for example realizations of the model with parameters $\beta = 1.6$, $\alpha_c = 30$, $\kappa_c = 0.5$, and different values of agent-agent local interaction strength $J_{ij}^{lm} \in [0.5, 0.75, 1, 1.25, 1.5]$.

close to $M^{(m)}(t) = 0$. These periods of stability in magnetization of the system intersperse with spans marked by the large fluctuations and significant spikes that occur in rearrangement periods. This effect is also visible in the rate of return signals. For high values of J_{ij}^{lm}, volatility clustering is amplified, and sharp changes of the returns are observed.

Differences in system dynamics and in the character of the generated signals for different agent-agent local interaction strength values are also visible in the statistical properties of the time series produced by the model. As shown in Figure 6.11 (panel (a)), due to lack of large fluctuations, the distribution of absolute returns for small J_{ij}^{lm} is not characterized by fat-tails. However, along with the increased J_{ij}^{lm}, the probability of large rates of return rise, and for high values of the interaction strength, the volatility cumulative distributions, to some degree (within range of returns $|r^{(m)}(t)| \in [2, 18]$) obey the power law with $\mu \approx 3$ for $J_{ij}^{lm} = 1.25$ and $J_{ij}^{lm} = 1.5$.

Furthermore, weakened collective behaviour of agents results in a relatively short range of the absolute returns autocorrelations (panel (c)), that for signals generated by the model with $J_{ij}^{lm} = 0.5$ last for 10^3 time steps. In comparison, non-linear dependencies for higher values of agent-agent interaction strengths maintain a significant level for approximately $6 * 10^3$ time steps. On the other hand, the influence level between agents does not affect the generated signal's linear dependencies. As shown in panel (b) of Figure 6.11, for all considered values of J_{ij}^{lm}, the autocorrelation function of returns, initially assumes slightly negative values (lags $\tau \in [2, 4]$) but converges to 0 after a few time steps ($\tau > 5$) and does not exceed statistical significance thresholds (marked as red dotted lines) thereafter.

The range of the non-linear correlations is also visible on the fluctuations function level (Figure 6.11, panels in section (e)). For weak agent-agent interaction ($J_{ij}^{lm} =$

0.5), the fluctuations function obeys the power law in the very limited range of scales ($s \in [20, 108]$). As the influence of communication among agents increases, the maximum of s for which scaling is observed rises as well (up to $s = 720$ and $s = 8100$, for $J_{ij}^{lm} = 0.75$ and $J_{ij}^{lm} = 1.25$, respectively).

Like the system under low temperature (i.e., large value of β), for the high levels of the agent-agent local interaction, the temporary equilibrium periods manifested by lack of fluctuations appear. This phenomenon is clearly visible in the distortion of $F_x(q, s)$ observed for negative q exponents (bottom panels of the section (e) of Figure 6.11). Interestingly, for large values of interaction strength parameter ($J_{ij}^{lm} = 1.5$), the deformation of the fluctuations function is noticeable, not only in the negative range of q exponents but also in the positive one.

Features of the generated signals discussed above reveal themselves on the multifractal spectra level as well. As shown in panel (d) of Figure 6.11 and in Table 6.2, $f(\alpha)$ functions of the signals produced by the model with weak interaction between agents ($J_{ij}^{lm} = 0.5$ and $J_{ij}^{lm} = 0.75$) are relatively narrow ($\Delta\alpha = 0.20 \pm 0.01$ and $\Delta\alpha = 0.19 \pm 0.02$), and are characterized by left-hand side asymmetry ($A_\alpha = 0.46 \pm 0.04$ and $A_\alpha = 0.77 \pm 0.07$). If a high value of J_{ij}^{lm} is assumed (e.g., $J_{ij}^{lm} = 1.25$), the singularity spectrum's right side develops, and as a result the asymmetry factor decreases ($A_\alpha = 0.34 \pm 0.12$), and the total width rises to $\Delta\alpha = 0.26 \pm 0.05$. It should be noted that signals generated by model with $J_{ij}^{lm} = 1.5$ are not fractals, and so the singularity spectrum for this case was not determined.

Again, in order to verify that measured multifractality of the time series generated by the model with different values of the agent-agent local interaction strength parameter is not a spurious effect, singularity spectra for randomly shuffled signals and Fourier surrogates were determined (left and right inset plots of panel (d), Figure 6.11, respectively). In both cases, width of the $f(\alpha)$ functions are significantly smaller than for the original signals and hover between $\Delta\alpha \approx 0.02$ and $\Delta\alpha \approx 0.07$ for shuffled signals, and between $\Delta\alpha \approx 0.01$ and $\Delta\alpha \approx 0.10$ for the signals modified according to Fourier surrogate procedure.

Table 6.2: Mean singularity spectrum $f(\alpha)$ properties of the time series generated by ten independent realizations of the single-asset variant of the model with the following parameters: $\beta = 1.6$, $\alpha_c = 30$, $\kappa_c = 0.5$, and different values of agent-agent local interaction strength $J_{ij}^{lm} \in [0.5, 0.75, 1, 1.25, 1.5]$.

	$\boldsymbol{J_{ij}^{lm} = 0.5}$	$\boldsymbol{J_{ij}^{lm} = 0.75}$	$\boldsymbol{J_{ij}^{lm} = 1.0}$	$\boldsymbol{J_{ij}^{lm} = 1.25}$
$\boldsymbol{\Delta\alpha}$	0.20 ± 0.01	0.19 ± 0.02	0.21 ± 0.02	0.26 ± 0.05
$\boldsymbol{A_\alpha}$	0.46 ± 0.04	0.77 ± 0.07	0.71 ± 0.08	0.34 ± 0.12
$\boldsymbol{H}$	0.40 ± 0.01	0.41 ± 0.02	0.42 ± 0.02	0.45 ± 0.03

Findings presented above show that collective behaviour of the agents besides being controlled by the temperature of the system (β parameter), can also be amplified (weaken) by the agent-agent local interaction strength J_{ij}^{lm}. Worth noting is that interaction strength J_{ij}^{lm} and parameter β constitute a pair of complementary quantities, whose manipulation, leads to similar effects with respect to multifractal properties of the time series generated by the model.

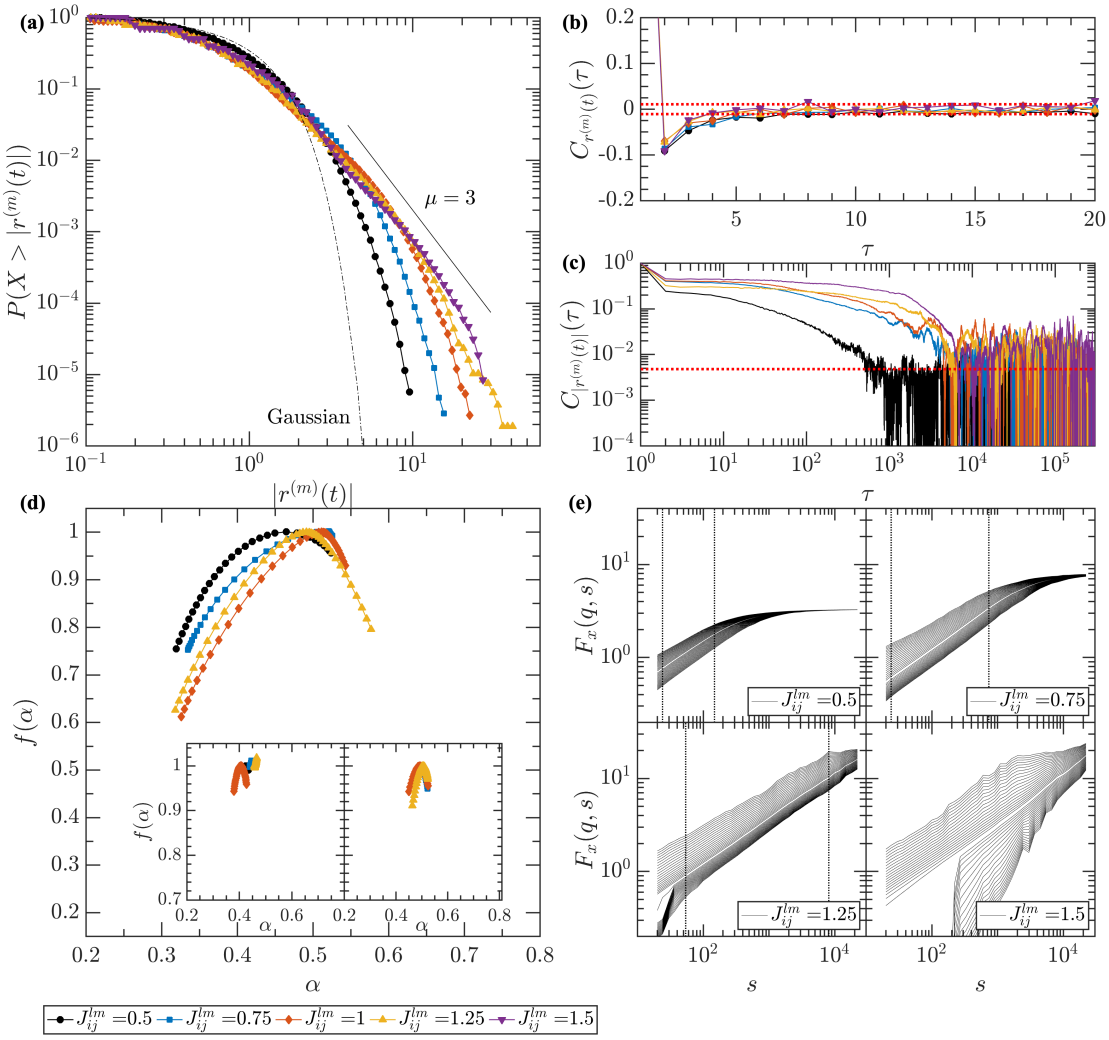

Figure 6.11: Mean statistical and multifractal properties of the time series generated by ten independent realizations of a single-asset model with the following parameters: $\beta = 1.6$, $\alpha_c = 30$, $\kappa_c = 0.5$, and different values of agent-agent local interaction strength $J_{ij}^{lm} \in [0.5, 0.75, 1, 1.25, 1.5]$. Panel **(a)**: distributions of the absolute returns; panel **(b)**: autocorrelation functions of returns; panel **(c)**: autocorrelation function of the absolute returns (volatility); panel **(d)**: singularity spectra $f(\alpha)$ (main plot) and result obtained for signals modified according to Fourier surrogates method and randomly shuffled series (inset plots on the right- and left-hand side, respectively); panels in section **(e)**: fluctuation functions of the signals. The red dotted lines in plots (b) and (c) denote the noise levels. The black dotted lines in section (e) indicate the range of scaling of $F_x(q,s)$ functions.

6.4 Agents strategies and their consequences

In addition to investor collective behaviour, the model incorporates individuals' possible pursuit of differing strategies. As discussed in the model description (section 5.2), entities can belong to one of two groups of traders: fundamentalists who seek to join the global minority, and chartists who follow market trends. Mathematically speaking, these strategies are reflected in the parameter $C_i^{(m)}(t)$ (here, $C_i^{(m)}(t) = S_i^{(m)}(t)$), which in the individual signal formula (see equation (5.3)) is multiplied by the absolute value of magnetization $M^{(m)}(t)$, and scaled by α_c parameter, here called

global coupling. This section contains a comprehensive investigation of the impact of global coupling parameter on the system dynamics and hierarchical organization of time series generated by the single-asset variant of the model.

In general, depending on an agent's strategy and the system magnetization value, the signal that a particular individual receives from neighbours can be amplified or weaken. For instance, assuming that agent i has state $S_i^{(m)} = -1$, and is surrounded by entities having the same position in the market, then the resultant individual signal is increased by the factor $\alpha_c|M^{(m)}(t)|$, consequently, decreasing the neighbors' influence and making the agent more likely to trade against individuals in its vicinity. However, the situation changes when agent i has state $S_i^{(m)} = +1$ (assuming that all neighbours have negative position in the market). In such a scenario, the $h_i^{(m)}$ value decreases, and, as a result, the probability that particular spin flips, decreases as well. In fact, for agents being inside the cluster of individuals having the same state, as long as α_c does not assume an enormous value, the effect described above does not significantly affect their investment decisions; however, the input coming from strategy-related term significantly influences the entities on the boundaries of the clusters (i.e., those who receive ambiguous signals from neighbours).

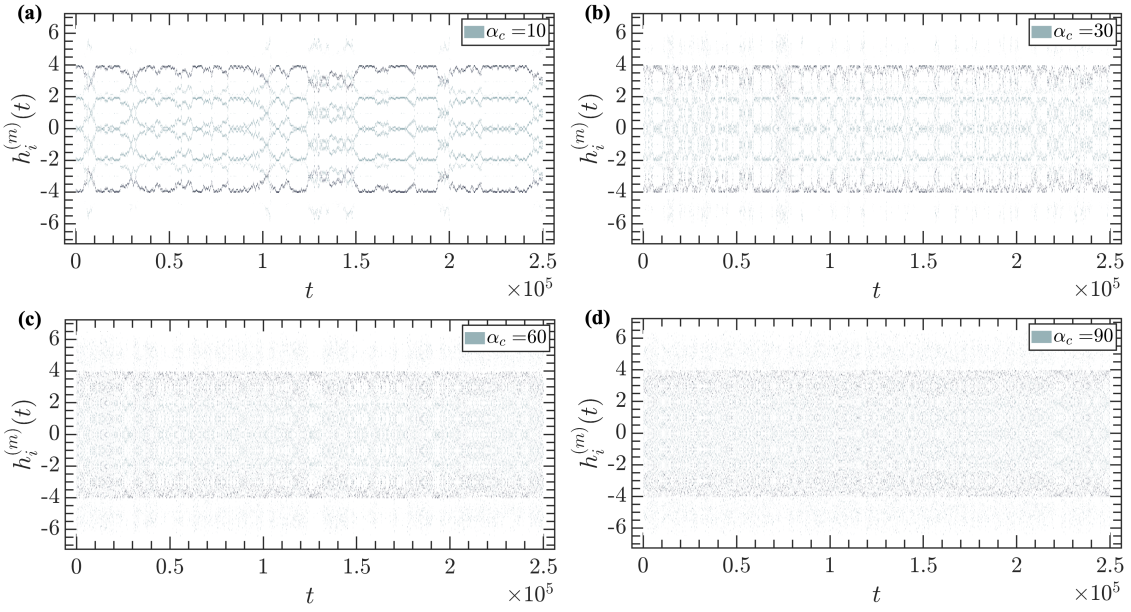

Figure 6.12: Two-dimensional, grayscale projection of an individual agent's signal histogram $h_i^{(m)}$ time evolution for simulations of the model with parameters $\beta = 1.6$, $J_{ij}^{lm} = 1$, $\kappa_c = 0.5$, and different values of global coupling parameter $\alpha_c \in [10, 30, 60, 90]$.

The global coupling parameter's influence is clearly visible in individual signal histograms' time evolution (Figure 6.12). For small values of parameter α_c the agent-agent local interaction term clearly dominates individual signal $h_i^{(m)}$. As a result, agents more willingly follow their neighbours and forms large, relatively stable clusters of the entities characterized by the same state. On the histogram level, it is manifested by the polarized distribution of $h_i^{(m)}$, which, during the rearrangement period, assume a more Gaussian-like shape (see panel (a), Figure 6.12). The dominance of the meta-stable configuration of the system is weakening as with global

coupling parameter increases. For high values of α_c ($\alpha_c = 60$ and $\alpha_c = 90$ - panels (c) and (d) of Figure 6.12) the system is constantly in the rearrangement phase, which evinces itself in the blurred $h_i^{(m)}(t)$ histograms. In such a scenario, the agents cannot form clusters, which are crucial in the context of the multifractal properties of the generated time series. In fact, individuals tend to constantly change state in a non-collective manner.

Naturally, changes in global coupling parameter value are manifested in the system's magnetization and corresponding rates of return (Figure 6.13, panels on the left- and right-hand side, respectively). For the small value of α_c the magnetization of the system changes relatively slowly, and has the trajectory, to some degree, similar to the price movements observed in financial market. As the global coupling parameter increases, fluctuations of magnetization increases and become more concentrated around $M^{(m)}(t) = 0$. On the rates of return level, the growth of α_c translates into a greater number of spikes and less pronounced, shorter volatility clusters. This effect is a result of the agent's pursuit of different strategies. When global coupling parameter assumes enormous value the signal that agents receive from neighbours is leveled by the term related to the agent's strategy. In consequence, the individual signal $h_i^{(m)}$ fluctuates closely to 0, and thus agents are trading in more random manner.

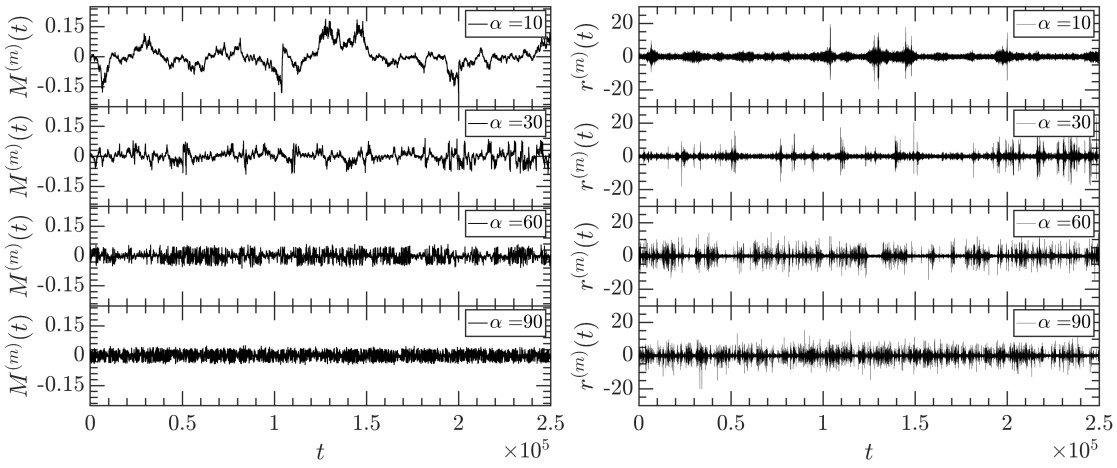

Figure 6.13: The magnetization (panels of the left-hand side) and corresponding rate of returns (panels on the right-hand side) generated by the single-asset variant of the model with parameters $\beta = 1.6$, $J_{ij}^{lm} = 1$, $\kappa_c = 0.5$ and different values of the global coupling parameter $\alpha_c \in [10, 30, 60, 90]$.

Although qualitative differences in the return's character are noticeable, the mean cumulative distribution functions do not vary substantially (Figure 6.14, panel (a)). For all analysed values of the global coupling parameter, the tails of the distributions of absolute returns are significantly heavier than those observed for Gaussian distribution; however, they do not obey the power law in its full range. The only significant difference is visible for the $\alpha_c = 10$ cumulative distribution where, for $|r^{(m)}(t)| \in [2, 6]$ a peculiar distortion occurs. For the small value of the global coupling parameter, agents' investment decisions are primarily driven by the signals received from neighbours. As a result, the transition between the meta-stable and rearrangement phase is more volatile than is observed for series generated by

a model characterised by stronger global coupling. On the magnetization level, this effect reveals itself in the sharp changes and smaller number of medium sized fluctuations, which in turn, cause deformation of the returns distribution.

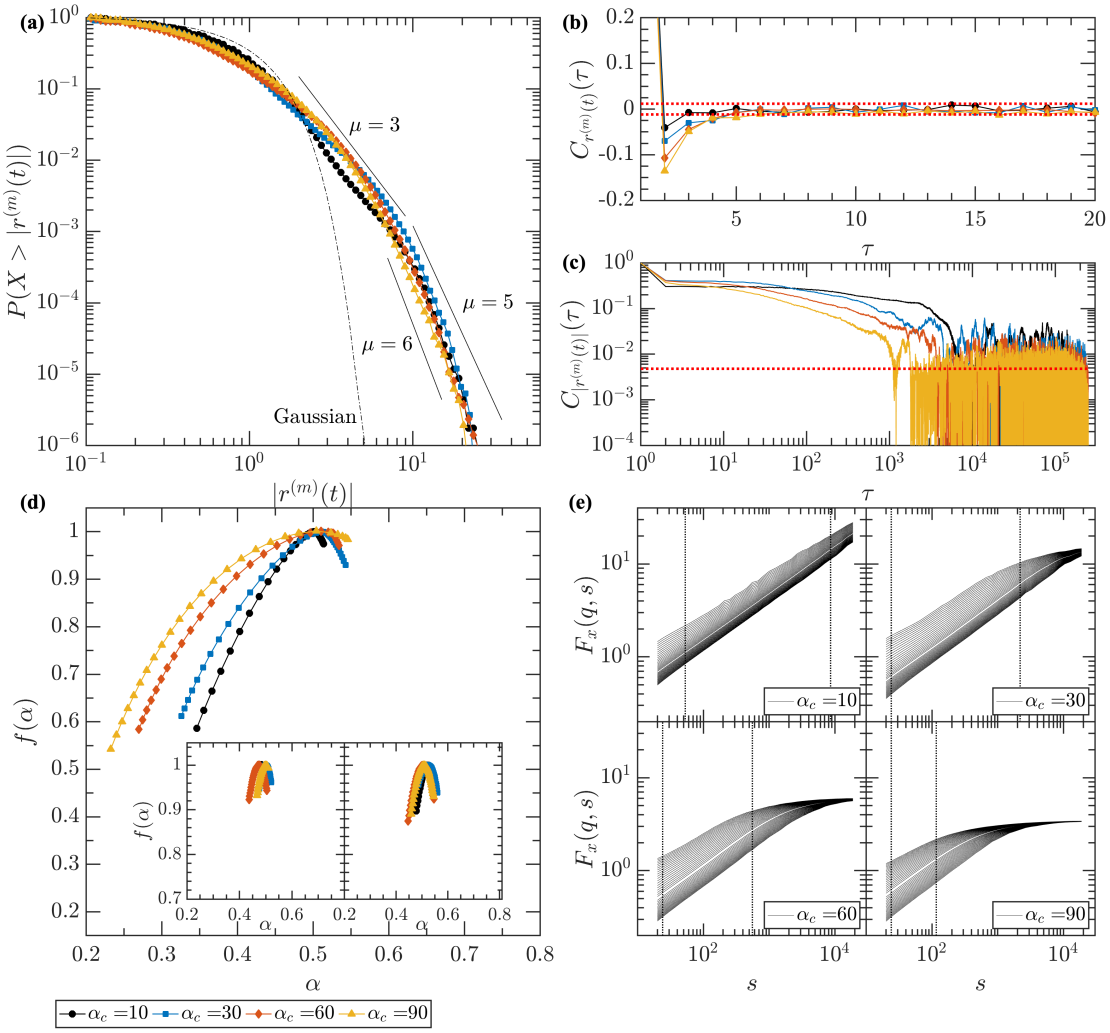

Figure 6.14: Mean statistical and multifractal properties of the time series generated by ten independent realizations of the single-asset version of the model with the following parameters $\beta = 1.6$, $J_{ij}^{lm} = 1$, $\kappa_c = 0.5$, and different values of the global coupling $\alpha_c \in [10, 30, 60, 90]$. Panel **(a)**: distribution of absolute returns; panel **(b)**: autocorrelation functions of returns; panel **(c)**: autocorrelation functions of absolute returns (volatility); panel **(d)**: singularity spectra $f(\alpha)$ of the generated signals (main plot) and result obtained for signals modified according to Fourier surrogates method and shuffled data (inset plots on the left- and right-hand side, respectively); panels in section **(e)**: fluctuation functions of the generated signals. The red dotted lines in plots (b) and (c) denote the noise levels. The black dotted lines in section (e) indicate range of scaling of the $F_x(q, s)$ functions.

Less pronounced clusters of the volatility observed for high values of global coupling parameter $\alpha_c \in [60, 90]$ are also visible on the level of the absolute returns autocorrelation functions, which maintain statistically significant level for lag $\tau \sim 10^3$, while for $\alpha_c = 30$ and $\alpha_c = 10$, they last for around $4 * 10^3$ time steps (Figure 6.14, panel (c)). Interestingly, the larger value of the global coupling parameter translates into stronger linear correlations of generated signals for $\tau = 1$. As shown in panel

(b) of Figure 6.14, the autocorrelation functions of the returns, for all analysed values of α_c, converges to 0 after a few time steps. However, for lag $\tau = 1$ significant differences are noticeable. As mentioned previously, for large values of α_c, agents tend to frequently change position to opposite, which, in turn reveal itself in the stronger negative autocorrelation observed for $\tau = 1$.

Value of the global coupling parameter, affects the range of non-linear correlations of returns produced by the model, that translates into different spans of scales for which fluctuation functions obey the power law (Figure 6.14, panel (e)). For low values of α_c parameter, the $F_x(q, s)$ function displays scale-free properties for $s \in [20, 10^4]$, while, along with the increase in global coupling parameter the span of scales for which the multifractal spectrum can be determined decreases to $s \in [20, 10^2]$. This effect is related to the length of fluctuation clusters. When parameter α_c is low, agent behaviour is more collective, and the rearrangement/meta-stable phases are longer, causing fluctuations clusters to span over a longer period of time. On the other hand, when an individual's decisions are mostly driven by the $\alpha_c S_i^{(m)} |M^{(m)}(t)|$ component, the agents behaviour is less collective, and thus the rearrangement/meta-stable periods are shorter and tend to change more frequently. In turn, volatility clusters are less pronounced, affecting the $F_x(q, s)$ function range of scaling.

The significant differences are also visible in the singularity spectra shapes (Figure 6.14, panel (d) and Table 6.3). While, for all analysed values of parameter α_c, function $f(\alpha)$ is characterized by strong left-hand side asymmetry (varying from $A_\alpha = 0.71 \pm 0.08$ for $\alpha_c = 30$ up to $A_\alpha = 0.85 \pm 0.21$ for $\alpha_c = 10$), the width of the singularity spectrum gradually growths, along with the α_c parameter, from $\Delta\alpha = 0.17 \pm 0.07$ for $\alpha_c = 10$ to $\Delta\alpha = 0.31 \pm 0.02$ for $\alpha_c = 90$. However, must be noted that the results obtained for large values of the global coupling parameter are based on the relatively short range of scales, and hence the free-scale properties of these signals are not convincing.

Furthermore, in order to verify that the observed multifractality is not a spurious effect, the singularity spectra for a randomly shuffled signals and Fourier surrogates were determined (inset plots on right- and left-hand in panel (d) of Figure 6.14, respectively). In both cases, the calculated $f(\alpha)$ functions' widths are significantly lower than for the original signals and vary from $\Delta\alpha = 0.06$ to $\Delta\alpha = 0.10$ for shuffled signal, and from $\Delta\alpha = 0.04$ to $\Delta\alpha = 0.06$ for signals modified according to the Fourier surrogate procedure.

Table 6.3: Mean singularity spectrum properties of the time series generated by ten independent realizations of the single-asset variant of the model with the following parameters $\beta = 1.6$, $J_{ij}^{lm} = 1$, $\kappa_c = 0.5$, and different values of the global coupling $\alpha_c \in [10, 30, 60, 90]$.

	$\boldsymbol{\alpha_c = 10}$	$\boldsymbol{\alpha_c = 30}$	$\boldsymbol{\alpha_c = 60}$	$\boldsymbol{\alpha_c = 90}$
$\boldsymbol{\Delta\alpha}$	0.17 ± 0.07	0.22 ± 0.03	0.26 ± 0.03	0.31 ± 0.02
$\boldsymbol{A_\alpha}$	0.85 ± 0.21	0.71 ± 0.08	0.82 ± 0.14	0.73 ± 0.11
$\boldsymbol{H}$	0.46 ± 0.04	0.44 ± 0.02	0.36 ± 0.01	0.34 ± 0.01

The results presented above confirm that an agent's ability to follow different

strategies, depending on the value of the α_c parameter, can significantly affect system dynamics. In general, when the individuals become more independent from their neighbours, the linear anti-persistence of the generated signals appears, and the volatility clusters become less pronounced. From the financial market perspective, it reflects the situation where investors are uncertain about their investment strategy and, therefore, continuously change the position in the market.

6.5 Transaction volume and threshold mechanism - how the *on-hold* state translates into a richer hierarchical organization of generated signals

The model's design incorporates another noticeable feature similar to the mechanism observed in real financial markets, namely, a positive correlation between volatility and transaction volume. In the model, this positive correlation is used to calculate threshold $\kappa^{(m)}(t)$, which determines whether agents actively participate in trading or not. This section focuses on the mentioned correlation and different types of threshold mechanisms, and quantitatively describes how it impacts the multiscale characteristics of the time series generated by the framework.

In the model, a transaction occurs when an agent changes its state to $S_i^{(m)} = +1$, which is considered as a 'buy' operation, or to $S_i^{(m)} = -1$, which is considered as a 'sell' action. Using such definitions of the transactions, the transaction volume V in particular time step t is equals the sum of buy $N_+^{(m)}(t)$ and sell $N_-^{(m)}(t)$ operations ($V^{(m)}(t) = N_+^{(m)}(t) + N_-^{(m)}(t)$). As the number of stocks and cash possessed by agents, besides of gradual decline of trading activity, does not significantly affect the multiscale correlations generated by the system (see Section 4.3.1), in the proposed model agents have unlimited resources, and the market is perfectly liquid. Practically, this means that individuals are always able to buy or sell an asset.

Figure 6.15 presents examples of the absolute returns signals and corresponding transaction volumes for four sets of the models parameters: default ($\beta = 1.6$, $\alpha_c = 30$, $J_{ij}^{lm} = 1$, $\kappa_c = 0.5$); high collectivity induced by low market temperature ($\beta = 2.0$, $\alpha_c = 30$, $J_{ij}^{lm} = 1$, $\kappa_c = 0.5$); increased local agent-agent interaction strength scenario ($\beta = 1.6$, $\alpha_c = 30$, $J_{ij}^{lm} = 1.25$, $\kappa_c = 0.5$); and strong global coupling case ($\beta = 1.6$, $\alpha_c = 90$, $J_{ij}^{lm} = 1$, $\kappa_c = 0.5$). As visual inspection reveals, volatility of generated time series is positively correlated with the number of transactions executed in system. Transaction volume peaks correspond to large returns, whereas small ones match with the periods of low activity of entities. Increased collectivity among individuals, caused by high value of β or strong agent-agent interaction do not affect the phenomenon significantly. Decorrelation between returns and transaction volume, however, is noticeable for signals generated by the model with high value of the global coupling parameter. In such a scenario, agents behave more independently; thus, the size of the peaks in transaction volume is not explicitly reflected in sizes of returns. A similar weakening of the dependence between transaction volume and volatility can be also observed for high temperatures (low β value) and low values of local agent-agent interaction strength parameter.

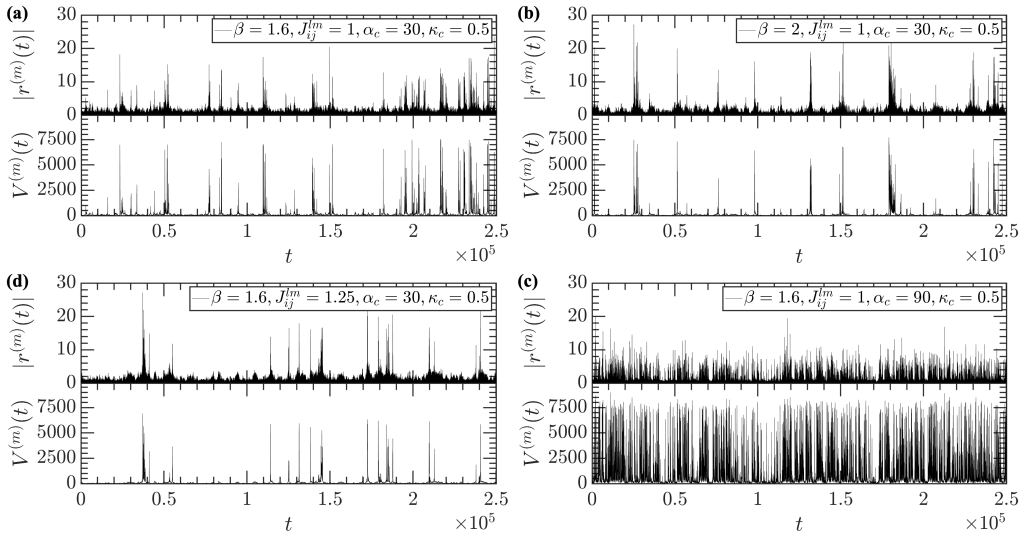

Figure 6.15: Examples of volatility and volume time series generated by the model with different sets of parameters: section **(a)**: $\beta = 1.6$, $\alpha_c = 30$, $J_{ij}^{lm} = 1$, $\kappa_c = 0.5$, section **(b)**: $\beta = 2.0$, $\alpha_c = 30$, $J_{ij}^{lm} = 1$, $\kappa_c = 0.5$, section **(c)**: $\beta = 1.6$, $\alpha_c = 30$, $J_{ij}^{lm} = 1.25$, $\kappa_c = 0.5$, section **(d)**: $\beta = 1.6$, $\alpha_c = 90$, $J_{ij}^{lm} = 1$, $\kappa_c = 0.5$.

The effect discussed above can be easily quantified by cross-correlation function C_{xy} (see equation 2.5). As panel (a) of Figure 6.16 shows, when collectivity among agents is relatively weak (i.e., large α_c value, orange line) and lags $\tau > 10$, function $C_{|r^{(m)}(t)|V^{(m)}(t)}$ assumes significantly lower values than are observed for other analysed sets of parameters. Moreover, the cross-correlation function maintains a statistically significant level for approximately $2.2 * 10^3$ time steps in the large global coupling scenario, versus $3.5 * 10^3 - 7 * 10^3$ for other cases that were considered. Such a result suggests that the correlation between volume and volatility might have a multiscale character. However, examination of the multifractal properties of the transaction volume time series produced by the model (Figure 6.16, panel (c)), shows that such a signal, in general, is not hierarchically organized. The $F_x(q, s)$ function of the number of transactions executed in the system does not obey the power law in small fluctuations regime ($q < 0$). For large returns ($q > 0$) and large scale $s \in [900, 10^4]$, as denoted by dotted trapeze in panel (c), $F_x(q, s)$ function has the appearance of power law dependence, however multifractal spectra calculated for this range of scales and scaling parameters does not assume inverted parabola shape typical for multifractal structures. As the autocorrelation of transaction volume signal does not have multifractal character, the dependency between the number of transaction and volatility is not multiscale as well.

The lack of hierarchical organization of the transaction volume time series in small scales regime is related to the model's intermittent on-off character. As the system transits between meta-stable and rearrangement phases, clusters of large returns develops, to some degree, in a gradual manner. Changes in transaction volume are less smooth, and in turn, the range of the observed values is poorer. For such a signal the hierarchical organization cannot develop. This effect is also visible on the cumulative distribution function level. As shown in panel (d) of Figure

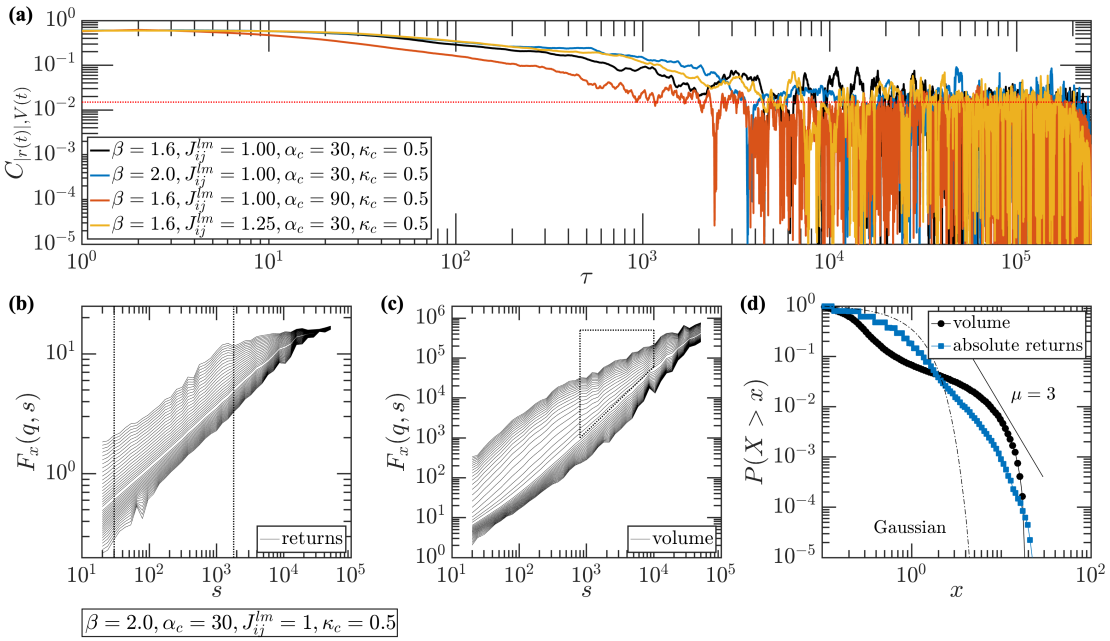

Figure 6.16: Cross-correlation between absolute returns and transaction volume signal generated by the model with different sets of parameter values (panel **(a)**). Panels **(b)** and **(c)** present the fluctuations function $F_x(q,s)$ of returns and transaction volume, respectively. Panel **(d)** display cumulative distribution functions of returns (black dots) and transaction volume signal (blue squares). The results presented on the plots (b)-(d) were generated by the model with parameters $\beta = 2.0$, $\alpha_c = 30$, $J_{ij}^{lm} = 1$, and $\kappa_c = 0.5$. The black dotted lines in panel (b) denote range of scaling. The black dotted trapeze in panel (c) presents the range of scales and q having an appearance of power law relationship.

6.16, the cumulative distribution function of the standardized transaction volume is curved in range $||V^{(m)}(t)|| \in [0.2, 0.9]$, indicating that the corresponding values of the standardized number of transactions are underrepresented.

Nevertheless, the correlation between the agent activity and volatility is successfully utilized in another element of the model, namely, in the threshold mechanism. The overall transaction volume is used for determining the threshold $\kappa^{(m)}$, based on which individuals decide to execute a transaction (i.e., assume state $S_i^{(m)}(t) = \pm 1$) or stay out of the market (i.e., assume on-hold state $S_i^{(m)}(t) = 0$).

The construction of the threshold mechanism and its connection with traders' activity significantly affects system dynamics. When individuals frequently change their positions in the market, the $\kappa^{(m)}$ value increases and prevents some of the entities from assuming active position. On the other hand, during quiet periods, the threshold decreases (entirely disappear, in extreme cases), and, as a result, all agents in the system assume a non-zero state. Practically speaking, the threshold mechanism does not affect the system in the meta-stable phase but, during rearrangement periods, it makes agents more likely to assume state $S_i^{(m)}(t) = 0$ and thus, enriches system dynamics overall. From the financial market perspective, the threshold can be interpreted as a risk-aversion factor. When investor activity increases, the market becomes volatile and so some of the traders assume a defensive strategy and prefer staying out of the market to secure their capital.

Naturally, increase of the κ_c leads to the growth of the number of individuals who

are inactive during the rearrangement periods. As shown in Figure 6.17, the size of the peak in the fraction of agents that assume $S_i^{(m)}(t) = 0$ span from $N_0^{(m)}/N \approx 0.15$ for $\kappa_c = 0.1$ up to $N_0^{(m)}/N \approx 0.9$ for $\kappa_c = 2$. Worth mentioning is that a further increase in κ_c value of leads to system collapse. When the threshold is sufficiently large, during the turbulent phase, all of individuals in the system become inactive, and, as magnetization drops to 0, the system never recovers.

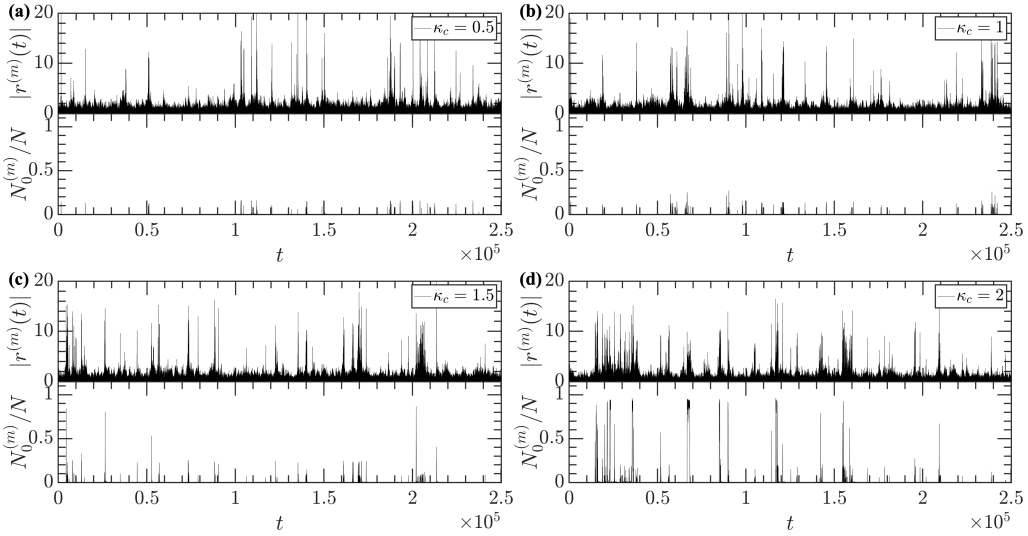

Figure 6.17: Absolute returns and normalized fraction of agents having state $S_i^{(m)} = 0$ generated by the model with parameters $\beta = 1.6$, $J_{ij}^{lm} = 1$, $\alpha_c = 30$, and different values of the threshold scaling coefficient $\kappa_c \in [0.5, 1, 1.5, 2]$.

While the influence of scaling factor κ_c on the number of agents out of the market is clearly visible, its impact on the returns generated by the system is not so obvious. Regardless of κ_c's value, volatility clustering and large single peaks in the returns time series occurs. Despite the lack of qualitative differences between returns generated by the model with a different value of κ_c, some discrepancies are visible on the cumulative distribution level. As shown in panel (a) of Figure 6.18 higher values of κ_c lead to slightly thinner absolute return distribution tails. During the rearrangement period when the system is volatile, the threshold mechanism works as a safety switch and reduces the number of agents actively participating in trading and, as a result, large fluctuations $|r^{(m)}(t)| > 10$ are less likely to occur. Quantitatively speaking, in the example series presented in Figure 6.17, the number of absolute returns that fulfill the inequality $|r^{(m)}(t)| > 10$ decreases from 141 for $k_c = 0.5$ to 52 for $k_c = 2$ (for $k_c = 1$ 136 data points fulfill the inequality, whereas, for $k_c = 1.5$ this number equals 104).

The slight discrepancies in the distribution of signals produced by the model with different values of the threshold scaling factor do not translate into the autocorrelation function of returns nor volatility. In the first case, regardless of the value of κ_c, $C_{r^{(m)}(t)}(\tau)$ converges to 0 for $\tau > 3$, whereas the absolute returns correlation function maintain substantial level for lags τ around $[3.7 * 10^3, 3.8 * 10^3]$, again without significant differences between results obtained for different values of κ_c.

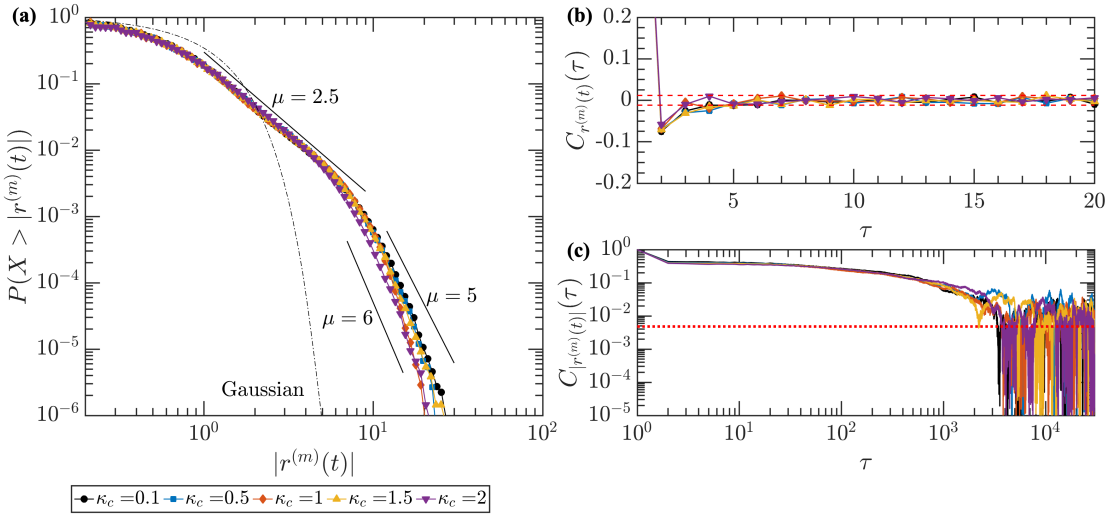

Figure 6.18: The mean cumulative distribution function (panel **(a)**), autocorrelation function of returns (panel **(b)**) and volatility (panel **(c)**) for signals generated by ten independent realizations of the single-asset variant of the model with parameters: $\beta = 1.6$, $J_{ij}^{lm} = 1$, $\alpha_c = 30$ and different values of the threshold scaling coefficient $\kappa_c \in [0.1, 0.5, 1, 1.5, 2]$.

The situation changes when the non-linear dependencies are considered. As shown in panel (a) of Figure 6.19 and Table 6.4, the mean multifractal spectrum calculated for signals generated by the model with $\kappa_c = 0.5$ is slightly wider than for other considered values of κ_c.

Few aspects of this result require further discussion. Firstly, introduction of the additional possible agent state enriches overall system dynamics. The presence of this new state is essential during rearrangement phases when the spatial organization of individuals is, at least partially, broken and entities are more likely to behave in a quasi-random manner. An agent's ability to assume on-hold position increases the complexity of the system configuration. Moreover, threshold size is directly linked to the previous time step's transaction volume (see equation (5.2)), which is correlated with volatility. As a result, the threshold mechanism introduces another medium of correlation propagation, which translates into amplification of non-linear dependencies of the signals generated by the model. However, it must be emphasized that an agent's ability to assume on-hold state, to some degree, cools down the entire system. Individuals, instead of changing the state, avoid taking any investment actions and, when a substantial number of the entities apply such a defensive strategy, system dynamics becomes poorer.

Last but not least, the threshold mechanism influence on the non-linear dependencies of the generated signal is amplified when system temperature is low. In fact, this impact gradually grows as the β parameter increases. As shown in Figure 6.20 the difference between the mean singularity spectrum width (panel (a)) of returns produced by a two-state variant of model $\kappa_c = 0$ and three state version with threshold scaling parameter $\kappa_c = 0.5$ is negligible when the system temperature is relatively high (up to $\beta \approx 1.5$). In such a scenario, the additional state does not significantly enrich the system's overall dynamics, because the rearrangement phases are not extremely turbulent. However, for sub-critical values of the inverse

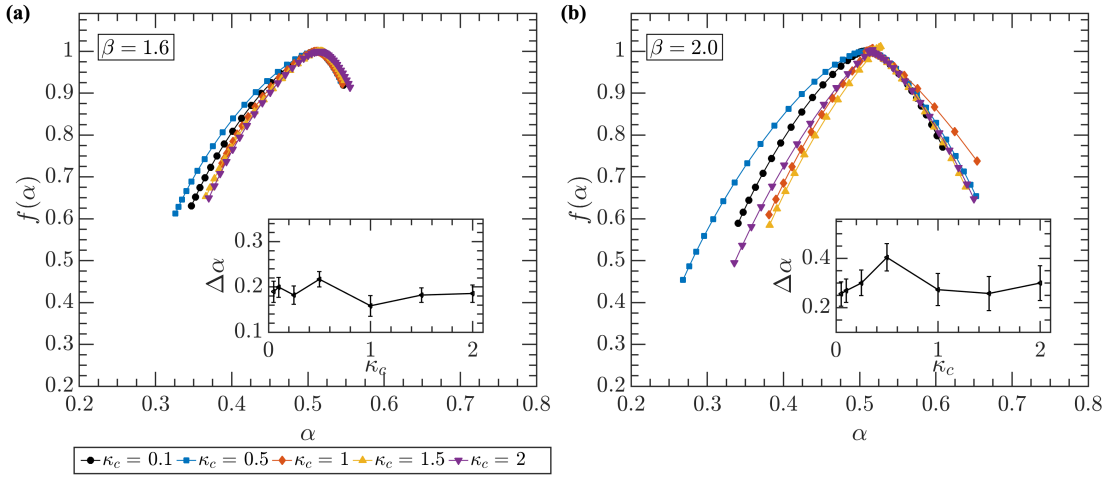

Figure 6.19: Mean singularity spectra of the time series generated by ten independent executions of the single-asset variant of the model with two values of the inverse temperature parameter $\beta = 1.6$ (panel **(a)**) and $\beta = 2.0$ (panel **(b)**) and different values of the threshold scaling coefficient $\kappa_c \in [0.1, 0.5, 1, 1.5, 2]$ (other parameters were set to: $J_{ij}^{lm} = 1$, $\alpha_c = 30$). Inset plots show the mean width $\overline{\Delta\alpha}$ of the presented spectra depending on κ_c's value.

Table 6.4: Mean singularity spectrum $f(\alpha)$ features of the time series generated by ten independent realizations of the single-asset variant of the model for two values of inverse temperature parameter $\beta = 1.6$ and $\beta = 2.0$, and different values of threshold scaling coefficient $\kappa_c \in [0.1, 0.5, 1, 1.5, 2]$ (other parameters were set to: $J_{ij}^{lm} = 1$, $\alpha_c = 30$).

$\beta = 1.6$	$\boldsymbol{\kappa_c = 0.1}$	$\boldsymbol{\kappa_c = 0.5}$	$\boldsymbol{\kappa_c = 1}$	$\boldsymbol{\kappa_c = 1.5}$	$\boldsymbol{\kappa_c = 2.0}$
$\boldsymbol{\Delta\alpha}$	0.19 ± 0.02	0.22 ± 0.02	0.15 ± 0.03	0.18 ± 0.02	0.18 ± 0.02
$\boldsymbol{A_\alpha}$	0.64 ± 0.16	0.71 ± 0.08	0.56 ± 0.05	0.64 ± 0.04	0.57 ± 0.03
$\boldsymbol{H}$	0.43 ± 0.02	0.44 ± 0.02	0.45 ± 0.02	0.45 ± 0.01	0.45 ± 0.02
$\beta = 2.0$	$\boldsymbol{\kappa_c = 0.1}$	$\boldsymbol{\kappa_c = 0.5}$	$\boldsymbol{\kappa_c = 1}$	$\boldsymbol{\kappa_c = 1.5}$	$\boldsymbol{\kappa_c = 2.0}$
$\boldsymbol{\Delta\alpha}$	0.26 ± 0.05	0.40 ± 0.05	0.27 ± 0.06	0.26 ± 0.07	0.29 ± 0.07
$\boldsymbol{A_\alpha}$	0.23 ± 0.10	0.29 ± 0.11	-0.06 ± 0.21	0.05 ± 0.16	0.12 ± 0.02
$\boldsymbol{H}$	0.45 ± 0.02	0.45 ± 0.02	0.50 ± 0.02	0.51 ± 0.01	0.48 ± 0.02

temperature $\beta \approx 2.0$, when the reconfiguration of the system is rough, the threshold mechanism's cooling-down aspect becomes important, as manifested by wider singularity spectra.

Regarding the influence of the on-hold state inclusion on non-linear dependencies in the signals produced by the model, another two possible ways of determining the trading friction were considered. The first, is based on the asymmetrical thresholds, calculated for positive and negative volume, respectively. In this case, buy and sell actions occurring in the system were counted and normalized separately, and as a result, two values of $\kappa_\pm^{(m)}$ were obtained. As shown in Figure 6.20 (blue squares), such modification does not significantly affect the richness of the time series generated by the model; however, the notable differences are observed in the singularity spectra asymmetry. For sub-critical values of $\beta \approx 2.0$ singularity spectra obtained for the asymmetric variant of the threshold mechanism are slightly more asymmetric than

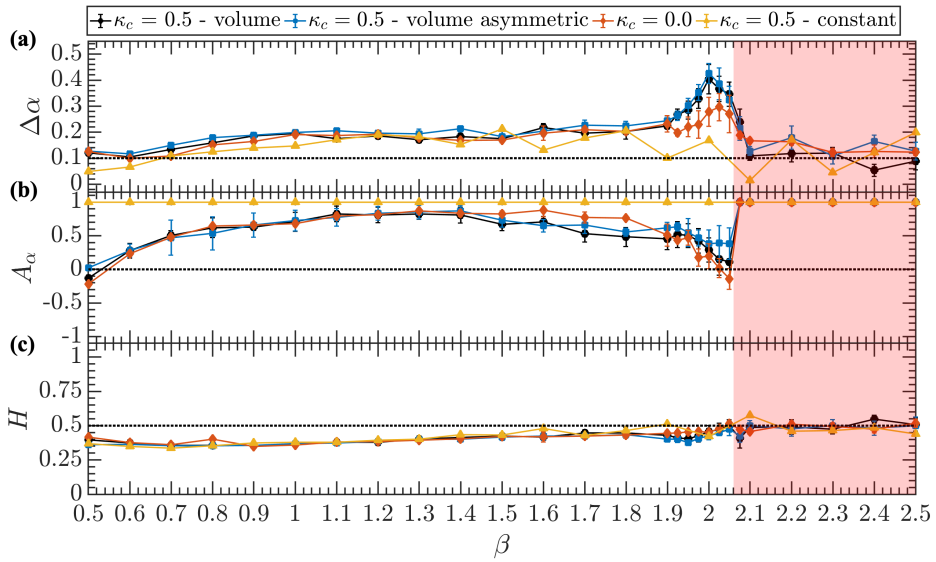

Figure 6.20: Mean spectrum width $\Delta\alpha$ (panel **(a)**), asymmetry A_α (panel **(b)**), and Hurst exponent H (panel **(c)**) in the dependence of $\beta \in [0.5, 2.5]$, obtained for ten independent realizations of the model with parameters $J_{ij}^{lm} = 1$, $\alpha_c = 30$, and different threshold mechanisms: volume depended with scaling $\kappa_c = 0.5$ (black dots), volume depended, asymmetric with scaling constant $\kappa_c = 0.5$ (blue squares), constant with $\kappa_c = 0.5$ (yellow triangles), and two-state version of the model with $\kappa_c = 0.0$ (orange diamonds). For the variant of the model with constant value of the threshold (yellow triangles), due to model instability, determination of reliable mean spectrum properties was not possible, thus the presented results are based on single realization only. The red zone indicates the range of β parameter for which scaling was observed only for positive q exponents.

spectra observed for threshold mechanism having symmetrical $\kappa^{(m)}$.

Moreover, the constant threshold variant was also studied (yellow triangles). In such a scenario, the value of $\kappa^{(m)}$ does not depend on transaction volume, but maintains the same level over the entire simulation. The dynamics of the signals generated by the model with such a variation of the threshold mechanism is characterised by full left-hand side asymmetry, and non-linear correlations are weaker, especially for sub-critical values of β. It must be emphasized that even a small value of the constant threshold leads to the model instability. When the threshold is constant, quite frequently all of agents in the system assume an on-hold state and system collapses[5].

The results presented above show that agent's ability to assume on-hold position in the market significantly affects system dynamics and non-linear correlations of returns generated by the model, especially when agents behaviour is highly collective ($\beta \approx 2.0$). The difference in hierarchical organization between two-state and three-state variants of the model, measured by generated time series singularity spectrum width, reaches 0.12 for $\beta = 2.0$. In practice, incorporation of on-hold state allows modeling of financial time series characterised by wide multifractal spectra, what is not possible with usage of either Bornholdt's or Iori's frameworks.

[5]Due to instability, the results presented in Figure 6.20 (yellow triangles) are based on the single, successful realization of the model.

6.6 Multifractal rolling window analysis of time series produced by the model

Examination of the multifractal properties of the time series provides valuable insights into the processes that govern the dynamics of the particular system. However, as long as the singularity spectrum is calculated for the entire signal, at once, averaged information is obtained. In this section, temporal evolution of the multifractal properties of the time series generated by the model is studied. As in Section 3.5, the analysis presented below is based on the rolling window technique.

The multifractal features of the financial time series, as shown in Section 3.5 and study [76] are constantly changing, and their dynamic is strongly influenced by critical market events such as crises and bubbles bursts. Interestingly, similar phenomena are observed in the time series generated by the model. Figure 6.21 shows the result of the rolling window analysis of signals produced by the model characterized by relatively high independence of agents: $\beta = 1.6$ (panels on the left-hand side) and increased collectivity: $\beta = 2.0$ (panels on the right-hand side). The remaining parameters were fixed at default values $\alpha_c = 30$, $J_{ij}^{lm} = 1.0$, and $\kappa_c = 0.5$. The analysis was performed for the windows containing 40000 data points with a step equal to 160 returns. Considering the signal produced by the model as hourly returns, such window corresponds to approximately 20 trading years, whereas a step is equivalent to approximately one trading month.

In both analysed cases, the singularity spectra have shape of the inverted parabola typical for the multifractal structures, and the $f(\alpha)$ maxima are located around $\alpha = 0.5$. Moreover, as in financial time series, signals produced by the model are characterized by strong non-linear dependencies of large fluctuations, as manifested by left-hand side asymmetry of multifractal spectra. The width of function $f(\alpha)$ varies from $\Delta\alpha \approx 0.2$ to $\Delta\alpha \approx 0.4$ for $\beta = 1.6$ and from $\Delta\alpha \approx 0.16$ to $\Delta\alpha \approx 0.48$ for $\beta = 2.0$. Such a difference in the richness of the hierarchical organization observed in returns generated by the model with different parameters has is based on changes in agent's collective behaviour, as was discussed in previous sections.

Regardless of the system temperature, the sharp changes in $\Delta\alpha$ calculated for different windows are noticeable. These fluctuations of singularity spectrum width typically correspond to large rates of return. Such a correlation suggests that variability of the multifractal spectrum properties might be rooted in the analysed signal's distribution changes. However, the fluctuations in $f(\alpha)$'s width for randomly shuffled data (blue squares) are significantly smaller (usually two times smaller) than those observed in the original signal. In fact, since the number of data points in the particular window is limited (40000 time steps), the variability of the multifractal spectrum width arises from a combination of the fluctuating level of non-linear correlations in the signal and changes in its distribution, with dominance of the former factor.

As mentioned above, left-hand asymmetry of the singularity spectra of returns generated by the model, can be observed in both analysed cases. However, the right wing of the $f(\alpha)$ function, which reflects the level of the hierarchical organization in the small fluctuations, is slightly more developed for the higher value of β. This effect is related to the system's ability to generate small returns. In low temperatures (i.e.,

high value of β), during a meta-stable period, a small number of agents change their position, and thus even minuscule fluctuations emerge. On the other hand, when the value of β is low, the number of agents actively participating in trading during quiet periods is significantly bigger, and, as a result, small returns rarely occur in the produced signal. Thus, the hierarchical structure in such a case is poorer.

Also worth noting is that, while the non-linear correlations of generated signals are significantly fluctuating over time, the long-range linear dependencies measured by the Hurst exponent (see Figure 6.21, section (e), bottom panels) maintain a level around $H = 0.42$ for $\beta = 1.6$ and around $H = 0.46$ for $\beta = 2.0$. The slightly anti-persistent signal generated by the system is a result of global coupling among agents (see Section 6.4 for more details).

Naturally, the features of the singularity spectra discussed above change along with the model parameters. Figure 6.22 presents the results of the rolling window analysis of signals generated by the model with decreased and increased value of the global coupling parameter (panels in section (a) - $\alpha_c = 10$, panels in section (b) - $\alpha_c = 90$) as well as amplified and weakened agent-agent interaction strength ($J_{ij}^{lm} = 0.75$ and $J_{ij}^{lm} = 1.25$, panels in sections (c) and (d), respectively). As can be observed in panels in sections (c) and (d), when the collectivity among agents is decreased the changes in $\Delta\alpha$ and A_α are significantly smoother than those existing for other analysed parameters sets. Moreover, due to the lack of highly pronounced volatility clusters, spectrum width stabilise around $\Delta\alpha \approx 0.3$ for increased global coupling scenario and leisurely fluctuates in range $\Delta\alpha \in [0.2, 0.4]$ for the $J_{ij}^{lm} = 0.75$ case.

On the other hand, when individual signal $h_i^{(m)}$ received by agents is dominated by information obtained from neighbours (i.e., resulting from decreased value of global coupling as shown in panel (a) or increased agent-agent interactionas shown in panel (d)), sharp changes in spectra width and asymmetry can be observed. Moreover, long periods of small fluctuations present in the signal generated by the model with a small value of α_c parameter result in the temporal monofractality of the series manifested by narrow and symmetrical singularity spectra (e.g., windows ending in range $t \in [5 * 10^3, 10^4]$). Furthermore, when agent investment decisions are primarily driven by the behaviour of other individuals in agent's vicinity (i.e., increased agent-agent local interaction as shown in panel (d)), the lack of hierarchical organization in small fluctuations emerges (marked by the red areas). As mentioned in previous sections, this effect is caused by the temporal freeze of the system configuration, which leads to zero returns. As a result, significant distortions in the fluctuation functions and, by extension, in the multifractal spectra are then observable.

Also noticeable are differences in long-range linear dependencies measured by Hurst exponent H. For a signal generated by the model with global coupling set to an immense value of (panel (b)), strong anti-persistence is noticeable $H \approx 0.31$. This effect is related to the increased dependence of agents' behaviour on the trading strategy (see Section 6.4). As a result, the spins are constantly flipping (changing from +1 to -1 and vice versa); thus, the clear trends manifested by subsequent positive/negative returns cannot develop. For other analysed parameter sets, the Hurst exponent fluctuates in a comparable range $H \in [0.32, 0.51]$.

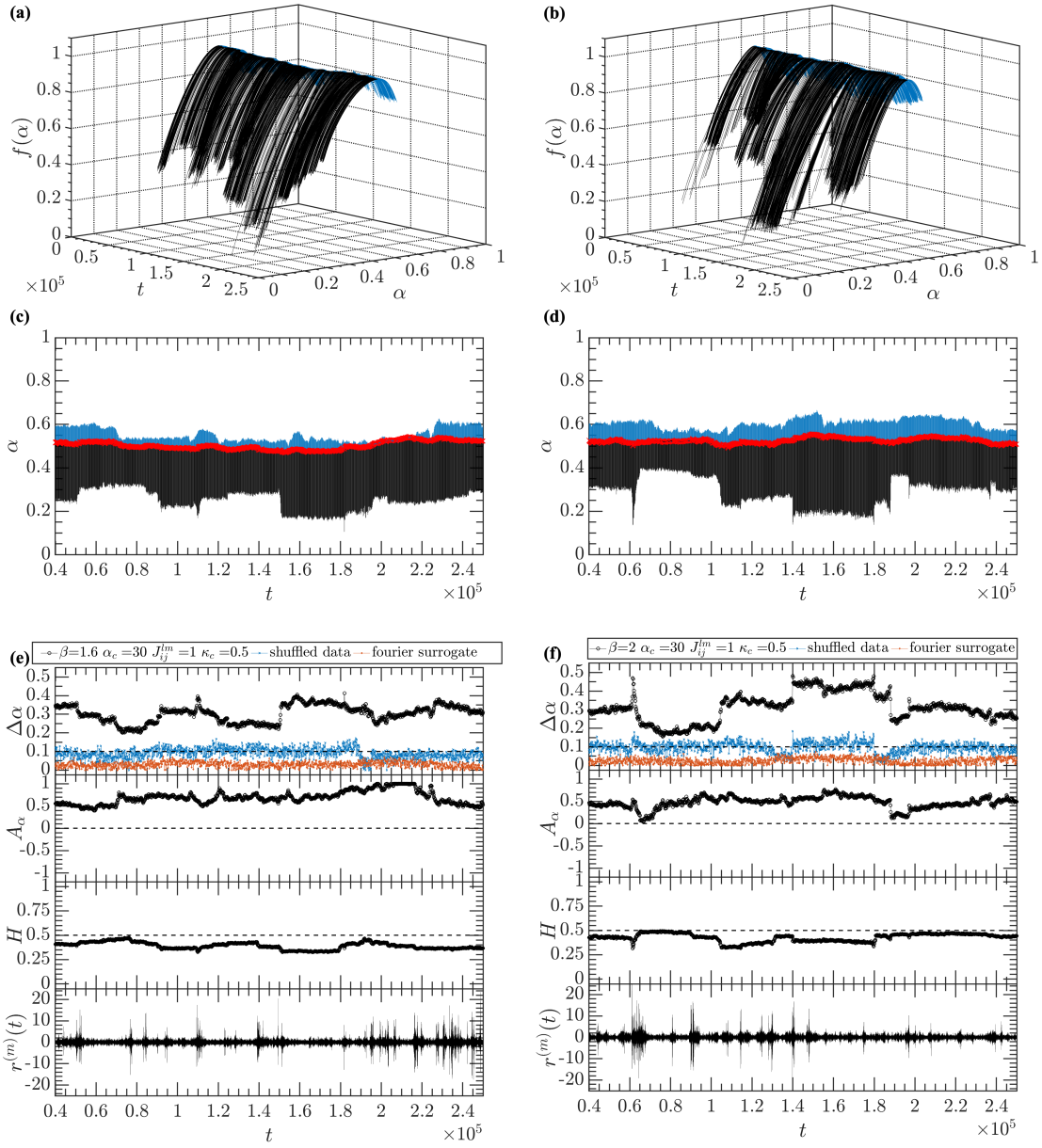

Figure 6.21: Multifractal rolling window analysis of the signals generated by the model with parameters: on the left-hand side: $\beta = 1.6$, $J_{ij}^{lm} = 1$, $\alpha_c = 30$, $\kappa_c = 0.5$ and on the right-hand side - $\beta = 1.6$, $J_{ij}^{lm} = 1$, $\alpha_c = 30$, $\kappa_c = 0.5$. Panels **(a)** and **(b)** present the three-dimensional view on the singularity spectra, where black and blue colors corresponds to left and right sides of the $f(\alpha)$, respectively. Panels **(c)** and **(d)** are projections of the multifractal spectra onto the time-α plane, with red crosses denoting $f(\alpha)$ maxima displacement. Panels in section **(e)** and **(f)** show the multifractal spectra properties (width $\Delta\alpha$, asymmetry A_α and Hurst exponent H, respectively) as well as analysed signal (panels at the bottom). The t value assigned to each data point corresponds to the end point within a window.

The multifractal rolling window analysis of the signals produced by the model shows that it can generate signals similar to those observed in financial data, including periods of singularity spectra's symmetrization and increased width. Moreover, manipulation of model parameters, allows generation of time series characterised

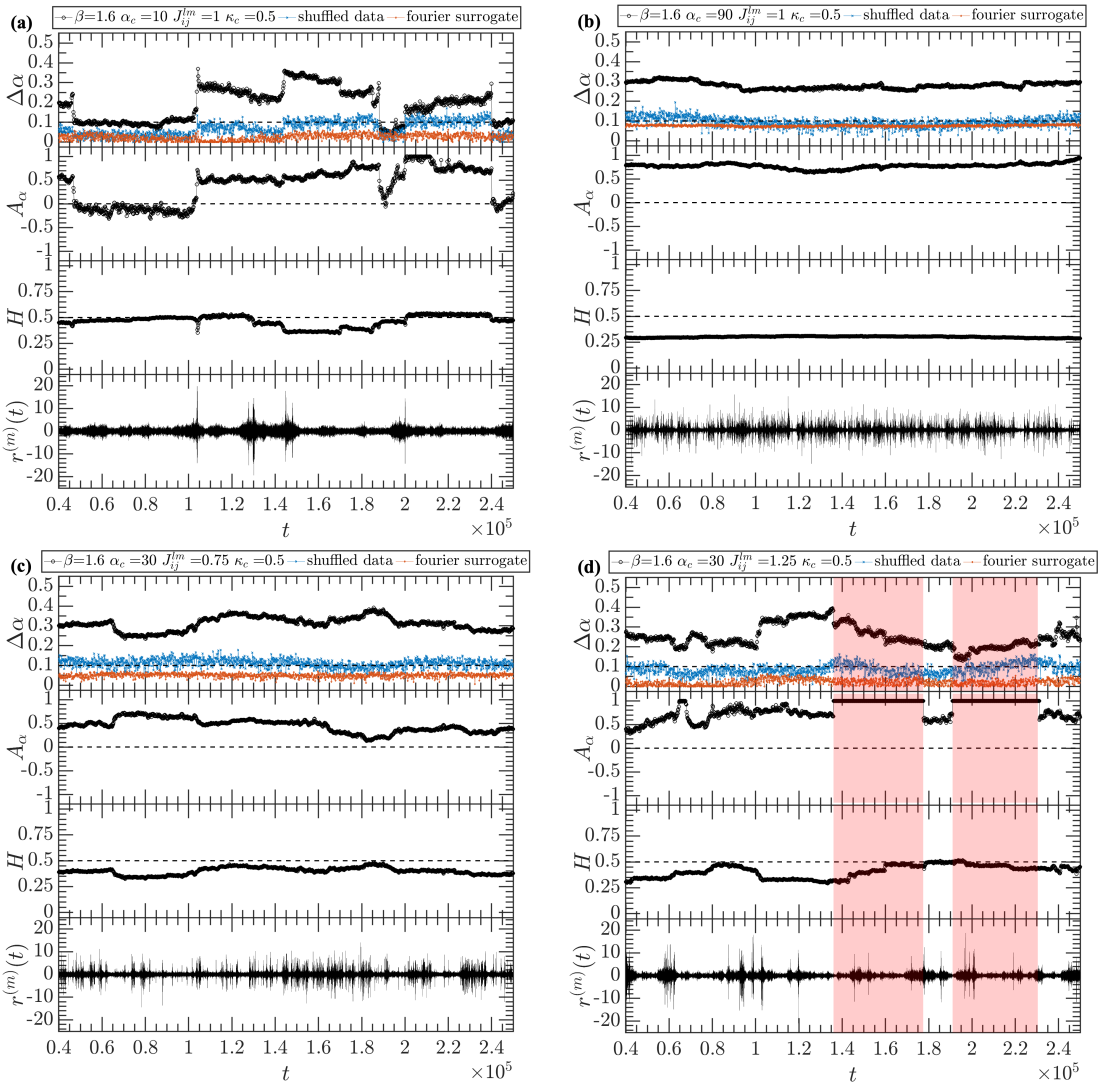

Figure 6.22: Time evolution of the multifractal properties of the returns generated by the single-asset variant of the model with decreased and increased value of the global coupling parameter ($\alpha_c = 10$ - panels in section **(a)** and $\alpha_c = 90$ - panels in section **(b)**) as well as amplified and weaken agent-agent local interaction strength ($J_{ij}^{lm} = 0.75$ and $J_{ij}^{lm} = 1.25$, panels in sections **(c)** and **(d)**, respectively). The red areas indicates the windows for which analysed signal was not fractal for negative values of the q parameter. The value of t assigned to each data point corresponds to the end point of a window.

by strong linear anti-persistence or temporal breakdown in scaling properties of the small fluctuations, which is typical for low liquidity assets (e.g., early years of bitcoin [83]), in the model represented by a variant with increased agent-agent local interaction parameter. From the financial market perspective, these results suggest that the primary force responsible for the dynamical variety of shapes observed in multifractal spectra of returns is caused by the continually changing collectivity among market participants.

Chapter 7

Multiscale correlations in the two-asset scenario

Key feature of the proposed model is its ability to simulate multiple, coupled financial instruments. In such a scenario, the entire system can be perceived as a set of linked subsystems, each representing an asset. Subsystems are connected on both global and local levels, and intensity of these connections is controlled by J_{ij}^{lm} and γ_{lm}, respectively (see equation (5.3) and Figure 5.1).

In this chapter, the influence of J_{ij}^{lm} and γ_{lm} values on generated signals' multiscale properties is examined. The following sections contain analysis of the framework's microscale dynamics in two-asset variant as well as examination of non-linear autocorrelations and cross-correlations of the signals produced by the model under differing combinations of cross-asset, agent-agent local interaction J_{ij}^{lm} and inter-asset global coupling γ_{lm} values.

7.1 Dynamics of multi-asset model variant

An investment decision of agent i regarding asset m can be influenced by the state of its neighbours in subsystem l and the magnetization of this subsystem scaled by the γ_{lm} parameter. From the financial market perspective, this model construction reflects a situation when an investor's decisions are driven not only by the positions of individuals in their vicinity and the price of the particular asset but also by the positions of those investors with respect to other assets quoted on the market and prices of these assets.

Naturally, extension of the model to a multi-asset scenario significantly affects its dynamics. As an example, consider a two-asset case, where each subsystem has the same parameters ($\beta = 1.6$, $\alpha_c = 30$, $\kappa_c = 0.5$) and connection between them is symmetrical $\gamma_{12} = \gamma_{21} = 0.1$ and $J_{ij}^{12} = J_{ij}^{21} = 0.01$, $J_{ij}^{11} = J_{ij}^{22} = 0.99$. As shown in Figure 7.1 (section (a)), analogous to the single-asset scenario, the dynamics observed on the subsystems configuration level is characterized by the metastable and rearrangement (turbulent) phases. Interestingly, even relatively weak cross-asset interactions between agents (i.e., a low value of $J_{ij}^{12} = J_{ij}^{21}$) lead to periods of synchronization in subsystems configurations, especially during the phases of low activity of agents. In these periods, individual's investments decisions regarding

traded assets are almost identical (Figure 7.1, section (a), inner panels).

The similarity between subsystems configurations is also visible during the rearrangement phases (Figure 7.1, section (a), panels on the right-hand side); however, due to decreased collectivity among agents, its level is significantly lower than is observed in quiet market periods. Furthermore, low values of J_{ij}^{lm} and γ_{lm} values prevent permanent synchronization of the subsystems. As shown on the left-hand side panels of section (a) of Figure 7.1, one subsystem may enter a turbulent phase, while another remains in its metastable phase.

The subsystems' synchronization and decoupling phases manifest themselves in the differences and similarities observed at the individual signal histograms level as well. As shown in section (b) of Figure 7.1, the distributions of $h_i^{(m)}$ during synchronization between assets (middle and right panels) are similar, whereas during decoupled period assume significantly different shapes - bell-like curve for the asset in the turbulent regime and polarized one for the stable subsystem. This phenomenon is even more visible in the time evolution of the individual signal histograms (Figure 7.1, section (c)). As in the single-asset scenario, most of the time, subsystems are in the metastable phase, which is occasionally interrupted by rearrangement periods, that can occur simultaneously in both subsystems or can be distinct. As a consequence, the increased volatility clusters in the signals produced by the subsystems often overlap.

From the practical application perspective, such behaviour of the system is highly desirable. The financial instruments tend to be coupled within the same basket; however, the correlations observed on the volatility level are not stable over time. During crises, most of the financial assets, regardless of their type, are volatile, which in the model is reflected by the overlapping volatility clusters. On the other hand, during stable periods, it is not unusual, that asset becomes volatile due to internal factors, such as disappointing earnings reports. These, in the model, are reflected by the distinct volatility clusters of fluctuations produced by the subsystems.

Worth noting is that extension of the model to a multi-asset scenario introduces additional potential values of $h_i^{(m)}$ that agents can receive, thus, enriching overall system dynamics. For example, in a system that consists of a single subsystem (i.e., single-asset scenario), assuming three-state variant of the model ($\kappa_c > 0$) and non-zero magnetization, an agent can receive 18 different values of $h_i^{(m)}$ (i.e., 9 possible values received from the neighbours multiplied by two possible values of the global coupling related term). When the model is extended to the two-assets variant and $J_{ij}^{ll} \neq J_{ij}^{lm}$, the spectrum of $h_i^{(m)}$ values increases to 82 (i.e., 41 possible values received from the neighbours multiplied by two possible values of the global coupling related term). Such enrichment of model dynamics, as shown in the following paragraphs, can positively impact the multiscale properties of the time series generated by the model.

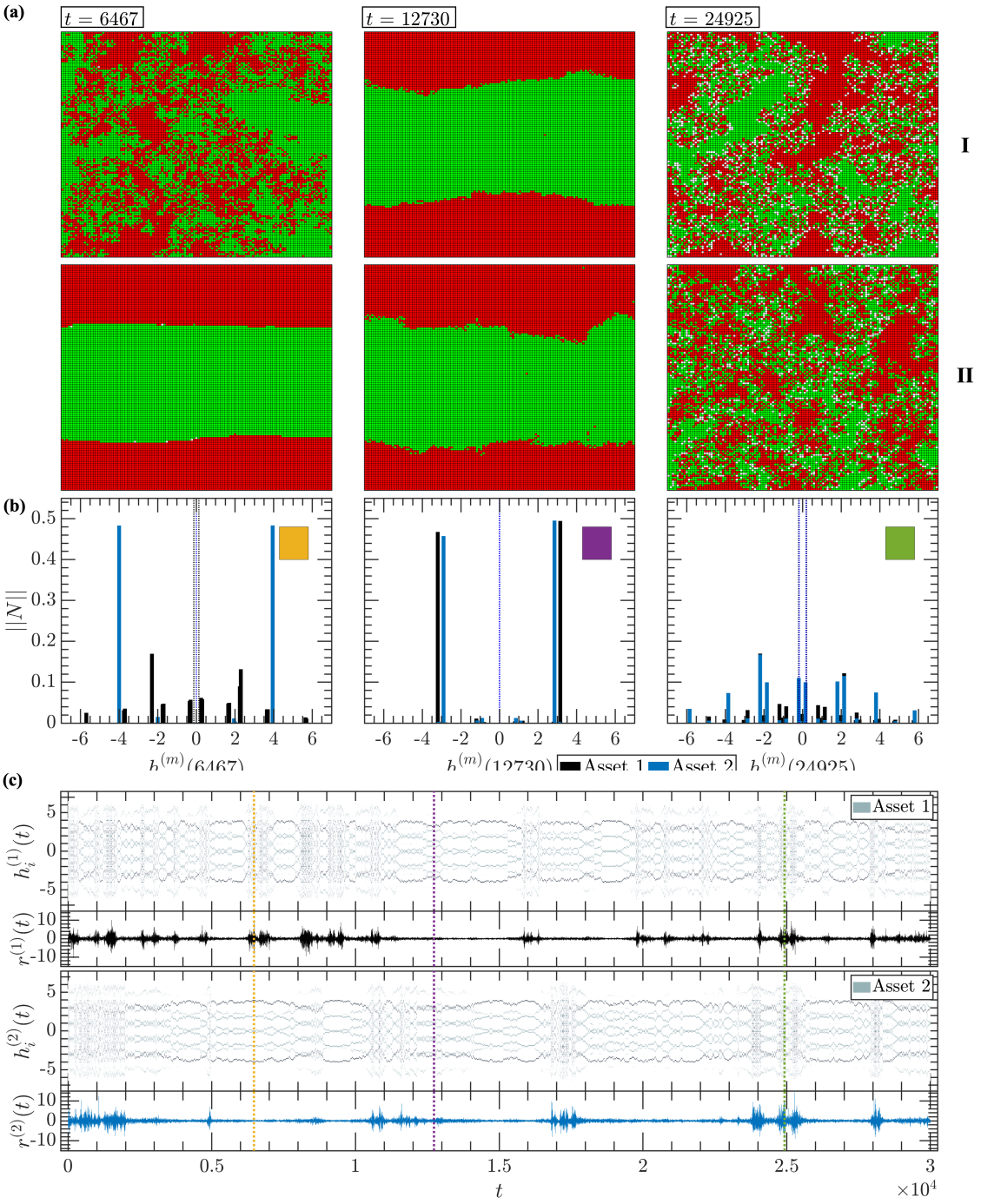

Figure 7.1: Dynamics of the two-asset variant of the model with parameters: $\beta = 1.6$,$J_{ij}^{12} = J_{ij}^{21} = 0.01$, $J_{ij}^{11} = J_{ij}^{22} = 0.99$, $\alpha_c = 30$, $\kappa_c = 0.5$, and $\gamma_{12} = \gamma_{21} = 0.1$. Section **(a)** shows subsystems configurations (Asset 1 - upper panels marked with I, Asset 2 - bottom panels, marked with II) in desynchronization period (panels on the left-hand side), synchronization in a metastable phase (middle panels) and partial synchronization in the rearrangement phase (panels on the right-hand side). Section **(b)** displays individual signal $h_i^m(t)$ histograms at time steps corresponding to the snapshots presented in section (a). Section **(c)** shows time evolution of individual signal histogram and generated returns time series (Asset 1 - upper panels, Asset 2 - bottom panels). Blue and black dotted lines in panels (b) indicate values of thresholds for Asset 1 and Asset 2, respectively. The color dotted lines in section (c) corresponds to individual signal histograms and rate of returns in section (c).

7.2 Influence of interactions between subsystems on non-linear self-dependencies of generated signals

The level of coupling between subsystems, as mentioned previously, can be controlled by two parameters, namely, the cross-asset agent-agent interaction strength J_{ij}^{lm} and inter-asset global coupling γ_{lm}. These parameters have slightly different influence on the agent's behaviour and, by extension, on the characteristics of the time series produced by the model. To get a sense of the impact of particular parameter, it is convenient to analyse them separately. Moreover, this analysis is narrowed to symmetrical cross-asset influence, meaning that: $J_{ij}^{lm} = J_{ij}^{ml}$ and $\gamma_{lm} = \gamma_{ml}$. In the two-asset scenario, the character of the relationship between subsystems (symmetrical or asymmetrical) does not significantly affect the produced time series. When the J_{ij}^{lm} and γ_{lm} are symmetrical, the generated signal can be perceived as a consensus between two subsystems, whereas, in the asymmetrical case, one asset acts as a leader is followed by another instrument. It should be noted here, that the situation is slightly more complicated when more than two assets are considered; this scenario is discussed in detail in Chapter 8.

Figure 7.2 presents the magnetization and corresponding rates of return generated by the model with different values of inter-asset global coupling factor $\gamma_{lm} \in [0.05, 0.1, 0.15, 0.2]$ and other parameters set to $\beta = 1.6$, $J_{ij}^{ll} = 1$, $J_{ij}^{lm} = 0$, $\alpha_c = 30$, and $\kappa_c = 0.5$. As is clearly visible the increased value of γ_{lm} leads to higher synchronization of the time series generated by the model (i.e., the overlap of more volatility clusters). However, for high values of the inter-asset global coupling ($\gamma_{lm} > 0.1$), undesirable effects on the magnetization level are observed. Specifically, the signals generated by the model, rather than fluctuating around $M(t) = 0$, drifts towards one of the equilibriums (e.g., for $\gamma_{lm} = 0.2$ it was $M(t) \approx \pm 0.1$), and, as the simulation continues, rapid transitions between these equilibrium zones occur. This effect is a result of the increased (decreased) value of the agent's individual signal.

The most convenient way to understand this phenomenon is to look at it from the perspective of the $h_i^{(m)}(t)$ histogram. When the value of γ_{lm} is sufficiently large, the entire histogram is shifted towards higher (or lower) values of the individual signal, depending on the magnetization of the other subsystem. As a result, the number of agents having positive (negative) individual signals becomes unbalanced, thereby possibly leading to positive (negative) magnetization of the system. These periods of unbalanced magnetization are occasionally broken during the rearrangement phases; however, the impact of the inter-asset global coupling rapidly pushes it towards one of the equilibrium zones. On the rates of return level, the biased agent's individual signal translates into the presence of pronounced volatility clusters that interlace with periods of small fluctuations, however these volatility clusters do not have shape observed in real financial time series.

Naturally, this effect is also noticeable on the multifractal properties level. Figure 7.3 shows the mean fluctuations functions and corresponding multifractal spectra calculated for time series of length $2.5 * 10^5$ data points generated by ten independent simulations. As shown on the left-hand side panels of the figure, the excessive value

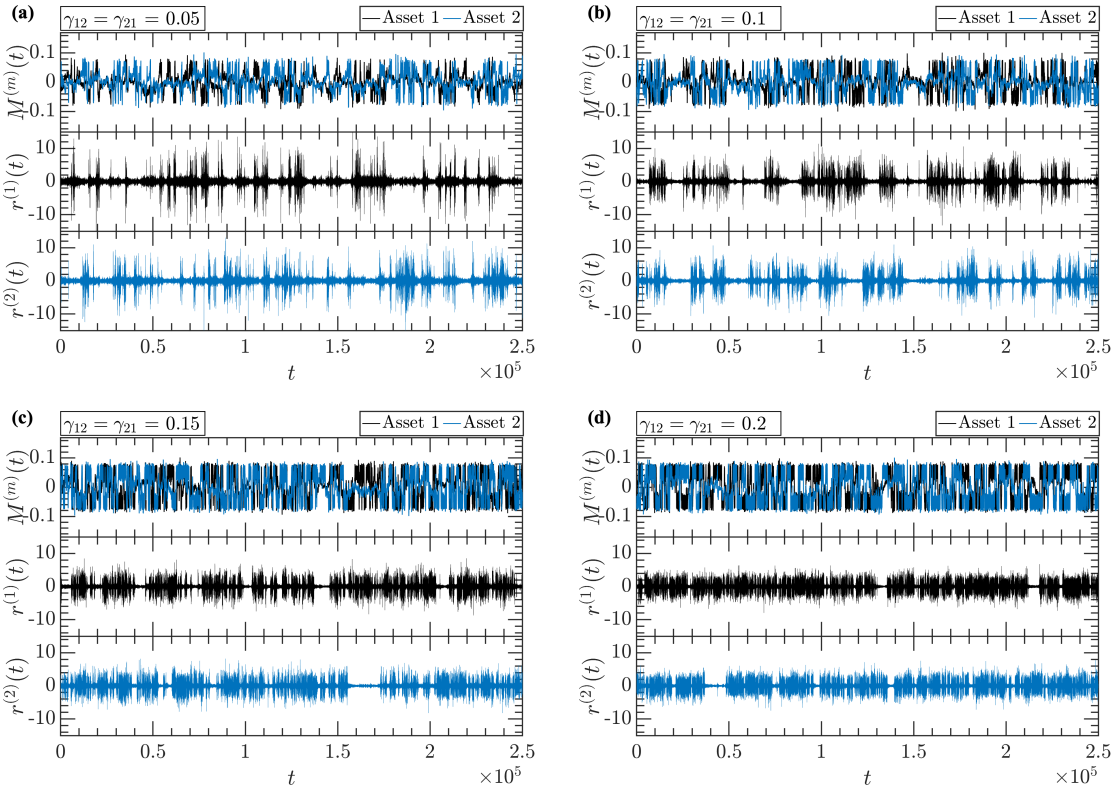

Figure 7.2: Examples of the magnetization and corresponding return time series generated by two-asset variant of the model with inter-asset global coupling coefficient: **(a)** $\gamma_{lm} = 0.05$, **(b)** $\gamma_{lm} = 0.1$; **(c)** $\gamma_{lm} = 0.15$, **(d)** $\gamma_{lm} = 0.2$, and values of other parameters set to: $J_{ij}^{ll} = 1$, $J_{ij}^{lm} = 0$, $\beta = 1.6$, $\alpha_c = 30$, and $\kappa_c = 0.5$.

of the inter-asset global coupling parameter ($\gamma_{lm} \in [0.15, 0.2]$) leads to the distortion of $F_x(q, s)$ observed for positive q exponents. The degree of deformation increases along with γ_{lm} and for $\gamma_{lm} = 0.2$ the function $F_x(q, s)$ significantly diverts from the expected power law characteristic. As mentioned previously, for strong inter-asset global coupling, generated signals are biased and tend to fluctuate in one of the equilibrium zones, occasionally switching between them. As the transition between high and low states of the magnetization is rapid, the volatility clusters assume rectangle-like shape, which is the main factor leading to the distortions observed in the fluctuations function. On the other hand, for small values of the inter-asset global coupling parameter ($\gamma_{lm} = [0.05, 0.1]$), this effect is not observed, and the scaling of function $F_x(q, s)$ is convincing and spans a considerable range of scales.

The differences in hierarchical organization are also visible on the multifractal spectra level. The panel (b) of Figure 7.3 shows the mean singularity spectra determined for $\gamma_{lm} = [0.05, 0.1, 0.15]$ (due to significant distortion of the fluctuations function, the case $\gamma_{lm} = 0.2$ is omitted). For weak inter-asset global coupling, $f(\alpha)$ functions are relatively broad ($\Delta\alpha = 0.16 \pm 0.02$ and $\Delta\alpha = 0.18 \pm 0.01$ for $\gamma = 0.05$ and $\gamma_{lm} = 0.1$ respectively) and are characterised by left-hand side asymmetry ($A_\alpha = 0.87 \pm 0.12$ and $A_\alpha = 0.59 \pm 0.20$ for $\gamma_{lm} = 0.05$ and $\gamma_{lm} = 0.1$, respectively), results similar to those obtained in the single-asset scenario. For

$\gamma_{lm} = 0.15$, widths of the singularity spectra are similar to those analysed above ($\Delta\alpha = 0.30 \pm 0.03$), however the multifractal spectrum reveals slight right-hand side asymmetry ($A_\alpha = -0.20 \pm 0.32$), which is related to poor scaling observed in the range of positive q values. Properties of obtained singularity spectra ($\Delta\alpha$, A_α and H) are also presented in Table 7.1.

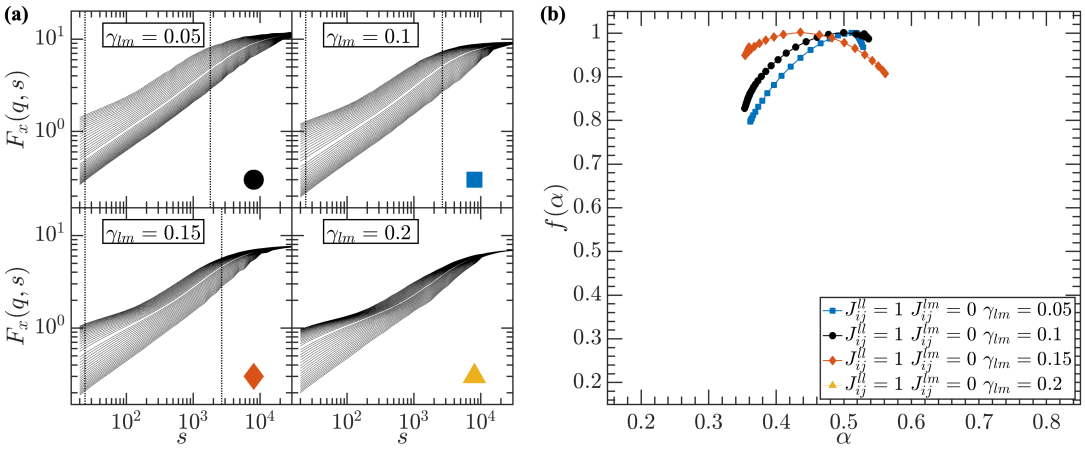

Figure 7.3: Mean fluctuations functions $F_x(q,s)$ (panels in section **(a)**) and corresponding multifractal spectra (panel in section **(b)**) of time series produced by ten independent executions of the multi-asset variant of the model with different values of inter-asset global coupling parameter $\gamma_{lm} \in [0.05, 0.1, 0.15, 0.2]$ and other coefficients fixed ($\beta = 1.6$, $J_{ij}^{ll} = 1$, $J_{ij}^{lm} = J_{ij}^{ml} = 0$, $\alpha_c = 30$, and $\kappa_c = 0.5$). The dotted black lines in the plots on the left-hand side denote the range of scales used for singularity spectrum calculations. Due to distortion of the fluctuations function for series produced by the model with $\gamma_{lm} = 0.2$, the singularity spectrum was not determined. The color markers in the fluctuation functions plots links to the corresponding singularity spectra presented on the right-hand side panel.

Table 7.1: Properties of mean singularity spectra determined for signals generated by ten independent executions of multi-asset variant of the model with different values of inter-asset global coupling parameter $\gamma_{lm} \in [0.05, 0.1, 0.15]$ and other coefficients fixed as follows: $\beta = 1.6$, $J_{ij}^{ll} = 1$, $J_{ij}^{lm} = J_{ij}^{ml} = 0$, $\alpha_c = 30$, and $\kappa_c = 0.5$.

	$\gamma_{lm} = 0.05$	$\gamma_{lm} = 0.1$	$\gamma_{lm} = 0.15$
$\Delta\alpha$	0.16 ± 0.02	0.18 ± 0.01	0.20 ± 0.03
A_α	0.87 ± 0.12	0.59 ± 0.20	-0.20 ± 0.32
H	0.39 ± 0.01	0.37 ± 0.01	0.36 ± 0.02

The characteristics of the signals produced by the model in which cross-asset interaction is limited only to the agent-agent interaction differ slightly. Figure 7.4 shows examples of time series generated by the model with different values of the cross-asset agent-agent interaction strength parameter, which were chosen in such a way that $J_{ij}^{ll} + J_{ij}^{lm} = 1$, i.e., $J_{ij}^{ll} \in [0.99, 0.96, 0.93, 0.9]$, and $J_{ij}^{lm} \in [0.01, 0.04, 0.07, 0.1]$ with the other parameters set as follows: $\beta = 1.6$, $\alpha_c = 30$, $\kappa_c = 0.5$, and $\gamma_{lm} = \gamma_{ml} = 0$. Naturally, as J_{ij}^{lm} increases, higher collectivity between time series emerges, and the magnetization of the subsystems aligns. It should be noted that, excessive value of the cross-asset agent-agent local interaction strength leads to the unwanted

features of the generated time series. That is, as J_{ij}^{lm} rises, the periods when the subsystems magnetization stabilizes around $M(t) \approx 0$ extend. This effect is caused by the significant influence that agent's neighbours positions in different assets have on agent's investment decisions. Thus, an imbalance between supply and demand appears less likely, as it has to develop in both subsystems simultaneously. Moreover, the same mechanism is responsible for the fewer large fluctuation clusters observed in returns signal.

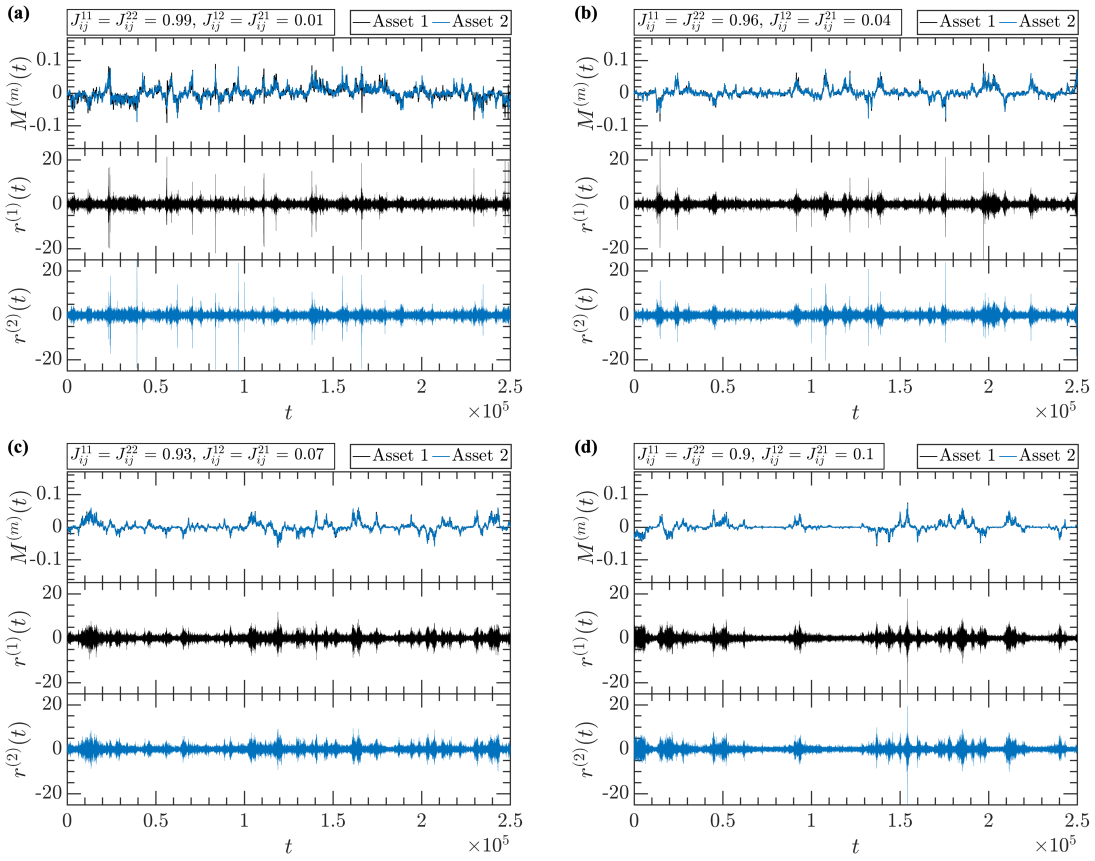

Figure 7.4: Examples of the magnetizations and corresponding returns time series generated by the two-asset variant of the model characterized by different values of the cross-asset agent-agent interaction strength parameter: **(a)** $J_{ij}^{ll} = 0.99$, $J_{ij}^{lm} = 0.01$; **(b)** $J_{ij}^{ll} = 0.96$, $J_{ij}^{lm} = 0.04$; **(c)** $J_{ij}^{ll} = 0.93$, $J_{ij}^{lm} = 0.07$; **(d)** $J_{ij}^{ll} = 0.9$, $J_{ij}^{lm} = 0.1$, and other parameters fixed as follows: $\beta = 1.6$, $\alpha_c = 30$, $\kappa_c = 0.5$, and $\gamma_{lm} = \gamma_{ml} = 0$.

The changes in time series characteristics that appear depending on the values of cross-asset agent-agent interaction strength are also visible on the hierarchical organization level. Figure 7.5 shows the mean fluctuations functions (panels in section (a)) and corresponding multifractal spectra (panel (b)) calculated for signals generated by the model with different sets of J_{ij}^{ll} and J_{ij}^{lm} parameters. As is clearly visible, for small values of $J_{ij}^{lm} \in [0.01, 0.04]$ the fluctuation functions obey the power law over a large range of scales ($s \in [20, 1000]$ and $s \in [20, 3932]$ for $J_{ij}^{lm} = 0.01$ and $J_{ij}^{lm} = 0.04$, respectively), whereas for the series generated by the model with $J_{ij}^{lm} = 0.07$ and $J_{ij}^{lm} = 0.1$ a significant distortion is observed for large s. This effect is caused by the subsystems synchronization observed for strong cross-asset agent-

agent interactions, which lead to stabilization of magnetization. In turn, obtained returns are characterised by a small number of large fluctuations, which are required to develop the hierarchical organization.

The multifractal spectra also manifest the differences in non-linear autocorrelations of the generated time series. As shown on panel (b) of Figure 7.5, the singularity spectra of signals produced by the model, for almost all analysed parameter sets (except for the $J_{ij}^{lm} = 0.1$ scenario), are characterized by strong left-hand side asymmetry (which varies from $A_\alpha = 0.31 \pm 0.36$ to $A_\alpha = 0.74 \pm 0.12$ for $J_{ij}^{lm} = 0.07$ and $J_{ij}^{ll} = 0.93$ and for $J_{ij}^{lm} = 0.01$ and $J_{ij}^{ll} = 0.99$, respectively), whereas width changes from $\Delta\alpha = 0.27 \pm 0.07$ for $J_{ij}^{lm} = 0.01$ and $J_{ij}^{ll} = 0.99$ to $\Delta\alpha = 0.16 \pm 0.10$ for $J_{ij}^{lm} = 0.07$ and $J_{ij}^{ll} = 0.93$. Interestingly, the singularity spectra obtained for the time series generated by the model with weak cross-asset agent-agent interactions are broader than those observed for the single-asset scenario with the same value of β parameter (see Figure 6.8, panel (b), blue squares). This amplification of non-linear self-dependencies in the produced signals could be related to the increase in number of possible values of the signal coming from the neighbours that was discussed in the previous section.

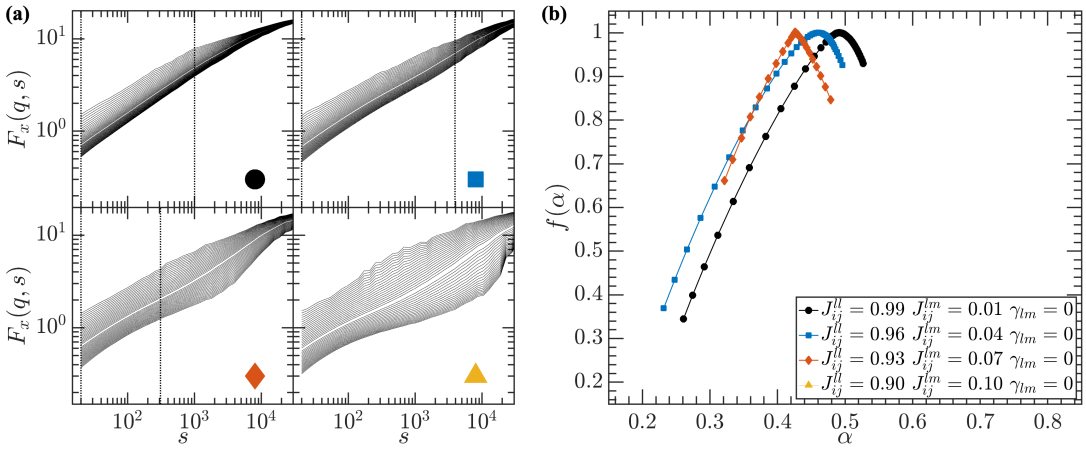

Figure 7.5: Mean fluctuations functions $F_x(q, s)$ (panels in section **(a)**) and corresponding multifractal spectra (panel **(b)**) of time series produced by ten independent executions of the multi-asset variant of the model with different values of cross-asset agent-agent local interaction strength parameters: $J_{ij}^{ll} \in [0.99, 0.96, 0.93, 0.9]$, $J_{ij}^{lm} = J_{ij}^{ml} \in [0.01, 0.04, 0.07, 0.1]$, and other coefficients set as follows: $\beta = 1.6$, $\alpha_c = 30$, $\kappa_c = 0.5$, and $\gamma_{lm} = 0$. The dotted black lines in the plots on the left-hand side denote the range of scales used for singularity spectrum calculations. Due to distortion of the fluctuation function for $J_{ij}^{ll} = 0.9$ and $J_{ij}^{lm} = 0.1$, the singularity spectrum for this case was not determined. The color markers in the fluctuations functions plots links to the corresponding singularity spectra presented on the right-hand side panel.

Besides the distortion of the hierarchical organization, another side effect is observed in signals produced by the model characterized by a large value of the cross-asset agent-agent local interaction strength parameter. The increased value of J_{ij}^{lm} introduces linear autocorrelations in the generated time series. As is noticeable, the multifractal spectra presented in panel (b) of Figure 7.5 drifts towards lower α values with an increase in J_{ij}^{lm}. The Hurst exponent of these signals indicates slight anti-persistence that varies from $H = 0.41 \pm 0.05$ for $J_{ij}^{lm} = 0.07$ and $J_{ij}^{ll} = 0.93$ to $H = 0.45 \pm 0.01$ for $J_{ij}^{lm} = 0.01$ and $J_{ij}^{ll} = 0.99$. Again, this effect is related to the

decrease in likelihood that an imbalance occurring between supply and demand in consecutive time steps develops, as it must develop in both subsystems simultaneously. Properties of obtained singularity spectra ($\Delta\alpha$, A_α and H) are also presented in Table 7.2.

Table 7.2: Mean singularity spectra properties determined for signals generated by ten independent executions of the multi-asset variant of the model with different values of cross-asset agent-agent local interaction strength parameter $J_{ij}^{ll} \in [0.99, 0.96, 0.93, 0.9]$, $J_{ij}^{lm} = J_{ij}^{ml} \in [0.01, 0.04, 0.07, 0.1]$, and other coefficients set as follows: $\beta = 1.6$, $\alpha_c = 30$, $\kappa_c = 0.5$, and $\gamma_{lm} = 0$.

	$J_{ij}^{ll} = 0.99, J_{ij}^{lm} = 0.01$	$J_{ij}^{ll} = 0.96, J_{ij}^{lm} = 0.04$	$J_{ij}^{ll} = 0.93, J_{ij}^{lm} = 0.07$
$\boldsymbol{\Delta\alpha}$	0.27 ± 0.07	0.26 ± 0.13	0.16 ± 0.10
$\boldsymbol{A_\alpha}$	0.74 ± 0.12	0.73 ± 0.14	0.31 ± 0.36
$\boldsymbol{H}$	0.45 ± 0.01	0.42 ± 0.04	0.41 ± 0.05

As the analysis presented in this section shows, both global and local cross-asset interactions between subsystems can amplify the non-linear autocorrelations of the time series generated by the model. However, the extreme values of the J_{ij}^{lm} or γ_{lm} coefficients lead to substantial distortion in the hierarchical organization of the produced signals, as the fluctuations functions deformation manifests.

7.3 Impact of cross-asset local and global interactions between agents on multiscale characteristics of produced time series

The crucial question that arises in the context of the analysis presented in previous section concerns the influence of combined inter-asset global coupling and cross-asset agent-agent interactions on the multifractality of the signals. Since the excessive values of any of these parameters lead to the distortion of hierarchical organization, the ranges of considered values of J_{ij}^{lm}, J_{ij}^{ll} and γ_{lm} were limited as follows: $J_{ij}^{lm} \in [0.01, 0.04]$, $J_{ij}^{ll} \in [0.99, 0.96]$ and $\gamma_{lm} \in [0.05, 0.1]$. As shown in Figure 7.6 (panels on the left-hand side), the fluctuations functions of returns generated by the model with such parameters obey the power law in a large range of scales (up to $s \sim 10^3$), whereas multifractal spectra (panel (b)) are characterized by left-side asymmetry (asymmetry coefficient varies from $A_\alpha = 0.66 \pm 0.09$ for $J_{ij}^{lm} = 0.04, J_{ij}^{ll} = 0.96, \gamma_{lm} = 0.05$ to $A_\alpha = 0.90 \pm 0.14$ for $J_{ij}^{lm} = 0.04, J_{ij}^{ll} = 0.96, \gamma_{lm} = 0.1$), and are relatively broad (from $\Delta\alpha = 0.18 \pm 0.02$ for $J_{ij}^{lm} = 0.04, J_{ij}^{ll} = 0.96, \gamma_{lm} = 0.1$ to $\Delta\alpha = 0.23 \pm 0.08$ for $J_{ij}^{lm} = 0.01, J_{ij}^{ll} = 0.99, \gamma_{lm} = 0.05$). In general, a model charachterised by relatively high global and local interactions between subsystems produces time series with the richest hierarchical organization ($J_{ij}^{ll} = 0.99, J_{ij}^{lm} = 0.01, \gamma_{lm} = 0.05$). Interestingly, the non-linear correlations of signals generated by the model with stronger global inter-asset coupling ($\gamma_{lm} = 0.1$) are slightly weaker than those observed when $\gamma_{lm} = 0.05$, suggesting that, in fact, the linkage between assets on a global level combined with local cross-asset interactions between agents negatively influences the hierarchical organization of the produced time series. The

reason for such a decrease in the multifractal spectra width could be related to the fact that both of these factors amplify the synchronization between subsystems configurations; thus, it becomes more stable (especially for large γ_{lm} values) and the overall dynamics of the model becomes poorer.

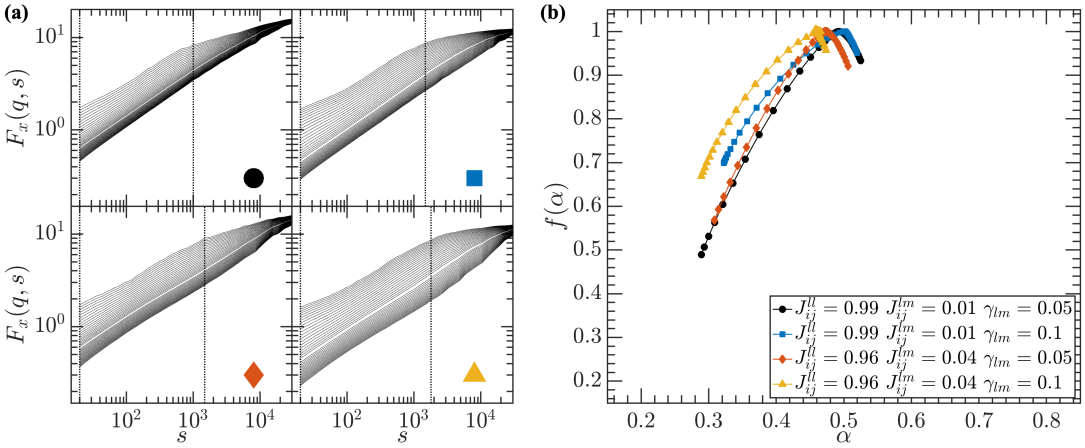

Figure 7.6: Mean fluctuations functions $F_x(q,s)$ (panels in section **(a)**) and corresponding multifractal spectra (panel **(b)**) of the time series generated by ten independent executions of the multi-asset variant of the model with different values of cross-asset agent-agent local interaction strength and inter-asset global coupling parameters $J_{ij}^{ll} \in [0.96, 0.99]$, $J_{ij}^{lm} \in [0.04, 0.01]$, $\gamma_{lm} \in [0.05, 0.1]$. Other coefficients were set as follows: $\beta = 1.6$, $\alpha_c = 30$, and $\kappa_c = 0.5$. The dotted black lines in $F_x(q,s)$ plots denote the range of scaling, and the color markers links to the corresponding singularity spectra presented in panel (b).

Table 7.3: Mean singularity spectra properties determined for signals generated by ten independent executions of the multi-asset variant of the model with different values of cross-asset agent-agent local interaction strength and inter-asset global coupling parameters $J_{ij}^{ll} \in [0.96, 0.99]$, $J_{ij}^{lm} \in [0.04, 0.01]$, $\gamma_{lm} \in [0.05, 0.1]$. Other coefficients were set as follows: $\beta = 1.6$, $\alpha_c = 30$, $\kappa_c = 0.5$.

	$J_{ij}^{ll} = 0.99, J_{ij}^{lm} = 0.01, \gamma_{lm} = 0.05$	$J_{ij}^{ll} = 0.99, J_{ij}^{lm} = 0.01, \gamma_{lm} = 0.1$
$\boldsymbol{\Delta\alpha}$	0.23 ± 0.08	0.19 ± 0.03
$\boldsymbol{A_\alpha}$	0.73 ± 0.15	0.82 ± 0.11
$\boldsymbol{H}$	0.43 ± 0.04	0.38 ± 0.02
	$J_{ij}^{ll} = 0.96, J_{ij}^{lm} = 0.04, \gamma_{lm} = 0.05$	$J_{ij}^{ll} = 0.96, J_{ij}^{lm} = 0.04, \gamma_{lm} = 0.1$
$\boldsymbol{\Delta\alpha}$	0.19 ± 0.05	0.18 ± 0.02
$\boldsymbol{A_\alpha}$	0.66 ± 0.09	0.90 ± 0.14
$\boldsymbol{H}$	0.42 ± 0.04	0.36 ± 0.02

Nonetheless, global coupling between subsystems positively impacts cross-dependencies between generated time series. As shown in panel (a) of Figure 7.7, volatility cross-correlations are stronger for signals produced by the model with a higher value of γ_{lm} (assuming that J_{ij}^{lm}, J_{ij}^{ll} are the same) and maintain a statistically significant level (denoted by the red line) for a longer period of time. The differences between the range of cross-correlations measured by $C_{xy}(\tau)$ function are also visible in the span of scales s, for which the dependencies between produced time series have multifractal character. The panels in section (b) of Figure 7.7, present mean cross

fluctuations functions $F_{xy}(q,s)$ for different sets of parameters. As indicated by the dotted black lines, the range of scales for which $F_{xy}(q,s)$ obeys the power law is slightly wider for signals generated by the model having a greater value of γ_{lm}, especially in the small-scales regime. Moreover, as is clearly visible in the middle panel (marked with orange diamond) and the panel on the right-hand side (marked with a purple triangle), the scaling of $F_{xy}(q,s)$ is more convincing for series produced by the model characterised by non-zero inter-asset global coupling.

The slight differences observed in the scaling range do not translate into strength of the multi-scale correlations. Plots in section (c) of Figure 7.7 present the mean $\rho^q_{xy}(s)$ for three values of q parameter (i.e., $q \in [2,3,4]$) depending on scale s. The differences in strength of the non-linear cross-correlations for different values of γ_{lm} are negligible, and the primary factor influencing level of the multi-scale cross dependencies is cross-asset agent-agent interaction, especially, if the middle range of scales is considered.

Interestingly, for small and large scales ($s < 10^2$ and $s > 10^4$, respectively), cross-correlations are on a similar level, regardless of the parameters of the model. In a small scales regime for all analysed parameters sets, multi-scale cross-correlations are weak, which is related to the model's stochastic character. Even though subsystems are, in general, synchronized, individuals are allowed to act, to some degree, independently, thus introducing desynchronization of the generated time series on small scales. Naturally, cross-correlations in the range of a small scales can be improved by decreasing agent's autonomy (by decreasing system temperature). However, as shown in section 6.2, increased value of parameter β, can cause 'freezing' of the system, which is highly undesirable effect.

On the other hand, when large scales are examined, almost perfect cross-correlation is observed, again, regardless of the model parameters. If sufficiently large spans of the generated time series are considered, differences in synchronization of subsystems observed on small scales become negligible, thus high cross-correlation is noticeable. Worth noting is that similar trajectories of the ρ^q_{xy} are observed in the financial markets (e.g. stock markets [112] or cryptocurrencies [200]).

In order to measure the multifractal character of cross-correlations between generated time series, $\lambda(q)$ (which measure the slope of function $F_{xy}(q,s)$) was compared to the mean value of generalized Hurst exponent $\overline{h(q)} = (h_x(q) + h_y(q))/2$. The smaller is the difference between these measures (i.e., $d(q) = \lambda(q) - \overline{h(q)}$) the more similar are the fractal structures in the signals, and for perfectly correlated series $d(q) = 0$. The most coherent time series are generated by the model with parameters $J^{ll}_{ij} = 0.99, J^{lm}_{ij} = J^{ml}_{ij} = 0.01$ and $\gamma_{lm} = \gamma_{ml} = 0.05$ (plot marked with the black dot). However, in this case, the result is burden with a significant error, thus from the practical applications point of view, the most valuable results are obtained for the following set of parameters: $J^{ll}_{ij} = 0.96, J^{lm}_{ij} = J^{ml}_{ij} = 0.04, \gamma_{lm} = \gamma_{ml} = 0.1$.

Worth noting is that the values of inter-asset global coupling and cross-asset agent-agent local interaction influence the repeatability of the generated signals. As the statistical errors (denoted by error bars) of multi-scale cross-correlation coefficient (section (c)) show, time series generated by the model with higher γ_{lm} (or J^{lm}_{ij}) parameters are characterized by smaller errors, especially in the range of medium scales ($s \in [10^2, 10^4]$). This effect is related to the stability of the system. Both

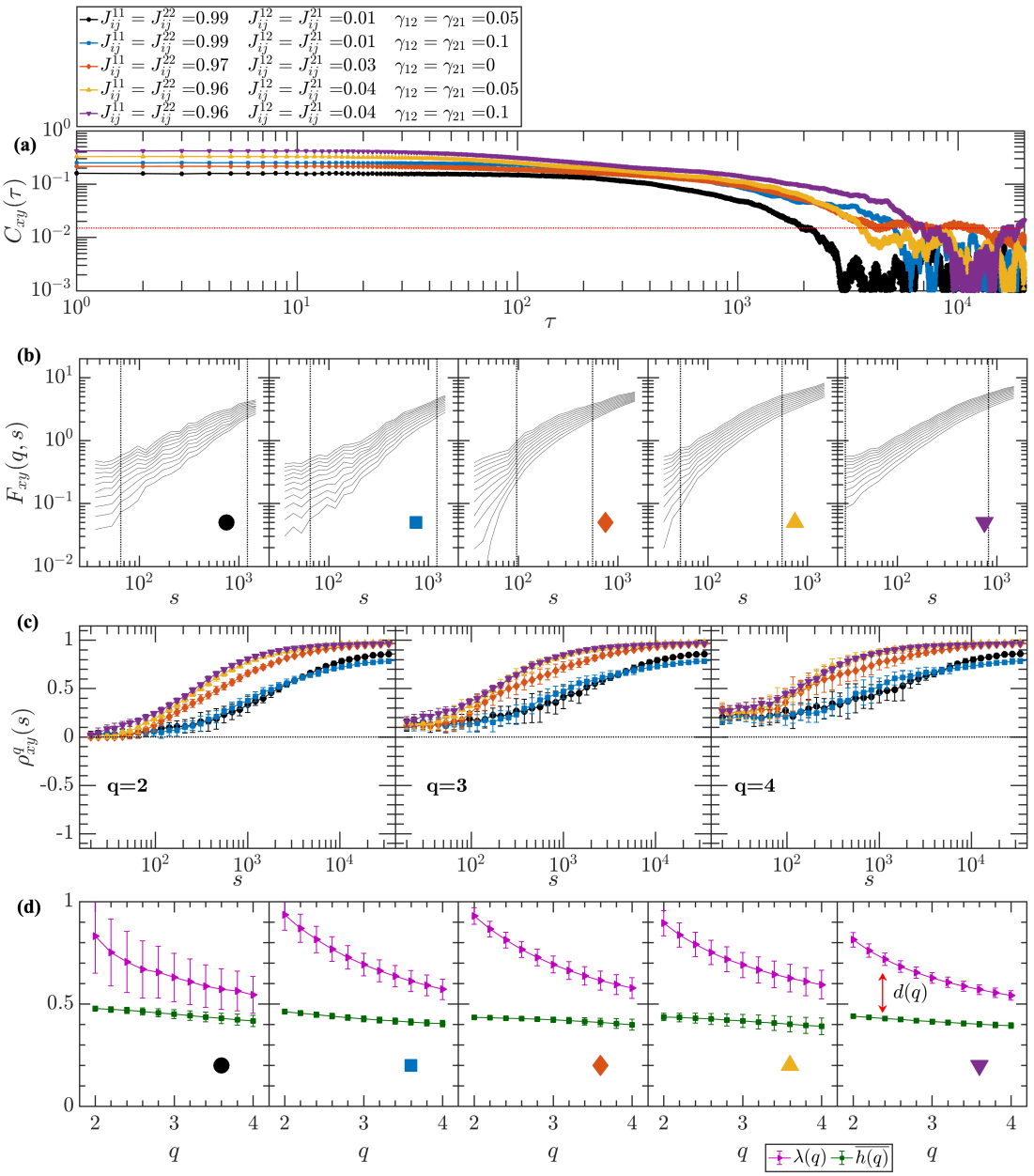

Figure 7.7: Mean volatility cross-correlation functions (section **(a)**), cross-fluctuation functions $F_{xy}(q,x)$ for $q \in [2,4]$ (section **(b)**), multi-scale cross-correlation coefficients $\rho_{xy}^{q}(s)$ (section **(c)**) and comparison of scaling exponent $\lambda(q)$ and mean generalized Hurst exponent $\overline{h(q)}$ (section **(d)**) of the time series generated by ten independent realizations of the multi-asset variant of the model with different values of the cross-asset agent-agent local interaction strength parameter $J_{ij}^{ll} \in 0.99, 0.96$, $J_{ij}^{lm} = J_{ij}^{ml} \in 0.01, 0.04$ and inter-asset global coupling $\gamma_{lm} = \gamma_{ml} \in [0, 0.05, 0.1]$, and fixed other parameters ($\beta = 1.6$, $\alpha_c = 30$, $\kappa_c = 0.5$). The dotted black lines in the plots in the section (b) plots denotes the range of scaling. The color markers in the plots in the section (b) and (d) links to corresponding cross-correlation and multi-scale cross-correlation functions (section (a) and (c), respectively).

of the considered parameters can improve the synchronization between subsystems and thereby reduce the stochastic character of the model.

As the analysis of the two-asset variant of the model shows, the proposed frame-

work is capable of reproducing multi-scale cross-correlations observed in financial markets. The strength of volatility cross-correlations measured by function $C_{xy}(\tau)$, and the value of coefficient $\rho^{q}_{xy}(s)$ depends primarily on the cross-asset agent-agent local interaction strength and to lesser extent on inter-asset global coupling. Taking into account that the price of the assets in financial markets are primarily driven by the transactions made by large, institutional investors (e.g., hedge funds, banks) suggests that the investment decisions of these market participants mostly depend on the positions of their competitors and to lesser extent on the price of the traded asset itself.

Chapter 8

Modeling of financial market cross-correlations

The huge advantage of the multi-asset three-state model is that no theoretical limitation regarding the number of simulated assets exist. In turn, it opens a possibility of modeling tens or even hundreds of coupled instruments and so reflecting the structures observed in real financial markets. In this chapter, proposed framework is used for building two artificial indices. The first, consisting of ten instruments grouped into three sectors is examined using rolling window technique analogous to analysis presented in Section 3.5. The second, aims at recreating multiscale cross-correlations structure of DJIA, thus it consists of thirty assets divided into six sectors and is examined using q-dependent MSTs introduced in Section 3.3.

8.1 Ten-assets artificial index

Modeling of multiple, coupled instruments using the multi-asset three-state model require careful selection of the framework parameters. When more than two instruments are simulated, especially compelling, is the cross-asset agent-agent interaction parameter. In the two-asset scenario, it does not make a significant difference whether the cross-asset local agent-agent interaction is symmetrical or not. In the symmetrical case, the subsystems seek a common equilibrium, which is occasionally broken during rearrangement phases. On the other hand, when the interaction between agents is not symmetrical, one subsystem acts as a leader, whereas another 'follows' this leader's configuration.

The situation is similar when more than two assets are considered; however, if cross-asset agent-agent interaction is symmetrical, as the number of modeled assets increases, the subsystems are more likely to remain aligned, and the probability of desynchronization decreases. Moreover, in such a scenario, a rearrangement phase occurs less often, as it has to develop in multiple subsystems simultaneously. Limiting cross-asset agent-agent local interaction to an asymmetric variant is sufficient to avoid permanent system stabilization. Additionally, Artificial index, in which one or few assets act as the leader for other instruments, reflects the dependencies observed in financial markets. Different stocks, depending on multiple factors (e.g., market capitalization), exert differing influence on other components. For instance,

ExxonMobil (XOM) is commonly perceived as the indicator for the entire Energy sector and significantly affects the valuation of other companies belonging to this basket. Another prominent example is General Electric (GE), which, with respect to non-linear correlations, seems to be one of the most influential stocks quoted on the New York Stock Exchange [125].

The second issue in index modeling is related to the excessive number of subsystems. Specifically, an increase in asset number dramatically affects the computational effort and memory footprint of the simulation. However, as shown in Section 3.5, proper selection of the assets representing different sectors allows construction of a proxy index that accurately mimics the behaviour of the original instrument, using only a fraction of its components.

Artificial index being considered in this section consists of ten assets that belong to three different sectors: **sector 1**: Assets 1-3, **sector 2**: Assets 4-7 and **sector 3**: Assets 8-10. Moreover, to reproduce correlations between instruments belonging to different baskets assets 1 and 10, as well as 3 and 4, are also linked on the cross-asset agent-agent local interaction and inter-asset global coupling levels (see equation (5.3)). Lastly, to avoid excessive value of the agent-agent interaction, which, as shown in Section 6.3 (see Figure 6.11) can cause system 'freeze', coefficients were chosen in such a way that sum of the signal received by an agent from the neighbour is equal to 1 ($\sum_m J_{ij}^{lm} = 1$). In addition, the inter-asset global coupling parameter was set relatively low ($\gamma_{lm} \in [0.025, 0.05]$). The cross-asset influence projection of J_{ij}^{lm} matrix (J^{lm}) and γ_{lm} matrix are presented below. In J^{lm} matrix, the diagonal describes the interaction strength within a given subsystem (values of J_{ij} for given subsystem m), other elements in the column indicate given asset's influence on other modeled instruments (on agent-agent interaction level) and the rows correspond to the influence of other subsystems on the given asset (again, on agent-agent interaction level). The γ_{lm} matrix was constructed analogously. The remaining parameters were set to values $\beta = 1.6$, $\alpha_c = 30$, and $\kappa_c = 0.5$, for each modeled instrument.

$$J^{lm} = \begin{bmatrix} 0.96 & 0 & 0 & 0 & 0 & 0 & 0 & 0 & 0 & 0.04 \\ 0.04 & 0.96 & 0 & 0 & 0 & 0 & 0 & 0 & 0 & 0 \\ 0 & 0.04 & 0.96 & 0 & 0 & 0 & 0 & 0 & 0 & 0 \\ 0 & 0 & 0.02 & 0.98 & 0 & 0 & 0 & 0 & 0 & 0 \\ 0 & 0 & 0 & 0.04 & 0.96 & 0 & 0 & 0 & 0 & 0 \\ 0 & 0 & 0 & 0.04 & 0 & 0.96 & 0 & 0 & 0 & 0 \\ 0 & 0 & 0 & 0.04 & 0 & 0 & 0.96 & 0 & 0 & 0 \\ 0 & 0 & 0 & 0 & 0 & 0 & 0 & 1.0 & 0 & 0 \\ 0 & 0 & 0 & 0 & 0 & 0 & 0 & 0.04 & 0.96 & 0 \\ 0.02 & 0 & 0 & 0 & 0 & 0 & 0 & 0.02 & 0 & 0.96 \end{bmatrix}$$

$$\gamma_{lm} = \begin{bmatrix} 0 & 0 & 0 & 0 & 0 & 0 & 0 & 0 & 0 & 0.05 \\ 0.05 & 0 & 0 & 0 & 0 & 0 & 0 & 0 & 0 & 0 \\ 0 & 0.025 & 0 & 0 & 0 & 0 & 0 & 0 & 0 & 0 \\ 0 & 0 & 0.025 & 0 & 0 & 0 & 0 & 0 & 0 & 0 \\ 0 & 0 & 0 & 0.05 & 0 & 0 & 0 & 0 & 0 & 0 \\ 0 & 0 & 0 & 0.05 & 0 & 0 & 0 & 0 & 0 & 0 \\ 0 & 0 & 0 & 0.05 & 0 & 0 & 0 & 0 & 0 & 0 \\ 0 & 0 & 0 & 0 & 0 & 0 & 0 & 0 & 0 & 0 \\ 0 & 0 & 0 & 0 & 0 & 0 & 0 & 0.05 & 0 & 0 \\ 0.025 & 0 & 0 & 0 & 0 & 0 & 0 & 0.025 & 0 & 0 \end{bmatrix}$$

The artificial index simulation consists of $2.5 * 10^5$ time steps; however, the first $5 * 10^4$ data points were considered as a thermalization period and so were omitted in the further analysis. Figure 8.1 shows the magnetization (panels on the left-hand side) and the corresponding rates of return (panels on the right-hand side) produced by each subsystem of the model. The returns of assets belonging to the same sectors overlap to a considerable degree (e.g., Assets 4 and 5), while those associated with different baskets appear to fluctuate more independently (e.g., Assets 7 and 8).

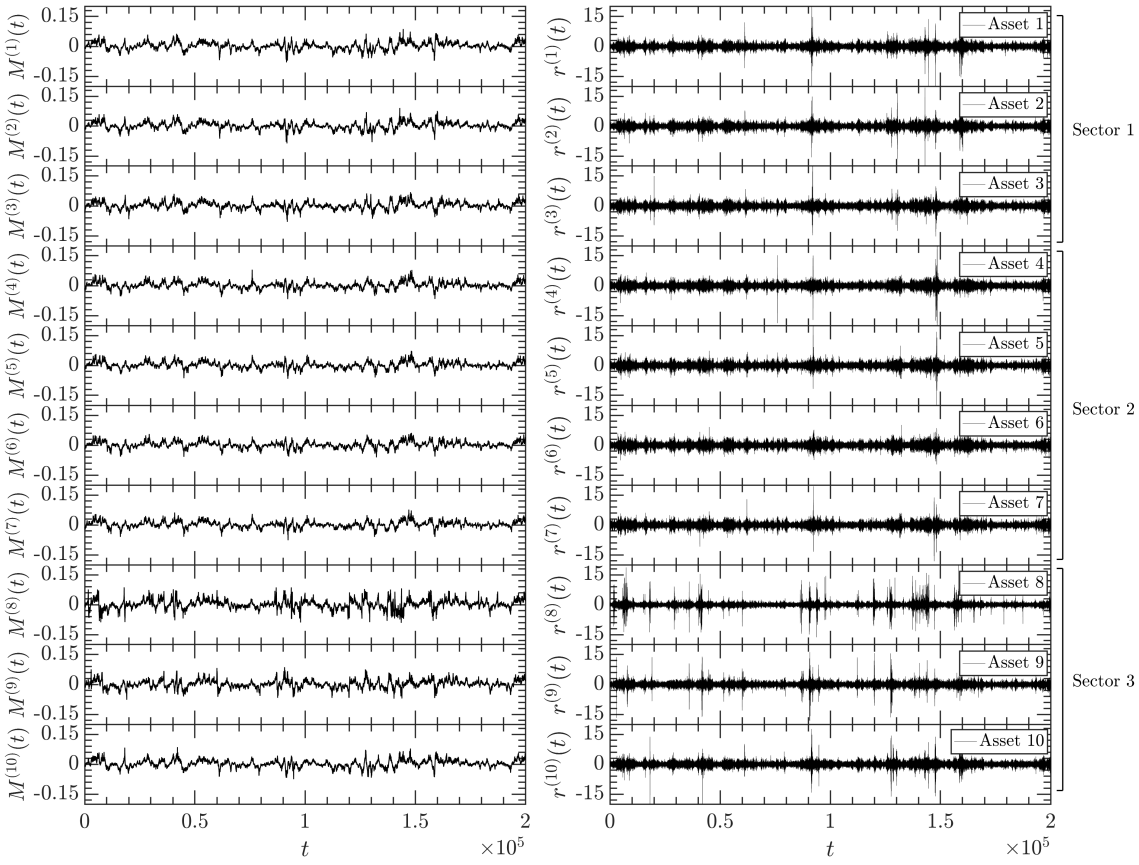

Figure 8.1: Magnetization (left panels) and corresponding rate of returns (right panels) generated by the particular subsystems of the ten asset variant of the model. The assets were coupled accordingly to the J^{lm} and γ_{lm} matrices presented above

The coupling between assets also reveals itself in the hierarchical organization of generated returns. As shown in the panels comprising section (a) of Figure 8.2, the fluctuations functions and their scaling ranges of instruments belonging to the same sector are similar. The span of the scales for which function $F_x(q, s)$ obeys the power law is wide and varies from approximately $s \in [20, 900]$ for Asset 8 (sector 3) to approximately $s \in [20, 3000]$ for Asset 4 (sector 2). Naturally, the similarities in non-linear self-dependencies are also noticeable on the singularity spectrum level. Panels in section (b) of Figure 8.2 present obtained $f(\alpha)$ functions, grouped by sectors. The shapes of the multifractal spectra for highly correlated assets is similar and characterized by comparable width $\Delta\alpha$ and asymmetry A_α which, depending on sector varies from $\overline{\Delta\alpha} \approx 0.31$ to $\overline{\Delta\alpha} \approx 0.24$ for Sectors 1 and 2, respectively, whereas asymmetry coefficient varies from $\overline{A_\alpha} \approx 0.56$ for Sector 2 to $\overline{A_\alpha} \approx 0.75$

for Sector 3. Moreover, as was already shown in Section 7.2, the cross-asset agent-agent interaction introduces weak negative linear self-dependencies in generated time series. In this case, mean Hurst exponent for different baskets varies from $\overline{H} = 0.437$ for Sector 1 to $\overline{H} = 0.443$ for Sector 2 (see Table 8.1 for more details).

Naturally, coupling level between assets is also visible in the cross fluctuations functions (section (c) of Figure 8.2). For assets belonging to the same sector, $F_{xy}(q, s)$ obeys the power law over considerable range of scales; however, significant distortions are observed for small s. For example, returns of Assets 1 and 2 (panel on the right-hand side in section (c) of Figure 8.2), even though they have overlapping volatility clusters, and both individually have a rich hierarchical organization, the pair's cross-fluctuations function is significantly distorted for scales $s \in [20, 50]$. This effect is caused primarily by model's stochastic character, and the fact that, even for relatively strong cross-asset agent-agent local interaction and inter-asset global coupling, agents are, to some degree, independent.

Comparing these results with the ones obtained for real data (see Section 3.5), another discrepancy stands out. For financial time series, even if the assets belong to different sectors, they are strongly correlated, especially when large scales are considered. In the cross fluctuation function, it is reflected by the substantial range of s for which $F_{xy}(q, s)$ obey the power law (see Figure 3.7, panels in section (a)). In the model, assets that represent different sectors are not cross-correlated in a multiscale manner. Both of these issues can be overcome by introducing stronger coupling between subsystems, however in such a scenario, the generated time series will fully align (see bottom right panel in section (a) of Figure 7.5), which is in contradiction to the situation observed in real financial markets.

Table 8.1: Spectrum width $\Delta\alpha$, asymmetry A_α, and Hurst exponent H of ten-assets artificial index components returns.

Asset:	**1**	**2**	**3**	**4**	**5**	**6**	**7**	**8**	**9**	**10**
$\boldsymbol{\Delta\alpha}$	0.34	0.29	0.29	0.26	0.24	0.18	0.27	0.30	0.27	0.27
$\boldsymbol{A_\alpha}$	0.71	0.66	0.68	0.71	0.49	0.37	0.70	0.83	0.83	0.61
$\boldsymbol{H}$	0.43	0.44	0.44	0.42	0.45	0.45	0.45	0.45	0.45	0.42

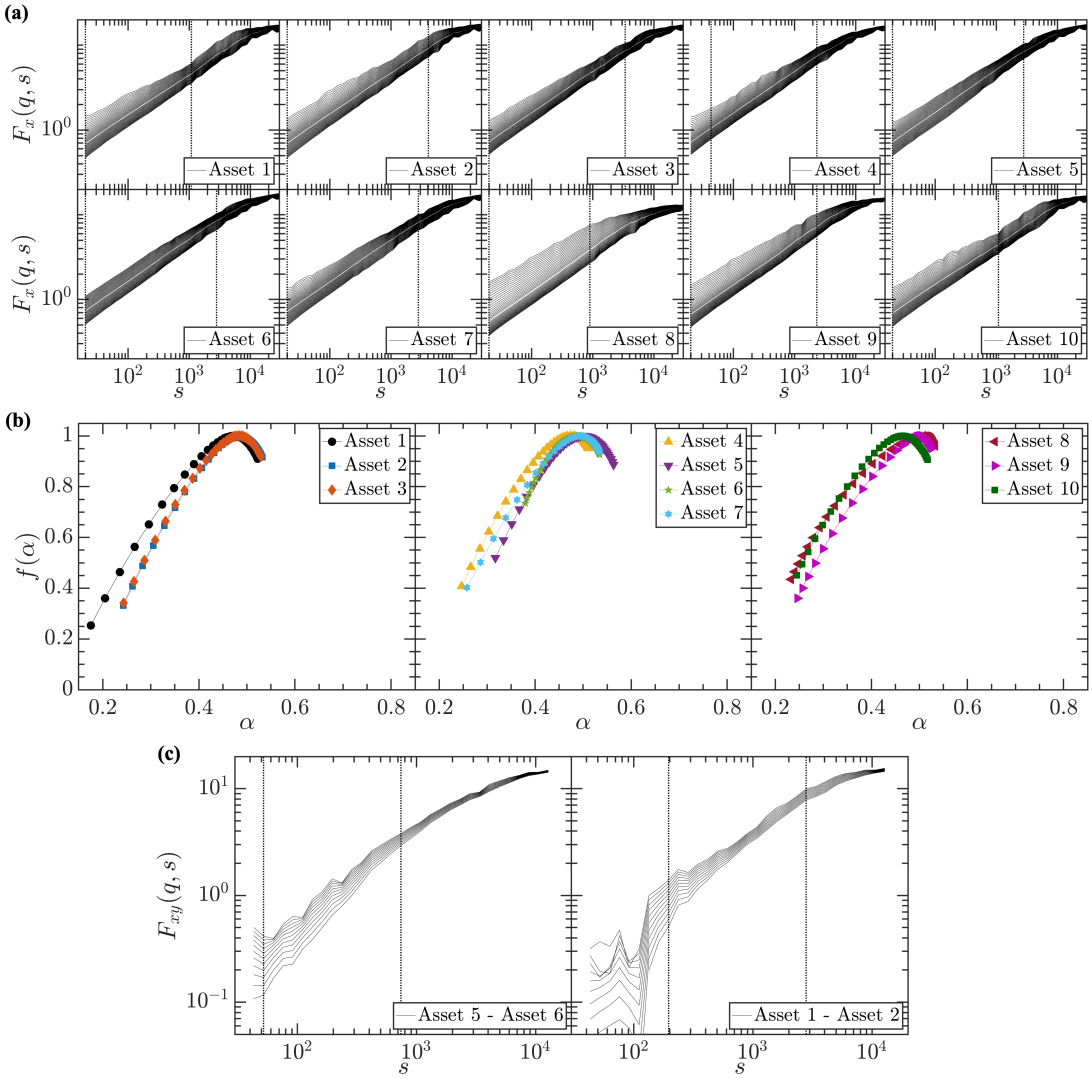

Figure 8.2: Fluctuation functions $F_x(q,s)$ (panels in section **(a)**) and corresponding multifractal spectra (panels in section **(b)**) calculated for returns of ten-assets artificial index components. Panel **(c)** shows the cross fluctuation functions $F_{xy}(q,s)$ for selected pairs of assets. Black dotted lines in plots in section (a) and (c) denote the range of scaling.

8.2 Variability of multiscale cross-dependencies between ten-assets artificial index and its components

Besides some discrepancies in $F_{xy}(q,s)$'s scaling range between real-world financial time series and returns generated by the model, the framework reflects the dynamic changes in the multifractal characteristics over time. In this section, the signals produced in ten-assets artificial index simulation are examined in the context of the multiscale features' variability. Analogously to the analysis performed in section 3.5, the rolling window technique was applied.

Figure 8.3 presents the result of the multifractal rolling window analysis conducted for ten-assets artificial index and components' fluctuations. Window length

was set to 40000 data points, and it was moved by 160 time steps. Assuming that the model generates hourly returns, the window length corresponds to approximately 20 trading years, whereas window step is approximately one trading month. Additionally, for more illustrative clarity, the multifractal spectra of the individual components are represented by the average value, calculated for each window separately.

As shown in panels (a) and (b), the singularity spectra calculated for ten asset artificial index as well as average $f(\alpha)$ functions of its components reveal significant changes in the hierarchical organization of generated signals. In both cases, obtained multifractal spectra are characterised by left-hand side asymmetry; however, the A_α coefficient for ten-assets artificial index assume higher values than it is observed for an average of the components. This effect is rooted in the stochastic character of the model. During the metastable periods, most of the agents preserve their positions over time; however, the form of the probability function p, which determines the spin of a particular agent in the given subsystem (see equation (5.1)), leaves room for less collective fluctuations. When these small oscillations are aggregated in the artificial index, the non-linear correlations are diminished, as manifested by the shrinkage of the right part of the singularity spectra. A similar effect is observed for large fluctuations (represented by the left part of the $f(\alpha)$ function). However in this case, the non-linear correlations are not entirely suppressed, and thus the left part of the singularity spectra do not disappear, but its width is substantially reduced. As a result, the multifractal spectra obtained for artificial index are never broader than the average of its components, which is in conscience with the observation made for real financial time series. Also worth noting is that the consequences of the aggregation performed to build the artificial index are also visible on the linear long-range correlations level. Hurst exponent for the ten-assets artificial index assumes values closer to $H = 0.5$ than it is observed for individual components average.

Importantly, the difference in richness of hierarchical organization between ten-assets artificial index and the average of its components is not constant in time. The multiscale rolling window analysis of the series generated by the model shows periods characterized by increased (green polygon) and decreased (red polygon) discrepancies in multifractal properties, suggesting that components returns exhibit phases of amplified and weaken cross-correlations, similar to those observed in the DJIA Proxy Index. To ascertain this, a correlation matrix analysis, analogous to the procedure presented in Section 3.5, was performed. Here, two different pairs of scales s and q exponents were considered, namely $s = 100, q = 2$ and $s = 344, q = 4$ (panels (b) and (c) of Figure 8.4, respectively). Moreover, the largest eigenvalue of the correlation matrix built of Pearson coefficients was analysed (panel (a) of Figure 8.4).

The maximum eigenvalue calculated for the correlation matrix composed of Pearson coefficients only occasionally and marginally assumes values above the noise regime, indicating that the linear correlations between the assets are negligible. Similar results were obtained for correlation matrix built of $\rho^2_{xy}(100)$. In this case, the maximum eigenvalue has comparable values in periods of increased and decrease coupling between instruments (green and red areas, respectively). Significant differences between these two phases are visible for cross-correlation matrix built of

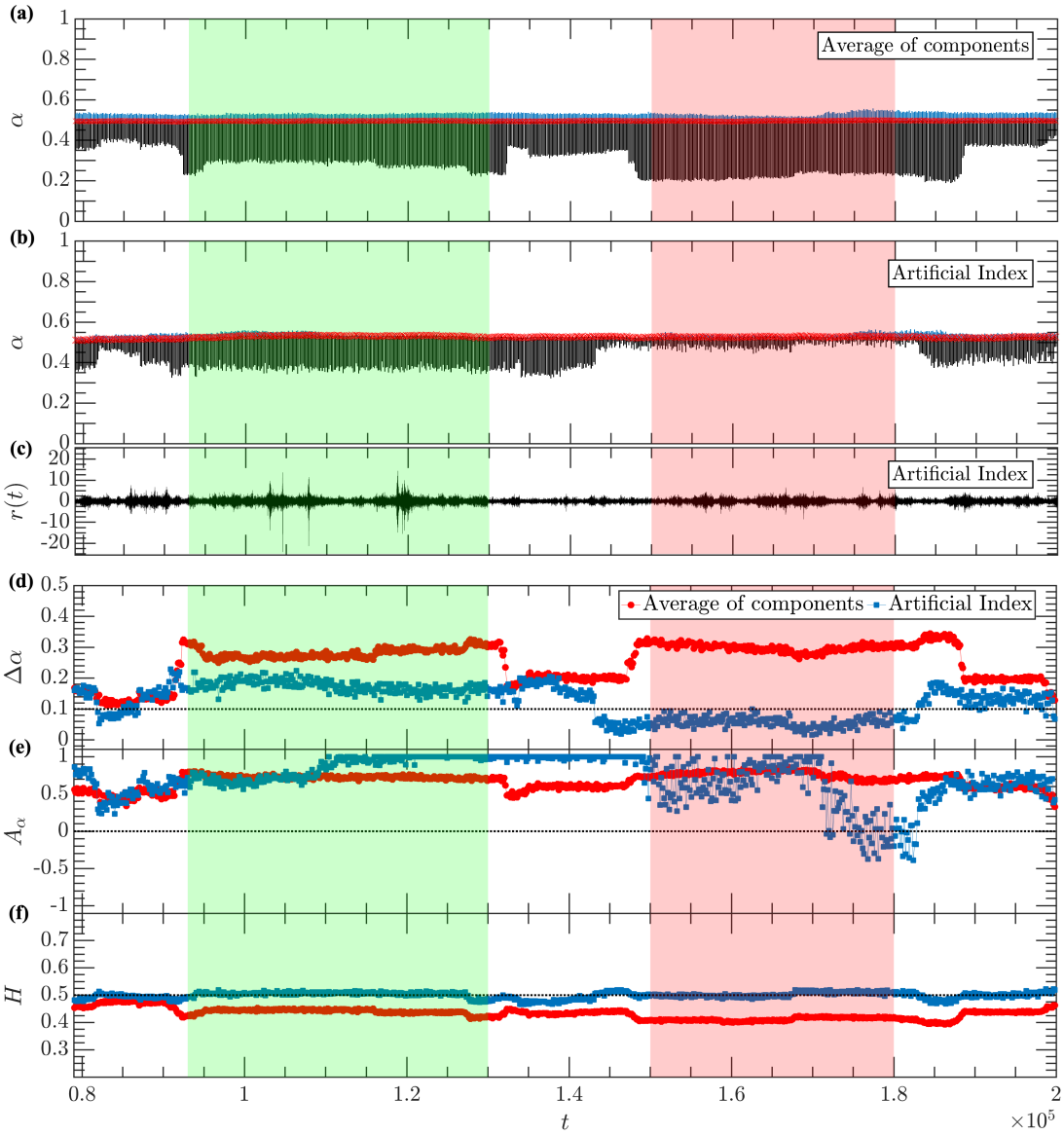

Figure 8.3: The multifractal rolling window analysis of the Artificial Index built of ten assets generated by the model with parameters defined in the previous section. Panels **(a)** and **(b)** presents projection of singularity spectra on α-t plane. The blue and black colors denotes right and left wing of the multifractal spectra respectively, whereas red crosses indicates the maxima of $f(\alpha)$. Panel **(c)** shows the rate of returns of the Artificial Index. Panels **(d)**, **(e)**, **(f)** contains obtained spectra width $\Delta\alpha$, asymmetry A_α as well as Hurst exponents H. The red circles indicates averaged multifractal properties of the individual components, whereas the blue squares represents the results obtained for the Artificial index. The green and red polygons indicate areas of increased and decreased coupling between the assets.

$\rho^4_{xy}(344)$. As shown in panel (c) of Figure 8.4 the maximal eigenvalue for $\rho^4_{xy}(344)$ for windows that end in period $t \in (9.3 * 10^4, 1.3 * 10^5)$ (marked by green polygon) assume significantly higher values than are observed for windows that end in $t \in (1.5 * 10^5, 1.8 * 10^5)$ (marked by red polygon). This analysis confirms that the signals generated by the model characterized by chosen parameters, for sufficiently large scales and large fluctuations ($q \in [3, 4]$) are cross-correlated; however, coupling between assets is not recreated when smaller scales and fluctuations are considered.

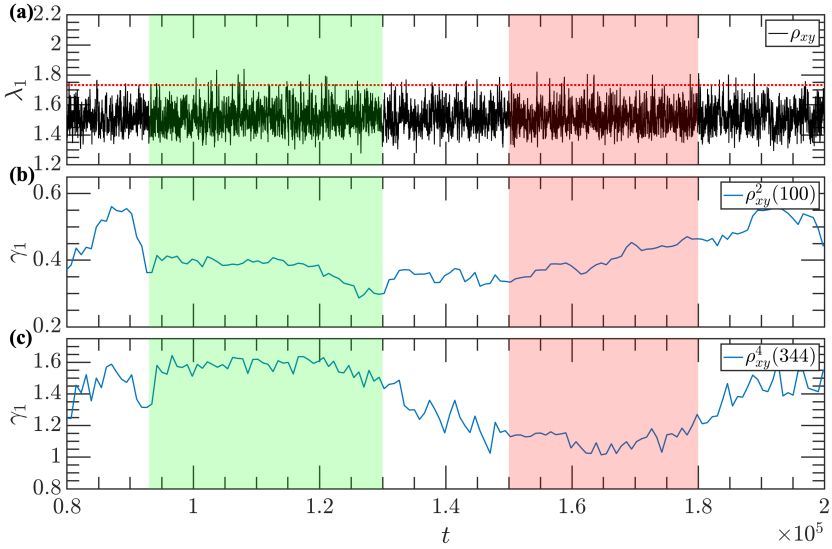

Figure 8.4: Rolling window analysis of the largest eigenvalue of the correlation matrix built of Pearson coefficients (panel **(a)**) and matrix composed of $\rho^q_{xy}(s)$ for $s = 100$, $q = 2$ (panel **(b)**) and $s = 344$, $q = 4$ (panel **(c)**), respectively. Horizontal red dotted line in plot (a) indicates the noise regime of the correlation matrix determined according to equation (3.37).

The periods of increased and decreased collectivity of the time series generated by the model have a stochastic nature, meaning that relatively weak coupling between particular components allows agents to behave, to some degree, independently from the information they receive from other subsystems. As a result, at some point of the simulation sectors desynchronize, which reduces the level of hierarchical organization of the artificial index. Worth noting is that estimating the time step at which such desynchronisation or excessive synchronization will occur is not possible. However, by changing the values of the J^{lm} and γ_{lm} matrices as the simulation progress, the modeler can, to some extent, control coupling between assets. Nonetheless, the time series generated by the model with such manual changes in cross-asset agent-agent interaction strength and inter-asset global coupling are still subject to stochastic fluctuations; thus, periods of stronger (weaker) cross-correlations may appear independently from parameters evolution introduced manually.

8.3 Modeling of DJIA non-linear cross-correlations structure

The intricacy of the financial markets, besides the dynamic changes of the return's multifractal properties, reveals itself in the complex structure of the non-linear correlations between the assets. As shown in section 3.3, multiscale interdependencies between financial instruments can be successfully analysed using complex network formalism. In the following paragraphs, this technique is applied to the signals generated by the DJIA-inspired artificial index that consisted of thirty components.

Thanks to the flexibility of the multi-asset three-state model, its ability to generate signals characterised by non-linear cross-correlations, and lack of theoretical limitations regarding the number of simulated assets, it is possible to, at least par-

tially, reflect the real financial market structure and its changes depending on the analysed scale and magnitude of returns. Naturally, an attempt to mimic financial market organization can lead to a complicated set of cross-asset agent-agent local interaction J^{lm} and inter-asset global coupling γ_{lm} parameters. Therefore, in this research, the emphasis was on simplest forms of these matrices, that could lead to recreating phenomena observed in the financial markets.

Constructed artificial index consisted of 30 subsystems grouped into 5 sectors as follows: Sector **(1)**: Assets 2-11, **(2)**: Assets 12-16, **(3)**: Assets 17-21, **(4)**: Assets 22-27, **(5)**: Assets 28-30. The first asset in each sector (i.e., 2, 12, 17, 22, 28) act as a leader which asymmetrically influences other components in the bucket with $J^{lm} = 0.04$ and $\gamma_{lm} = 0.05$. Moreover, the entire system has a leader (Asset 1) that is connected with leaders of Sectors 1-4 asymmetrically, again with parameters $J^{lm} = 0.04$ and $\gamma_{lm} = 0.05$. Moreover, the leader of Sector 5 (Asset 28) is not linked directly to the central subsystem, but it is connected to the Asset 27. Such choice of the parameters intends to reflect the relation between Healthcare and Consumer Goods sectors observed in DJIA (e.g., panel (g) of Figure 3.8), as well as the star-like layout of the MST graph[1]. Other parameters were set to the values: $\beta = 1.6$, $\alpha_c = 30$, and $\kappa_c = 0.5$ for each subsystem. For the model specified in such a way, a simulation containing $2.5 * 10^5$ time steps was performed, however first $5 * 10^4$ data points were removed (thermalization period); thus, the effective length of the analysed signal was $2 * 10^5$ time steps.

Figure 8.5 shows MSTs built upon generalized cross-correlation coefficients $\rho^q_{xy}(s)$ constructed according to the procedure presented in Section 3.3. The analysis covers three exponents $q \in [2, 3, 4]$ and three different scales $s \in [42, 645, 17335]$ with node color corresponds to the sector to which given asset belongs and node size indicating the value of the betweenness coefficient, according to the legend presented at the bottom of the figure.

For small scales $s = 42$, regardless of the considered scale, MSTs assume chain-like shape, and nodes are not grouped by the sector. Such a structure results from weak correlations between time series produced by the model in a small scales regime, which on average vary from $\overline{\rho^2_{xy}(42)} = 0.07$ to $\overline{\rho^4_{xy}(42)} = 0.24$ (see Table 8.2).

Considering medium scale $s = 645$, MSTs have a chain-like structure as well; however, nodes representing companies belonging to the same sector are typically close to each other. As the graphs have an elongated structure, there are a few nodes with increased betweenness. Importantly, for small and medium scales, the node 1, which suppose to be an index leader is marginalised.

As larger q exponents are considered, correlations between assets become stronger, although they depend less on the sector to which particular instrument belongs (see Table 8.2). This effect is manifested by the lower convergence between J^{lm},γ_{lm} matrices and the graph structure. For example, a few nodes that for $q = 2, s = 645$ and $q = 2, s = 645$ are surrounded by nodes belonging to the same or connected sector, whereas for $q = 4, s = 645$ are attached to completely different basket (e.g., node 30 and 19). Stronger cross-correlations between large fluctuations of components belonging to different sectors, as was shown in Section 3.3, are also observed in real financial markets.

[1]The entire J^{lm} and γ_{lm} matrices are available in Appendix B.

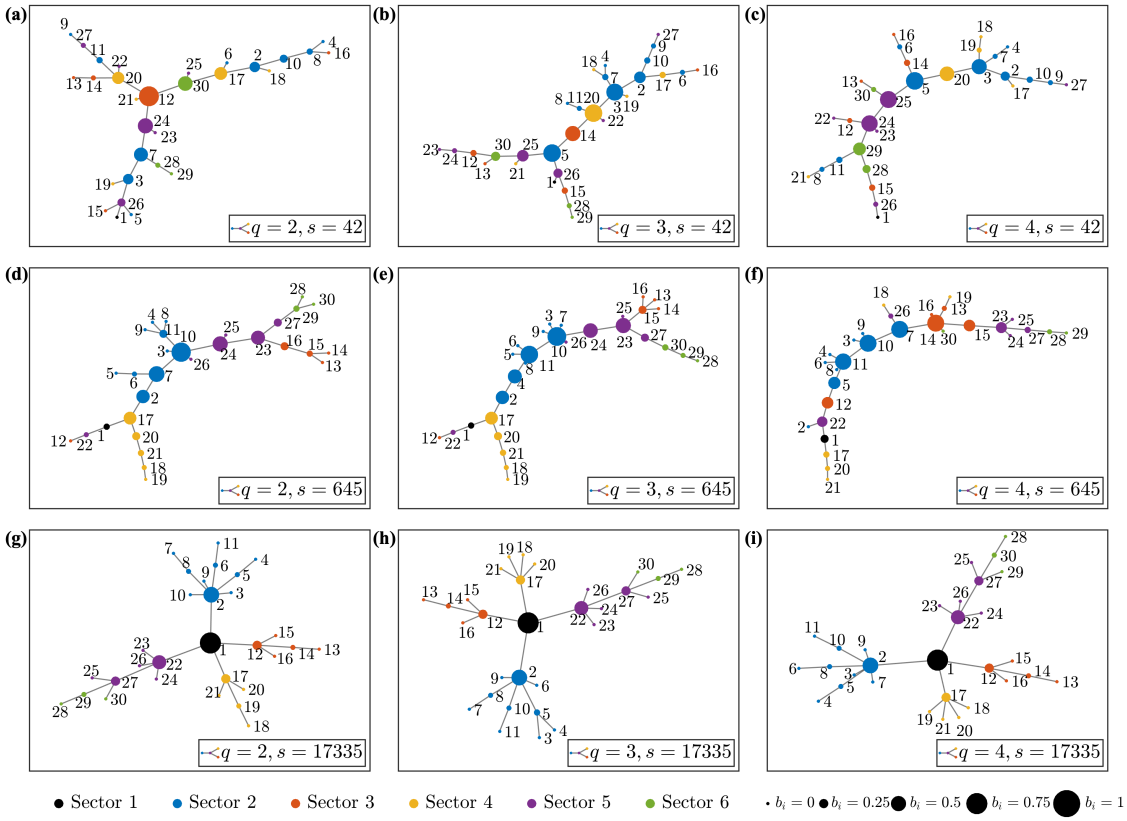

Figure 8.5: Minimal spanning trees built upon multiscale cross-correlation coefficient $\rho^q_{xy}(s)$ between returns of DJIA-inspired artificial index components for scales $s \in [42, 645, 17335]$ and exponents $q \in [2, 3, 4]$. Each row of panels corresponds to a single scale s, whereas each column contains graphs calculated for different q parameter. Nodes colors indicate the sector to which the particular asset belongs (black: 'central node', blue: Sector 1, orange: Sector 2, yellow: Sector 3, green: Sector 4 and purple: Sector 5). Node size denotes the value of the betweenness coefficient, according to the legend presented at the bottom of the figure.

The highest consistency between structure defined in J^{lm} and γ_{lm} matrices and obtained MSTs is visible for the largest scales (panels (g)-(i) of Figure 8.5). In this case, clusters of nodes denoting different sectors are clearly visible. Moreover, Asset 1 assumes a central position in the graph and links different sectors regardless of the considered size of the fluctuations. Naturally, the importance of this node measured by its betweenness is the highest for each q parameter - $b_1 \approx 0.75$. Minor discrepancies between the J^{lm} and γ_{lm} matrix structures and obtained MSTs are noticeable in the composition of cluster. Not all nodes that belong to given sector are connected to sector leader. Naturally, these discrepancies have roots in the stochastic character of the model and the fact that time series are not fully synchronized as the agents, to some degree, behave independently.

In order to quantitatively describe MSTs build upon generalized cross-correlations coefficients of the generated time series, the node degree distribution and average path length were determined. Because the simulation consisted of a limited number of subsystems (30), it was not possible to clearly affirms if the node degree distribution obeys power law typical for the financial markets; however, seedbeds

for this type of dependence are visible, especially when larger scales are considered $s \in [645, 17335]$.

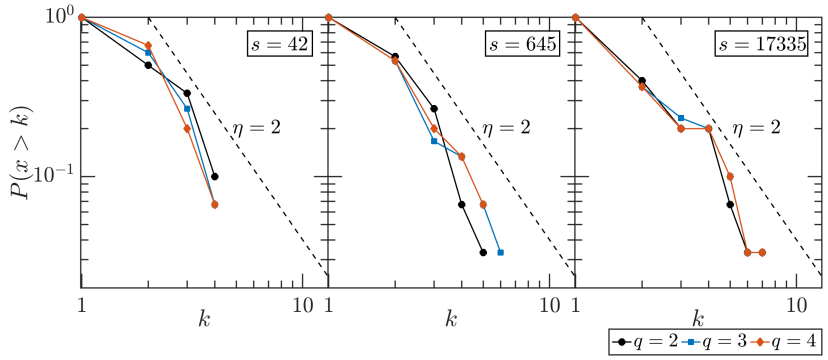

Figure 8.6: Cumulative distribution of the node degree of MSTs built upon the multiscale cross-correlation coefficient $\rho^q_{xy}(s)$, determined for three different scales: $s = 42$ (panel on the left-hand side), $s = 645$ (panel in the middle), $s = 17335$ (panel on the right-hand side) and three different scaling parameters $q = 2$ (black circles), $q = 3$ (blue squares), $q = 4$ (orange diamonds).

Moreover, changes in the coupling between assets and market organization are reflected in the average shortest path length L (Table 8.2). For small and medium scales, the average shortest path length increases along with increase in q parameter, which is consistent with the results obtained for real financial markets. For the largest considered scale $s = 17335$ graphs layouts almost fully align with the J^{lm} and γ_{lm} matrices structure; thus, the average shortest path lengths do not change significantly with increase in q exponent.

Table 8.2: Average path length L (upper table) of the MSTs built upon non-linear cross-correlation coefficients $\rho^q_{xy}(s)$ between components of the DJIA-inspired artificial index determined for the three exponents $q \in [2, 3, 4]$ and the three scales $s \in [42, 645, 17335]$. The table at the bottom presents the average value of the generalized cross-correlation coefficient $\overline{\rho^q_{xy}(s)}$ for each scale and q exponent considered.

L	$q = 2$	$q = 3$	$q = 4$
$s = 42$	5.04	5.21	5.32
$s = 645$	5.20	5.34	5.37
$s = 17335$	3.72	3.73	3.68

$\overline{\rho^q_{xy}(s)}$	$q = 2$	$q = 3$	$q = 4$
$s = 42$	0.07 ± 0.06	0.14 ± 0.08	0.24 ± 0.11
$s = 645$	0.39 ± 0.11	0.45 ± 0.12	0.50 ± 0.13
$s = 17335$	0.89 ± 0.03	0.90 ± 0.03	0.90 ± 0.03

The network analysis of the non-linear cross-correlations of the artificial index inspired by DJIA demonstrates that the proposed model is able to recreate some of the market's structure features. Even a relatively simple definition of the dependencies between subsystems that covered five sectors linked by a single asset is able to sufficiently reflect strong interdependencies between assets belonging to the same

basket as well as changes of the MSTs structure observed for different q exponents. Increasing dispersion of the MST along with the rise of q exponent is noticeable in small and middle scales regime. When large fluctuations are considered, the DJIA-inspired artificial market structure does not break-down, whereas, in the case of DJIA components, such disorganization was observed (see Figure 3.8). Nevertheless, some discrepancies between the real market structure and one recreated by the model do not prevent its practical application. Moreover, the proposed framework is highly adjustable; thus, the various configurations of the market structures could be reproduced by proper manipulation of the J^{lm} and γ_{lm} matrices as well as other parameters of the model.

Chapter 9

Summary

The financial market is an example of a complex system with an enormous number of dependencies and intricate non-linear correlations between components. Analysis of such systems requires applying sophisticated mathematical tools, whereas its modeling using a traditional top-down approach seems to be a breakneck task. The research described in this dissertation, based on the difficulties mentioned above, can be divided into two blocks. The first focuses on identification and quantification of financial time series properties, with extra emphasis on non-linear autocorrelations and cross-correlations, including temporal evolution of these features. The research was conducted for daily returns of five indices that represent major stock exchanges (DJIA, NASDAQ, DAX, FTSE, and NIKKEI) and individual companies quoted within DJIA (list of analysed indices and components is available in Appendix A). The second, part of this dissertation, comprehensively describes usage of agent-based models inspired by physical phenomena in reproducing not only financial time series non-linear autocorrelations but also reflecting the cross-dependencies between assets. In this block, two variations of the Ising Model were discussed (Iori's model and Bornholdt's model), and, based on their pros and cons, the generalized multi-asset three-state model of a financial market was proposed and then comprehensively studied in the context of reproducing complex phenomena observed in real financial markets.

The financial time series analysis confirmed existence of so-called, stylized facts. As has been demonstrated, the cumulative distributions of the financial indices and individual components daily returns, are leptokurtic with an elongated central part and heavy tails, regardless of the market on which they are quoted. Moreover, analysis of the correlations of returns and volatility has confirmed the absence of any significant linear dependencies; however, it also showed that these signals are characterized by strong, long-range non-linear autocorrelations. Additionally, analysis of the cross-correlation function of volatility demonstrated that assets could be strongly coupled. The strongest cross-dependencies, measured by function C_{xy}, were observed for indices that, in part, are built upon common components, as the DJIA and NASDAQ, as well as between companies belonging to the same sector as IBM and HPQ (see Figure 2.5).

To quantitatively describe non-linear self and inter-dependencies between considered financial assets, advanced multifractal formalism was introduced. In Chap-

ter Three, two multiscale analysis methods, namely, MFDFA and MFCCA, were comprehensively described and applied to financial time series. **The singularity spectra obtained for major instruments are broad and typically reveal left-hand side asymmetry, which indicates great complexity of the analysed signal, especially in large fluctuations** (see Figure 3.5). Similar properties of the multifractal spectra were observed for the the DJIA components' time series; however, in this case, the non-linear correlations in small fluctuations were stronger, as manifested by more symmetrical $f(\alpha)$ functions. Such a discrepancy between indices' and components' singularity spectra is rooted in the nature of the latter instrument. Since indices are constructed of components that may have different multiscale characteristics, the global hierarchical organization of the index (which is sum of components) becomes distorted, and the multifractal spectrum then becomes asymmetric.

Non-trivial multiscale characteristics are also observable on the level of asset cross-dependencies. **The cross-fluctuations functions of analysed financial instruments obey the power law over a large range of scales**. The exception here is the DJIA-NIKKEI pair, which, as was shown, in the considered period does not have linear nor non-linear cross-correlations. On the grounds of the obtained $F_{xy}(q, s)$ functions, generalized cross-correlation coefficients $\rho^q_{xy}(s)$ were determined. The strongest dependencies were observed for the DJIA-NASDAQ pair, as these instruments have common components. On individual companies level, the highest cross-correlations were observed for components representing the same sector, such as HPQ and IBM (see Figure 3.7). Interestingly, the differences in the value of $\rho^q_{xy}(s)$ between assets belonging to the same basket and companies which operates in distinct business areas disappear along with an increase in scale s or when large fluctuations are considered. In the former case, the global trends that exist on large scales play a significant role, whereas the latter has its roots in the higher coupling between stock shares in volatile market periods (e.g., during bubble crashes).

Additionally, the non-linear cross-correlations were investigated using complex network formalism. Based on the $\rho^q_{xy}(s)$ coefficients obtained for 30 components of the DJIA, minimal spanning trees for three different scales s and three values of q exponent were built. **This analysis showed that, depending on considered scales and fluctuation sizes, market components correlation structure is changing** (see Figure 3.8). Due to limited number of analysed assets, the quantitative description of observed graph structure was constricted; however, some signatures of power law characteristic of node degree distribution and the star-like structures with General Electric (or United Technologies) as a central node, were observed, aligning with findings for high frequency data reported in study [125].

Financial market complexity was also captured in the time dimension. For this purpose, the singularity spectra of the major stock indices and components from the DJIA were determined in windows of approximately twenty years in length and moved by a window step of around one trading month. **Obtained results showed that the hierarchical organization of the financial time series is continually evolving through a variety of shapes**. The changes are visible on the level of singularity spectra width and its asymmetry, and are usually linked to major financial market events such as the Black Monday Crash or the bankruptcy of Lehman

Brothers (see Figure 3.10). However, the intensity of these effects varies depending on analysed assets. For instance, DAX's multifractal properties are relatively steady over the considered period of time, whereas NIKKEI, from the multiscale analysis perspective, was not significantly affected by Black Monday Crash; however, substantial changes were observed after the Japanese asset price bubble burst in 1991. As was demonstrated in subsequent sections of this study, the changes in hierarchical organization visible in the index can be linked with periods of higher and lower degree of correlations among its components. The multifractal rolling window analysis of the DJIA proxy index and its components confirmed this hypothesis (see Figures 3.13 and 3.14).

The second, more critical part of this thesis focuses on modeling previously quantified multiscale features of financial time series using agent-based models. The first framework considered in the context of its ability to reproduce stylized facts, including non-linear correlations of returns, was modified Random Field Ising Model proposed by Gulia Iori. As was demonstrated in Section 4.3.1, this framework can recreate the vast majority of financial time series properties (see Figure 4.6); however, these features appear for near-critical parameters of the model, specifically for interaction probabilities close to the percolation threshold, which translates into framework instability (see Figure 4.5). Moreover, Iori model is not able to resemble the vibrant hierarchical organization ($\Delta\alpha > 0.3$) often observed in financial time series.

The second examined framework was the one introduced by Bornholdt. In this case, the primary modification compared to the classic Ising Model is that agents can follow one of two different strategies. Practically speaking, this means that individuals are divided into two groups: fundamentalists and chartists. As shown in Section 4.3.2, model construction results in the system's intermittent on-off behaviour manifested by metastable and rearrangement phases. The analysed solution, like the one proposed by Iori, can recreate stylized facts; however, the distributions of generated do not obey inverse cubic law. On the other hand, the hierarchical organization of the produced time series is richer than that observed in Iori model; nonetheless, it was still insufficient to model instruments characterised by rich non-linear correlations (see Figure 4.8). The study of Iori's and Bornholdt's models revealed following limitations of these frameworks in the context of multiscale correlations generation:

- Neither could produce time series characterised by a rich hierarchical organization (having singularity spectrum width $\Delta\alpha > 0.3$).
- They are not able to simulate multiple coupled assets.
- In Bornholdt's model, agents are not allowed to stay out of the market (i.e., the model incorporates only two states: buy and sell).
- Iori's framework simulations for agent-agent interaction probability p close to the percolation threshold are unstable.

To fill these gaps, a new, **multi-asset three-state model of financial market** was proposed. The framework is inspired by the Ising Model and, similarly to the solution introduced by Bornholdt, incorporates a minority game mechanism that divides agents into two groups: fundamentalist and chartists. Moreover, the new

framework allows agents to assume an on-hold state. Another significant improvement of the proposed framework is the ability to simulate multiple coupled assets. **The coupling between instruments is realized on the local and global levels. Agents exchange information with the nearest neighbours about their position in other assets (local interaction) and are influenced by overall sentiment of investors regarding these instruments (global interaction)**.

As shown in Section 6.1, the microscopic dynamics of the single-asset variant of the model can be described as interlaced phases of metastability, when agents form large clusters of individuals having the same state, and rearrangements, which are characterised by the spatial disorganisation and breakdown of the clustered structure (see Figure 6.1). In this context, the metastable and rearrangement periods have much in common with phase transitions from ordered to unordered states observed in physical systems (e.g., phase transition in ferromagnetic materials). Notably, considered phases directly corresponded to increased and decreased collectivity among agents, which reveals itself in small and large fluctuations in the generated returns. Collective behaviour of agents themselves was identified as a primary source of fluctuations clustering observed in produced signals. The obtained result suggests that the hierarchical organization of the financial time series is related to the market participants' collective behavior and the fact that, besides observing asset valuation, investors consider other traders' positions.

In the model, level of collectivity among agents and, by extension, the degree of hierarchical organization of the generated time series can be controlled several ways. The first one relies on changing market temperature (i.e., increasing/decreasing β parameter, which result in steeper/more steady probability function p, see Figure 6.4), whereas the second is based on modification of agent-agent local interaction strength J_{ij}^{lm}. These two parameters are, to some degree, complementary. Practically speaking, by increasing or decreasing one or another, similar results can be obtained. Moreover, as shown by manipulation of β parameter, excessive collectivity among agents leads to another phenomenon having the appearance of phase transition (see Figure 6.8). Assuming that singularity spectrum width of signal generated by the model is the measure of system order, then the plunge in $\Delta\alpha$ caused by temporal freeze of system configuration (i.e., system configuration remains the same over consecutive time steps) observed for $\beta > 2.0$ can be perceived as a phase transition (see Figure 6.8). In the financial markets, such effects are related to the asset liquidity and are observed in assets characterised by low transaction volume (e.g., early years of the Bitcoin)

In the context of the non-linear autocorrelations of signals generated by the model, another element of the framework is noteworthy, namely, agents ability to assume on-hold position and related threshold mechanism, which positively impacts the hierarchical organization of generated returns, especially when the collectivity of the individuals is high (see Figure 6.20). By design, the threshold mechanism is directly linked to the system's transaction volume. Thanks to that, when the market is quiet (i.e., in a meta-stable phase), agents willingly participate in trading; on the other hand, when the market is volatile (i.e., in a rearrangement phase), some of the individuals perceive this situation as too hazardous and assume on-hold position. As a result, **signals generated by the single-asset variant of**

the model are characterized by broad singularity spectrum - $\overline{\Delta\alpha} \approx 0.4$. By introducing an on-hold state, the framework can be applied in modeling of the financial instruments characterised by rich multifractal structure, which, as was demonstrated, is not possible using well-known frameworks proposed in [71] or [70].

From the perspective of the hierarchical organization of the time series produced by the model, not without significance is an agent's ability to follow different strategies. As shown in Section 6.4, when the individuals become more independent from their neighbours (i.e. have higher value of α_c) the linear anti-persistence of the generated signals appear, and the volatility clusters become less pronounced, whereas the range of scaling of the fluctuations functions shrinks (see Figure 6.14). Such behaviour of agents corresponds to the situation when investors are uncertain about their investment strategy and therefore frequently change market position.

The multifractal rolling window analysis of the signals produced by the single-asset variant of the model, presented in Section 6.6, showed that the **model can generate signals that are charaterised by periods of symmetrization as well as increased width of the singularity spectra** (see Figures 6.21 and 6.22). Moreover, manipulating model parameters, can generate time series characterised by strong linear antipersistence or temporal breakdown in scaling properties of small fluctuations (typical of low liquidity assets).

In Chapter Seven, analysis of the model characteristics was extended to two-asset scenario. As was demonstrated, **the model by incorporation of global and local interactions between assets is able to generate pair of signals characterised by multiscale cross-correlations**. Moreover, it was shown that the cross-asset agent-agent local interaction is the main factor responsible for non-linear cross dependencies between produced signals; however, the most convincing results were obtained for the simulations in which both: local and global interactions were incorporated (see Figure 7.7). This suggests that the correlations between financial instruments primarily come from direct interactions between investors and, to lesser degree, from asset valuation itself. Since transactions made by large, institutional investors (e.g., hedge funds, banks) are the primary drivers of asset prices implies that these market participants, in their investment decision look closely at positions of their competitors in different instruments and to lesser degree are driven by financial instrument price.

As was demonstrated in Chapter Eight, new **framework can be applied to building multi-assets artificial indices that reproduce non-linear correlations between many financial instruments** (see Figure 8.2). In section 8.2, based on ten-assets artificial index it was presented that signals generated by the model, like financial time series, are characterised by phases of increased and decreased cross-dependencies (see Figures 8.3). The second artificial index considered in this thesis was inspired by DJIA and consisted of thirty assets divided into different sectors. In this case, the analysis focused on investigation of the multiscale cross-correlations captured within complex network formalism. Using q-dependent minimal spanning trees, it was demonstrated that **the model can reflect different market structures on different scales, including star-like and chain-like organization** (see Figure 8.5). Even though the framework does not generate signals cross-correlated on small scales, it can model real financial market structure ob-

served for large scales and large returns. As the structure of dependencies between components of artificial indices can be controlled by J_{ij}^{lm} and γ_{lm} matrices, thereby, **further modification of the local and global coupling between modeled assets is possible. In turn, the framework can be applied to recreating multiscale cross-dependencies structure observed in various systems**.

To sum up, analysis of the multiscale properties of the major indices and of DJIA components confirmed that financial time series are characterised by non-linear autocorrelations and cross-correlations. Quantification of these features helped in modeling them using authorial agent-based model. The proposed Ising-inspired multi-asset three-state model by allowing agents to stay out of the market and by incorporating coupling between assets on the local and global levels is able to accurately reproduce major multiscale characteristics of the financial data as well as facilitate understanding of the market mechanisms that underlie the hierarchical organization observed in returns signals.

Appendix A
List of symbols

List of stock indices and exchanges

Symbol	Name	Exchange
DAX	Deutscher Aktienindex	Frankfurt Stock Exchange
DJIA	Dow Jones Industrials Average	New Your Stock Exchange
FTSE	Financial Times Stock Exchange	London Stock Exchange
NASDAQ	NASDAQ	NASDAQ stock market
NIKKEI	Nikkei heikin kabuka	Tokyo Stock Exchange

List of analysed DJIA components

Symbol	Name	Sector
AA	Alcoa	Energy
AAPL	Apple Inc.	IT
AIG	AIG	Finance
AXP	American Express	Finance
BA	Boeing	Industrials
C	Citigroup	Finance
CAT	Caterpillar	Industrials
CVX	Chevron Corporation	Energy
DIS	The Walt Disney Company	Consumer Goods
GE	General Electric	Industrials
GT	Goodyear	Industrials
HON	Honeywell	Industrials
HPQ	Hewlett-Packard Company	IT
IBM	International Business Machines	IT
INTC	Intel	IT
JNJ	Johnson & Johnson	Healthcare
JPM	JPMorgan Chase	Finance
KO	The Coca-Cola Company	Consumer Goods
MCD	McDonalds	Consumer Goods
MMM	3M	Industrials
MO	Altria	Consumer Goods
MRK	Merck & Co.	Healthcare
NKE	Nike	Consumer Goods
PFE	Pfizer	Healthcare
PG	Procter & Gamble	Consumer Goods
RTX	Raytheon Technologies (United Technologies Corporation)	Industrials
TRV	The Travelers Companies	Finance
WBA	Walgreens Boots Alliance	Consumer Goods
WMT	UnitedHealth Group	Healthcare
XOM	ExxonMobil	Energy

Appendix B
Parameters of artificial index

Cross-asset agent-agent interaction strength matrix projection

$$J^{lm}=\begin{bmatrix}
1 & 0 & 0 & 0 & 0 & 0 & 0 & 0 & 0 & 0 & 0 & 0 & 0 & 0 & 0 & 0 & 0 & 0 & 0 & 0 & 0 & 0 & 0 & 0 & 0 & 0 & 0 & 0 & 0 & 0 \\
0.04 & 0.96 & 0 & 0 & 0 & 0 & 0 & 0 & 0 & 0 & 0 & 0 & 0 & 0 & 0 & 0 & 0 & 0 & 0 & 0 & 0 & 0 & 0 & 0 & 0 & 0 & 0 & 0 & 0 & 0 \\
0 & 0.04 & 0.96 & 0 & 0 & 0 & 0 & 0 & 0 & 0 & 0 & 0 & 0 & 0 & 0 & 0 & 0 & 0 & 0 & 0 & 0 & 0 & 0 & 0 & 0 & 0 & 0 & 0 & 0 & 0 \\
0 & 0.04 & 0 & 0.96 & 0 & 0 & 0 & 0 & 0 & 0 & 0 & 0 & 0 & 0 & 0 & 0 & 0 & 0 & 0 & 0 & 0 & 0 & 0 & 0 & 0 & 0 & 0 & 0 & 0 & 0 \\
0 & 0.04 & 0 & 0 & 0.96 & 0 & 0 & 0 & 0 & 0 & 0 & 0 & 0 & 0 & 0 & 0 & 0 & 0 & 0 & 0 & 0 & 0 & 0 & 0 & 0 & 0 & 0 & 0 & 0 & 0 \\
0 & 0.04 & 0 & 0 & 0 & 0.96 & 0 & 0 & 0 & 0 & 0 & 0 & 0 & 0 & 0 & 0 & 0 & 0 & 0 & 0 & 0 & 0 & 0 & 0 & 0 & 0 & 0 & 0 & 0 & 0 \\
0 & 0.04 & 0 & 0 & 0 & 0 & 0.96 & 0 & 0 & 0 & 0 & 0 & 0 & 0 & 0 & 0 & 0 & 0 & 0 & 0 & 0 & 0 & 0 & 0 & 0 & 0 & 0 & 0 & 0 & 0 \\
0 & 0.04 & 0 & 0 & 0 & 0 & 0 & 0.96 & 0 & 0 & 0 & 0 & 0 & 0 & 0 & 0 & 0 & 0 & 0 & 0 & 0 & 0 & 0 & 0 & 0 & 0 & 0 & 0 & 0 & 0 \\
0 & 0.04 & 0 & 0 & 0 & 0 & 0 & 0 & 0.96 & 0 & 0 & 0 & 0 & 0 & 0 & 0 & 0 & 0 & 0 & 0 & 0 & 0 & 0 & 0 & 0 & 0 & 0 & 0 & 0 & 0 \\
0 & 0.04 & 0 & 0 & 0 & 0 & 0 & 0 & 0 & 0.96 & 0 & 0 & 0 & 0 & 0 & 0 & 0 & 0 & 0 & 0 & 0 & 0 & 0 & 0 & 0 & 0 & 0 & 0 & 0 & 0 \\
0 & 0.04 & 0 & 0 & 0 & 0 & 0 & 0 & 0 & 0 & 0.96 & 0 & 0 & 0 & 0 & 0 & 0 & 0 & 0 & 0 & 0 & 0 & 0 & 0 & 0 & 0 & 0 & 0 & 0 & 0 \\
0.04 & 0 & 0 & 0 & 0 & 0 & 0 & 0 & 0 & 0 & 0 & 0.96 & 0 & 0 & 0 & 0 & 0 & 0 & 0 & 0 & 0 & 0 & 0 & 0 & 0 & 0 & 0 & 0 & 0 & 0 \\
0 & 0 & 0 & 0 & 0 & 0 & 0 & 0 & 0 & 0 & 0 & 0.04 & 0.96 & 0 & 0 & 0 & 0 & 0 & 0 & 0 & 0 & 0 & 0 & 0 & 0 & 0 & 0 & 0 & 0 & 0 \\
0 & 0 & 0 & 0 & 0 & 0 & 0 & 0 & 0 & 0 & 0 & 0.04 & 0 & 0.96 & 0 & 0 & 0 & 0 & 0 & 0 & 0 & 0 & 0 & 0 & 0 & 0 & 0 & 0 & 0 & 0 \\
0 & 0 & 0 & 0 & 0 & 0 & 0 & 0 & 0 & 0 & 0 & 0.04 & 0 & 0 & 0.96 & 0 & 0 & 0 & 0 & 0 & 0 & 0 & 0 & 0 & 0 & 0 & 0 & 0 & 0 & 0 \\
0 & 0 & 0 & 0 & 0 & 0 & 0 & 0 & 0 & 0 & 0 & 0.04 & 0 & 0 & 0 & 0.96 & 0 & 0 & 0 & 0 & 0 & 0 & 0 & 0 & 0 & 0 & 0 & 0 & 0 & 0 \\
0.04 & 0 & 0 & 0 & 0 & 0 & 0 & 0 & 0 & 0 & 0 & 0 & 0 & 0 & 0 & 0 & 0.96 & 0 & 0 & 0 & 0 & 0 & 0 & 0 & 0 & 0 & 0 & 0 & 0 & 0 \\
0 & 0 & 0 & 0 & 0 & 0 & 0 & 0 & 0 & 0 & 0 & 0 & 0 & 0 & 0 & 0 & 0.04 & 0.96 & 0 & 0 & 0 & 0 & 0 & 0 & 0 & 0 & 0 & 0 & 0 & 0 \\
0 & 0 & 0 & 0 & 0 & 0 & 0 & 0 & 0 & 0 & 0 & 0 & 0 & 0 & 0 & 0 & 0.04 & 0 & 0.96 & 0 & 0 & 0 & 0 & 0 & 0 & 0 & 0 & 0 & 0 & 0 \\
0 & 0 & 0 & 0 & 0 & 0 & 0 & 0 & 0 & 0 & 0 & 0 & 0 & 0 & 0 & 0 & 0.04 & 0 & 0 & 0.96 & 0 & 0 & 0 & 0 & 0 & 0 & 0 & 0 & 0 & 0 \\
0 & 0 & 0 & 0 & 0 & 0 & 0 & 0 & 0 & 0 & 0 & 0 & 0 & 0 & 0 & 0 & 0.04 & 0 & 0 & 0 & 0.96 & 0 & 0 & 0 & 0 & 0 & 0 & 0 & 0 & 0 \\
0.04 & 0 & 0 & 0 & 0 & 0 & 0 & 0 & 0 & 0 & 0 & 0 & 0 & 0 & 0 & 0 & 0 & 0 & 0 & 0 & 0 & 0.96 & 0 & 0 & 0 & 0 & 0 & 0 & 0 & 0 \\
0 & 0 & 0 & 0 & 0 & 0 & 0 & 0 & 0 & 0 & 0 & 0 & 0 & 0 & 0 & 0 & 0 & 0 & 0 & 0 & 0 & 0.04 & 0.96 & 0 & 0 & 0 & 0 & 0 & 0 & 0 \\
0 & 0 & 0 & 0 & 0 & 0 & 0 & 0 & 0 & 0 & 0 & 0 & 0 & 0 & 0 & 0 & 0 & 0 & 0 & 0 & 0 & 0.04 & 0 & 0.96 & 0 & 0 & 0 & 0 & 0 & 0 \\
0 & 0 & 0 & 0 & 0 & 0 & 0 & 0 & 0 & 0 & 0 & 0 & 0 & 0 & 0 & 0 & 0 & 0 & 0 & 0 & 0 & 0.04 & 0 & 0 & 0.96 & 0 & 0 & 0 & 0 & 0 \\
0 & 0 & 0 & 0 & 0 & 0 & 0 & 0 & 0 & 0 & 0 & 0 & 0 & 0 & 0 & 0 & 0 & 0 & 0 & 0 & 0 & 0.04 & 0 & 0 & 0 & 0.96 & 0 & 0 & 0 & 0 \\
0 & 0 & 0 & 0 & 0 & 0 & 0 & 0 & 0 & 0 & 0 & 0 & 0 & 0 & 0 & 0 & 0 & 0 & 0 & 0 & 0 & 0.04 & 0 & 0 & 0 & 0 & 0.96 & 0 & 0 & 0 \\
0 & 0 & 0 & 0 & 0 & 0 & 0 & 0 & 0 & 0 & 0 & 0 & 0 & 0 & 0 & 0 & 0 & 0 & 0 & 0 & 0 & 0 & 0 & 0 & 0 & 0 & 0.04 & 0.96 & 0 & 0 \\
0 & 0 & 0 & 0 & 0 & 0 & 0 & 0 & 0 & 0 & 0 & 0 & 0 & 0 & 0 & 0 & 0 & 0 & 0 & 0 & 0 & 0 & 0 & 0 & 0 & 0 & 0.04 & 0 & 0.96 & 0 \\
0 & 0 & 0 & 0 & 0 & 0 & 0 & 0 & 0 & 0 & 0 & 0 & 0 & 0 & 0 & 0 & 0 & 0 & 0 & 0 & 0 & 0 & 0 & 0 & 0 & 0 & 0.04 & 0 & 0 & 0.96
\end{bmatrix}$$

Inter-asset global coupling coefficients matrix

$$\gamma_{lm}=\begin{bmatrix}
0&0&0&0&0&0&0&0&0&0&0&0&0&0&0&0&0&0&0&0&0&0&0&0&0&0&0&0&0&0\\
0.05&0&0&0&0&0&0&0&0&0&0&0&0&0&0&0&0&0&0&0&0&0&0&0&0&0&0&0&0&0\\
0&0.05&0&0&0&0&0&0&0&0&0&0&0&0&0&0&0&0&0&0&0&0&0&0&0&0&0&0&0&0\\
0&0.05&0&0&0&0&0&0&0&0&0&0&0&0&0&0&0&0&0&0&0&0&0&0&0&0&0&0&0&0\\
0&0.05&0&0&0&0&0&0&0&0&0&0&0&0&0&0&0&0&0&0&0&0&0&0&0&0&0&0&0&0\\
0&0.05&0&0&0&0&0&0&0&0&0&0&0&0&0&0&0&0&0&0&0&0&0&0&0&0&0&0&0&0\\
0&0.05&0&0&0&0&0&0&0&0&0&0&0&0&0&0&0&0&0&0&0&0&0&0&0&0&0&0&0&0\\
0&0.05&0&0&0&0&0&0&0&0&0&0&0&0&0&0&0&0&0&0&0&0&0&0&0&0&0&0&0&0\\
0&0.05&0&0&0&0&0&0&0&0&0&0&0&0&0&0&0&0&0&0&0&0&0&0&0&0&0&0&0&0\\
0&0.05&0&0&0&0&0&0&0&0&0&0&0&0&0&0&0&0&0&0&0&0&0&0&0&0&0&0&0&0\\
0&0.05&0&0&0&0&0&0&0&0&0&0&0&0&0&0&0&0&0&0&0&0&0&0&0&0&0&0&0&0\\
0.05&0&0&0&0&0&0&0&0&0&0&0&0&0&0&0&0&0&0&0&0&0&0&0&0&0&0&0&0&0\\
0&0&0&0&0&0&0&0&0&0&0&0.05&0&0&0&0&0&0&0&0&0&0&0&0&0&0&0&0&0&0\\
0&0&0&0&0&0&0&0&0&0&0&0.05&0&0&0&0&0&0&0&0&0&0&0&0&0&0&0&0&0&0\\
0&0&0&0&0&0&0&0&0&0&0&0.05&0&0&0&0&0&0&0&0&0&0&0&0&0&0&0&0&0&0\\
0&0&0&0&0&0&0&0&0&0&0&0.05&0&0&0&0&0&0&0&0&0&0&0&0&0&0&0&0&0&0\\
0.05&0&0&0&0&0&0&0&0&0&0&0&0&0&0&0&0&0&0&0&0&0&0&0&0&0&0&0&0&0\\
0&0&0&0&0&0&0&0&0&0&0&0&0&0&0&0&0.05&0&0&0&0&0&0&0&0&0&0&0&0&0\\
0&0&0&0&0&0&0&0&0&0&0&0&0&0&0&0&0.05&0&0&0&0&0&0&0&0&0&0&0&0&0\\
0&0&0&0&0&0&0&0&0&0&0&0&0&0&0&0&0.05&0&0&0&0&0&0&0&0&0&0&0&0&0\\
0&0&0&0&0&0&0&0&0&0&0&0&0&0&0&0&0.05&0&0&0&0&0&0&0&0&0&0&0&0&0\\
0.05&0&0&0&0&0&0&0&0&0&0&0&0&0&0&0&0&0&0&0&0&0&0&0&0&0&0&0&0&0\\
0&0&0&0&0&0&0&0&0&0&0&0&0&0&0&0&0&0&0&0&0&0.05&0&0&0&0&0&0&0&0\\
0&0&0&0&0&0&0&0&0&0&0&0&0&0&0&0&0&0&0&0&0&0.05&0&0&0&0&0&0&0&0\\
0&0&0&0&0&0&0&0&0&0&0&0&0&0&0&0&0&0&0&0&0&0.05&0&0&0&0&0&0&0&0\\
0&0&0&0&0&0&0&0&0&0&0&0&0&0&0&0&0&0&0&0&0&0.05&0&0&0&0&0&0&0&0\\
0&0&0&0&0&0&0&0&0&0&0&0&0&0&0&0&0&0&0&0&0&0.05&0&0&0&0&0&0&0&0\\
0&0&0&0&0&0&0&0&0&0&0&0&0&0&0&0&0&0&0&0&0&0&0&0&0&0&0.05&0&0&0\\
0&0&0&0&0&0&0&0&0&0&0&0&0&0&0&0&0&0&0&0&0&0&0&0&0&0&0.05&0&0&0\\
0&0&0&0&0&0&0&0&0&0&0&0&0&0&0&0&0&0&0&0&0&0&0&0&0&0&0.05&0&0&0
\end{bmatrix}$$

Bibliography

[1] J. Kwapień and S. Drożdż, "Physical approach to complex systems," *Physics Reports*, vol. 515, no. 3-4, pp. 115–226, 2012.

[2] W. B. Arthur, "Complexity and the economy," *Science*, vol. 284, no. 5411, pp. 107–109, 1999.

[3] J. D. Farmer, M. Gallegati, C. Hommes, A. Kirman, P. Ormerod, S. Cincotti, A. Sanchez, and D. Helbing, "A complex systems approach to constructing better models for managing financial markets and the economy," *The European Physical Journal Special Topics*, vol. 214, no. 1, pp. 295–324, 2012.

[4] D. Sornette, *Critical phenomena in natural sciences: chaos, fractals, selforganization and disorder: concepts and tools*. Springer Science & Business Media, 2006.

[5] J. D. Farmer, "Market force, ecology and evolution," *Industrial and Corporate Change*, vol. 11, no. 5, pp. 895–953, 2002.

[6] D. Sornette, *Why stock markets crash: critical events in complex financial systems*. Princeton University Press, 2017.

[7] E. Mayr, *The growth of biological thought: Diversity, evolution, and inheritance*. Harvard University Press, 1982.

[8] E. Wilson, *The insect societies*. Harvard University Press, 1971.

[9] L. H. Hartwell, J. J. Hopfield, S. Leibler, and A. W. Murray, "From molecular to modular cell biology," *Nature*, vol. 402, no. 6761, pp. C47–C52, 1999.

[10] B. N. Danforth, "Female foraging and intranest behavior of a communal bee, perdita portalis (hymenoptera: Andrenidae)," *Annals of the Entomological Society of America*, vol. 84, no. 5, pp. 537–548, 1991.

[11] J. H. Miller and S. E. Page, *Complex adaptive systems: An introduction to computational models of social life*. Princeton University Press, 2009.

[12] N. Luhmann, *Social systems*. Stanford University Press, 1995.

[13] T. E. Drabek and D. A. McEntire, "Emergent phenomena and the sociology of disaster: lessons, trends and opportunities from the research literature," *Disaster Prevention and Management: An International Journal*, 2003.

[14] R. M. Raafat, N. Chater, and C. Frith, "Herding in humans," *Trends in Cognitive Sciences*, vol. 13, no. 10, pp. 420–428, 2009.

[15] J. H. Holland, *Emergence: From chaos to order*. Oxford University Press, 2000.

[16] P. W. Anderson, "More is different," *Science*, vol. 177, no. 4047, pp. 393–396, 1972.

[17] H. Y. Hwang, Y. Iwasa, M. Kawasaki, B. Keimer, N. Nagaosa, and Y. Tokura, "Emergent phenomena at oxide interfaces," *Nature Materials*, vol. 11, no. 2, pp. 103–113, 2012.

[18] P. W. Anderson, *Basic notions of condensed matter physics*. CRC Press, 2018.

[19] R. Dorner, J. Goold, C. Cormick, M. Paternostro, and V. Vedral, "Emergent thermodynamics in a quenched quantum many-body system," *Physical Review Letters*, vol. 109, no. 16, 2012.

[20] L. Bachelier, *Théorie de la spéculation*. Annales scientifiques de l'École normale supérieure, 1900.

[21] F. Black and M. Scholes, "The pricing of options and corporate liabilities," *Journal of Political Economy*, vol. 81, no. 3, pp. 637–654, 1973.

[22] X. Gabaix, P. Gopikrishnan, V. Plerou, and H. E. Stanley, "A theory of power-law distributions in financial market fluctuations," *Nature*, vol. 423, no. 6937, pp. 267–270, 2003.

[23] R. N. Mantegna and H. E. Stanley, *Introduction to econophysics: correlations and complexity in finance*. Cambridge University Press, 1999.

[24] Y. Liu, P. Gopikrishnan, and H. E. Stanley, "Statistical properties of the volatility of price fluctuations," *Physical Review E*, vol. 60, no. 2, p. 1390, 1999.

[25] P. Gopikrishnan, V. Plerou, L. A. N. Amaral, M. Meyer, and H. E. Stanley, "Scaling of the distribution of fluctuations of financial market indices," *Physical Review E*, vol. 60, no. 5, p. 5305, 1999.

[26] S. Drożdż, J. Kwapień, F. Grummer, F. Ruf, and J. Speth, "Are the contemporary financial fluctuations sooner converging to normal?," *Acta Physica Polonica B*, vol. 34, no. 8, p. 4293, 2003.

[27] J. J. Binney, N. J. Dowrick, A. J. Fisher, and M. E. Newman, *The theory of critical phenomena: an introduction to the renormalization group*. Oxford University Press, 1992.

[28] S.-K. Ma, *Modern theory of critical phenomena*. Routledge, 2018.

[29] B. Mandelbrot, "The variation of certain speculative prices," *The Journal of Business*, vol. 36, no. 4, pp. 394–419, 1963.

[30] J.-F. Muzy, E. Bacry, R. Baile, and P. Poggi, "Uncovering latent singularities from multifractal scaling laws in mixed asymptotic regime. application to turbulence," *Europhysics Letters*, vol. 82, no. 6, 2008.

[31] A. R. Subramaniam, I. A. Gruzberg, and A. W. Ludwig, "Boundary criticality and multifractality at the two-dimensional spin quantum hall transition," *Physical Review B*, vol. 78, no. 24, p. 245105, 2008.

[32] P. C. Ivanov, L. A. N. Amaral, A. L. Goldberger, S. Havlin, M. G. Rosenblum, Z. R. Struzik, and H. E. Stanley, "Multifractality in human heartbeat dynamics," *Nature*, vol. 399, no. 6735, pp. 461–465, 1999.

[33] A. L. Goldberger, L. A. Amaral, J. M. Hausdorff, P. C. Ivanov, C.-K. Peng, and H. E. Stanley, "Fractal dynamics in physiology: alterations with disease and aging," *Proceedings of the National Academy of Sciences*, vol. 99, no. suppl 1, pp. 2466–2472, 2002.

[34] H. E. Stanley and P. Meakin, "Multifractal phenomena in physics and chemistry," *Nature*, vol. 335, no. 6189, pp. 405–409, 1988.

[35] V. Udovichenko and P. Strizhak, "Multifractal properties of copper sulfide film formed in self-organizing chemical system," *Theoretical and Experimental Chemistry*, vol. 38, no. 4, pp. 259–262, 2002.

[36] A. Witt and B. D. Malamud, "Quantification of long-range persistence in geophysical time series: conventional and benchmark-based improvement techniques," *Surveys in Geophysics*, vol. 34, no. 5, pp. 541–651, 2013.

[37] L. Telesca, V. Lapenna, and M. Macchiato, "Multifractal fluctuations in earthquake-related geoelectrical signals," *New Journal of Physics*, vol. 7, no. 1, p. 214, 2005.

[38] M. Ausloos, "Generalized hurst exponent and multifractal function of original and translated texts mapped into frequency and length time series," *Physical Review E*, vol. 86, no. 3, p. 031108, 2012.

[39] S. Drożdż, P. Oświęcimka, A. Kulig, J. Kwapień, K. Bazarnik, I. Grabska-Gradzińska, J. Rybicki, and M. Stanuszek, "Quantifying origin and character of long-range correlations in narrative texts," *Information Sciences*, vol. 331, pp. 32–44, 2016.

[40] L. Calvet and A. Fisher, "Multifractality in asset returns: theory and evidence," *Review of Economics and Statistics*, vol. 84, no. 3, pp. 381–406, 2002.

[41] P. Oświęcimka, J. Kwapień, and S. Drożdż, "Multifractality in the stock market: price increments versus waiting times," *Physica A: Statistical Mechanics and its Applications*, vol. 347, pp. 626–638, 2005.

[42] J. Perelló, J. Masoliver, A. Kasprzak, and R. Kutner, "Model for interevent times with long tails and multifractality in human communications: An application to financial trading," *Physical Review E*, vol. 78, no. 3, p. 036108, 2008.

[43] M. Ausloos and K. Ivanova, "Multifractal nature of stock exchange prices," *Computer Physics Communications*, vol. 147, no. 1-2, pp. 582–585, 2002.

[44] A. Turiel and C. J. Pérez-Vicente, "Role of multifractal sources in the analysis of stock market time series," *Physica A: Statistical Mechanics and its Applications*, vol. 355, no. 2-4, pp. 475–496, 2005.

[45] W.-X. Zhou, "Multifractal detrended cross-correlation analysis for two nonstationary signals," *Physical Review E*, vol. 77, no. 6, p. 066211, 2008.

[46] S. Drożdż, J. Kwapień, P. Oświęcimka, and R. Rak, "The foreign exchange market: return distributions, multifractality, anomalous multifractality and the epps effect," *New Journal of Physics*, vol. 12, no. 10, p. 105003, 2010.

[47] D. Grech, "Alternative measure of multifractal content and its application in finance," *Chaos, Solitons & Fractals*, vol. 88, pp. 183–195, 2016.

[48] E. Bacry, J. Delour, and J.-F. Muzy, "Modelling financial time series using multifractal random walks," *Physica A: Statistical Mechanics and its Applications*, vol. 299, no. 1-2, pp. 84–92, 2001.

[49] T. Lux, "The markov-switching multifractal model of asset returns: Gmm estimation and linear forecasting of volatility," *Journal of business & economic statistics*, vol. 26, no. 2, pp. 194–210, 2008.

[50] J.-P. Bouchaud and M. Potters, *Theory of financial risk and derivative pricing: from statistical physics to risk management*. Cambridge University Press, 2003.

[51] H. M. Markowitz, "Foundations of portfolio theory," *The Journal of Finance*, vol. 46, no. 2, pp. 469–477, 1991.

[52] A. Troisi, V. Wong, and M. A. Ratner, "An agent-based approach for modeling molecular self-organization," *Proceedings of the National Academy of Sciences*, vol. 102, no. 2, pp. 255–260, 2005.

[53] G. Y. Vichniac, "Simulating physics with cellular automata," *Physica D: Nonlinear Phenomena*, vol. 10, no. 1-2, pp. 96–116, 1984.

[54] N. F. Johnson, D. M. Smith, and P. M. Hui, "Multi-agent complex systems and many-body physics," *Europhysics Letters*, vol. 74, no. 5, p. 923, 2006.

[55] D. J. Barnes and D. Chu, *Guide to Simulation and Modeling for Biosciences*. Springer, 2015.

[56] G. An, Q. Mi, J. Dutta-Moscato, and Y. Vodovotz, "Agent-based models in translational systems biology," *Wiley Interdisciplinary Reviews: Systems Biology and Medicine*, vol. 1, no. 2, pp. 159–171, 2009.

[57] Z. Wang, J. D. Butner, R. Kerketta, V. Cristini, and T. S. Deisboeck, "Simulating cancer growth with multiscale agent-based modeling," *Seminars in Cancer Biology*, vol. 30, pp. 70–78, 2015.

[58] A. Crooks, C. Castle, and M. Batty, "Key challenges in agent-based modelling for geo-spatial simulation," *Computers, Environment and Urban Systems*, vol. 32, no. 6, pp. 417–430, 2008.

[59] A. T. Crooks and A. J. Heppenstall, "Introduction to agent-based modelling," in *Agent-based models of geographical systems*, pp. 85–105, Springer, 2012.

[60] D. Valbuena, P. H. Verburg, A. K. Bregt, and A. Ligtenberg, "An agent-based approach to model land-use change at a regional scale," *Landscape Ecology*, vol. 25, no. 2, pp. 185–199, 2010.

[61] K. Sznajd-Weron and J. Sznajd, "Opinion evolution in closed community," *International Journal of Modern Physics C*, vol. 11, no. 06, pp. 1157–1165, 2000.

[62] A. Kowalska-Styczeń, K. Malarz, and K. Paradowski, "Model of knowledge transfer within an organisation," *Journal of Artificial Societies and Social Simulation*, vol. 21, no. 2, pp. 1–3, 2018.

[63] L. An, "Modeling human decisions in coupled human and natural systems: Review of agent-based models," *Ecological Modelling*, vol. 229, pp. 25–36, 2012.

[64] B. Müller, F. Bohn, G. Dreßler, J. Groeneveld, C. Klassert, R. Martin, M. Schlüter, J. Schulze, H. Weise, and N. Schwarz, "Describing human decisions in agent-based models–odd+ d, an extension of the odd protocol," *Environmental Modelling & Software*, vol. 48, pp. 37–48, 2013.

[65] I. Benenson, K. Martens, and S. Birfir, "Parkagent: An agent-based model of parking in the city," *Computers, Environment and Urban Systems*, vol. 32, no. 6, pp. 431–439, 2008.

[66] J. D. Farmer and D. Foley, "The economy needs agent-based modelling," *Nature*, vol. 460, no. 7256, pp. 685–686, 2009.

[67] T. Lux, "Estimation of an agent-based model of investor sentiment formation in financial markets," *Journal of Economic Dynamics and Control*, vol. 36, no. 8, pp. 1284–1302, 2012.

[68] S. Thurner, "Systemic financial risk: agent based models to understand the leverage cycle on national scales and its consequences," *IFP/FGS Working Paper*, vol. 14, 2011.

[69] E. Samanidou, E. Zschischang, D. Stauffer, and T. Lux, "Agent-based models of financial markets," *Reports on Progress in Physics*, vol. 70, no. 3, p. 409, 2007.

[70] G. Iori, "A microsimulation of traders activity in the stock market: the role of heterogeneity, agents' interactions and trade frictions," *Journal of Economic Behavior & Organization*, vol. 49, no. 2, pp. 269–285, 2002.

[71] S. Bornholdt, "Expectation bubbles in a spin model of markets: intermittency from frustration across scales," *International Journal of Modern Physics C*, vol. 12, no. 05, p. 667–674, 2001.

[72] K. Sznajd-Weron, "Sznajd model and its applications," *Acta Physica Polonica B*, vol. 36, p. 2537, 2005.

[73] M. Denys, T. Gubiec, and R. Kutner, "Reinterpretation of Sieczka-hołyst Financial Market Model," *Acta Physica Polonica A*, vol. 3, no. 123, pp. 513–517, 2013.

[74] D. Sornette, "Physics and financial economics (1776–2014): puzzles, ising and agent-based models," *Reports on Progress in Physics*, vol. 77, no. 6, p. 062001, 2014.

[75] I. Giardina and J.-P. Bouchaud, "Bubbles, crashes and intermittency in agent based market models," *The European Physical Journal B-Condensed Matter and Complex Systems*, vol. 31, no. 3, pp. 421–437, 2003.

[76] S. Drożdż, R. Kowalski, P. Oświęcimka, R. Rak, and R. Gębarowski, "Dynamical variety of shapes in financial multifractality," *Complexity*, vol. 2018, 2018.

[77] T. C. Schelling, "Dynamic models of segregation," *Journal of Mathematical Sociology*, vol. 1, no. 2, pp. 143–186, 1971.

[78] C. W. Reynolds, "Flocks, herds and schools: A distributed behavioral model," *Proceedings of the 14th annual conference on Computer graphics and interactive techniques*, pp. 25–34, 1987.

[79] F. S. Mishkin, *The economics of money, banking, and financial markets*. Pearson Education, 2007.

[80] R. F. Engle, "Autoregressive conditional heteroscedasticity with estimates of the variance of united kingdom inflation," *Econometrica: Journal of the Econometric Society*, pp. 987–1007, 1982.

[81] Z. Zheng, Z. Qiao, T. Takaishi, H. E. Stanley, and B. Li, "Realized volatility and absolute return volatility: a comparison indicating market risk," *PloS one*, vol. 9, no. 7, 2014.

[82] L. Forsberg and E. Ghysels, "Why do absolute returns predict volatility so well?," *Journal of Financial Econometrics*, vol. 5, no. 1, pp. 31–67, 2007.

[83] S. Drożdż, R. Gębarowski, L. Minati, P. Oświęcimka, and M. Wątorek, "Bitcoin market route to maturity? Evidence from return fluctuations, temporal correlations and multiscaling effects," *Chaos: An Interdisciplinary Journal of Nonlinear Science*, vol. 28, no. 7, p. 071101, 2018.

[84] B. Gutenberg and C. F. Richter, "Earthquake magnitude, intensity, energy, and acceleration," *Bulletin of the Seismological Society of America*, vol. 46, no. 2, pp. 105–145, 1956.

[85] E. T. Lu and R. J. Hamilton, "Avalanches and the distribution of solar flares," *The Astrophysical Journal*, vol. 380, pp. L89–L92, 1991.

[86] R. E. Wyllys, "Empirical and Theoretical Bases of Zipf's law," *Science*, vol. 53, 1981.

[87] A. Kulig, J. Kwapień, T. Stanisz, and S. Drożdż, "In narrative texts punctuation marks obey the same statistics as words," *Information Sciences*, vol. 375, pp. 98–113, 2017.

[88] A. Klaus, S. Yu, and D. Plenz, "Statistical analyses support power law distributions found in neuronal avalanches," *PloS one*, vol. 6, no. 5, 2011.

[89] M. E. Newman, "Power laws, Pareto distributions and Zipf's law," *Contemporary Physics*, vol. 46, no. 5, pp. 323–351, 2005.

[90] C. Hill and D. G. Musaev, *Complexity in Chemistry and Beyond: Interplay Theory and Experiment: New and Old Aspects of Complexity in Modern Research*. Springer, 2013.

[91] S. Drożdż, M. Forczek, J. Kwapień, P. Oświęcimka, and R. Rak, "Stock market return distributions: From past to present," *Physica A: Statistical Mechanics and its Applications*, vol. 383, no. 1, pp. 59–64, 2007.

[92] B. B. Mandelbrot, *The Fractal Geometry of Nature*, vol. 173. W.H. Freeman, 1982.

[93] W. Sierpiński, "Sur une courbe dont tout point est un point de ramification," *Comptes rendus de l'Académie des Sciences*, vol. 160, pp. 302–305, 1915.

[94] H. von Koch, "Sur une courbe continue sans tangente, obtenue par une construction geometrique elementaire," *Arkiv för Matematik, Astronomi och Fysik*, vol. 1, pp. 681–702, 1904.

[95] A. Bunde and S. Havlin, *Fractals and disordered systems*. Springer Science & Business Media, 2012.

[96] K. J. Falconer, *The Geometry of Fractal Sets*. Cambridge University Press, 1986.

[97] J.-F. Muzy, E. Bacry, and A. Arneodo, "The multifractal formalism revisited with wavelets," *International Journal of Bifurcation and Chaos*, vol. 4, no. 02, pp. 245–302, 1994.

[98] K. Falconer, *Fractal Geometry: Mathematical Foundations and Applications*. John Wiley & Sons, 2004.

[99] T. Gneiting, H. Ševčíková, and D. B. Percival, "Estimators of fractal dimension: Assessing the roughness of time series and spatial data," *Statistical Science*, pp. 247–277, 2012.

[100] A. Górski, S. Drożdż, A. Mokrzycka, and J. Pawlik, "Accuracy analysis of the box-counting algorithm," *Acta Physica Polonica A*, vol. 121, no. 2B, 2012.

[101] A. Arneodo, E. Bacry, and J. Muzy, "The thermodynamics of fractals revisited with wavelets," *Physica A: Statistical Mechanics and its Applications*, vol. 213, no. 1-2, pp. 232–275, 1995.

[102] P. Grassberger and I. Procaccia, "Measuring the strangeness of strange attractors," in *The Theory of Chaotic Attractors*, pp. 170–189, Springer, 2004.

[103] J. W. Kantelhardt, S. A. Zschiegner, E. Koscielny-Bunde, S. Havlin, A. Bunde, and H. E. Stanley, "Multifractal detrended fluctuation analysis of nonstationary time series," *Physica A: Statistical Mechanics and its Applications*, vol. 316, no. 1-4, pp. 87–114, 2002.

[104] J. W. Kantelhardt, E. Koscielny-Bunde, D. Rybski, P. Braun, A. Bunde, and S. Havlin, "Long-term persistence and multifractality of precipitation and river runoff records," *Journal of Geophysical Research: Atmospheres*, vol. 111, no. D1, 2006.

[105] S. Drożdż and P. Oświęcimka, "Detecting and interpreting distortions in hierarchical organization of complex time series," *Physical Review E*, vol. 91, no. 3, p. 030902, 2015.

[106] A. Wawrzaszek and W. M. Macek, "Observation of the multifractal spectrum in solar wind turbulence by ulysses at high latitudes," *Journal of Geophysical Research: Space Physics*, vol. 115, no. A7, 2010.

[107] C. Xue, P. Shang, and W. Jing, "Multifractal detrended cross-correlation analysis of bvp model time series," *Nonlinear Dynamics*, vol. 69, no. 1-2, pp. 263–273, 2012.

[108] R. Lopes and N. Betrouni, "Fractal and multifractal analysis: a review," *Medical Image Analysis*, vol. 13, no. 4, pp. 634–649, 2009.

[109] L. Czarnecki and D. Grech, "Multifractal dynamics of stock markets.," *Acta Physica Polonica, A.*, vol. 117, no. 4, 2010.

[110] B. B. Mandelbrot and R. L. Hudson, *The (mis) behaviour of markets: a fractal view of risk, ruin and reward*. Profile books, 2010.

[111] P. Oświęcimka, J. Kwapień, and S. Drożdż, "Wavelet versus detrended fluctuation analysis of multifractal structures," *Physical Review E*, vol. 74, no. 1, p. 016103, 2006.

[112] P. Oświęcimka, S. Drożdż, M. Forczek, S. Jadach, and J. Kwapień, "Detrended cross-correlation analysis consistently extended to multifractality," *Physical Review E*, vol. 89, no. 2, p. 023305, 2014.

[113] C.-K. Peng, S. V. Buldyrev, S. Havlin, M. Simons, H. E. Stanley, and A. L. Goldberger, "Mosaic organization of dna nucleotides," *Physical Review E*, vol. 49, no. 2, p. 1685, 1994.

[114] P. Oświęcimka, S. Drożdż, J. Kwapień, and A. Górski, "Effect of detrending on multifractal characteristics.," *Acta Physica Polonica, A.*, vol. 123, no. 3, 2013.

[115] B. B. Mandelbrot, A. J. Fisher, and L. E. Calvet, "A multifractal model of asset returns," *Cowles Foundation Discussion Papers*, no. 1165, 1997.

[116] B. Podobnik and H. E. Stanley, "Detrended cross-correlation analysis: a new method for analyzing two nonstationary time series," *Physical Review Letters*, vol. 100, no. 8, p. 084102, 2008.

[117] L. Kristoufek, "Multifractal height cross-correlation analysis: A new method for analyzing long-range cross-correlations," *Europhysics Letters*, vol. 95, no. 6, p. 68001, 2011.

[118] W.-X. Zhou, "The components of empirical multifractality in financial returns," *Europhysics Letters*, vol. 88, no. 2, p. 28004, 2009.

[119] D. Grech and G. Pamula, "On the multifractal effects generated by monofractal signals," *Physica A: Statistical Mechanics and its Applications*, vol. 392, no. 23, pp. 5845–5864, 2013.

[120] J. Kwapień, P. Oświęcimka, and S. Drożdż, "Components of multifractality in high-frequency stock returns," *Physica A: Statistical Mechanics and its Applications*, vol. 350, no. 2-4, pp. 466–474, 2005.

[121] S. Drożdż, J. Kwapień, P. Oświęcimka, and R. Rak, "Quantitative features of multifractal subtleties in time series," *Europhysics Letters*, vol. 88, no. 6, p. 60003, 2010.

[122] R. Rak and D. Grech, "Quantitative approach to multifractality induced by correlations and broad distribution of data," *Physica A: Statistical Mechanics and its Applications*, vol. 508, pp. 48–66, 2018.

[123] T. Schreiber and A. Schmitz, "Surrogate time series," *Physica D: Nonlinear Phenomena*, vol. 142, no. 3-4, pp. 346–382, 2000.

[124] K. Okina, M. Shirakawa, and S. Shiratsuka, "The asset price bubble and monetary policy: Japan's experience in the late 1980s and the lessons," *Monetary and Economic Studies (special edition)*, vol. 19, no. 2, pp. 395–450, 2001.

[125] J. Kwapień, P. Oświęcimka, M. Forczek, and S. Drożdż, "Minimum spanning tree filtering of correlations for varying time scales and size of fluctuations," *Physical Review E*, vol. 95, no. 5, p. 052313, 2017.

[126] J. B. Kruskal, "On the shortest spanning subtree of a graph and the traveling salesman problem," *Proceedings of the American Mathematical Society*, vol. 7, no. 1, pp. 48–50, 1956.

[127] S. Aparicio, J. Villazón-Terrazas, and G. Álvarez, "A model for scale-free networks: application to twitter," *Entropy*, vol. 17, no. 8, pp. 5848–5867, 2015.

[128] Y. Ding, "Scientific collaboration and endorsement: Network analysis of coauthorship and citation networks," *Journal of Informetrics*, vol. 5, no. 1, pp. 187–203, 2011.

[129] H. Ebel, L.-I. Mielsch, and S. Bornholdt, "Scale-free topology of e-mail networks," *Physical Review E*, vol. 66, no. 3, p. 035103, 2002.

[130] M. Steyvers and J. B. Tenenbaum, "The large-scale structure of semantic networks: Statistical analyses and a model of semantic growth," *Cognitive Science*, vol. 29, no. 1, pp. 41–78, 2005.

[131] A.-L. Barabási and E. Bonabeau, "Scale-free networks," *Scientific American*, vol. 288, no. 5, pp. 60–69, 2003.

[132] J. Kwapień, S. Gworek, S. Drożdż, and A. Górski, "Analysis of a network structure of the foreign currency exchange market," *Journal of Economic Interaction and Coordination*, vol. 4, no. 1, p. 55, 2009.

[133] R. Rak and E. Rak, "The fractional preferential attachment scale-free network model," *Entropy*, vol. 22, no. 5, p. 509, 2020.

[134] J.-P. Onnela, A. Chakraborti, K. Kaski, J. Kertész, and A. Kanto, "Dynamics of market correlations: Taxonomy and portfolio analysis," *Physical Review E*, vol. 68, p. 056110, 2003.

[135] A. Hüttner, J.-F. Mai, and S. Mineo, "Portfolio selection based on graphs: Does it align with markowitz-optimal portfolios?," *Dependence Modeling*, vol. 6, no. 1, pp. 63–87, 2018.

[136] T. Callen and J. D. Ostry, *Japan's lost decade: policies for economic revival*. International Monetary Fund, 2003.

[137] F. Hayashi and E. C. Prescott, "The 1990s in japan: A lost decade," *Review of Economic Dynamics*, vol. 5, no. 1, pp. 206–235, 2002.

[138] R. Matousek, S. T. Papadamou, A. Šević, and N. G. Tzeremes, "The effectiveness of quantitative easing: evidence from japan," *Journal of International Money and Finance*, vol. 99, p. 102068, 2019.

[139] S. Drożdż, F. Grummer, A. Górski, F. Ruf, and J. Speth, "Dynamics of competition between collectivity and noise in the stock market," *Physica A: Statistical Mechanics and its Applications*, vol. 287, no. 3-4, pp. 440–449, 2000.

[140] V. A. Marčenko and L. A. Pastur, "Distribution of eigenvalues for some sets of random matrices," *Mathematics of the USSR-Sbornik*, vol. 1, no. 4, p. 457, 1967.

[141] S. Drożdż, J. Kwapień, F. Grümmer, F. Ruf, and J. Speth, "Quantifying the dynamics of financial correlations," *Physica A: Statistical Mechanics and its Applications*, vol. 299, no. 1-2, pp. 144–153, 2001.

[142] C. M. Macal and M. J. North, "Tutorial on agent-based modeling and simulation," in *Proceedings of the Winter Simulation Conference, 2005.*, IEEE, 2005.

[143] C. Macal and M. North, "Introductory tutorial: Agent-based modeling and simulation," in *Proceedings of the Winter Simulation Conference 2014*, IEEE, 2014.

[144] E. Bonabeau, "Agent-based modeling: Methods and techniques for simulating human systems," *Proceedings of the National Academy of Sciences*, vol. 99, no. suppl 3, pp. 7280–7287, 2002.

[145] M. Wooldridge and N. R. Jennings, "Intelligent agents: Theory and practice," *The Knowledge Engineering Review*, vol. 10, no. 2, pp. 115–152, 1995.

[146] J. M. Epstein, "Agent-based computational models and generative social science," *Complexity*, vol. 4, no. 5, pp. 41–60, 1999.

[147] N. Brandon, K. L. Dionisio, K. Isaacs, R. Tornero-Velez, D. Kapraun, R. W. Setzer, and P. S. Price, "Simulating exposure-related behaviors using agent-based models embedded with needs-based artificial intelligence," *Journal of Exposure Science & Environmental Epidemiology*, pp. 1–10, 2018.

[148] J. D. Farmer, "Toward agent-based models for investment," *Developments in Quantitative Investment Models*, no. 7, pp. 61–71, 2001.

[149] M. Lovric, U. Kaymak, and J. Spronk, "Modeling investor sentiment and overconfidence in an agent-based stock market," *Human Systems Management*, vol. 29, no. 2, pp. 89–101, 2010.

[150] L. Tesfatsion, "Agent-based computational economics: A constructive approach to economic theory," *Handbook of computational economics*, vol. 2, pp. 831–880, 2006.

[151] M. Gardner, "Mathematical games," *Scientific American*, vol. 222, no. 6, pp. 132–140, 1970.

[152] C. Hofer, G. Jäger, and M. Füllsack, "Including traffic jam avoidance in an agent-based network model," *Computational Social Networks*, vol. 5, no. 1, p. 5, 2018.

[153] L. Zhang, Z. Wang, J. A. Sagotsky, and T. S. Deisboeck, "Multiscale agent-based cancer modeling," *Journal of Mathematical Biology*, vol. 58, no. 4-5, pp. 545–559, 2009.

[154] J. L. Segovia-Juarez, S. Ganguli, and D. Kirschner, "Identifying control mechanisms of granuloma formation during m. tuberculosis infection using an agent-based model," *Journal of Theoretical Biology*, vol. 231, no. 3, pp. 357–376, 2004.

[155] W. Rand, "Machine learning meets agent-based modeling: when not to go to a bar," in *Conference on Social Agents: Results and Prospects*, 2006.

[156] S. Taylor, *Agent-based Modeling and Simulation.* Springer, 2014.

[157] M. K. Brunnermeier and K. Markus, *Asset pricing under asymmetric information: Bubbles, crashes, technical analysis, and herding.* Oxford University Press, 2001.

[158] T. Lux, "Herd behaviour, bubbles and crashes," *The Economic Journal*, vol. 105, no. 431, pp. 881–896, 1995.

[159] B. LeBaron, "Agent-based computational finance," *Handbook of Computational Economics*, vol. 2, pp. 1187–1233, 2006.

[160] J. Duffy and M. U. Ünver, "Asset price bubbles and crashes with near-zero-intelligence traders," *Economic Theory*, vol. 27, no. 3, pp. 537–563, 2006.

[161] J. Geanakoplos, R. Axtell, J. D. Farmer, P. Howitt, B. Conlee, J. Goldstein, M. Hendrey, N. M. Palmer, and C.-Y. Yang, "Getting at systemic risk via an agent-based model of the housing market," *American Economic Review*, vol. 102, no. 3, pp. 53–58, 2012.

[162] R. Axtell, D. Farmer, J. Geanakoplos, P. Howitt, E. Carrella, B. Conlee, J. Goldstein, M. Hendrey, P. Kalikman, and D. Masad, "An agent-based model of the housing market bubble in metropolitan washington, d.c.," in *Whitepaper for Deutsche Bundesbank's Spring Conference on "Housing markets and the macroeconomy: Challenges for monetary policy and financial stability*, 2014.

[163] W. B. Arthur, J. H. Holland, B. LeBaron, R. Palmer, and P. Tayler, *The Economy As An Evolving Complex System II*, vol. 27. CRC Press, 1996.

[164] R. G. Palmer, W. B. Arthur, J. H. Holland, B. LeBaron, and P. Tayler, "Artificial economic life: a simple model of a stockmarket," *Physica D: Nonlinear Phenomena*, vol. 75, no. 1-3, pp. 264–274, 1994.

[165] D. Stauffer, "Percolation models of financial market dynamics," *Advances in Complex Systems*, vol. 04, p. 19–27, Mar 2001.

[166] D. Stauffer and D. Sornette, "Self-organized percolation model for stock market fluctuations," *Physica A: Statistical Mechanics and its Applications*, vol. 271, p. 496–506, Sep 1999.

[167] D. P. Landau and K. Binder, *A guide to Monte Carlo simulations in statistical physics*. Cambridge University Press, 2014.

[168] L. D. Landau and E. M. Lifshitz, *Course of Theoretical Physics*. Elsevier, 2013.

[169] A. Kasprzak, R. Kutner, J. Perelló, and J. Masoliver, "Higher-order phase transitions on financial markets," *The European Physical Journal B*, vol. 76, no. 4, pp. 513–527, 2010.

[170] J. Jurczyk, T. Rehberg, A. Eckrot, and I. Morgenstern, "Measuring critical transitions in financial markets," *Scientific Reports*, vol. 7, no. 1, pp. 1–6, 2017.

[171] D. Sornette, "Stock market speculation: Spontaneous symmetry breaking of economic valuation," *Physica A: Statistical Mechanics and its Applications*, vol. 284, no. 1-4, pp. 355–375, 2000.

[172] D. Sornette and A. Johansen, "Significance of log-periodic precursors to financial crashes," *Quantitative Finance*, vol. 1, no. 4, pp. 452–471, 2001.

[173] S. Drożdż, J. Kwapień, and P. Oświęcimka, "Criticality characteristics of current oil price dynamics," *Acta Physica Polonica A*, vol. 114, no. 4, pp. 699–702, 2008.

[174] M. Wątorek, S. Drożdż, and P. Oświęcimka, "World financial 2014-2016 market bubbles: Oil negative-us dollar positive," *Acta Physica Polonica A*, vol. 129, no. 5, pp. 932–936, 2016.

[175] S. G. Brush, "History of the lenz-ising model," *Reviews of Modern Physics*, vol. 39, no. 4, p. 883, 1967.

[176] E. Ising, "Beitrag zur theorie des ferromagnetismus," *Zeitschrift für Physik*, vol. 31, no. 1, pp. 253–258, 1925.

[177] L. Onsager, "Crystal statistics. i. a two-dimensional model with an order-disorder transition," *Physical Review*, vol. 65, no. 3-4, p. 117, 1944.

[178] J. Honerkamp, *Statistical physics: an advanced approach with applications*. Springer Science & Business Media, 2012.

[179] N. Metropolis, A. W. Rosenbluth, M. N. Rosenbluth, A. H. Teller, and E. Teller, "Equation of state calculations by fast computing machines," *The Journal of Chemical Physics*, vol. 21, no. 6, pp. 1087–1092, 1953.

[180] R. J. Glauber, "Time-dependent statistics of the ising model," *Journal of Mathematical Physics*, vol. 4, no. 2, pp. 294–307, 1963.

[181] J.-S. Wang and R. H. Swendsen, "Cluster monte carlo algorithms," *Physica A: Statistical Mechanics and its Applications*, vol. 167, no. 3, pp. 565–579, 1990.

[182] R. Cont and J.-P. Bouchaud, "Herd behavior and aggregate fluctuations in financial markets," *Macroeconomic Dynamics*, vol. 4, no. 2, pp. 170–196, 2000.

[183] A. Ponzi and Y. Aizawa, "Criticality and punctuated equilibrium in a spin system model of a financial market," *Chaos, Solitons & Fractals*, vol. 11, no. 11, pp. 1739–1746, 2000.

[184] D. Heymann, R. Perazzo, and A. Schuschny, "Learning and contagion effects in transitions between regimes: Some schematic multiagent models," *Journal of Management and Economics*, vol. 2, no. 6, 1998.

[185] G. Iori and S. Jafarey, "Criticality in a model of banking crises," *Physica A: Statistical Mechanics and its Applications*, vol. 299, no. 1-2, pp. 205–212, 2001.

[186] P. Sieczka, D. Sornette, and J. A. Hołyst, "The Lehman Brothers effect and bankruptcy cascades," *The European Physical Journal B*, vol. 82, no. 3-4, p. 257, 2011.

[187] D. Belanger and A. Young, "The Random Field Ising Model," *Journal of magnetism and magnetic materials*, vol. 100, no. 1-3, pp. 272–291, 1991.

[188] F.-Y. Wu, "The potts model," *Reviews of Modern Physics*, vol. 54, no. 1, p. 235, 1982.

[189] M. Mézard, G. Parisi, and M. Virasoro, *Spin glass theory and beyond: An Introduction to the Replica Method and Its Applications*, vol. 9. World Scientific Publishing Company, 1987.

[190] T. Lux and M. Marchesi, "Scaling and criticality in a stochastic multi-agent model of a financial market," *Nature*, vol. 397, no. 6719, pp. 498–500, 1999.

[191] T. Lux and M. Marchesi, "Volatility clustering in financial markets: a microsimulation of interacting agents," *International Journal of Theoretical and Applied Finance*, vol. 3, no. 04, pp. 675–702, 2000.

[192] S.-H. Chen, T. Lux, and M. Marchesi, "Testing for non-linear structure in an artificial financial market," *Journal of Economic Behavior & Organization*, vol. 46, no. 3, pp. 327–342, 2001.

[193] J. Kukacka and L. Kristoufek, "Do complex financial models really lead to complex dynamics? Agent-based models and multifractality," *Journal of Economic Dynamics and Control*, vol. 113, p. 103855, 2020.

[194] D. Marković and C. Gros, "Power laws and self-organized criticality in theory and nature," *Physics Reports*, vol. 536, no. 2, pp. 41–74, 2014.

[195] T. Yamano, "Bornholdt's spin model of a market dynamics in high dimensions," *International Journal of Modern Physics C*, vol. 13, no. 01, pp. 89–96, 2002.

[196] T. Kaizoji, S. Bornholdt, and Y. Fujiwara, "Dynamics of price and trading volume in a spin model of stock markets with heterogeneous agents," *Physica A: Statistical Mechanics and its Applications*, vol. 316, no. 1-4, pp. 441–452, 2002.

[197] W. Lee, "Risk-based asset allocation: A new answer to an old question?," *Journal of Portfolio Management*, vol. 37, no. 4, p. 11, 2011.

[198] P. Sieczka and J. Hołyst, "A threshold model of financial markets," *Acta Physica Polonica A*, vol. 3, no. 114, pp. 525–530, 2008.

[199] T. Takaishi, "Multiple time series Ising Model for financial market simulations," in *Journal of Physics: Conference Series*, vol. 574, p. 012149, IOP Publishing, 2015.

[200] S. Drożdż, L. Minati, P. Oświęcimka, M. Stanuszek, and M. Wątorek, "Signatures of the crypto-currency market decoupling from the forex," *Future Internet*, vol. 11, no. 7, p. 154, 2019.